Blended fuel droplet heating, evaporation and combustion

Al-Esawi, Nawar

Award date:
2021

Awarding institution:
Coventry University

BLENDED FUEL DROPLET HEATING, EVAPORATION AND COMBUSTION

By

Nawar Al-Esawi

July 2020

A thesis submitted in partial fulfilment of the University's requirements for the Degree of Doctor of Philosophy

Content removed on data protection grounds

Certificate of Ethical Approval

Applicant:

Nawar Al-Esawi

Project Title:

Blended fuel droplets heating, evaporation and ignition

This is to certify that the above named applicant has completed the Coventry University Ethical Approval process and their project has been confirmed and approved as Low Risk

Date of approval:

17 September 2019

Project Reference Number:

P94213

Abstract

The previously developed models for fuel droplet heating and evaporation processes, mainly the Discrete Multi Component Model (DMCM), and Multi-Dimensional Quasi-Discrete Model (MDQDM) are studied, improved and generalised for a broad range of bio-fossil fuel blends so that the application areas are broadened with increased accuracy. The main distinctive features of these models are that they consider the impacts of species thermal conductivities and diffusivities within the droplets to account for the temperature gradient, transient diffusion of species and recirculation. The research carried out in this thesis is focused on four key aspects: (1) application of the previously developed models for a broad range of fossil fuels, biofuels and their blends including ethanol/gasoline, biodiesel/diesel, E85-diesel (E85 refers to 85% ethanol and 15% gasoline) and ethanol/biodiesel/diesel fuel blends; (2) formulation of fuel surrogates, using a new model referred to as ''Complex Fuel Surrogate Model (CFSM)'', and analysing their heating, evaporation and combustion characteristics; (3) modelling of fuel droplet heating and evaporation, using a modified version of the MDQDM with a new transient algorithm referred to as ''Transient Multi-Dimensional Quasi-Discrete Model (TMDQDM)''; and (4) providing a proof of concept with the implementation of the developed model into a commercial CFD code ANSYS-Fluent, for the three-dimensional modelling of complete combustion processes. A case study is made for the CFD modelling of gas-turbine engine using kerosene fuel surrogate. The non-ideal vapour-liquid equilibrium is accounted for, using the Universal Quasi-Chemical Functional–group Activity Coefficient (UNIFAC) model.

The heating and evaporation of ethanol/gasoline and biodiesel/diesel fuel blends are investigated using the DMCM. The combination of ethanol and gasoline fuels has a noticeable impact on droplet heating and evaporation. For biodiesel/diesel blend, the predicted droplet lifetimes of biodiesel/diesel blends with 5% biodiesel and 95% diesel are only 1% less than that of pure diesel. The application of the MDQDM has improved the computational efficiency significantly with minimal sacrifice in accuracy. It is found that the original DMCM predicts ethanol/gasoline fuel droplet lifetimes with errors up to 5.7% compared to those predicted using the same model but with the ACs obtained from the UNIFAC model.

A new approach to the formulation of fuel surrogates in application to gasoline, diesel, and their biofuel blends (including blends of biodiesel/diesel and ethanol/gasoline) is proposed. This new approach, described as a ''CFSM'', is based on a modified version of the MDQDM. The CFSM is aimed to reduce the full composition of fuel to a much smaller number of components based on their mass fractions, and to formulate fuel surrogates. A new algorithm for the auto-selection of Components/Quasi-Components in MDQDM is suggested and applied to the analysis of fuel droplet heating and evaporation. In contrast to the MDQDM, the new model takes into account the transient contributions of all groups of hydrocarbons, aiming for higher accuracy of the selection of quasi-components than that produced using the original MDQDM. Finally, a surrogate for kerosene is proposed using the CFSM. The model is implemented into ANSYS-Fluent via a user-defined function in order to provide the first full simulation of the combustion process. Detailed chemical mechanism is also implemented into ANSYS CHEMKIN for the combustion study.

Acknowledgements

First of all, I would like to express my deepest and sincere gratitude towards my supervisors, Dr Mansour Al Qubeissi and Dr Bidur Khanal, and Professor Mike Blundell, for their encouragement and guidance throughout the years of study. This thesis would not have been possible without their invaluable support.

I am grateful to Professor Sergei S. Sazhin for the invaluable support throughout the years of study. I would also like to express my gratitude to Dr Mohammed Ghaleeh, Dr Ruslana Kolodnytska, Dr Nwabueze Emekwuru, Mr. Reece Whitaker, Mr. Geng Wang, and Dr Oyuna Rybdylova for their valuable collaboration.

I am very grateful to the Institute for Future Transport and Cities, Coventry University for the fully funded studentship (Project Ref. ECR019), and the in-kind support of the Faculty of Engineering, Environment and Computing, Coventry University, in facilitating the work on this project.

The division of Combustion Physics, Lund University is gratefully acknowledged for providing a training course on Laser Imaging of Spray Systems. This course was provided by Dr Edouard Berrocal, Dr Elias Kristensson, Professor Mark Linne and Dr Sven-Inge Moller.

The UK Fluids network is gratefully acknowledged for its support of the Special Interest Group 'Sprays in engineering applications: modelling and experimental studies'. This group was a platform for the exchange of ideas between researchers working on various aspects of spray research.

Many thanks to my beloved wife Marwah for all the efforts, support, and patience she provided throughout the years of my study. My truthful love is dedicated to you and to our beloved Asal and Hasan. I would also like to thank my father Hasan and my mother Azhar for their immense support and love to continuously spur me on through this period.

Contents

Abstract III
Acknowledgements IV
Nomenclature VII
List of Figures XIV
List of Tables XIX
Dissemination of Results XXI
CHAPTER ONE: Introduction 1
1.1. Motivation 4
1.2. Aim and Objectives 5
1.3. Thesis Structure 5
CHAPTER TWO: Literature Review 7
2.1. Overview 7
2.2. Infinite Diffusivity/Infinite Thermal Conductivity Based Models 7
2.3. Discrete Multi-Component Model 13
2.4. Quasi-Component Models 17
2.5. Formulation of Fuel Surrogates 20
2.6. Summary of Chapter 2 24
CHAPTER THREE: Computational Methodology 26
3.1. Overview 26
3.2. Droplet Heating 28
3.3. Species Diffusion 31
3.4. Droplet Evaporation 33
3.5. Vapour-Liquid Equilibrium 35
3.6. Multi-Dimensional Quasi-Discrete Model 40
3.7. Solution Algorithm 41
CHAPTER FOUR: Ethanol/Gasoline Fuel Blends 44
4.1. Overview 44
4.2. Impacts of Fuel Blends and Ambient Conditions 45
4.2.1. Fuel compositions 45
4.2.2. Model validation 46
4.2.3. Impacts of ethanol/gasoline fuel blends 47
4.2.4. Impacts of ambient conditions 51
4.3. Impacts of the Activity Coefficient 57
4.3.1. Model validation 57
4.3.2. Predictions of heating and evaporation 58
4.4. Summary of Chapter 4 64
CHAPTER FIVE: Bio/Diesel-Fuel Blends 66
5.1. Overview 66
5.2. Biodiesel/Diesel Fuel Blends 66
5.2.1. Fuel compositions 67
5.2.2. Impacts of biodiesel/diesel fuel blends 71
5.2.3. Impacts of ambient conditions 76

5.3. E85-Diesel Fuel Blends 81
5.3.1. Model validation 82
5.3.2. Predictions of the DMCM 83
5.3.3. Predictions of the MDQDM 89
5.4. Ethanol/Biodiesel/Diesel Fuel Blends 92
5.4.1. Heating and evaporation 93
5.4.2. Cetane number and viscosity 96
5.4.3. Heating value 99
5.5. Summary of Chapter 5 101
CHAPTER SIX: Complex Fuel Surrogates 103
6.1. Overview 103
6.2. The Complex Fuel Surrogates Model 103
6.3. Diesel Fuel Surrogates 105
6.4. Gasoline Fuel Surrogates 116
6.5. Blended Ethanol/Gasoline Surrogates 119
6.6. Blended Biodiesel/Diesel Surrogate 122
6.7. Summary of Chapter 6 125
CHAPTER SEVEN: Auto-Selection of Quasi-Components of Fuel Blends 127
7.1. Overview 127
7.2. The Transient Multi-Dimensional Quasi-Discrete Model 128
7.3. E85-Diesel Fuel Blend 132
7.4. Summary of Chapter 7 144
CHAPTER EIGHT: Combustion of Fuel Surrogate 146
8.1. Overview 146
8.2. Surrogate Formulation 146
8.3. Implementation of DMCM 148
8.4. Combustion and Ignition Time Delay 152
8.5. Summary of Chapter 8 164
CHAPTER NINE: Conclusions and Recommendations 165
9.1. Conclusions 165
9.2. Recommendations 171
References 173
Appendix A. Thermodynamic Properties of Air 191
Appendix B. Thermodynamic Properties of Gasoline 192
Appendix C. Thermodynamic Properties of Ethanol 200
Appendix D. Supporting Results of Chapter 4 204
Appendix E. Thermodynamic Properties of Diesel 209
Appendix F. Thermodynamic Properties of Biodiesel 218
Appendix G. Diffusion Coefficients 222
Appendix H. Blending Rules 224
Appendix I. Components/Quasi-Components 225

Nomenclature

Abbreviations

AC	Activity Coefficient
ADC	Approximate Discrete Components
B#	#% Biodiesel/diesel volume fraction
BME	Butter Methyl Ester
C/QC	Components/Quasi-Components
CAN	Canola Methyl Ester
CFD	Computational Fluid Dynamics
CFSM	Complex Fuel Surrogate Model
CME	Coconut Methyl Ester
CML	Camelina Methyl Ester
CN	Cetane Number
CNE	Corn Methyl Ester
CO	Carbon monoxide
CO_2	Carbon dioxide
CPU	Central Processing Unit
CSE	Cottonseed Methyl Ester
DB	Double Bond
Diff	Difference
DLM	Diffusion Limit Model
DMCM	Discrete Multi-Component Model
E#	#% Ethanol/gasoline volume fraction
EM#	#% Ethanol/gasoline molar fraction
EW#	#% Ethanol/gasoline weight fraction

EBD	Ethanol/Biodiesel/Diesel
ED	Effective Diffusivity
E/D	Ethanol/Diesel
ETC	Effective Thermal Conductivity
FACE	Fuel used in Advanced Combustion Engines
FAME	Fatty Acid Methyl Ester
GGE	Greenhouse Gas Emissions
FGM	Flamelet Generated Manifold
GTE	Gas-Turbine Engines
HC	Hydrocarbons
H/C	Hydrogen/Carbon
HME1	Hempseed-oil, produced in Ukraine
HME2	Hempseed-oil, produced in the EU
HV	Heating Value
ICE	Internal Combustion Engine
ID	Infinite Diffusivity
ITC	Infinite Thermal Conductivity
JTR	Jatropha Methyl Ester
LME	Lard Methyl Ester
LNE	Linseed Methyl Ester
MDQDM	Multi-Dimensional Quasi-Discrete Model
MON	Motor Octane Number
MW	Molar Weight
NO_x	Nitrogen Oxides
Nu	Nusselt number
NRTL	Non-Random Two Liquids

ON	Octane Number
Pe	Peclet number
PME	Palm Methyl Ester
PMK	Palm kernel Methyl Ester
Pr	Prandtl number
RMM	Rapid Mixing Model
PTE	Peanut Methyl Ester
QDM	Quasi-Discrete Model
Re	Reynolds number
RME	Rapeseed Methyl Ester
RON	Research octane number
Sc	Schmidt number
SCM	Single Component Model
SFE	Safflower Methyl Ester
Sh	Sherwood number
SME	Soybean Methyl Ester
SNE	Sunflower Methyl Ester
Sur#	Surrogate number
TGE	Tung Methyl Ester
TMDQDM	Transient Multi-Dimensional Quasi-Discrete Model
TME	Tallow Methyl Ester
UNIFAC	Universal Quasi-Chemical Functional–group Activity Coefficient
WCO	Waste Cooking Oil
YGR	Yellow Grease Methyl Ester

Symbols

a	Group interaction parameter
B_M	Spalding mass transfer number
B_T	Spalding heat transfer number
c	Specific heat capacity
C_F	Friction drag coefficient
c_{pv}	Specific heat capacity of the fuel vapour at constant pressure
D	Diffusion coefficient
Ea	Activation energy
$F(B_M)$	Mass film thickness correction factor
$F(B_T)$	Heat film thickness correction factor
G	Group mass fraction
$\Delta^* g^{EC}$	Parameter introduced at Equation 38
$\Delta^* g^{RC}$	Parameter introduced at Equation 38
h	Convective heat transfer coefficient
h_{OT}	Parameter introduced at Equation 10
h_{OY}	Parameter introduced at Equation 21
k	Thermal conductivity
L	Latent heat of evaporation
Le	Lewis number
m	Hydrocarbon group number or mass of the droplet
$\dot{m}$	Evaporation rate of droplets
n	Carbon number
N	Number of atoms
p	Pressure

q	Sum of the group area parameter
q_n	Parameter introduced at Equation 10
Q	Molecular van der Waals surface area parameter
Q_L	Power spent on the droplet heating
r	Sum of the group volume parameter
R	Droplet Radius, molecular van der Waals volume parameter or universal gas constant
$\dot{R}$	Rate of change in droplet radius
t	Time
T	Temperature
U	Velocity
v	Volume fraction or kinematic viscosity
v_n	Parameter introduced at Equation 10
V	Volume
W	Weight
x	Molar fraction
y	Mass fraction

Greek Symbols

α	Parameter defined by Equation 19
β	Parameter value for octane or cetane numbers
γ	Activity coefficient
θ	Area fraction
ϵ	Evaporation rate of specie
ε	Error
κ	Effective thermal diffusivity

μ	Dynamic viscosity
ρ	Density
$\tilde{\rho}$	Relative density
v	Number of structure groups in molecule i
ψ	Group interaction parameter
Γ	Group residual activity coefficient
Φ	Segment fraction
ϕ	Equivalence ratio
φ	Parameter introduced in Equation 28 or fugacity coefficient
τ	Time instant in transient states or ignition time delay
σ	Stefan-Boltzmann constant
λ	Eigenvalues
ω	Acentric factor
χ	Recirculation coefficient
Δ	Difference

Subscripts

av	Average
b	Boiling
B	Biodiesel
c	Critical
C	Carbon
d	Droplet
D	Diesel
E	Evaporation or Ethanol
eff	Effective

g	Gas
H	Hydrogen
i	Index of individual components
ign	Ignition
iso	Isolated
j	Molecular group of mixed type
k, m, n	Molecular group of one type used in the UNIFAC model
l	Liquid
m	Mixture
r	Reduced
rad	Radiation
s	Surface
T	Temperature
v	Vapour
∞	Far from the droplet surface

Superscripts

C	Combinatorial term
R	Residual term
Sat	Saturation
$*$	Modified values

List of Figures

Figure 1. Schematic of injection, breakup, heating, evaporation and ignition processes inside the combustion chamber of an ICE [14]....2

Figure 2. The effect of internal recirculation on temperature distribution inside a droplet moving with relative velocities (a) 0.2 m.s^{-1}, (b) 1 m.s^{-1} and (c) 3 m.s^{-1} [11]. 13

Figure 3. Liquid kinetic and hydrodynamic regions near the surface of the droplet. T_s is the droplet surface temperature, ρ_{si} is the vapour density of component i in the immediate vicinity of the droplet surface, T_{Rd} is the temperature at the outer boundary of the kinetic region and ρ_{Rdi} is the vapour density of component i at the outer boundary of the kinetic region....27

Figure 4. Predicted and experimentally measured [134] normalised radii of the EW30, EW70 and EW100 droplets. 47

Figure 5. The plots of droplet radii versus time for various ethanol/gasoline blends. 48

Figure 6. The plots of droplet surface temperatures versus time for various ethanol/gasoline blends. 49

Figure 7. The plots of surface mass fractions of representative components of EM50, Ys, versus time. The plots of the following components are shown: n-$C_{12}H_{26}$ (1), iso-C_8H_{18} (2), iso-$C_{11}H_{24}$ (3), C_9H_{12} (4), C_9H_{10} (5) and C_2H_6O (6). 51

Figure 8. The estimated droplet lifetimes versus radiative temperatures T_{rad} for EM0–EM100 fuel blends, using the DMCM. 52

Figure 9. The effect of ambient pressures on droplet lifetimes for EM0–EM100 fuel blends, estimated at ambient gas temperature 650 K, using the DMCM. The effects of thermal radiation are ignored. 53

Figure 10. The effect of ambient temperatures on droplet lifetimes for EM0–EM100 fuel blends, estimated at ambient pressure of 3 bar, using the DMCM. The effects of thermal radiation are ignored. 54

Figure 11. The effect of ambient temperatures on droplet lifetimes for EM0–EM100 fuel blends, estimated at ambient pressure of 30 bar, using the DMCM. The effects of thermal radiation are ignored. 55

Figure 12. The effect of ambient pressures on droplet lifetimes for EM0–EM100 fuel blends, estimated at ambient temperature 400 K, using the DMCM. The effects of thermal radiation are ignored. 56

Figure 13. The predicted and experimentally observed total vapour pressures of ethanol/gasoline blends at various temperatures and ethanol volume fractions in the liquid phase [143]. 58

Figure 14. Total vapour pressure of various ethanol/gasoline molar blends (EM0–EM100), predicted by Raoult's law and the UNIFAC model at $T = 296$ K and 350 K....59

Figure 15. Droplet surface temperatures and radii versus time for EM5 (a), EM20 (b), EM85 (c) and EM85 (d) blends for various approaches to calculating the total vapour pressures at droplet surfaces.....62

Figure 16. Droplet surface temperatures and radii versus time for various SME/diesel fuel blends.....71

Figure 17. Droplet surface temperatures and radii versus time for various WCO/diesel fuel blends.....72

Figure 18. The estimated droplet lifetimes versus radiation temperatures T_{rad} for B0 – B100 SME/diesel fuel blends.....76

Figure 19. The estimated droplet lifetimes versus radiation temperatures T_{rad} for B0 – B100 WCO/diesel fuel blends.....77

Figure 20. The impact of ambient pressures on droplet lifetimes for B0 – B100 of SME/diesel fuel blends at T_g = 800 K.....78

Figure 21. The impact of ambient pressures on droplet lifetimes for B0 – B100 of WCO/diesel fuel blends at T_g = 800 K.....79

Figure 22. The impact of ambient temperatures on droplet lifetimes for B0 – B100 of SME/diesel fuel blends at p_g = 30 bar.....79

Figure 23. The impact of ambient temperatures on droplet lifetimes for B0 – B100 of WCO/diesel fuel blends at p_g = 30 bar.....80

Figure 24. Normalised squared diameters of diesel fuel (represented by 6 components) droplets versus time [163,164].....83

Figure 25. Droplet radii versus time for various E85-diesel blends.....84

Figure 26. Droplet surface temperatures versus time for various E85-diesel blends.....84

Figure 27. Temperature inside droplet versus normalised distance from the centre of droplet for E85-5 blend at time instants 0.02, 0.3, 0.5 and 1 ms.....86

Figure 28. Droplet surface temperature versus percentage volume recovered as distillate for E85-5 and pure E85 using the ETC/ED models.....87

Figure 29. Evolution of droplet radii and surface temperatures for E85-5 and E85-20 blends.....88

Figure 30. The plots of surface mass fractions Y_{lis} of 9 representative components of the E85-5 blend versus time. The plots for the following components are shown: $C_{10}H_{22}$ (1), $C_{19}H_{40}$ (2), $C_{27}H_{56}$ (3), $C_{20}H_{40}$ (4), $C_{27}H_{54}$ (5), $C_{12}H_{18}$ (6), $C_{24}H_{42}$ (7), C_8H_{18} (8) and C_2H_5OH (9).....89

Figure 31. Droplet radii versus time for six approximations of E85-5: 119 components using the DMCM, and 90, 63, 45, 20 and 16 C/QC (numbers near the curves) using the MDQDM.....90

Figure 32. Droplet surface temperatures versus time for six approximations of the E85-5 blend: 119 components using the DMCM, and 90, 63, 45, 20, and 16 C/QC (numbers near the curves) using the MDQDM. 90

Figure 33. The evolution of droplet radii for pure diesel (indicated as D100), pure biodiesel (indicated as B100), pure ethanol (indicated as E100), and three different EBD blends. ... 94

Figure 34. The evolution of droplet surface temperatures for the same fuels and their blends as in Figure 40..... 95

Figure 35. The predicted heating value, experimentally measured in [148], for ethanol, biodiesel, diesel, and their blends. The x-axis blend cases are illustrated in Table 20..... 100

Figure 36. Evolution of droplet surface temperatures and radii predicted for the full compositions of diesel fuel (98 components) using DMCM, 6 approximate discrete components using CFSM, and 6 quasi-components using MDQDM. 107

Figure 37. The values of droplet surface temperatures (a) and radii (b) versus ADC and C/QC at time instant 0.5 ms..... 108

Figure 38. The values of droplet surface temperatures (a) and radii (b) versus ADC and C/QC at time instant 1 ms. 109

Figure 39. The values of droplet surface temperatures (a) and radii (b) versus ADC and C/QC at time instant 1.5 ms..... 110

Figure 40. The values of droplet surface temperatures (a) and radii (b) versus ADC and C/QC at time instant 2 ms. 111

Figure 41. Evolutions of droplet surface temperatures and radii for the full compositions of diesel fuel and the 3 surrogates (Sur1, Sur2 and Sur3). 114

Figure 42. Evolutions of droplet radii and surface temperatures for the full compositions of gasoline and its 3 suggested surrogates: Sur4 (derived using the CFSM), Sur5 (inferred from [31]) and Sur6 (inferred from [80]). 117

Figure 43. Evolution of the droplet radii and surface temperatures for the full compositions of E20 and the two surrogates (Sur7 and Sur8). 121

Figure 44. Evolutions of droplet radii and surface temperatures for the full compositions of B10 and a suggested surrogate. The same ambient conditions and model as in the case shown in Figure 41 were used. 125

Figure 45. Flowchart of the new algorithm, where the minimum change in mass fraction ratio $K = 0.1$, reduction factor $F = 0.75$ and the minimum ratio of droplet radii $\varepsilon = 10^{-6}$. 131

Figure 46. Evolutions of droplet radii versus time for 98 components of pure diesel fuel using the DMCM and two approximations of the original MDQDM and MDQDM with the new transient algorithm (indicated as TMDQDM). 133

Figure 47. Evolution of droplet surface temperatures of pure diesel fuel using the DMCM, original MDQDM and the MDQDM with the new transient algorithm (indicated as TMDQDM)..... 134

Figure 48. Evolutions of droplet radii versus time for 119 components for E85-5 (95% diesel and 5% E85) using the DMCM and two approximations of the original MDQDM and MDQDM with the new transient algorithm (indicated as TMDQDM)..... 135

Figure 49. Evolution of droplet surface temperatures versus time for 119 components for E85-5 (95% diesel and 5% E85) using the DMCM, original MDQDM and the MDQDM with the new transient algorithm (indicated as TMDQDM)..... 135

Figure 50. Evolutions of droplet radii versus time for 119 components for E85-20 (80% diesel and 20% E85) using the DMCM and two approximations of the original MDQDM and MDQDM with the new transient algorithm (indicated as TMDQDM)..... 136

Figure 51. Evolution of droplet surface temperatures versus time for 119 components for E85-20 (80% diesel and 20% E85) using the DMCM, original MDQDM and the MDQDM with the new transient algorithm (indicated as TMDQDM)..... 136

Figure 52. Evolutions of droplet radii versus time for 119 components for E85-50 (50% diesel and 50% E85) using the DMCM and two approximations of the original MDQDM and MDQDM with the new transient algorithm (indicated as TMDQDM)..... 137

Figure 53. Evolution of droplet surface temperatures versus time for 119 components for E85-50 (50% diesel and 50% E85) using the DMCM, original MDQDM and the MDQDM with the new transient algorithm (indicated as TMDQDM)..... 137

Figure 54. Evolutions of droplet radii versus time for 21 components for E85 (100% E85) using the DMCM and two approximations of the original MDQDM and MDQDM with the new transient algorithm (indicated as TMDQDM). 138

Figure 55. Evolutions of droplet surface temperature versus time for 21 components for E85 (100% E85) using the DMCM and two approximations of the original MDQDM and MDQDM with the new transient algorithm (indicated as TMDQDM). 138

Figure 56. Droplet radii in μm (a) and surface temperatures in K (b) versus the numbers of C/QC predicted by the TMDQD algorithm (▲), the DMCM (●) and the original MDQDM (■) at time instants (0.3 ms, 0.5 ms, 1 ms, 1.5 ms and 2 ms) for various numbers of C/QC.... 141

Figure 57. CPU time (wide bars) and errors (narrow bars) of various modelling approaches, compared with the prediction of the DMCM for three modelling approaches as error %=100 ×($time_{DMCM}$-$time_{model}$)/$time_{DMCM}$, for E85-5 fuel blend..... 143

Figure 58. The droplet evaporation versus time for kerosene using the DMCM, MDQDM and surrogate (CFSM)..... 147

Figure 59. The can combustor geometry, showing (a) the internal walls of the system, and (b) the polyhedral mesh, used in the CFD simulation. The cell volume range is 0.0057647 – 470 mm^3, the face cell area range is 0.014 – 8 mm^2, and the total number of cells is 262,255. 149

Figure 60. The evolutions of droplet diameter using the three modelling approaches: 1 refers to Standard ANSYS-Fluent results, with constant properties, 2 refers to ANSYS-Fluent results, with in-house properties using UDF, and 3 refers to ANSYS-fluent results incorporating the CFSM using UDF. 150

Figure 61. Profile of droplet diameter starting from the injection until the full evaporation. 151

Figure 62. The validation of the models for the normalised squared droplet diameters predicted by the standard ANSYS-Fluent (solid curve), and ANSYS-Fluent incorporating the CFSM (dotted curve), using data reported in [207] (bold triangles) for kerosene fuel. 152

Figure 63. The species distribution (dimensionless mass fraction), (a) NO_X and (b) CO_2, at the symmetry plane of the combustion chamber using the suggested kerosene surrogate (53.4% iso-decane and 46.6% cyclododecane). Black arrows show the species diffusion from the high concentration content to the lower concentration content. 155

Figure 64. Species formation and distribution across the can combustor at four planes, showing (a) the four planes along the combustor, and (b) the profile contours for the four planes..... 156

Figure 65. The species distribution, (a) NO_X and (b) CO_2, at the symmetry plane of the combustion chamber using ANSYS kerosene surrogate ($C_{12}H_{23}$)..... 157

Figure 66. Ignition time delay of the full composition of kerosene fuel and its surrogates (suggested surrogate and Ansys surrogate) at pressure of 4 bar and equivalence ratio of 1. 160

Figure 67. Ignition time delay of the proposed kerosene surrogate at different equivalence ratios and pressure of 1 bar. 161

Figure 68. Ignition time delay of the proposed kerosene surrogate at different equivalence ratios and pressure of 4 bar. 161

Figure 69. Ignition time delay of the proposed kerosene surrogate at different pressures and equivalence ratio of 0.5. 162

Figure 70. Ignition time delay of the proposed kerosene surrogate at different pressures and equivalence ratio of 1..... 162

Figure 71. Ignition time delay of the proposed kerosene surrogate at different pressures and equivalence ratio of 1.5. 163

List of Tables

Table 1. Van der Waals volumes (R_k) and surface areas (Q_k) for various molecules and atoms. 37

Table 2. The m-group and n-group interaction parameters (a_{mn}) in K, used in the UNIFAC model. 38

Table 3. The approximation of the missing structure groups for the predictions of the ACs. 39

Table 4. The molar composition (%) of gasoline FACE C fuel. 46

Table 5. The impact of ethanol/gasoline fuel blends on estimated droplet lifetimes (in ms); 49

Table 6. The blended fuel droplet lifetimes when the effects of thermal radiation are taken into account and the estimated differences compared with the predictions of the model when radiation is ignored (Table 5). 52

Table 7. The impact of ethanol/gasoline fuel blends on estimated droplet lifetimes (in ms) and surface temperatures (in K) taking into account transient multi-component ACs. 63

Table 8. The estimated errors in prediction of droplet lifetimes (in ms) based on Raoult's law compared to the case where the transient UNIFAC approach is used. 64

Table 9. The estimated errors in prediction of droplet surface temperatures (in K) based on Raoult's law compared to the case where the transient UNIFAC approach is used. 64

Table 10. Molar fraction (%) of diesel fuel components. 67

Table 11. Biodiesel fuel compositions (:0,1,2,3,4 refer to the number of double bonds in the component's structure) [63]. 69

Table 12. Biodiesel fuel compositions (continued). 70

Table 13. Estimation of the droplet lifetimes (in ms) of biodiesel/diesel blends and their differences compared with B0 droplet lifetime (2.25 ms). 73

Table 14. Estimation of biodiesel and biodiesel/diesel fuel droplets lifetimes (in ms) and their differences compared with those of B0 fuel (2.25 ms). 74

Table 15. The blended fuel droplet lifetimes (in ms) under radiative effects and their estimated differences for the case when radiation is ignored. 77

Table 16. The impact of reducing the number of components on CPU time (in sec). 91

Table 17. The volume fractions and parameters of each group of diesel fuel and their predicted CN. 97

Table 18. Predicted CN of biodiesel, diesel, ethanol, and their blends. 98

Table 19. Predicted viscosity (at $T = 40$ °C) of biodiesel, diesel, ethanol, and their blends. 99

Table 20. The cases of EBD blends used in Figure 42. 100

Table 21. Quasi-Components (QC) and Approximate Discrete Components (ADC), representing the groups of species in diesel fuel. 106

Table 22. The molar fractions of the three surrogates (Sur1, Sur2, and Sur3) of diesel fuel. 113

Table 23. The CNs and viscosities (in cP) of diesel fuel and its three surrogates (Sur1, Sur2 and Sur3) 115

Table 24. The molar fractions of the three surrogates (Sur4, Sur5 and Sur6) of gasoline fuel. 116

Table 25. The calculated vapour pressures (in kPa) and densities (in $kg \cdot m^{-3}$) for gasoline fuel and its surrogates (Sur4, Sur5 and Sur6) at 296 K. 118

Table 26. The RONs, H/C ratios and MWs (in $g \cdot mole^{-1}$) of gasoline fuel and its surrogates. 119

Table 27. The RONs and densities (in $kg \cdot m^{-3}$) of ethanol/gasoline fuel blends 120

Table 28. The molar fractions of E20 surrogates (Sur7 and Sur8). 121

Table 29. The RONs, H/C ratios and MWs (in $g \cdot mole^{-1}$) of gasoline fuel and its surrogates. 122

Table 30. The CNs of biodiesel/diesel fuel blends. 123

Table 31. The molar fractions of the B10 surrogate (Sur9). 124

Table 32. Droplet lifetimes (ms) of various E85/diesel blends, predicted using the MDQDM with the new algorithm implemented into it (TMDQD) and the original MDQDM, and the errors of their predictions compared to the predictions using the DMCM. 139

Table 33. CPU time (in sec) required for each blend using two approximations of the TMDQDM and MDQDM and their saved time compared to the DMCM 144

Table 34. Molar fractions of kerosene fuel, inferred from [203,204]. 146

Table 35. The input parameters used for the combustion simulation. 154

Table 36. Thermodynamic characteristics of the combustion process 158

Dissemination of Results

The original results, presented in this work so far, have been reported in some international refereed journals, conference proceedings and other research communications as follows:

Refereed journal articles

1. **Nawar Al-Esawi**, Mansour Al Qubeissi. " A new approach to formulation of complex fuel surrogates." Fuel 283, (2021): 118923.

2. Mansour Al Qubeissi, **Nawar Al-Esawi**, Sergei S. Sazhin. " Auto-selection quasi-components/components in the multi-dimensional quasi-discrete model." Fuel, (2021) (in Press).

3. **Nawar Al-Esawi,** Mansour Al Qubeissi, Reece Whitaker, Sergei S. Sazhin. "Blended E85–Diesel fuel droplet heating and evaporation." Energy & fuels 33 (3), (2019): 2477-2488.

4. **Nawar Al-Esawi,** Mansour Al Qubeissi, Ruslana Kolodnytska. "The impact of biodiesel fuel on ethanol/diesel blends." Energies 12 (9), (2019): 1804.

5. **Nawar Al-Esawi,** Mansour Al Qubeissi, Sergei S. Sazhin, Reece Whitaker. "The impacts of the activity coefficient on heating and evaporation of ethanol/gasoline fuel blends." International Communications in Heat and Mass Transfer 98 (2018): 177-182.

6. Mansour Al Qubeissi, **Nawar Al-Esawi,** Sergei S. Sazhin, Mohammad Ghaleeh. "Ethanol/gasoline droplet heating and evaporation: Effects of fuel blends and ambient conditions." Energy & fuels 32 (6), (2018): 6498-6506.

7. Luke Poulton, Oyuna Rybdylova, IA Zubrilin, SG Matveev, NI Gurakov, Mansour Al Qubeissi, **Nawar Al-Esawi**, Tajwali Khan, Vlad M Gun'ko, Sergei S Sazhin. "Modelling of multi-component kerosene and surrogate fuel droplet heating and evaporation characteristics: A comparative analysis." Fuel 269, (2020): 117115.

Refereed conference papers

8. Mansour Al Qubeissi, Geng Wang, **Nawar Al-Esawi**, Oyuna Rybdylova, Sergei S Sazhin. "The heating, evaporation and combustion of kerosene droplets in a gas-turbine combustor: CFD modelling using the discrete component approach". 16th UK Heat Transfer Conference, 4-6 Sep. 2019, Nottingham, UK.

9. **Nawar Al-Esawi**, Mansour Al Qubeissi, Sergei S. Sazhin. "The impact of fuel blends and ambient conditions on the heating and evaporation of diesel and biodiesel fuel droplets." 16th International Heat Transfer Conference (IHTC16); Begellhouse: Beijing, China, 2018; 6641-6648.

10. Mansour Al Qubeissi, **Nawar Al-Esawi**, Sergei S. Sazhin. "Droplets heating and evaporation: an application to diesel-biodiesel fuel mixtures". Proc. of 28th Liquid Atom. and Sp. Sys. Euro. Conf. (ILASS28). Universitat Politècnica València, Spain, 5-7 Sep 2017. 1060-1067.

11. Mansour Al Qubeissi, Sergei S. Sazhin, Nawar Al-Esawi. "Models for automotive fuel droplets heating and evaporation". Proc. of 28th Liquid Atom. and Sp. Sys. Euro. Conf. (ILASS28). Universitat Politècnica València, Spain, 5-7 Sep 2017. 1044-1051

Book chapter

12. Mansour Al Qubeissi, **Nawar Al-Esawi**, Ruslana Kolodnytska. "Atomization of Bio-Fossil Fuel Blends". In Advances in Biofuels and Bioenergy; Nageswara-Rao, M., Soneji, J. R., Eds.; InTech, 2018.

Abstracts/ research communications

13. **Nawar Al-Esawi**, Mansour Al Qubeissi, Sergei S. Sazhin, Nwabueze Emekwuru, Mike V. Blundell. "Impact of corrected activity coefficient on the estimated droplet heating and evaporation". Proc. of the 11th Int. Conf. Therm. Eng. Theory Appl., Feb.2018, Doha, Qatar.

14. **Nawar Al-Esawi**, Mansour Al Qubeissi. Heating, evaporation and combustion of ethanol-biodiesel-diesel Blends. Faculty of Engineering Research Symposium, 5th June 2019, Coventry University, UK.

15. **Nawar Al-Esawi**, Mansour Al Qubeissi. A new model for the heating and evaporation of blended multi-component fuels, using a transient MDQD approach. UK Fluid Network - Special Interests Group (SIG) 4th meeting, Sprays in Engineering Applications: Modelling and Experimental Studies, 18–19 September 2018, University of Oxford, UK.

16. **Nawar Al-Esawi**, Mansour Al Qubeissi. Automotive fuel droplets. Osborne Reynolds Day Competitions, 3rd September 2018, University of Manchester, UK.

17. **Nawar Al-Esawi**, Mansour Al Qubeissi. Heating and evaporation of bio-fossil fuel blends. Faculty of Engineering Research Symposium, 6th June 2018, Coventry University, UK.

18. **Nawar Al-Esawi**, Mansour Al Qubeissi. MDQD model for E85-diesel fuel mixtures. UK Fluid Network - Special Interests Group (SIG) 3rd meeting, Sprays in Engineering Applications: Modelling and Experimental Studies, 3-4 May 2018, Coventry University, UK.

19. **Nawar Al-Esawi**, Mansour Al Qubeissi. Impact of in-cylinder conditions on fuel droplet heating and evaporation. UK Fluid Network - Special Interests Group (SIG) 2nd meeting, Sprays in Engineering Applications: Modelling and Experimental Studies, 4–5 December 2017, University of Brunel, UK.

20. **Nawar Al-Esawi**, Mansour Al Qubeissi. Biodiesel fuel droplet heating and evaporation. Faculty of Engineering Research Symposium, 29th March 2017, Coventry University, UK.

Candidate declaration	
The candidate herein confirms that he has used 9 of published research outputs and other 2 accepted/submitted research outputs in his thesis. All those publication were made with significant contribution by the candidate, and in collaboration with co-authors. The contrinbution of the candidate is entailed by taking part in conceptualisation, development of the models, formal analysis, writing up, validations, formatting and resources.	
Candidates Signature: Content removed on data protection grounds	**Date: 11/07/2020**

CHAPTER ONE: Introduction

The energy demand is sharply increasing along with the increase in worldwide population and global fossil fuel consumption. This demand is expected to grow at an average annual growth rate of around 1% [1]. Currently, more than 99% of the transport sector is powered by combustion engines, which contribute to around 14% of Greenhouse Gas Emissions (GGE) [1]. Due to the need for reducing GGE, which contribute to global warming, and the depletion of fossil fuels, governments and industries are aiming to shift from the dependency on fossil fuels to renewable energy sources (e.g., biofuels) [2,3]. The use of mixture of biofuels (e.g., biodiesel and ethanol) with fossil fuels in standard propulsion systems can reduce GGE and lead to complete combustion [4].

According to the US environment protection agency, all gasoline engine vehicles can use a blend of gasoline fuel with up to 10% volume fraction of ethanol without the need for engine modification [5]. The reduction in CO_2 emissions without loss of engine performance is noticeable for this mixture [6]. According to the European Renewable Ethanol Association, replacing the European gasoline with a mixture of 10% ethanol and 90% gasoline (known as E10) would reduce the GGE by 6% [7]. Mixtures with up to 15% of ethanol and 85% of gasoline fuel have been approved for use in 2001 and newer vehicles, under the U.S. federal standards for renewable fuel [8]. Unsurprisingly, this increase in the ethanol content in the baseline fuel would reduce the GGE even further. For diesel fuel, it is known that mixtures with up to 85% diesel and 15% ethanol are used in standard diesel engines without significant impacts on these engines [9]. It has been reported in [10] that ethanol can be blended with diesel fuel at up to 20% ethanol in diesel engines. Likewise, the use of such fuel blends in Gas-Turbine Engines (GTE) has also become common nowadays. These blends have indeed been stimulated by the depletion of fossil fuel and most importantly the environmental concerns.

Based on scientific ground of the applicability of bio-fossil fuel blends in conventional gasoline and diesel engines [11], governments set targets for the use of biofuels by increasing their fractions in the baseline fuel (gasoline and diesel). According to the UK Department for Transport, the British Government has legislated a new policy for increasing the percentage of bio/fossil fuel blends from 4.75% in 2018 to 9.75% in 2020 and to 12.4% in 2032 to achieve its obligations regarding reducing the GGE by 6% by the end of 2020 [12]. Recently, the US administration gave approval for the compulsory use of E15 [13].

The feasibility of mixing fuel from different origins (i.e. bio and fossil fuels) starts from their storage to their final ignition and releasing the needed energy. The processes inside the combustion chamber of an Internal Combustion Engine (ICE) are illustrated in Figure 1.

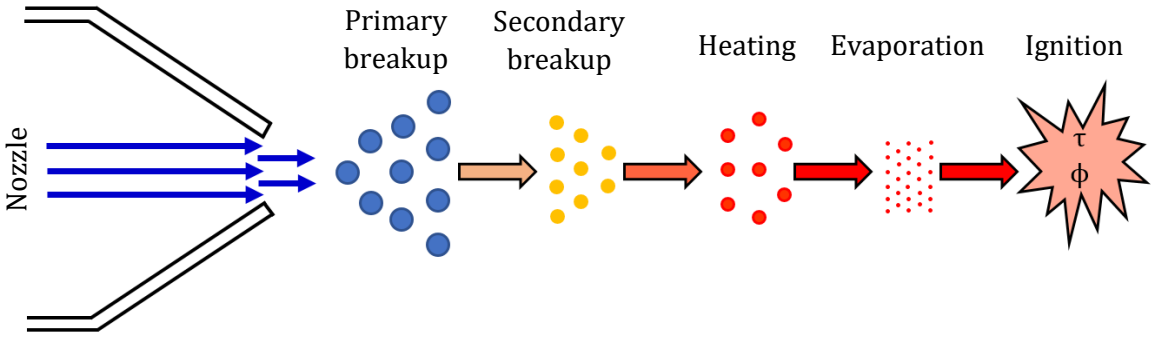

Figure 1. Schematic of injection, breakup, heating, evaporation and ignition processes inside the combustion chamber of an ICE [14].

In typical ICE chamber, the fuel is injected in a high pressure cylinder (up to 1000 bar [15]) in the form of large ligaments which are part of the primary breakup. These ligaments will undergo a secondary breakup to form fuel droplets. These fuel droplets are then heated and evaporated and then a gaseous phase of the fuel vapour and air is formed which is eventually ignited to release the needed energy that drives the ICE. The importance of multi-component fuel droplets heating and evaporation processes has been highlighted in literature [11,16]. These processes precede the onset of ignition, and play an essential role in the performance of engines due to their very short time before the ignition of the air/fuel

mixture [17]. Incomplete combustion and high levels of pollutant are expected when the fuel is not well mixed with air and completely evaporated. As such, understanding these processes is crucial to the design and optimum operation of ICE.

Different models were developed for the simulation of multi-component fuel droplet heating and evaporation [18–21]. In most cases, the modelling of heating and evaporation of multi-component droplets were represented by single components, for instance gasoline was represented by iso-octane [22] and diesel was represented by n-dodecane [23,24]. These approaches were based on two assumptions: 1) the effect of species diffusion inside droplets during the evaporation process and 2) the effect of finite thermal conductivity with droplets could be ignored. Most of these studies (e.g. [25,26]) relied on these assumptions to reduce the model complexity and the computational cost (CPU time).

The importance of considering the effect of species diffusion inside droplets and finite thermal conductivity was highlighted in many studies and they were modelled using the Effective Thermal Conductivity/Effective Diffusivity (ETC/ED) models [27–29]. The importance of the latter models was represented by the fact that they took into account the recirculation, temperature gradient and species diffusion inside droplets. Recent models were developed to take into account ETC/ED models including the Discrete Multi-Component Model (DMCM), Quasi-Discrete Model (QDM) and Multi-Dimensional Quasi-Discrete Model (MDQDM).

The combustion studies were always based on the approximation of the composition of a fuel by certain number of components to match the real combustion characteristics of the fuel [30,31]. These approximations, commonly known as fuel surrogates, were mainly used due to the unavailability of the chemical mechanisms of many components and the lack of the computational resources. Although fuel surrogates were good representatives of the real fuel composition in terms of their chemical behaviour, these surrogates might not be able to match the physical characteristics of that fuel.

Like the reciprocating engines, in GTE the understanding of the evaporation and combustion processes of liquid fuels involving hundreds of components is crucial for the improvements of these engines. The surrogates' formulation of those fuels for GTE can also be a substantial step in the accurate modelling of the heating and evaporation processes in some GTE with less computational time.

1.1. Motivation

There are several gaps in the current state of fuel droplet heating and evaporation research and formulation of fuel surrogates, which are outlined below. These form the main basis for the motivation in this research:

- There are limited attempts to cover a broad range of biofuel/diesel fuel blends (including, biodiesel/diesel, E85-diesel (E85 refers to 85% vol. ethanol and 15% vol. gasoline) and ethanol/biodiesel/diesel) heating and evaporation.
- The impact of ethanol/gasoline fuel blends has only been investigated in the literature by approximating the full composition of gasoline with iso-octane.
- The non-ideal vapour-liquid equilibrium has not been considered for the multi-component heating and evaporation.
- The selection of quasi-components in the recently suggested MDQDM has been based on trial and error, and on the initial fuel fraction (not transient); hence, the model is not applicable for implementation into CFD software for real engineering applications.
- The previous studies have been mainly focussed on the formulation of chemical surrogates to match the combustion characteristics of the full fuel compositions. There have not been any attempts to formulate fuel surrogates that can match both the chemical and physical characteristics of such a broad range of fuels and their blends.
- There has not been a study that considered the implementation of heating and evaporation models into CFD codes for the modelling of GTE combustion system.

1.2. Aim and Objectives

The aim of this study is to provide an accurate and CPU efficient approach for the modelling of major processes preceding the onset of combustion (fuel droplet heating and evaporation), with an application to the blends of multi-component bio-fossil fuel droplets. Additionally, a new approach is introduced for the formulation of fuel surrogates to capture the major physical and chemical fuel characteristics. The models are applied in conditions relevant to direct injection internal combustion and GTE.

The following objectives were set as milestones and conducted to achieve the project aim:

- To understand the underlying physics related to automotive fuel droplet heating and evaporation, and chemistry of fuel ignition.
- To calculate the detailed thermodynamic and transport properties of all types of fuels covered in this work, including their mixtures.
- To further develop the multi-component modelling approach for the heating and evaporation of different fuels and their blends.
- To formulate suitable fuel surrogates that can match both the physical and chemical behaviour of blended fuels.
- To implement the models into a commercial CFD code for a broad range of combustion applications. A proof of concept is presented in application to a GTE combustion system.

1.3. Thesis Structure

The thesis is structured in the following frame of chapters and topics:

- In Chapter 2, a comprehensive literature review for the recent models for the simulation of fuel droplet heating and evaporation, and for the formulation of fuel surrogates is offered.

- In Chapter 3, the basic equations and mathematical expressions for the prediction of fuel droplet heating and evaporation, and vapour liquid equilibrium are illustrated.
- In Chapter 4, the DMCM, taking into account the Universal Quasi-Chemical Functional–group Activity Coefficient (UNIFAC) model, is applied for the predictions of ethanol/gasoline fuel droplet heating and evaporation.
- In Chapter 5, the DMCM and MDQDM are applied for the analysis of biodiesel/diesel blends, E85-diesel blends and ethanol/biodiesel/diesel fuel blends.
- In Chapter 6, a new suggested Complex Fuel Surrogate Model (CFSM) is used for the formulation of fuel surrogates for a broad range of automotive fuels.
- In Chapter 7, a new ''Transient MDQDM'' is suggested and tested for the predictions of blended fuel droplet heating and evaporation.
- In Chapter 8, the developed model in Chapter 6 is used for the formulation of kerosene surrogates and then implemented into ANSYS-Fluent, via the user-defined function, for the simulation of heating, evaporation and combustion of kerosene fuel in a GTE.
- In Chapter 9, the main key findings of the thesis are summarised and recommendations for future work are highlighted.

CHAPTER TWO: Literature Review

2.1. Overview

The physical delay of fuel combustion due to droplets heating and evaporation processes is crucial for the performance of Internal Combustion Engines (ICE) and Gas-Turbine Engines (GTE). The understanding of these processes is essential to the design and enhancement of ICE. The heating and evaporation, as dominant processes to proceed combustion, are complex processes due to the intervention of hundreds of chemical components in them. Measurements related to these processes are commonly expensive, time consuming, and not always available.

Also, the numerical simulation of such large numbers of components, including their detailed thermodynamic and transport properties, is computationally expensive. Instead, analytical modelling provides an alternative approach to fully understand these processes. As such, the recent analytical studies about fuel droplets heating and evaporation are summarised to identify the research gaps, challenges and rooms for improvement. The major combustion characteristics and research findings for fuels used in automotive engineering, including gasoline, diesel, ethanol, biodiesel and their blends and their formulated surrogates, are reviewed.

2.2. Infinite Diffusivity/Infinite Thermal Conductivity Based Models

In previous studies, two approaches were used for the modelling of multi-component automotive fuel droplet heating and evaporation. These approaches were based on the analysis of approximating large number of components, such as the distillation curve model [18,19] and the continuous thermodynamics model [20,21]. These approaches relied on crude assumptions for modelling automotive fuel droplets; for example, species inside droplets were assumed to either mix infinitely quickly (leading to Infinite

Diffusivity/Infinite Thermal Conductivity (ID/ITC) models), or do not mix at all (leading to Single Component Model (SCM)).

The ID/ITC approaches are widely used in research and Computational Fluid Dynamics (CFD) codes, despite their simplicity. Different findings were relied on these approaches. The continuous thermodynamics approach was utilised in [32] to model the multi-component diesel fuel and compared to the SCM. Shorter evaporation time was predicted by the multi-component model than that of SCM. This was due to the early evaporation of lighter components, while the single component model might be represented by a heavy component which took more time to evaporate.

The influence of ambient temperature on the evaporation time of normal decane was predicted in [33] using the Diffusion Limit Model (DLM) and the Rapid Mixing Model (RMM). Compared to the DLM, it was observed in this study that the RMM underpredicted the droplet temperature and resulted in a slightly faster droplet heating. Results also showed that the evaporation time decreased as a result of increasing the ambient temperature. In addition, the impact of ambient pressure on the evaporation time of a mixture of normal heptane and decane was investigated. Predictions showed that increasing the ambient pressure from 1 bar to 8 bar led to a significant increase in the evaporation time.

The impact of ambient temperatures on the evaluation of droplet lifetime was also studied in [34]. In this study, the droplet was represented by n-heptane. Similar behaviour to [33] was obtained where the evaporation rate increased with increasing the ambient gas temperature. The impact of ambient pressure on normal heptane and decane droplet lifetime was investigated in [35] using three dimensional numerical simulation. The ambient pressure was in the range of 0.1-0.2 MPa. Numerical simulation showed that, at low gas temperature, droplet lifetimes for both components increased with increasing the ambient pressure. However, they decreased with increasing the ambient pressure at high gas temperature.

The continuous thermodynamic evaporation model was facilitated in [25] to analyse the evaporation of biodiesel fuel droplet. Predictions showed that the difference in the evaporation time of both the saturated and unsaturated Fatty Acid Methyl Ester (FAME) groups was negligible. The evaporation of biodiesel fuel droplet, represented by Rapeseed and Soybean methyl ester separately, was investigated in [36] using the ITC model. The ambient pressure was 1 bar and the ambient temperature was in the range of 550-1050 K. The numerical work showed that the droplet lifetime decreased with increasing the ambient temperature for both types of biodiesel fuels. Good agreement was observed by comparing the numerical predictions with the experimental work provided in [37].

The evaporation process of normal decane, two components surrogate (normal decane and trimethyl-benzene) and three components surrogate (normal dodecane, iso-octane and toluene) was investigated in [38], assuming uniform temperature and composition inside droplets . The evaporation rate of the three components surrogate was noticed to be faster in the initial period and slower in the subsequent period than those of n-dodecane and two components surrogate. This was attributed to the fact that iso-octane and toluene in the three components surrogate had higher volatilities, while dodecane had lower volatility.

Numerical study was performed in [39] to study the evaporation of ethanol/iso-octane droplet using ANSYS-Fluent. The Universal Functional Activity Coefficient (UNIFAC) model was used to address the non-ideal equilibrium behaviour. The temperature was found to be the most effective parameter in evaporation time. The evaporation rate was found to be faster with increasing the ambient temperature. The impact of UNIFAC model on the predictions of ethanol/iso-octane was also investigated in [40]. Significant difference in the evaporation rate was observed as a result of considering the non-ideal vapour-liquid equilibrium compared to the case where vapour-liquid equilibrium was treated as ideal.

The impact of non-ideal vapour-liquid equilibrium on the evaporation of ethanol/iso-octane droplets was investigated in [41]. The non-random two liquids (NRTL) model was used to

describe the non-ideal equilibrium behaviour. Significant drop in the evaporation rate was observed when the non-ideal behaviour was accounted for. However, the droplet temperature was significantly decreased especially when the ethanol fraction increased. Different predictions were observed at low ambient temperature. The evaporation time was seen to be decreased when the non-ideal behaviour was considered. At high ambient temperature, the impact of the non-ideal behaviour led to small difference in the evaporation time compared to the case when the non-ideal behaviour was ignored. The non-ideal behaviour of vapour-liquid equilibrium in ethanol/gasoline fuel blends was investigated in [42] by adapting the UNIFAC model. Consistent evaporation rate was predicted by the numerical model due to the incorporation of the non-ideal behaviour compared to the case when it was ignored.

The modelling of ethanol/gasoline fuel droplet evaporation was presented in [43]. The evaporation model was developed using real solvent approach based on COSMO-RS theory. In this study, the gasoline was approximated by 15 components. The evaporation time was decreased with increasing the ethanol fraction. The evaporation of ethanol/iso-octane was investigated numerically and experimentally in [44]. The non-random two liquids (NRTL) model was used to describe the non-ideal equilibrium behaviour. It was found that the evaporation rate decreased with increase the ethanol fraction. Hybrid multi-component evaporation model was formulated and tested for multi-component fuel evaporation based on reduced number of components [45]. This model was based on the assumption that composition distribution inside the droplet was uniform. The developed model improved the computational efficiency compared to the case when the full number of components was considered.

All the results discussed in this section so far relied on the ID/ITC models. The limitations of these models are well known and defined in [28]. In these models, the following balanced energy equation is used to model the droplet heating:

$$C_{pl} m_d \frac{dT}{dt} = 2\pi \mathrm{Nu} k_g R_d (T_g - T_s) + L\dot{m}_d + q_{\mathrm{int}} \quad (1)$$

where, C_{pl} is the specific heat capacity of liquid, m_d and R_d are the mass and radius of the droplet, respectively, Nu is the Nusselt number, k_g is the thermal conductivity of gas, T_g and T_s are gas and surface temperatures, respectively, L is the latent heat of evaporation, and q_{int} is the heat supplied.

The assumption of effects of temperature gradients inside droplets can be ignored was the main support of the derivation of equation 1 [46–56]. This assumption was supported by the fact that the thermal conductivity of gas is much lower than that of liquid [57]. That means the ratio of the heat transfer coefficient of the gas phase and the conductivity of liquid (i.e. Biot number) is very small (<0.1). In some studies, Lewis number becomes relevant in the case of multi-components evaporation due to the significant differences in thermal conductivities and diffusion coefficients of components involved in the fuel mixture. However, a comparison of the liquid and gas thermal diffusivities should be performed and used as a base for the aforesaid assumption when modelling transient processes. In most engineering applications, the thermal diffusivity of gas is much higher than that of liquid. Equation 1, therefore, cannot be used for the modelling of transient heating process [57]. Moreover, the rapid evaporation of light components at the surface of the droplet leads to a high gradient of component mass fractions inside the droplet which is another important factor that also needs to be considered.

In response to the importance of considering the thermal diffusivity, the impacts of temperature gradient, species diffusion and recirculation inside droplet are taken into account through: 1) the analytical solution to the transient heat conduction and mass transfer equations assuming that all the processes inside the droplet are spherically symmetric [27,28]; or 2) the numerical solution to the energy equation. The models that account for the temperature gradient, species diffusion and recirculation inside droplet are

referred as Effective Thermal Conductivity/Effective Diffusivity (ETC/ED) models. A typical distribution of temperature inside a moving droplet taking into account the ETC model is shown in Figure 2 [11].

Based on the solutions of the heat and mass transfer equations and by taking into account the ETC/ED models, several models have been developed during the last 15 years [58–60]. These models have been facilitated for the analysis of droplet heating and evaporation of gasoline, diesel and biodiesel.

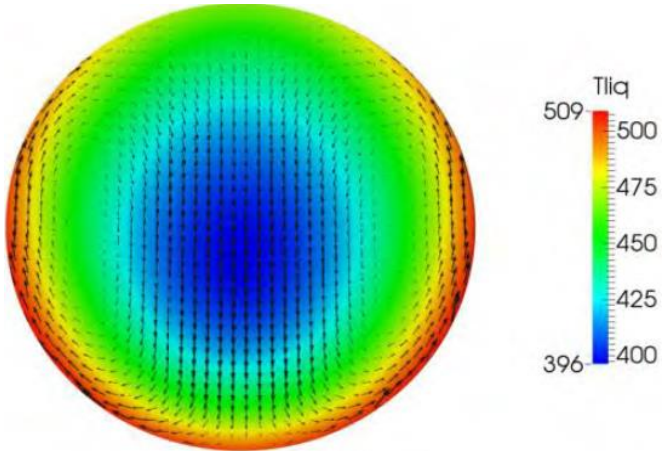

(a)

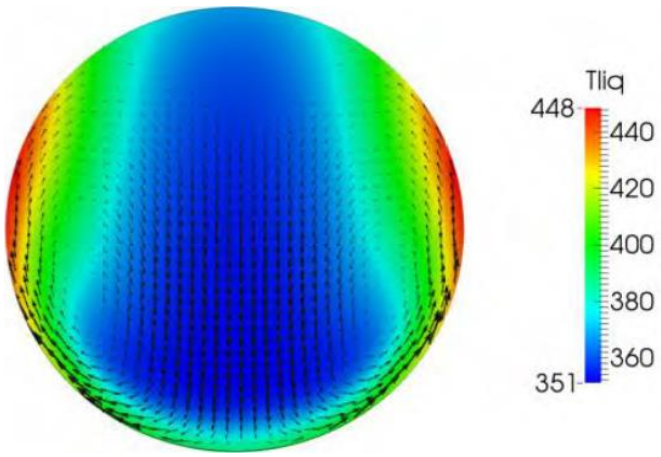

(b)

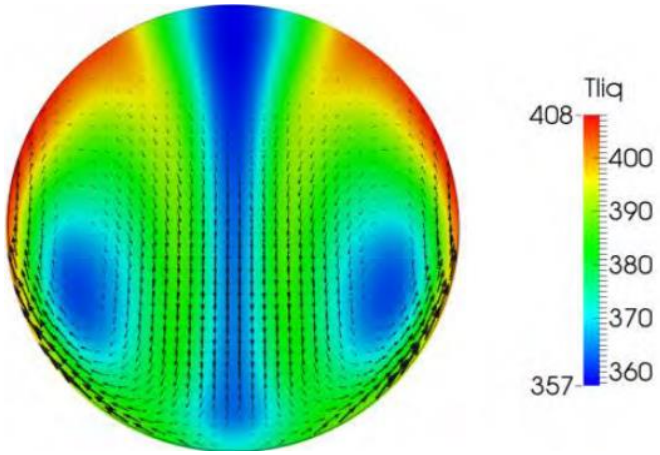

(c)

Figure 2. The effect of internal recirculation on temperature distribution inside a droplet moving with relative velocities (a) 0.2 m.s^{-1}, (b) 1 m.s^{-1} and (c) 3 m.s^{-1} [11].

2.3. Discrete Multi-Component Model

This approach (Discrete Multi-Component Model (DMCM)) was based on the consideration of all components of fuel without any approximation using the ETC/ED models. It was based, in most cases reviewed in this section unless otherwise stated, on the analytical solutions to the heat and mass transfer equations as will be discussed in Chapter 3. It was originally suggested in [27] for the heating of non-evaporating droplets and then generalised for evaporating droplets. It was used for the simulation of 2 components and up to 105 components. This model was used extensively for the modelling of droplet heating and evaporation.

One of the early developments of the DMCM was introduced in [61] to model the evaporation process of gasoline and diesel fuel. The work was based on an approximate solution to the quasi-steady energy equation accounting for the ETC/ED models. The authors of [61] observed a significant difference between the predictions of their suggested model and those obtained from the SCM. Also, a significant difference in the predicted droplet lifetime was noticed between the case of considering the ETC model and the case of ignoring it. The evaporation process of biodiesel/diesel fuel blends was investigated numerically in [26] using the DMCM . In this study, the model was based on the numerical

solutions of the heat and mass transfer equations rather than the analytical solution. Predictions showed that the fuel blending ratio had a significant impact of the droplet lifetime. The evaporation time and droplet surface temperature tended to increase with increasing the biodiesel fraction in the fuel at certain ambient conditions and droplet sizes. The impact of the ambient temperature was also highlighted in this study. Droplet lifetime was observed to be decreasing with increasing the ambient temperature for all fuel fractions.

In [62], four types of biodiesel fuel combined of methyl ester groups had been analysed by means of heating and evaporation processes. These were Rapeseed, Soybean, Hemp oil and Palm. Different models were used in this study and compared to identify the deviation in droplet lifetimes and surface temperatures. It was found that the approximation of biodiesel fuel by single component led to 2.4% deviation in droplet surface temperature compared to the DMCM. Four biodiesel fuel types were analysed in [58] using the DMCM . These biodiesel fuels were combined of methyl ester groups which were: Palm, Rapeseed, Hemp-oil and Soybean having 15 different methyl esters. It was found through this study that the approximation of biodiesel fuel by single component gave 5.5% underprediction in droplet lifetime as compared to multi-components. This difference was seen rather close for all types of biodiesel.

Heating and evaporation of a broad range of biodiesel fuels were investigated in [63]. Several types of biodiesel fuel (up to 19) combined of methyl ester groups were analysed. These were Lard, Tallow, Butter, Palm, Palm Kernel, Waste cooking-oil, Cottonseed, Peanut, Corn, Tung, Sunflower, Hemp-oil 1, produced from Hemp seed oil in Ukraine, Linseed, Hemp-oil 2, produced in European Union, Canola, Safflower, Soybean, Coconut and Rapeseed. Several models were used in this study. The first model was the DMCM which took into account the contribution of all the methyl ester groups in the biodiesel fuels, recirculation, species diffusion and temperature gradient inside droplet (i.e. ED/ETC

model). The second approach was the DMCM which also took into account the contribution of all the methyl ester groups in the biodiesel fuels, however, the thermal conductivity and diffusivity were assumed infinitely large (i.e. ID/ITC model). The last model was similar to the first model, but the fuel was approximated by a single component. The single component model predicted up to 5.5% and 2.4% deviation in droplet lifetime and surface temperature, respectively, compared to the DMCM.

Heating and evaporation of these types of fuels were also analysed in [64]. The study was performed to analyse the blend of standard diesel fuel and waste cooking oil (WCO). The DMCM was used to investigate the effect of fuel compositions on the droplet lifetime. It was found that increasing the fraction of biodiesel from pure diesel (B0) to pure WCO biodiesel (B100) had a noticeable impact on droplet lifetime. For B100, the predicted droplet lifetime was roughly 11% less than that of B0.

Hybrid approach was suggested in [65] to simulate the evaporation of diesel/biodiesel fuel blend, where the biodiesel fuel was represented by soybean methyl ester. This approach included the DMCM for biodiesel fuel and the continuous thermodynamic model for diesel fuel. It was found that the evaporation time increased with increasing the biodiesel fraction. This increase in droplet lifetime was due to the low volatility associated with biodiesel fuel. The same approach was used in the same study to analyse the ethanol/gasoline fuel droplet heating and evaporation. Different fractions of this type of blend were analysed. It was highlighted that increasing the ethanol fraction led to increasing in droplet lifetime. This was due to the higher latent heat of vaporisation associated with ethanol.

Droplets heating and evaporation of FACE A gasoline fuel were investigated in [30], using the DMCM described in [61]. According to the US department of energy, the term FACE is defined as fuels for advanced combustion engines, while A refers to paraffin-rich gasoline fuel. As mentioned in [30], FACE A gasoline fuel consisted of n-paraffins, iso-paraffins, aromatics, naphthenes and olefins with compositions of 10.57%, 68.12%, 0.37%, 2.49% and

0.45% respectively. Firstly, three surrogates were analysed based on their ability to match the ignition time delay, the research octane number or the hydrogen to carbon ratio. These surrogates, however, could not accurately predict the evolution of droplet surface temperature and radii. Therefore, new surrogates were suggested after reducing the Sixty-six components of this fuel to 19 components. Different surrogates were analysed and compared with the reduced FACE A gasoline fuel (19 components). It was found that one of these suggested surrogates gave the best prediction as compared with FACE A, where the error in the time evolution of surface temperature and droplet lifetime was up to 0.25% and 5% respectively.

FACE I gasoline fuel droplet heating and evaporation was investigated in [66] using the DMCM . Five surrogates were formed and compared to FACE I gasoline in this study. FACE I gasoline consisted of 33 hydrocarbon components and it had intermediate octane number which was around 70. Among the five suggested surrogates, one of them, which had eight components, gave closer predictions to those obtained by full compositions of FACE I gasoline fuel (i.e. less deviation in droplet lifetime and surface temperature).

New discrete model was suggested in [59] for the modelling of droplet heating and evaporation. This model was referred as the quasi-dimensional multi-component model. In contrast to the DMCM used in [16,27], this model was based on the polynomial approximations of the temperature gradient and mass fractions distributions of species inside droplets rather than the analytical solution to the heat and mass transfer equations inside droplets. In [59], the authors believed that the predictions of their model were a reasonable compromise between the analytical solutions of the DMCM and the simplified model in which temperature gradient and mass fractions distributions of species inside droplets were ignored.

The authors of [67] presented an evaporation model for aviation kerosene and butanol blend. In their study, the non-ideal behaviour of the mixture and impact of recirculation

inside the droplet were considered through the activity coefficient. It was found that the droplet lifetime increased with increasing the butanol content. Additionally, it was observed that the evaporation rate was impacted significantly by the convection velocity due to the increase in Sherwood number and Reynolds number.

2.4. Quasi-Component Models

The DMCM, reviewed in Section 2.3, was generally applicable to cases of relatively small number of components. The application of this model to real fuel composition (where the number of components exceeds several dozens) make it computationally expensive. To address this issue, the Quasi-Discrete Model (QDM) was suggested in [68]. This model was based on the assumption that the components with close carbon numbers could be replaced with representative components called Quasi-Components (QC) having non-integer carbon number.

The QDM was tested for the predictions of diesel fuel droplet heating and evaporation in [68]. In this study, the diesel fuel was approximated by 20 and 5 quasi normal alkane components. Predictions showed that droplet radii and surface temperatures were almost the same for both 20 and 5 QC and closer to the diesel fuel than the single component approach did. The model that was suggested in [68] was further developed in [69] by taking into account the dependency of viscosity, density, thermal conductivity and heat capacity of liquid components on temperature and carbon number rather than approximated all the previously mentioned properties of 20 QC by n-dodecane. The new model predicted 10% longer droplet lifetimes than that where all the liquid properties were approximated by n-dodecane. In the latter study, the QDM was also used for the investigation of the evaporation characteristics of gasoline fuel droplets. The model was based on the replacement of the actual number of components in gasoline fuel by certain QC. The gasoline fuel was approximated by 13, 3 and 1 QC. Results showed that the droplet lifetime for the 13 QC was

two times higher than that of SCM when the ambient temperature and pressure were relatively low, 450 K and 3 bar, respectively.

The effect of fuel approximations on gasoline fuel droplets heating and evaporation was investigated in [70] using the QDM. Different gasoline fuel approximations were formed. These approximations consisted of three normal alkanes: Surrogate I (C_6H_{14}, $C_{10}H_{22}$ and $C_{14}H_{30}$ with compositions of 83%, 15.6% and 1.4% respectively) and Surrogate II (C_7H_{16}, $C_{11}H_{24}$ and $C_{15}H_{32}$ with compositions of 83%, 15.6 and 1.4% respectively). Also, another two surrogates were proposed, these consisted of not only normal alkane but iso-alkane and aromatic components, Surrogate A (n-C_7H_{16}, iso-C_8H_{18} and C_7H_8 with compositions of 56%, 28% and 17% respectively) and Surrogate B (n-C_7H_{16}, iso-C_8H_{18} and C_7H_8 with compositions of 63%, 20% and 17% respectively). The predicted results were compared with those predicted in [69], where the gasoline fuel was approximated by 13, 3 and 1 QC. It was illustrated that Surrogate II gave better predictions than the other three surrogates (Surrogate I, Surrogate A and Surrogate B) compared to the approximation of 13 QC using the QDM by means of less deviation in droplet lifetimes and surface temperatures.

The importance and efficiency of the QDM was clearly demonstrated in [68–70]. This model, however, turned out to have some significant limitations. The obvious one was that the model was based on the approximation of diesel and gasoline fuels by the n-alkanes hydrocarbon group only. These two fuels, however, had more than six hydrocarbon groups and n-alkanes group represents only 40% of the total fractions of these fuels [60,71]. Therefore, the QDM was generalised to take into account the contribution of all hydrocarbon groups in diesel and gasoline via a new suggested model called the Multi-Dimensional Quasi-Discrete Model (MDQDM) [60].

The MDQDM was tested for the analysis of diesel fuel droplet heating and evaporation [60]. The diesel fuel, used in this study, matched the standard European Union diesel fuel (EN590). N-alkanes and iso-alkanes groups were considered separately in contrast to [68]

where they are taken into account as one group of alkanes. The actual components of diesel fuel were replaced by 15 QC. Results showed that this reduction in the number of components of diesel fuel led to 1.6% and 2.5% difference in droplet surface temperatures and lifetimes, respectively. However, the CPU time was noticed to be 6 times less than that required when all the diesel components were taken into account, and that made this approach computationally efficient.

In [72], the diesel fuel was approximated by 20 normal alkane components and single component (n-dodecane). In this study, the DMCM was used to investigate the heating and evaporation of this fuel and compared to the case where all the components in diesel fuel were considered. Results showed that droplet lifetimes deviated by 22% for the case of 20 alkane components and 50% for the case of single component. However, the deviation did not exceed 3% when diesel fuel was replaced by 15 QC, which represent all the hydrocarbon groups in diesel fuel rather than considering the normal alkane group only.

The MDQDM was used for the modelling of heating and evaporation processes of FACE C gasoline fuel droplets [71]. The authors were able to reduce the number of components from 83 to 20 components. This was done by grouping the same components (components having the same carbon number, see [71]) and replace them by one component. It was highlighted in this study that replacing the actual number of gasoline components by 6 QC resulted in errors in the estimated evaporation times and droplet surface temperatures of approximately 6.6% and 0.9% respectively. The main advantage of this model was that the CPU time was reduced by 70 % when the 6 QC scenario was compared to the case of 20 gasoline fuel components.

A recent study was conducted in [73] to analyse the heating and evaporation of blended biodiesel/diesel fuel droplet using the MDQDM. In this study, the biodiesel fuel was represented by the widely used biodiesel fuel 'soybean methyl ester (SME)'. Different biodiesel/diesel fuel compositions were used. It was found that using a blend of 95% diesel

and 5% biodiesel fuels with the approximation of this blend by 17 C/QC led to 9% underpredictions in droplet lifetime and up to 4% in the case of 50% diesel and 50% biodiesel as compared to the DMCM when 105 components were considered (98 components of diesel and 7 components of SME fuel).

The limitation of the MDQDM is the generation of components with non-integer carbon numbers (i.e. QC). These QC cannot be used for the prediction of reaction pathways and combustion simulations. The approximations of MDQDM, however, can still be useful for reducing the large numbers of components to much smaller ones. In order to utilise this benefit for the combustion applications, the formulation of surrogates will be investigated.

2.5. Formulation of Fuel Surrogates

Commercial fuels are complex mixtures of many hydrocarbon components [74,75]. Due to the lack of chemical data and complexities in the combustions processes (including heating, evaporation and ignition) of these fuels, surrogate fuels are used to match the physical and chemical behaviour of such fuels. In fact, surrogate fuels are usually including one, bi, or multi components which are much less than the actual number of components in a commercial fuel such as gasoline and diesel. A wide range of fuel surrogates have been formulated to emulate either the physical or chemical behaviour of the full composition of the real fuel using small number of components [31,66,76–84].

Due not only to the lack of chemical complexities in the combustions processes, but also the limitations of the computational resources, studies started by approximating the fuel by single component, where diesel and gasoline were represented by n-dodecane and iso-octane, respectively [22,23,85,86]. However, as the chemical mechanism became available for a wide range of components and the increase in the computational efficiency, researchers started to approximate the fuel by a certain number of components blended together to mimic any desirable characteristic of a certain fuel. Some surrogates were

generated to match the chemical properties such as ignition time delay, H/C ratio and Research Octane Number (RON), while others were generated to match the physical properties such as droplet lifetime and surface temperature, distillation curve, density and molecular weight (MW). Therefore, there have been two directions for the models developed for the formulation of fuel surrogates.

A new gasoline surrogate was proposed in [87] to analysis the gasoline fuel droplet heating and evaporation using the batch distillation approach. The surrogate approximation was composed of iso-C5, n-C7, toluene, iso-C8, n-propyl cyclohexane and iso-C11. Good agreement with experimental data was obtained with up to 3% deviation. This deviation, where the gasoline evaporated faster that the formed surrogate, was due to the more volatile components in gasoline fuel compared to the new surrogate. A new computational methodology of different software tools was proposed in [80] to generate surrogates for gasoline FACE A and C. The methodology combined the detailed hydrocarbon analysis for the selection of species types, the NIST Reference Fluid Thermodynamic and Transport Properties Database and MATLAB code for the predictions of distillation curve and physical properties and CHEMKIN for the predictions of RON via the ignition time delay. Predictions revealed that the generated surrogates, using the proposed computational methodology, gave a very good agreement compared to the full compositions of the fuel. The distillation curve model was used in [82] to generate surrogates for gasoline fuel. In this study, it was found that the specific generated surrogate cannot match two properties. In other words, there should be two surrogates to match the vapour pressure and the distillation profiles by each individual surrogate.

A decoupling approach for detailed and simplified oxidation mechanisms was suggested in [88] to reproduce the heat release, ignition time delay, flame propagation and other combustion characteristics using small number components. In that approach, detailed mechanisms were considered for Hydrogen (H_2), Carbon monoxide (CO) and methane (C_1),

while simplified oxidation mechanisms were used for C_2-C_n. The decoupling approach was used to generate a simplified oxidation mechanism for a surrogate of n-decane, iso-octane, toluene, and methyl-cyclohexane. The decoupling approach was motivated by: 1) the predictions of flame propagation and extinction characteristics were dominated by small radical and molecular species even when considering fuels with large hydrocarbon chains and this had been proven in [89–91], 2) the heat release during the combustion of any fuel mainly originated from the conversion of CO to carbon dioxide (CO_2) as have been investigated in [92], therefore, it was important to approximate the oxidation of CO in details as the heat release has significant impact on the performance of the ICE and emissions, and 3) the ignition time delay of large hydrocarbons can be accurately predicted using a very simplified oxidation mechanisms of C_4-C_n, which was also proven previously in [93]. The final generated mechanisms involved 70 species and 220 reactions. The predictions of the heat release, ignition time delay, flame propagation and extinction using the suggested simplified chemical oxidation mechanism for the surrogate were compared to experimental data. Results showed that all the modelled characteristics were in good agreement with those obtained from the experimental measurements. This agreement confirmed the assumptions of ignoring the detailed oxidation mechanism of C_2-C_n.

A model, widely known as the Physical Surrogate Group Chemistry Representation approach, was developed in [94] to model the combustion processes of multi-component fuel. The developed model combined physical multi-component model and the reduced chemical mechanism model. The combination of these two models were performed to match the physical and chemical characteristics of surrogate fuels. In this study, detailed chemical mechanisms were used for components with available chemical pathways, and generic chemical mechanisms were used for components with unavailable chemical pathways. Findings showed that the developed model matched the combustion behaviour

of the multi-component fuels and improved the computational efficiency using the reduced mechanisms of the physical surrogates.

New approaches, based on chemical functional hydrocarbon groups, were suggested recently. In [95] an approach was suggested to generate fuel surrogates based on the molecular structure. The approach was applied for biodiesel and jet fuels. For jet fuel, the functional groups were CH_3, CH_2, CH, C and phenyl, while for biodiesel fuel, they were CH_3, CH_2, CH_2=CH=CH, and COO-CH_3. It was observed that the generated hydrocarbon and oxygenated surrogates were able to match the combustion characteristics of real fuels. A minimalist functional group approach was suggested in [96] for the formulation of gasoline FACE A, C, F, G and I surrogates. The approach was based on the different functional group which were: paraffinic Ch_3, CH_2 and CH, naphthenic CH-CH_2, and aromatic C-CH groups. The model was able to generate surrogates with fewer components to reduce the computational expenses and the complexity of chemical kinetics without noticeable losing to the accuracy.

In [97], a framework was developed to reduce the hundreds of species and their thousands of reactions of kerosene fuel. The considered kerosene consisted of n-dodecane, methylcyclohexane and m-xylene. The target was to match the laminar flame speed and the ignition strain rate using two sets of surrogates, one with 42 species and the other with 17 species. Results revealed that both the premixed and non-premixed structures of the flame were well predicted using the reduced surrogates. Compared to the original fuel, it was found that the reduced mechanism saved up to 19 times of the computational time.

An aviation kerosene surrogate of two components was generated by targeting the ignition time delay [98]. The formulated surrogate included 8% n-propylbenzene and 92% n-decane on molar basis, with a detailed mechanism of 308 species and 1865 reactions. The latter mechanism was simplified to 45 species and 151 reactions. Through the numerical simulation using CHEMKIN tool, results showed that there was a good agreement in the

ignition time delay and flame propagation predicted by the simplified mechanism and those computed using the detailed mechanism.

A recent study by Liu et al. [99] developed a new surrogate for RP-3 kerosene fuel targeting the average molar weight, low heating value, hydrogen/carbon ratio, cetane number, density and viscosity. The developed surrogate was composed of 14 mol.% n-decane, 10 mol.% n-dodecane, 30 mol.% iso-cetane, 36 mol.% methylcyclohexane and 10 mol.% toluene. The six targeted properties predicted by the developed surrogate were compared to those predicted using the original RP-3 fuel which showed excellent agreement. Moreover, the predicted laminar combustion velocities and the ignition time delays of the surrogate were compared to those of the original RP-3 fuel experimentally which also showed a good agreement.

2.6. Summary of Chapter 2

Despite the recent progress in the development of rigorous models for the predictions of droplet heating and evaporation, the simplified models, assuming no gradients of species fraction and temperature inside droplet, are still widely used for modelling these processes, including those in most of CFD codes. In fact, much simpler model based on the assumption that the droplet temperature is constant over time is still used by some authors for the modelling of droplet evaporation. The latter assumption leads to the commonly known d^2 model.

In response to that, a number of models have been developed based on the analytical solutions to the heat and mass transfer equations. These models are the DMCM, QDM and MDQDM. The importance of these models is attributed to the fact that they take into account the recirculation, temperature gradient and species diffusion inside droplets via the ETC/ED models. Noticeable progress was made to reduce the computational time without losing the accuracy. This was achieved through the development of the MDQDM by reducing

the number of fuel components to much less number of representative components called QC. However, there is still no rigorous algorithm for the reduction in the number of components in each chemical functional group in the recently suggested models.

Fewer models were developed for the formulation of fuel surrogates as most of the studies relied on the experimental work and trial and error for the generation of surrogates. These fewer models were used to generate surrogates that either match the physical or chemical delays. No sufficient universal models have been suggested to match both chemical and physical properties. Also, very limited surrogates have been suggested for bio-fossil fuel blends.

CHAPTER THREE: Computational Methodology

3.1. Overview

The models, presented in this research, are based on the analytical solutions to the heat and mass transfer equations. The droplet movement relevant to ambient gas (air) is considered to account for the Effective Thermal Conductivity (ETC) and Effective Diffusivity (ED) using the ETC/ED models [100]. Note that the modelling, provided in this work, is based on the following assumptions:

1. All processes are assumed to be spherically symmetric. The shapes of some droplets in Internal Combustion Engine (ICE) applications, however, can be far from sphericity. On the other hand, developing a general model for droplet heating and evaporation for arbitrary shapes is not possible in most cases. Attempts have been made in [101,102] to model the heating and evaporation of spheroidal droplets. In most cases, the heating and evaporation of non-spherical droplets are investigated based on the numerical solutions to the heat and mass transfer equations not their exact (analytical) solutions [103,104].

2. The modelling is based on an isolated droplet. In other words, the coupling effect of interaction between droplets on their heating and evaporation is ignored. This assumption is open to question because the evaporation rate decreases when the number of droplets per unit volume increases [105]. In ICE, however, positions of evaporated moving droplets are rather complex. It is not obvious yet how this complex interaction between moving droplets can be accounted for when modelling single droplet heating and evaporation.

3. The non-ideal gas behaviour of the gas phase is not considered as the current work focuses on the effects of multicomponent fuel composition on the processes in the liquid phase. One of the most recent investigations of these effects in the gas phase was presented by Tonini and Cossali [106]. The latter analysis is beyond the scope of this thesis.

4. The modelling of droplet heating and evaporation is based on the hydrodynamic approximation. In this approximation, it is assumed that the vapour at the surface of droplet is saturated and the evaporation process is modelled on the basis of the vapour diffusion from the surface of the droplet to the ambient gas. In the immediate vicinity of droplets, the kinetic region was introduced in some studies (see Figure 3 [107]). This region was simulated using the Boltzmann equations, to determine the evaporation coefficient and collisions between molecules for the correction of the temperature and vapour density. This region, however, was only introduced for the modelling of up to three component [107]. The values of evaporation coefficients are obtained from the molecular dynamic simulations based on the United Atom Model [29]. It is far too complex to consider the inelastic collisions between tens of molecules in a multi-component fuel such as gasoline and diesel in order to predict their evaporation coefficients. Additionally, this region was showing very minor effects on the scope of this thesis interest. For example, the droplet lifetime was only affected by less than 0.6% when using this model for a typical ICE ambient conditions [107].

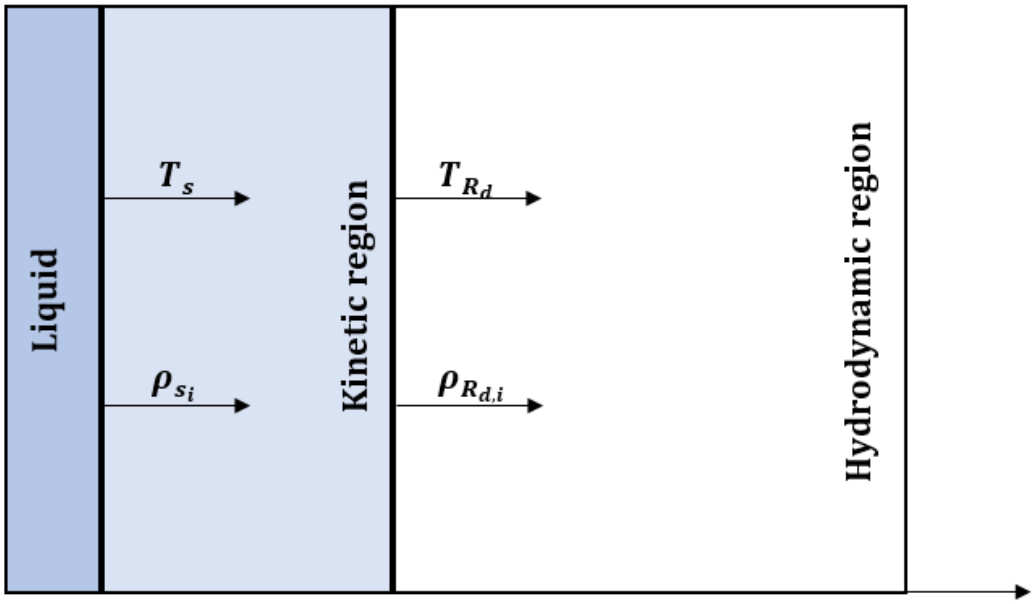

Figure 3. Liquid kinetic and hydrodynamic regions near the surface of the droplet. T_s is the droplet surface temperature, ρ_{s_i} is the vapour density of component i in the immediate vicinity of the droplet surface, T_{R_d} is the temperature at the outer boundary of the kinetic region and ρ_{Rd_i} is the vapour density of component i at the outer boundary of the kinetic region.

All the relevant equations used in producing the results and thesis analysis are described in the following sub-sections.

3.2. Droplet Heating

The heating of spherical droplets is described by the unsteady heat conduction equation [108,109]:

$$\frac{\partial T}{\partial t} = \kappa\left(\frac{\partial^2 T}{\partial R^2} + \frac{2}{R}\frac{\partial T}{\partial R}\right), \tag{2}$$

where $T = T(t, R)$ is the temperature in the liquid phase, t is time, R is the distance from the centre of droplet, and κ is the effective thermal diffusivity [110,111]:

$$\kappa = k_{\text{eff}}/c_l\rho_l, \tag{3}$$

ρ_l is the liquid density, c_l is the liquid specific heat capacity, and k_{eff} is the Effective Thermal Conductivity (ETC), defined as [112]:

$$k_{\text{eff}} = \chi k_l, \tag{4}$$

$$\chi = 1.86 + 0.86\tanh\left[2.225\log_{10}\left(\text{Pe}_{d(l)}/30\right)\right], \tag{5}$$

$\text{Pe}_l = \text{Re}_{d(l)}\text{Pr}_l$, $\text{Re}_{\text{d}(l)} = \frac{2\rho_l U_s R_d}{\mu_l}$ is the droplet Reynolds number in the liquid phase, $U_s = \frac{1}{32}\Delta U\left(\frac{\mu_g}{\mu_l}\right)\text{Re}_d C_F$ is the maximum surface velocity inside a droplet, $\Delta U = |U_g - U_d|$, $C_F = \frac{12.69}{\text{Re}_d{}^{2/3}(1+B_M)}$ is the friction drag coefficient, $\text{Pr}_l = \frac{c_l\mu_l}{k_l}$ is the Prandtl number, U_{g} is the velocity of gas, U_d is the velocity of the droplet, μ_l is the liquid dynamic viscosity, k_l is the liquid thermal conductivity, Re_d is the Reynolds number of droplet, and B_M is the Spalding mass transfer number defined later [28]. The initial and boundary conditions for Eq. (2) are:

$$\left.\begin{aligned} T(t=0) &= T_{d0}(R) \\ h\left(T_g - T_s\right) &= k_{\text{eff}} \left.\frac{\partial T}{\partial R}\right|_{R=R_d-0} \end{aligned}\right\}, \tag{6}$$

where $T_s = T_s(t)$ is the droplet surface temperature, $T_g = T_g(t)$ is the ambient gas temperature, R_d is the droplet radius, and $h = h(t)$ is the convective heat transfer coefficient, found as a function of the Nusselt number (Nu), as:

$$h = \text{Nu}\, k_g / 2R_d, \tag{7}$$

k_g is the thermal conductivity in the gas phase.

In contrast to [58,71,113], this work has taken into consideration both the convective and radiative heating of droplets. A more rigorous approach to modelling the radiative heating of droplets would take into account the semi-transparency of droplets as described in [28]. This approach, however, would involve measurement of the absorption properties of gasoline, diesel, biodiesel and ethanol fuel components in the visible and infrared ranges which is currently not available. The presented approach is based on the estimation of the maximal possible radiative absorption in droplets, which allows the author to use a simplified model of the process.

In the suggested approach, the droplet is assumed to be opaque and non-reflective (emissivity equal to 1). The following boundary condition, which represents an energy balance at the droplet-gas interface, is applied at its surface:

$$k_{\text{eff}} \left.\frac{\partial T}{\partial R}\right|_{R=R_d} = \rho L \frac{dR_d}{dt} + h\left(T_g - T_s\right) + \sigma T_{\text{rad}}^4, \tag{8}$$

where $k_{\text{eff}} = \chi k_l$ is the effective thermal conductivity, k_l is the liquid thermal conductivity, χ is the circulation coefficient (see [114] for details), ρ is the liquid density, L is the latent heat of evaporation, $\frac{dR_d}{dt}$ is the rate of droplet radius change due to evaporation, h is the

convection heat transfer coefficient, T_g is the ambient temperature, and $\sigma = 5.6703\ 10^{-8}$ W m^{-2}K^{-4} is the Stefan-Boltzmann constant. The radiative temperature T_{rad} is equal to gas temperature in the case of optically thick gas and external temperature in the case of optically thin gas. The analysis will focus on the latter case when the impact of thermal radiation is expected to be the strongest for engine conditions.

The radiation flux emitted by the droplet σT_d^4 to the ambient gas is assumed to be negligible, compared with the radiation flux hitting the droplet $\sigma T_{\mathrm{rad}}^4$ (e.g. due to remote flames). The effect of radiation is considered within the analytical solution to the heat transfer equation, described in [103,107], by replacing the gas temperature with the effective temperature:

$$T_{\mathrm{eff}} = T_g + \frac{\rho L \frac{dR_d}{dt}}{h} + \frac{\sigma T_{\mathrm{rad}}^4}{h}, \tag{9}$$

$\dot{R}_{dE}$ is the droplet radius change rate due to evaporation, and L is the latent heat of evaporation.

Within any given time step Δt, R_d is assumed constant and is updated at the end of Δt, as $R_{d(new)} = R_{d(old)} + \dot{R}_d \Delta t$, where the value of $\dot{R}_d$ is influenced by the droplet evaporation rate and thermal swelling (see Equations (31) - (33)).

The analytical solution to Equation (2) at the end of each time step ($t = t_1$) was obtained as [115]:

$$T(R,t) = \frac{R_d}{R} \sum_{n=1}^{\infty} \begin{Bmatrix} q_n \exp[-\kappa_R \lambda_n^2 t] - \frac{\sin \lambda_n}{\|v_n\|^2 \lambda_n^2} \mu_0(0) \exp[-\kappa_R \lambda_n^2 t] \\ -\frac{\sin \lambda_n}{\|v_n\|^2 \lambda_n^2} \int_0^t \frac{d\mu_{0(\tau)}}{d\tau} \exp[-\kappa_R \lambda_n^2 (t-\tau)] d\tau \end{Bmatrix} \sin\left(\lambda_n \frac{R}{R_d}\right) + T_{\mathrm{eff}}(t), \tag{10}$$

where $\|v_n\|^2 = \frac{1}{2}\left(1 - \frac{sin\ 2\lambda_n}{2\lambda_n}\right) = \frac{1}{2}\left(1 + \frac{h_{0T}}{h_{0T}^2 + \lambda_n^2}\right)$, $q_n = \frac{1}{R_d \|v_n\|^2} \int_0^{R_d} \tilde{T}_0(R) \sin\left(\lambda_n \frac{R}{R_d}\right) dR$,

$\tilde{T}_0(R) = R\ T_{d0}(R)/R_d$, $k_R = \frac{k_{\mathrm{eff}}}{c_l \rho_l R_d^2}$, $\mu_0(t) = \frac{h T_g(t) R_d}{k_{\mathrm{eff}}}$, $h_{l0} = \left(\frac{h R_d}{k_{\mathrm{eff}}}\right) - 1$.

A set of positive eigenvalues λ_n, $n > 0$ (the trivial solution $\lambda = 0$ is not considered), is determined from the solution to the following relation:

$$\lambda \cos\lambda + h_{l0} \sin\lambda = 0. \tag{11}$$

In the limit $k_{\text{eff}} \to \infty$, the prediction of Expression (10) will reduce to that of the so-called 'Infinite Thermal Conductivity' (ITC) model [24]. The value of Nu for an isolated moving droplet is calculated as [110]:

$$\text{Nu}_{\text{iso}} = 2\frac{\ln(1+B_T)}{B_T}\left[1 + \frac{(1+\text{Re}_\text{d}\text{Pr}_\text{d})^{1/3}\max\{1, \text{Re}_\text{d}^{0.077}\}-1}{2\,F(B_T)}\right], \tag{12}$$

where $F(B_T) = (1+B_T)^{0.7}\frac{\ln(1+B_T)}{B_T}$, B_T is the Spalding heat transfer number:

$$B_T = \frac{C_{pv}(T_g - T_s)}{L_{\text{eff}}}, \tag{13}$$

c_{pv} is the specific heat capacity of the fuel vapour at constant pressure,

$$L_{\text{eff}} = L + \frac{Q_L}{\dot{m}_d} = \sum_i \epsilon_i L_i + \frac{Q_L}{\sum_i \dot{m}_i}, \tag{14}$$

Q_L is the power spent on the droplet heating, $\epsilon_i = \epsilon_i(t)$ are the evaporation rates of species i, and $\dot{m}_i = \epsilon_i\,\dot{m}_d$ ($\dot{m}_d = \sum_i \dot{m}_i$). The interactions among droplets are ignored (these are discussed in [111,116,117]). The analysis of the evaporation process is based on the assumption that a mixture of vapour species and air can be treated as a separate gas (see Equation (24)).

3.3. Species Diffusion

The mass fractions of liquid species $Y_{li} \equiv Y_{li}(t, R)$ are described by the transient diffusion equations for spherical droplets as [27]:

$$\frac{\partial Y_{li}}{\partial t} = D_{\text{eff}}\left(\frac{\partial^2 Y_{li}}{\partial R^2} + \frac{2}{R}\frac{\partial Y_{li}}{\partial R}\right), \tag{15}$$

where $i = 1,2,3,\ldots$ refers to species, D_{eff} is the effective diffusivity of species in liquid phase, determined as a function of the liquid diffusivity D_l as:

$$D_{\text{eff}} = \chi_Y D_l, \tag{16}$$

coefficient χ_{Y} is approximated as:

$$\chi_{\text{Y}} = 1.86 + 0.86\tanh\left[2.225\log_{10}\left(\text{Re}_{\text{d}(l)}\text{Sc}_l/30\right)\right], \tag{17}$$

$\text{Pe}_l = \text{Re}_{\text{d}(l)}\,\text{Sc}_l, \text{Sc}_{\text{d}(l)} = \frac{v_l}{D_l}$ is the liquid Schmidt number, $\text{Re}_{\text{d}(l)}$ is the Reynolds number, as in Equation (5), and v_l is the kinematic viscosity of liquid phase. The model based on Equations (15)-(17) is known as the Effective Diffusivity (ED) model [16,110].

The following boundary condition, which also represents an energy balance at the droplet-gas interface, is considered for the solution to Equation (15) [100]:

$$\alpha(\epsilon_i - Y_{lis}) = -D_{\text{eff}}\frac{\partial Y_{li}}{\partial R}\Big|_{R=R_d-0}, \tag{18}$$

where $Y_{lis} = Y_{lis}(t)$ are liquid components' mass fractions at the droplet surface,

$$\alpha = \frac{|\dot{m}_d|}{4\pi\rho_l R_d^2} = \left|\dot{R}_{dE}\right|, \tag{19}$$

$\dot{m}_d$ is the droplet evaporation rate, the calculation of which is discussed in Section 3.4 (see Equation (24)).

The initial condition is $Y_{li}\ (t = 0) = Y_{li0}(R)$,

Assuming no impacts of species in the ambient gas, the values of ϵ_i were obtained as [27,118,119]:

$$\epsilon_i = \frac{Y_{vis}}{\sum_i Y_{vis}}. \tag{20}$$

The following analytical solution to Equation (15) at the end of each time step was obtained [27]:

$$Y_{li} = \epsilon_{\mathrm{i}} + \frac{1}{R}\left\{ \begin{array}{l} \left[\exp\left[D_{\mathrm{eff}}\left(\frac{\lambda_0}{R_d}\right)^2 t\right][q_{i0} - \epsilon_i Q_0]\sinh\left(\lambda_0 \frac{R}{R_d}\right) + \\ \sum_{\mathrm{n}=1}^{\infty}\left[\exp\left[-D_{\mathrm{eff}}\left(\frac{\lambda_n}{R_d}\right)^2 t\right][q_{in} - \epsilon_i Q_n]\ \sin\left(\lambda_n \frac{R}{R_d}\right)\right. \end{array} \right\}, \tag{21}$$

where λ_0 and λ_n are calculated from $\tanh\lambda_0 = -\lambda_0/h_{0Y}$ and $\tanh\lambda_n = -\lambda_n/h_{0Y}$ (for $\mathrm{n} \geq 1$), respectively, $h_{0Y} = -\left(1 + \frac{\alpha R_d}{D_{\mathrm{eff}}}\right)$,

$$Q_n = \left\{ \begin{array}{ll} -\frac{1}{\|v_o\|^2}\left(\frac{R_d}{\lambda_0}\right)^2 (1 + h_0)\sinh\lambda_0 & \text{when } \ n = 0 \\ \frac{1}{\|v_n\|^2}\left(\frac{R_d}{\lambda_n}\right)^2 (1 + h_{0Y})\sin\lambda_n & \text{when } \ n \geq 1 \end{array} \right\}, \tag{22}$$

Where $\|v_n\|^2 = \frac{1}{2}\left(1 - \frac{sin\ 2\lambda_n}{2\lambda_n}\right) = \frac{1}{2}\left(1 + \frac{h_{0Y}}{h_{0Y}^2 + \lambda_n^2}\right)$, and:

$$q_{in} = \left\{ \begin{array}{ll} \frac{1}{\|v_0\|^2}\int_0^{R_d} R\ Y_{li0}(R)\sinh\left(\lambda_0 \frac{R}{R_d}\right) dR & \text{when } \ n = 0 \\ \frac{1}{\|v_n\|^2}\int_0^{R_d} R\ Y_{li0}(R)\sin\left(\lambda_n \frac{R}{R_d}\right) dR & \text{when } \ n \geq 1 \end{array} \right\}. \tag{23}$$

Solution (21) is incorporated in the Discrete Multi Component Model (DMCM), which is used in the analysis of droplet heating.

3.4. Droplet Evaporation

For multi-component fuels, droplet evaporation depends on the diffusion rate of individual species in the gas phase; the evaporation rate of each component is affected by the evaporation rate of other components [27,116]. Following [120], however, the relative

diffusion of individual components in the gas phase is not considered. The analysis of droplet evaporation rate ($\dot{m}_d$) is based on the following expression:

$$\dot{m}_d = -2\pi R_d D_v \rho_{\text{total}} B_M \, \text{Sh}_{\text{iso}}, \tag{24}$$

where D_v is the binary diffusion coefficient of vapour in gas (air), $\rho_{total} = \rho_a + \rho_v$ is the total density of the mixture of air (ρ_a) and fuel vapour (ρ_v), B_M is the Spalding mass transfer number defined as [121]:

$$B_M = \frac{\rho_{vs} - \rho_{v\infty}}{1 - \rho_{vs}} = \frac{Y_{vs} - Y_{v\infty}}{1 - Y_{vs}}, \tag{25}$$

Y_v is the vapour mass fraction, ρ_{vs} and $\rho_{v\infty}$ are densities of vapour near the droplet surface and at a large distance from it, Sh_{iso} is the Sherwood number for isolated droplets approximated as [110]:

$$\text{Sh}_{\text{iso}} = 2\frac{\ln(1+B_M)}{B_M}\left[1 + \frac{(1+\text{Re}_\text{d}\text{Sc}_\text{d})^{1/3}\max\{1, \text{Re}_\text{d}{}^{0.077}\} - 1}{2\,F(B_M)}\right], \tag{26}$$

Sc_d is the Schmidt number for the gas phase, $F(B_M)$ is the same as in (12) but with B_T replaced with B_M [29]. B_T and B_M are linked by the following formula [110]:

$$B_T = (1 + B_M)^{\varphi} - 1, \tag{27}$$

$$\varphi = \left(\frac{c_{pv}}{c_{pa}}\right)\left(\frac{\text{Sh}^*}{\text{Nu}^*}\right)\frac{1}{\text{Le}}, \tag{28}$$

$\text{Le} = k_g/(c_p\,\rho_g\,D_v)$ is the Lewis number, and Sh^* and Nu^* are the modified Sherwood and Nusselt Numbers, respectively, calculated as:

$$\text{Sh}^* = 2\left[1 + \frac{(1+\text{Re}_d\text{Sc}_d)^{1/3}\max\{1,\text{Re}_d^{0.077}\} - 1}{2F(B_M)}\right], \tag{29}$$

$$\text{Nu}^* = 2\left[1 + \frac{(1+\text{Re}_d\text{Pr}_d)^{1/3}\max\{1,\text{Re}_d^{0.077}\} - 1}{2F(B_T)}\right], \tag{30}$$

The ratio $\frac{\mathrm{Sh}^*}{\mathrm{Nu}^*}$ is equal to 1 for stationary droplets. This ratio was sometimes assumed equal to 1 for slowly moving droplets [27,28]. Such an assumption turned out to be too crude in some cases. Hence, Expressions (29) and (30) are used to estimate φ based on Equation (26). Note that $\dot{m}_d \leq 0$.

When calculating the value of $\dot{R}_d$, both droplets evaporation and thermal swelling during the time step were taken into account [122]:

$$\dot{R}_d = \dot{R}_{dT} + \dot{R}_{dE}, \tag{31}$$

where $\dot{R}_{dT}$ is the rate of change in droplet radius, caused by thermal expansions or contractions, calculated as [122]:

$$\dot{R}_{dT} = \frac{R_d(T_{av,0})}{\Delta t}\left[\left(\frac{\rho_l(T_{av,0})}{\rho_l(T_{av,1})}\right)^{1/3} - 1\right], \tag{32}$$

$T_{av,0}$ and $T_{av,1}$ are average droplet temperatures at the beginning $t = t_0$ and the end $t = t_1$ of the time-step. The value of $\dot{R}_{dE}$ is controlled by droplet evaporation [100]:

$$\dot{R}_{dE} = \frac{\dot{m}_d}{4\pi R_d^2 \rho_l}. \tag{33}$$

3.5. Vapour-Liquid Equilibrium

Vapour mass fraction of individual species i are calculated from the vapour molar fractions at the droplet surface (X_{vis}) using modified Raoult's law:

$$X_{vis} = \gamma_i \frac{X_{lis}\, p_{is}^{\mathrm{sat}}}{\varphi_i p}, \tag{34}$$

where p is the total (ambient) pressure, X_{lis} is the liquid molar fraction of the i^{th} species at the surface of the droplet, γ_i is the AC of the i^{th} species, p_{is}^{sat} is the saturated pressure of the

i^{th} species in the absence of other species, p is the total pressure, and φ_i is the fugacity coefficient. It has been shown, in some studies (example [41]), that the non-ideality mainly originates from the liquid phase, while it is very low at the gas phase for the parameters used in this study. Hence the fugacity coefficient can be assumed equal to unity,

In contrast to [60,63,71,123–126], where Raoult's law is assumed to be valid ($\gamma_i = 1$), this study accounts for the values of ACs taking into consideration the effect of corrected partial pressures of vapour components. The UNIFAC model is used for the estimation of the ACs of 21, up to 114 and 119 components of ethanol/gasoline, biodiesel/diesel and E85-diesel fuel blends, respectively. This model includes two terms: the combinatorial term (C) and residual term (R), taking into account the contribution of the excess entropy and the effect of the excess enthalpy, respectively. The excess entropy is inferred from various shapes and sizes of molecules or functional groups of atoms, while the excess enthalpy is inferred from interactions between molecules or groups [127,128]. The UNIFAC equation for the AC of component *i* in a multi-component mixture is presented as [129]:

$$\ln \gamma_{\mathrm{i}} = \ln \gamma_{\mathrm{i}}^{\mathrm{C}} + \ln \gamma_{\mathrm{i}}^{\mathrm{R}} \tag{35}$$

where $\ln \gamma_{\mathrm{i}}^{\mathrm{C}} = \ln \frac{\Phi_i}{X_i} + \frac{z}{2} q_i \ln \frac{\theta_i}{\Phi_i} + l_i - \frac{\Phi_{\mathrm{i}}}{X_i} \sum_{\mathrm{j}} X_j l_j$ is the combinatorial part, $\ln \gamma_i^R = \sum_k v_k^i (\ln \Gamma_k - \ln \Gamma_k^i)$ is the residual part, $l_i = \frac{Z}{2} (r_i - q_i) - (r_i - 1), Z = 10, \theta_i = \frac{q_i X_i}{\sum_j q_j X_j}$ is the area fraction of each molecule in the mixture, $\Phi_i = \frac{r_i X_i}{\sum_j r_j X_j}$ is the segment (volume) fraction of each molecule, $r_i = \sum_k v_k^i R_k$ is the volume parameter, $q_i = \sum_k v_k^i Q_k$ is the surface parameter, $\ln \Gamma_k = Q_k \left[1 - \ln(\sum_m \theta_m \psi_{mk}) - \sum_m \frac{\theta_m \psi_{km}}{\sum_n \theta_n \psi_{nm}}\right]$, $\theta_m = \frac{Q_m X_m}{\sum_n Q_m X_m}$ is the area fraction of group m, X_i is the molar fraction of liquid component i (the same as X_{lis} in Equation (2)), X_m is the molar fraction of group m, and R_k and Q_k are the van der Waals volumes and surface areas for each group, respectively [128,129]. R_k is the volume occupied by each group in the molecule, while Q_k is the surface area occupied by each group in the

molecule. Both R_k and Q_k are functions of bond distances, bond angles, contact distances, and shapes that are characteristic of the group [130]. v_k^i is the number of groups in molecule i. Γ_k is the residual AC of group k in the mixture and Γ_k^i is the residual AC of group k in a reference solution containing only molecules of type i (for example Γ_k^i for the CH_2OH group in ethanol refers to a solution containing 50% CH_2OH and 50% CH_3, while CH_2OH in 1-pentanol refers to a solution of 20% CH_2OH, 60% CH_2, and 20% CH_3). In other words, Γ_k^i deals with each group in each molecule, while Γ_k deals with each group in the mixture. $\psi_{mn} = e^{-(\frac{a_{mn}}{T})}$ is the interaction and temperature dependent coefficient, a_{mn} is the group-interaction parameter between groups m and n, m and n refer to the group in the mixture (in the case of Γ_k) or in the molecule (in the case of Γ_k^i) [129]. T is the interface temperature. The R_k and Q_k for different groups in ethanol, biodiesel, and gasoline components are shown in Table 1, which are inferred from [129].

Table 1. Van der Waals volumes (R_k) and surface areas (Q_k) for various molecules and atoms.

Name	Group	Group number	R_k	Q_k
alkanes	CH_3	1	0.9011	0.848
	CH_2	1	0.6744	0.540
	CH	1	0.4469	0.228
olefin	CH_2=CH	2	1.3454	1.176
benzene	ACH	3	0.5313	0.400
alkylbenzenes	$ACCH_3$	4	1.2663	0.968
	$ACCH_2$	4	1.0396	0.660
	ACCH	4	0.8121	0.348
ethanol	OH	5	1.0000	1.200
methyl ester	CH_2COO	11	1.6764	1.188

In Table 1, there are six groups in ethanol, biodiesel, and gasoline fuels, and each group interacts with the other five groups. The a_{mn} between these groups are shown in Table 2 [129].

Table 2. The m-group and n-group interaction parameters (a_{mn}) in K, used in the UNIFAC model.

Group number	n = 1	2	3	4	5	11
m = 1	0.0	86.02	61.13	76.50	986.5	232.11
2	−35.36	0.0	38.81	74.15	524.1	37.85
3	−11.12	3.446	0.0	167.0	636.1	5.994
4	−69.70	−113.6	−146.8	0.0	803.2	5688
5	156.4	457.0	89.6	25.82	0.0	101.1
11	114.8	132.1	85.84	−170.0	245.4	0.0

The structure of the groups and the values of R_k and Q_k in E85-diesel fuel blends are the same as those shown in [131] for the ethanol/gasoline blend. Diesel fuel, however, has 5 more groups of molecules than gasoline fuel, namely, bicycloalkanes, naphthalenes, tricycloalkanes, diaromatics and phenanthrenes. The values of parameters R_k and Q_k for these five groups in the composition of diesel fuel are not provided anywhere in the literature, to the best of the author's knowledge. The structures of these groups of molecules are approximated to the nearest available structures for which the values of parameters R_k and Q_k are known, taking into account the number of groups in each molecule. For example, when the aromatic molecule $C_{10}H_{14}$ (its structure group is available in [128,129]) has 1 aromatic ring (C_6), 3 CH_2 and 1 CH_3 (the numbers 1, 3 and 1 refer to v_k^i which is the number of groups in molecule i), the diaromatic molecule $C_{12}H_{16}$ is approximated by 2 aromatic rings (C_6). Thus, the diaromatic group is approximated by 2 single aromatic groups, as shown in Table 3. This approximation allowed the author to predict the activity coefficients for all components of the E85-diesel fuel blend.

Table 3. The approximation of the missing structure groups for the predictions of the ACs.

Group name	Group structure	
	Missing group	Approximation
Bicycloalkanes	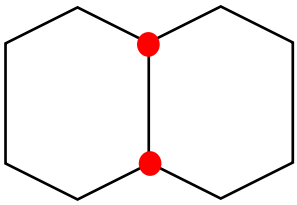 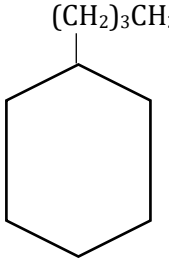 The bicyclo-$C_{10}H_{18}$ is approximated by Cyclo-C_6, 3 CH_2 and 1 CH_3.	
Naphthalenes	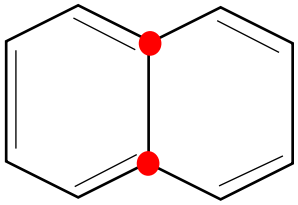 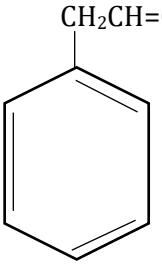 The naphthalenes $C_{10}H_8$ is approximated by 1 aromatic C_6, 1 CH_2, 1 CH=CH and 1 CH_3.	
Tricycloalkanes	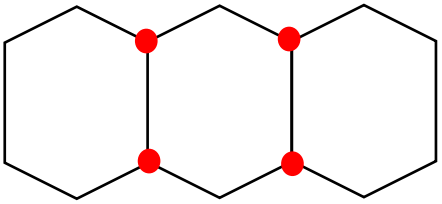 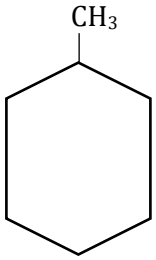 The tricycloalkane $C_{14}H_{24}$ is approximated by 2 cyclo C_6 and 2 CH_3.	
Diaromatics	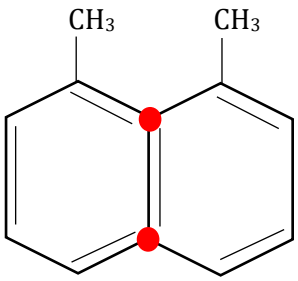 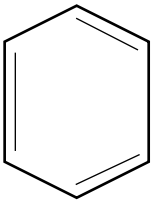 The diaromatic $C_{12}H_{16}$ is approximated by 2 aromatic C_6.	

Phenanthrenes	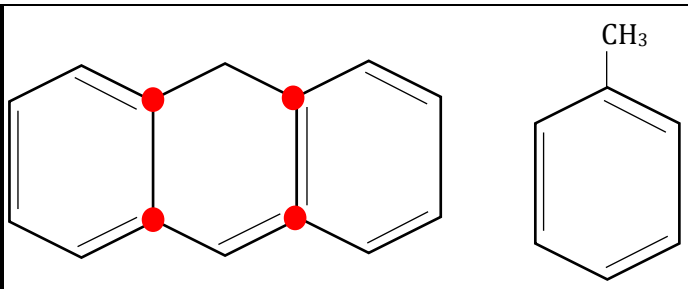 The phenanthrene $C_{14}H_{11}$ is approximated by 2 aromatic C_6 and 2 CH_3

3.6. Multi-Dimensional Quasi-Discrete Model

The Multi-Dimensional Quasi-Discrete Model (MDQDM) was introduced in [60] which was a generalised model to the original Quasi-Discrete Model (QDM) introduced in [68]. In the MDQDM, the generation of the Components/Quasi-Components (C/QC) was based on the molar fraction contribution of each component instead of distribution function used for the generation of the C/QC by the QDM. The matrix X_{nm} describes the distribution function, where *n* represents the carbon number, and *m* represents the group (e.g. aromatics).

For each *m*, the values of n_{jm} of C/QC can be produced as:

$$n_{1m} = \frac{\sum_{n=n_{1m}}^{n=n_{(\varphi_m+1)m}} (nX_{nm})}{\sum_{n=n_{1m}}^{n=n_{(\varphi_m+1)m}} (X_{nm})}$$

$$n_{2m} = \frac{\sum_{n=n_{(\varphi_m+2)m}}^{n=n_{(2\varphi_m+2)m}} (nX_{nm})}{\sum_{n=n_{(\varphi_m+2)m}}^{n=n_{(2\varphi_m+2)m}} (X_{nm})}$$

$$n_{3m} = \frac{\sum_{n=n_{(2\varphi_m+3)m}}^{n=n_{(3\varphi_m+3)m}} (nX_{nm})}{\sum_{n=n_{(2\varphi_m+3)m}}^{n=n_{(3\varphi_m+3)m}} (X_{nm})} \quad (36)$$

$$n_{4m} = \frac{\sum_{n=n_{(3\varphi_m+4)m}}^{n=n_{(4\varphi_m+4)m}} (nX_{nm})}{\sum_{n=n_{(3\varphi_m+4)m}}^{n=n_{(4\varphi_m+4)m}} (X_{nm})}$$

.....

$$n_{\ell m} = \frac{\sum_{n=n_{((\ell-1)\varphi_m+\ell)m}}^{n=n_{km}} (nX_{nm})}{\sum_{n=n_{((\ell-1)\varphi_m+\ell)m}}^{n=n_{km}} (X_{nm})}$$

where n_{1m} and n_{km} are the minimal and maximal values of n, respectively for which $X_{nm} \neq 0$, $\ell = \text{int.}((k_m + \varphi_m)/(\varphi_m + 1))$. The value of φ_m is always assumed to be integer and the same for all generated C/QC within each group m; $\varphi_m + 1$ is the number of components to be grouped and form a QC. The MDQDM becomes the DMCM (i.e. the number of C/QC is equal to the number of actual components) when the parameter $\varphi_m = 0$ which leads to $\ell = k$.

The molar fractions of the generated C/QC can be estimated as follows:

$$\begin{aligned}
X_{1m} &= \sum_{n=n_{1m}}^{n=n_{(\varphi_m+1)m}} X_{nm} \\
X_{2m} &= \sum_{n=n_{(\varphi_m+2)m}}^{n=n_{(2\varphi_m+2)m}} X_{nm} \\
X_{3m} &= \sum_{n=n_{(2\varphi_m+3)m}}^{n=n_{(3\varphi_m+3)m}} X_{nm} \\
X_{4m} &= \sum_{n=n_{(3\varphi_m+4)m}}^{n=n_{(4\varphi_m+4)m}} X_{nm} \\
&\ldots\ldots\ldots\ldots\ldots\ldots\ldots\ldots\ldots\ldots\ldots\ldots\ldots\ldots \\
X_{lm} &= \sum_{n=n_{((\ell-1)\varphi_m+\ell)m}}^{n=n_{km}} X_{nm}
\end{aligned} \tag{37}$$

3.7. Solution Algorithm

The following algorithmic steps are used in the droplet heating and evaporation analysis [60]:

1. The temperature distribution and species molar fractions are provided inside the droplet (initial homogeneous or inferred from the previous time step). The species molar fractions are converted into species mass fractions.
2. The liquid thermal conductivity and effective thermal conductivity of the droplet are calculated for each individual component using the appropriate physical properties

presented in Appendices B, C, E and F. The blending rule for the thermal conductivity, presented in Appendix I, is used to make up the thermal conductivity of the mixture. All other needed properties are calculated in the same way.

3. The partial pressures and molar fractions in the gas phase are calculated, using Equation (34).
4. The Spalding mass transfer number is calculated, using Equation (25).
5. The liquid heat capacity and the mixture diffusivity of vapour species in air, and species evaporation rates (ϵ_i) are calculated, using Equation (20).
6. The Spalding heat transfer number is calculated, using Equations (27) – (30).
7. The Nusselt and Sherwood numbers are calculated for isolated droplets, using Equations (12) and (26).
8. Nu^* and Sh^* are determined, using Equations (29) and (30).
9. The change rate of droplet radius is found, using Equations (31) – (33).
10. The effective temperature is found, using Equation (9).
11. The temperature distribution inside the droplet is found, based on Equation (10), with 44 terms in the series [60].
12. The species distribution inside the droplet is found, based on Equation (21), with 33 terms in the series [60].
13. The droplet radii are calculated at the end of each time step Δt using Equations (31) – (33). The ratio of the calculated radius to the initial radius should be higher than an *à priori* small number of $\varepsilon_s = 10^{-6}$ to go to the next step; otherwise, the droplet is assumed to be completely evaporated [28]. It should be noted that ε_s is a safety net for closing the calculation loop before droplet size reaches 'nil', which does not affect the accuracy of the results.
14. The temperature and species distributions for the droplet with the new radius, found in the previous steps, are used back in Steps 1-12 until the condition in Step 13 is satisfied.

The equations for heating and evaporation processes presented in this chapter as well as the physical properties presented in Appendices B, C, E or F were solved in a FORTRAN code. A one-dimensional numerical analysis was made for the liquid phase model in a droplet of 300 layers; while a 0-dimensional analysis was made for the modelling the gas phase.

Due to the importance of the DMCM for the simulation of advanced combustion, several attempts have been made to implement it in some of the combustion processes (mainly fuel injection). In [122], the authors focused on the influence of the selected heating and evaporation model on the predicted amounts of fuel vapour and in-cylinder pressure of a diesel engine. In most recent studies (e.g., [57]), the DMCM was implemented for the modelling of single droplets and sprays evaporation. However, the model has not been implemented in any CFD code for the full engine cycle simulation including combustion. In real efforts to address this issue, in Chapter 8, the developed FORTRAN code was translated to C# language for the implementation into Ansys Fluent via its User-Defined Function. This first of its kind approach has been made to showcase the impact of the model accuracy on the fuel combustion in a typical GTE, due to the capability of such engines to deal with broader variety of fuels than the ICE.

CHAPTER FOUR: Ethanol/Gasoline Fuel Blends

4.1. Overview

Gasoline is a volatile fuel, combining middle distillate of petroleum derivatives and liquid mixture of hydrocarbons in the range of C_4-C_{12} [70,132,133]. It is the most common fuel in the automotive sector for spark ignition engines [31]. With 40% of global transport energy is used in passenger cars, about 80% of these cars are powered by spark ignition engines. Due to that demand on gasoline fuel, it is therefore essential to fully understand its combustion characteristics which could result in modifications of engines' design for better performance. Many investigations focused on the replacement of gasoline with ethanol/gasoline blends to improve those characteristics [41,43,134]. These have been mainly driven by the importance of reducing Greenhouse Gas Emissions (GGE) and dependency on fossil fuels.

In several studies (e.g. [41,135–137]), gasoline fuel was approximated by iso-octane, whilst in reality commercial gasoline fuel grades consist of hundreds of hydrocarbons [138]. Multi-component fuel droplet heating and evaporation are essential processes in ICE, which strongly depend on ambient (in-cylinder) conditions and controlled spray combustion behaviour.

The UK government policy allows using up to 5% mixture of biofuel with gasoline [12]. However, it is revealed recently that gasoline can be mixed with 10 % ethanol with minimal or no impacts on the engines [8]. According to the UK Department for Transport [139], increasing the content of ethanol in gasoline from 5% to 10% could cut the CO_2 emissions by a further 750,000 tonnes per year. This is equivalent to taking 350,000 cars away from UK roads.

In this chapter, the impacts of ethanol (a typical biofuel blend for gasoline) on gasoline droplets heating and evaporation are investigated, accounting for several in-cylinder conditions, including the radiative temperature. In addition, the model is improved, taking into account the vapour-liquid equilibrium of the blend with the adjusted calculation of activity coefficient. In previous studies (e.g. [28]) Raoult's law was assumed to be valid (the activity coefficient (AC) was assumed equal to one) for the predictions of vapour-liquid equilibrium. Unlike fossil fuels, ethanol fuel is polar liquid. Therefore, Raoult's law may not be suitable for predicting the vapour pressures of such fuel blends [140].

4.2. Impacts of Fuel Blends and Ambient Conditions

This section focuses on the effects of ambient pressure, ambient and radiative temperatures, and blending ratios on the evaporation characteristics of ethanol/gasoline fuel droplets. The Discrete Multi Component Model (DMCM) was applied to the analysis of heating and evaporation of gasoline FACE C (fuel used in advanced combustion engines, type C), ethanol and their blends.

4.2.1. Fuel compositions

Gasoline FACE C (Fuel for Advanced Combustion Engines Type C) fuel was used in this study (inferred from [71]). In [71], the number of the components with identical chemical formulae and close thermodynamic and transport properties were replaced with characteristic components leading to reducing the original composition of gasoline fuel (83 components) to 20 components only, represented by 6 hydrocarbon groups as presented in Table 4.

Table 4. The molar composition (%) of gasoline FACE C fuel.

carbon no	n-alkanes	iso-alkanes	alkylbenzenes	cycloalkanes	naphthalenes	olefins
C4	3.905	0.092	-	-	-	-
C5	13.87	7.456	-	-	-	-
C6	10.842	2.98	-	-	-	-
C7	-	11.67	-	-	-	-
C8	-	42.17	0.242	1.49	-	-
C9	-	0.137	3.521	-	0.104	0.346
C10	0.01	0.36	0.44	-	-	-
C11	-	0.113	0.055	-	-	-
C12	0.012	-	-	-	-	-
Total%	28.64	64.98	4.26	1.49	0.104	0.346

In this research, the physical properties of air used are presented in Appendix A. While those for gasoline and ethanol are illustrated in Appendices B and C, respectively.

4.2.2. Model validation

Firstly, the results of application of the DMCM to the evaporation of an ethanol/gasoline (combined iso-octane and heptane) mixture droplet were validated for mixtures EW30, EW70, and EW100 (EWX refers to a mixture with X% weight fraction of ethanol and $(100 - X)$% weight fraction of gasoline) against experimental data inferred from [134]. The results are shown in Figure 4. The mixtures of weight fractions EW30 and EW70 are approximately equivalent to the mixtures of volume fractions 27% ethanol/73% gasoline and 67% ethanol/33% gasoline, respectively. Droplets of 23.6 μm initial radius and 280.15 K initial temperature were suspended in stationary dry air at 1 atm.

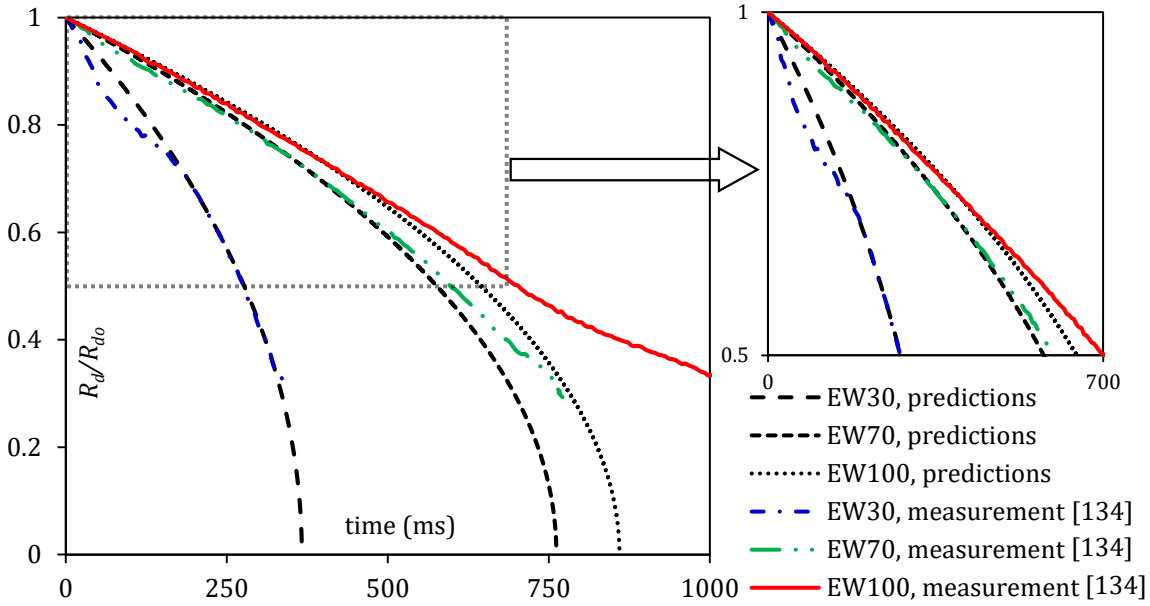

Figure 4. Predicted and experimentally measured [134] normalised radii of the EW30, EW70 and EW100 droplets.

As can be seen from Figure 4, the predicted initial evolutions of droplet radii are close to those inferred from experimental data. However, clear deviations between model predictions and experimental data can be seen at the final stages of droplet evaporation. This deviation is attributed to the experimental procedure used in [134]. As noted by the authors of [134] this is caused by the water uptake from the ambient gas into fuel droplet during the measurement, the impact of which is outside the scope of the used model. The impact of such measurement uncertainty becomes more significant for higher fractions of ethanol, hence experimental results near the end of EW70 – EW100 droplet evaporations are not reliable.

4.2.3. Impacts of ethanol/gasoline fuel blends

In the following analysis, the effects on droplet heating and evaporation on various molar fractions of ethanol in the mixture were investigated. The following molar fractions of ethanol were considered: 100%, 85%, 50%, 20%, 5% and 0%. The corresponding molar mixtures were referred to as EM100, EM85, EM50, EM20, EM5 and EM0 as in the case when volume fractions of ethanol were considered. In this case, mixtures EM85, EM50, EM20 and

EM5, are approximately equivalent to the mixtures with volume fractions 70% ethanol/30% gasoline, 29% ethanol/71% gasoline, 9% ethanol/91% gasoline, and 2% ethanol/98% gasoline, respectively. The plots of droplet surface temperatures T_s and radii R_d versus time for various ethanol/gasoline fuel blends, taking into account the contributions of all 21 components in ethanol/gasoline fuel blends, are shown in Figures 5 and 6 respectively. As in [71], the initial droplet radius was taken to be $R_{do} = 12$ µm, based on the measured SMD of gasoline fuel droplets, and its constant axial velocity in still air and initial temperature were assumed equal to $U_d = 24\ \mathrm{m.s^{-1}}$ and T_{do} = 296 K, respectively. The ambient air pressure and temperature were assumed constant and equal to p_g = 9 bar and $T_g = 545$ K, respectively.

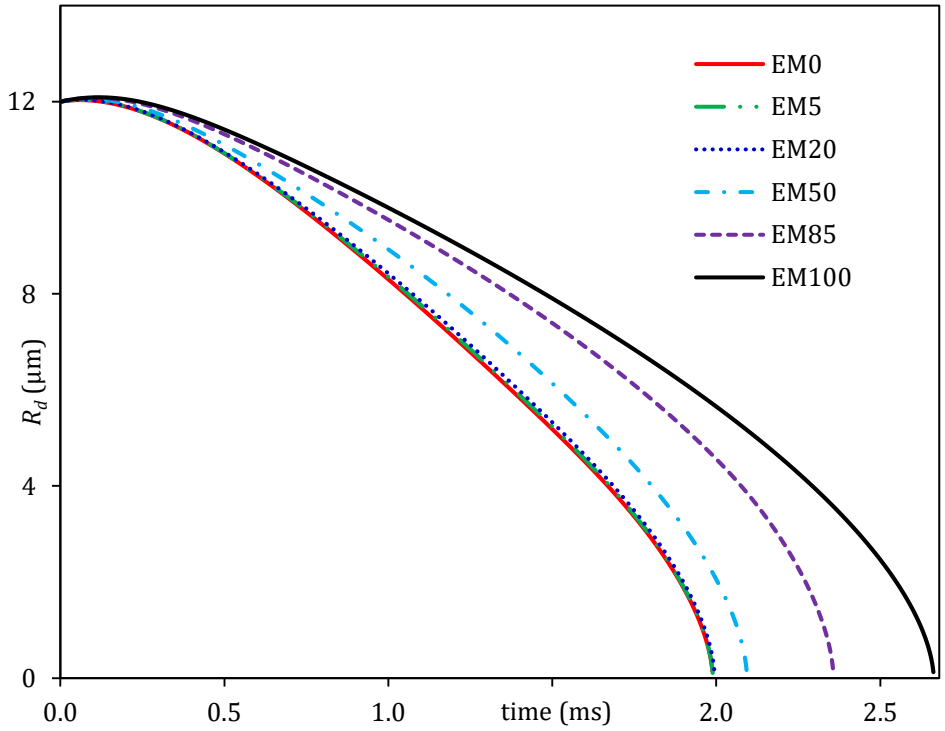

Figure 5. The plots of droplet radii versus time for various ethanol/gasoline blends.

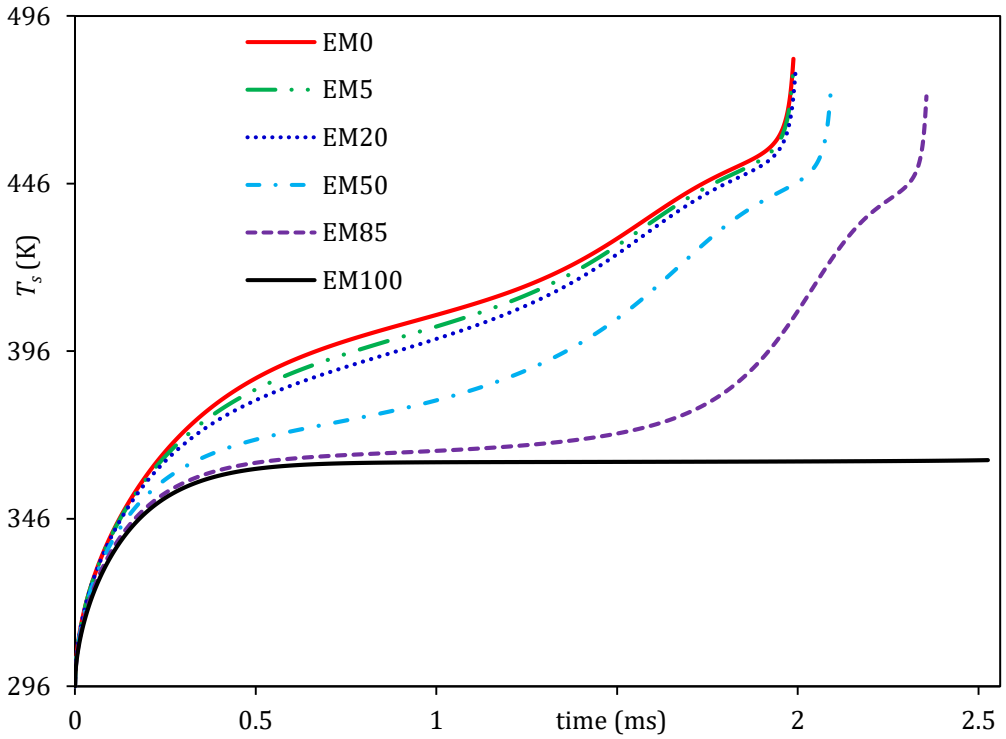

Figure 6. The plots of droplet surface temperatures versus time for various ethanol/gasoline blends.

The plots for droplet radii and surface temperatures are shown for six blends of ethanol/gasoline fuel (EM0–EM100). The impact of ethanol/gasoline fuel blends on droplet lifetimes, compared to the case of pure gasoline FACE C fuel (EM0), is shown in Table 5.

Table 5. The impact of ethanol/gasoline fuel blends on estimated droplet lifetimes (in ms); Diff % $= \frac{\text{lifetime(blend)} - \text{lifetime(E0)}}{\text{lifetime(E0)}} \times 100$.

Blend	Lifetime	Diff %
EM0	1.988	-
EM5	1.989	0.050
EM20	1.994	0.302
EM50	2.093	5.282
EM85	2.356	18.511
EM100	2.662	33.903

As evident from Figure 5, the droplet lifetime for pure gasoline fuel (EM0) is shorter than for any of the blends. It increases as the fraction of ethanol increases. This trend is similar to that reported in [43,134]. The difference reaches 33.9% for EM100. This can be attributed to the different thermodynamic and transport properties of ethanol and gasoline. For example, the latent heat of evaporation of ethanol is much higher than those of averaged gasoline fuel components. In Figure 6, the predicted droplet surface temperature for EM100 is up to 24.3% lower than that predicted for EM0. However, the volatility of ethanol is lower than gasoline due to the difference between their vapour pressures which leads to a lower droplet wet bulb surface temperature for the blends compared with the pure gasoline fuel. The sudden increase in the multi-component droplet surface temperatures is due to the sudden drop in droplet size at the final stage of evaporation. For a single component (e.g. pure ethanol), however, it is plateau because there is smooth evaporation.

The results presented in Figures 5 and 6 are based on a droplet with radius $R_{do} = 12$ μm, based on the estimated SMD of gasoline fuel droplets. It is obvious that droplet lifetimes of larger droplets will be longer. The impact of droplet radii, however, was not investigated as the focus was on the modelling of heating and evaporation process of droplet with average size similar to that of real applications.

The time evolution of surface mass fractions of representative components of the fuel mixture, predicted by the author's solver, is shown in Figure 7.

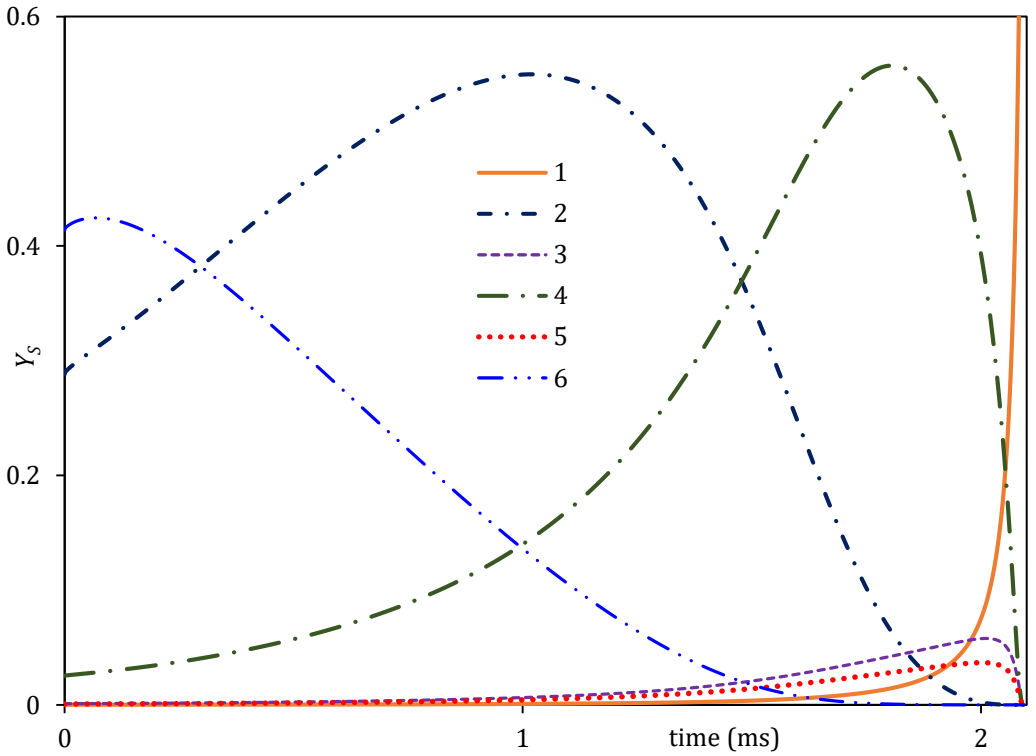

Figure 7. The plots of surface mass fractions of representative components of EM50, Y_S, versus time. The plots of the following components are shown: n-$C_{12}H_{26}$ (1), iso-C_8H_{18} (2), iso-$C_{11}H_{24}$ (3), C_9H_{12} (4), C_9H_{10} (5) and C_2H_6O (6).

As follows from Figure 7, the mass fractions of heavy components monotonically increase with time at the expense of lighter components. The mass fractions of the intermediate components (iso-C_8H_{18}) initially increase but then decrease with time. This is consistent with the results from a previous study on this phenomenon [28]. One can expect this complex behaviour of different components to significantly affect the distributions of mass fractions of components inside the combustion chamber in realistic engine-like conditions, where the ambient gas temperatures are not homogeneous.

4.2.4. Impacts of ambient conditions

As mentioned earlier, in contrast to previous studies (e.g. [112,115]), the suggested model takes into account the impact of thermal radiation on droplet heating. The focus is on a reasonable range of petrol engine injection conditions, accounting for different radiative temperatures and in-cylinder pressures and temperatures for EM0–EM100 fuel mixtures.

The ambient pressures, gas and radiative temperatures were considered in the ranges 3–30 bar, 400–650 K, and 1000–2000 K, respectively. Transient diffusion of 21 hydrocarbons, temperature gradient, and recirculation inside droplets were accounted for in the model. The impact of radiative temperatures is shown in Figure 8.

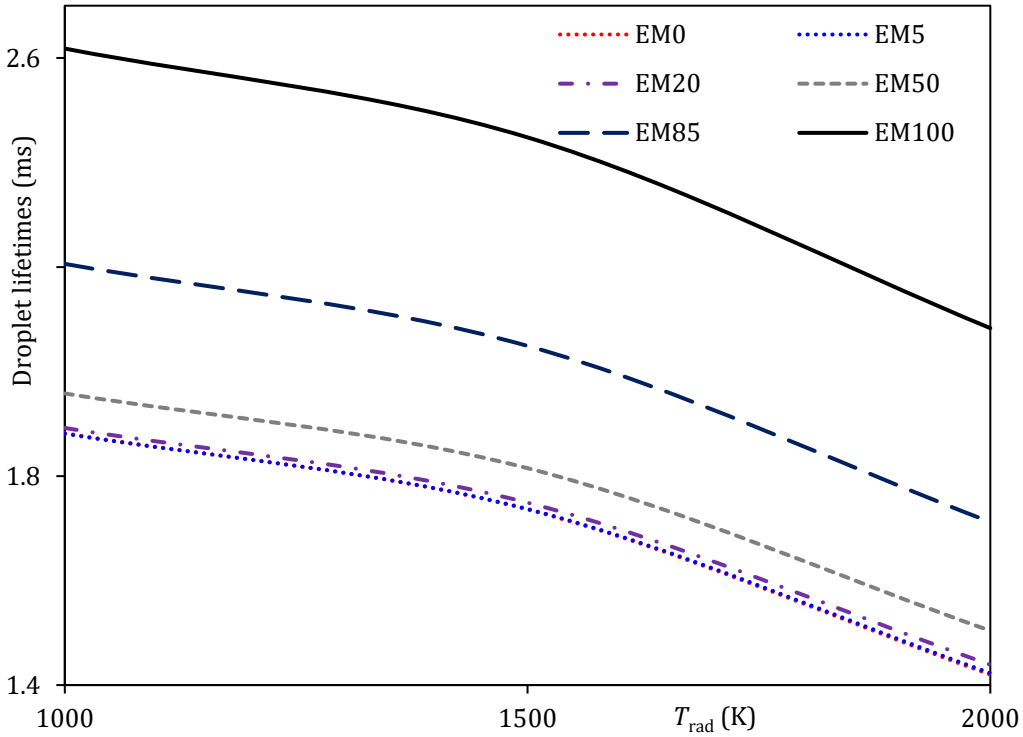

Figure 8. The estimated droplet lifetimes versus radiative temperatures T_{rad} for EM0–EM100 fuel blends, using the DMCM.

Table 6. The blended fuel droplet lifetimes when the effects of thermal radiation are taken into account and the estimated differences compared with the predictions of the model when radiation is ignored (Table 5), $\left(\text{Diff \%} = \frac{\text{time}_{\text{no rad}} - \text{time}_{\text{rad}}}{\text{time}_{\text{no rad}}} \times 100\right)$.

Blends	T_{rad}= 1000 K		T_{rad}= 1500 K		T_{rad}= 2000 K	
	time	Diff %	time	Diff %	time	Diff %
E0	1.882	5.33	1.736	12.67	1.420	28.57
E5	1.881	5.43	1.737	12.67	1.423	28.46
E20	1.892	5.11	1.749	12.29	1.439	27.83
E50	1.958	6.45	1.815	13.28	1.504	28.14
E85	2.206	6.37	2.049	13.03	1.712	27.33
E100	2.618	1.65	2.448	8.04	2.083	21.75

From Figure 8, it is clearly evident that the potential for radiation to reduce droplet lifetimes becomes more significant at higher radiative temperatures, as expected. Further illustrations of this effect are presented in Figure D1 in Appendix D. The blended fuel droplet lifetimes with and without accounting the effects of thermal radiation are presented in Table 6. From the latter table, one can see that the impact of radiation is less significant for blends with higher ethanol ratios compared to the cases when gasoline is dominant in the blends. This is related by the fact that the lifetimes of the droplets with high ethanol ratios are the longest.

The effect of ambient pressures on droplet lifetimes for EM0–EM100 fuel blends at ambient gas temperature 650 K is shown in Figure 9.

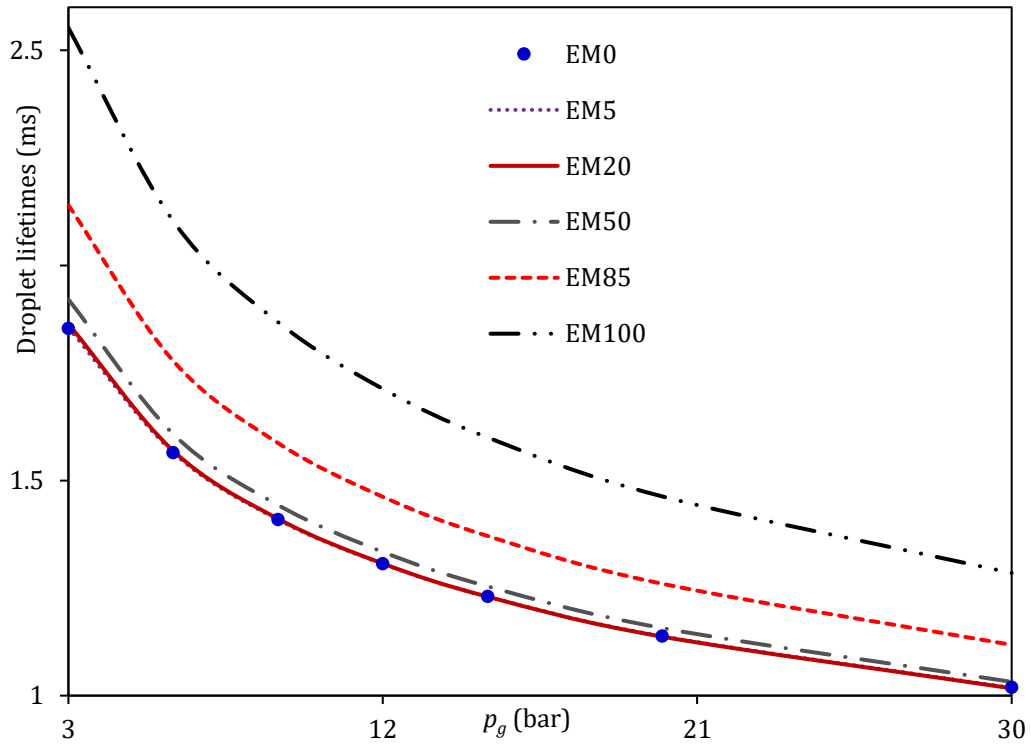

Figure 9. The effect of ambient pressures on droplet lifetimes for EM0–EM100 fuel blends, estimated at ambient gas temperature 650 K, using the DMCM. The effects of thermal radiation are ignored.

As shown in Figure 9, increasing the ambient pressure at a relatively high ambient temperature (650 K) leads to a reduction in estimated droplet lifetimes with almost the same effect for all mixtures (EM0–EM100, with higher droplet lifetimes for EM100 and

lower ones for EM0). Similar trends are observed when ambient temperatures are increased at a relatively low ambient pressure (3 bar) (see Figure 10).

As can be seen in Figure 10, at a relatively low ambient pressure (3 bar), increasing the ambient temperature noticeably reduces droplet lifetime. This effect becomes more significant at higher ambient pressure (30 bar), as shown in Figure 11.

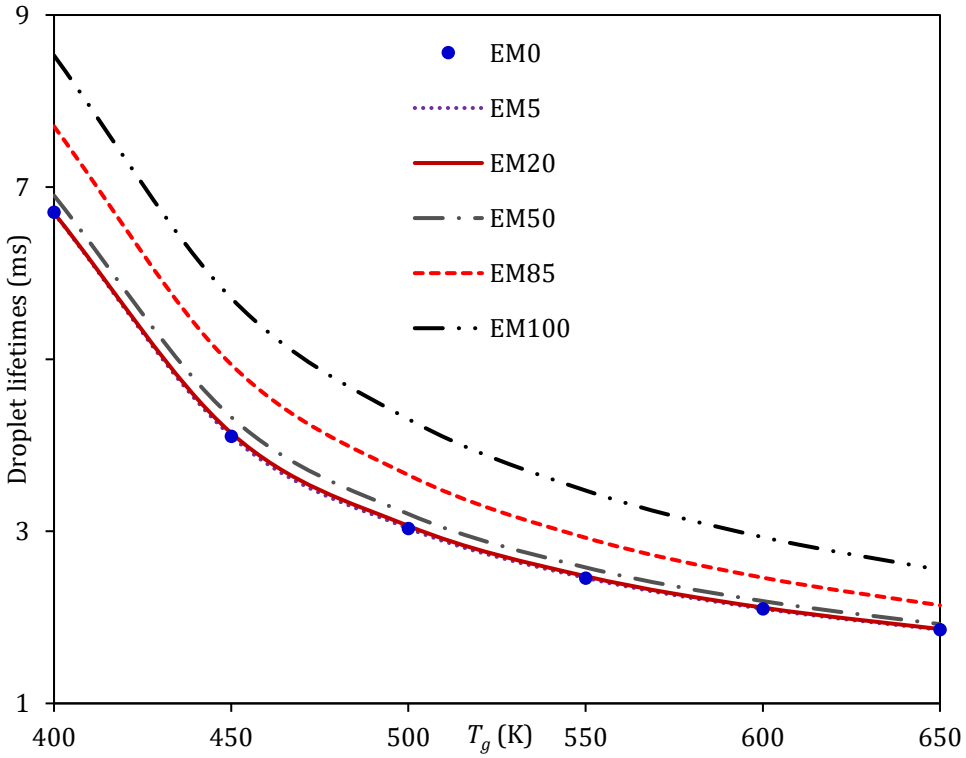

Figure 10. The effect of ambient temperatures on droplet lifetimes for EM0–EM100 fuel blends, estimated at ambient pressure of 3 bar, using the DMCM. The effects of thermal radiation are ignored.

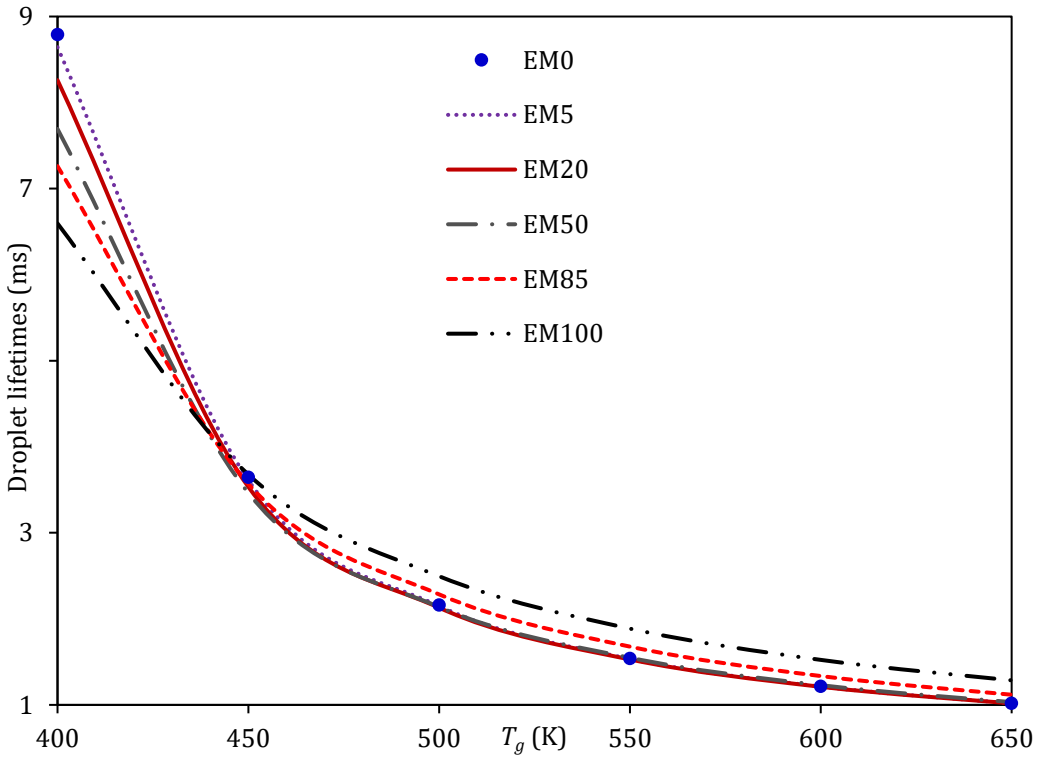

Figure 11. The effect of ambient temperatures on droplet lifetimes for EM0–EM100 fuel blends, estimated at ambient pressure of 30 bar, using the DMCM. The effects of thermal radiation are ignored.

To summarise, increasing radiative temperature, ambient pressure, or ambient temperature, always leads to a faster evaporation of ethanol/gasoline droplets, regardless of their blending fractions.

In Figures 5, 9 and 11, the general trends indicate slower evaporation for ethanol (EM100) droplets than for gasoline and ethanol/gasoline blend droplet (EM0–EM85). However, these trends are not the same at relatively low ambient gas temperatures ($\leq$ 400 K), as can be seen from Figure 12. At these temperatures, as follows from the latter figure, EM100 droplet evaporation can become slightly faster than that of EM0-EM85 droplets. The droplet lifetimes versus gas pressure for all mixtures under consideration for ambient gas temperature 400 K are presented in Figure 12.

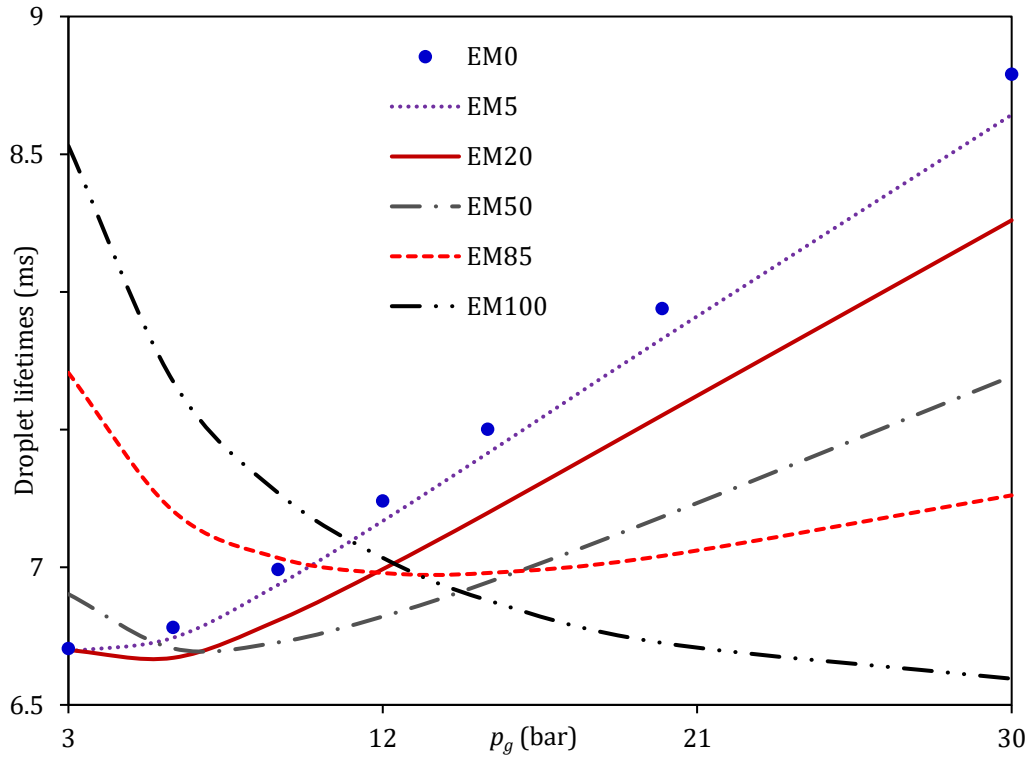

Figure 12. The effect of ambient pressures on droplet lifetimes for EM0–EM100 fuel blends, estimated at ambient temperature 400K, using the DMCM. The effects of thermal radiation are ignored.

As can be seen in Figure 12, ambient pressures have a different effect on the lifetimes of EM0–EM100 droplets to those shown in Figures 6 and 11 for the same fuels, but at higher ambient temperatures (> 400 K). The full evolution of droplet radii and surface temperatures of EM0, presented in Figures 9-12, are shown in Figures D2-D5 in Appendix D. The uncommon in-cylinder conditions, relatively low ambient temperatures (≤ 400 K) and high ambient pressures (≥ 12 bar), lead to lower droplet lifetimes for EM100 than for E0. This can be attributed to the different responses of the thermodynamic and transport properties of these fuels under these unique ambient conditions. This is due to the fact that, at high ambient pressure, the vapour pressure becomes more effective than the evaporation rate and diffusion coefficient. Hence, E100 has longer droplet lifetime than that of E0 at high pressures (≥ 12 bar). The opposite response is observed at low pressures (≤ 12 bar).

4.3. Impacts of the Activity Coefficient

As ethanol and gasoline form a highly non-ideal solution, the partial vapour pressure must be corrected by taking into account the AC. In some studies (e.g. [141]), the Wilson equation was used for the predictions of ACs. The Wilson equation is a simple approach but limited to binary components. In the general case, the UNIFAC model is believed to be the most suitable for prediction of the multi-component ACs [39,127].

In [142], the UNIFAC model was used to predict the ACs of 20 components in gasoline FACE C and 98 components in diesel fuel. This approach, however, was based on the initial molar fractions of components and droplet surface temperatures. In the current analysis, the impact of transient ACs on the evolutions of blended ethanol/gasoline fuel droplet temperatures and radii is investigated. The transient droplet surface temperatures and diffusion of 21 components are considered using the UNIFAC model.

4.3.1. Model validation

The total vapour pressure of E0–E100 ethanol/gasoline blends, predicted using the UNIFAC model, was validated against experimental data provided in [143] as shown in Figure 13. Note that the difference between the vapour pressure predicted by the transient UNIFAC model and the experimental results presented in [143] can be at least partly attributed to the differences between gasoline FACE C and the gasoline used in the experiments (New Zealand regular grade unleaded gasoline). None the less, the thermodynamic and transport properties of these fuels, however, were found to be reasonably close.

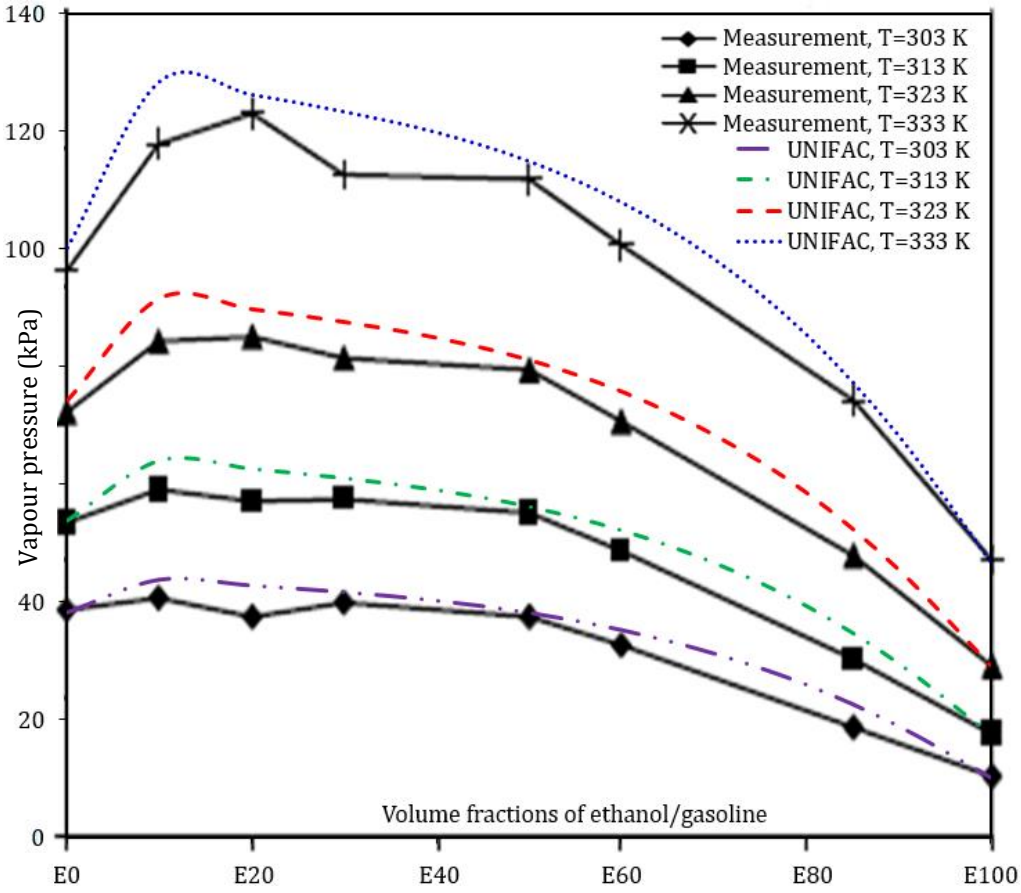

Figure 13. The predicted and experimentally observed total vapour pressures of ethanol/gasoline blends at various temperatures and ethanol volume fractions in the liquid phase [143].

4.3.2. Predictions of heating and evaporation

The total vapour pressures versus molar fractions of ethanol/gasoline in the liquid phase (indicated as EMX, where X is the percentage of ethanol in the mixture) at 296 K and 350 K are presented in Figure 14. In this figure, a comparison between the two approaches, Raoult's and UNIFAC, is shown. In Raoult's law, the AC is equal to unity, while in the UNIFAC model, the values of multi-component ACs are used.

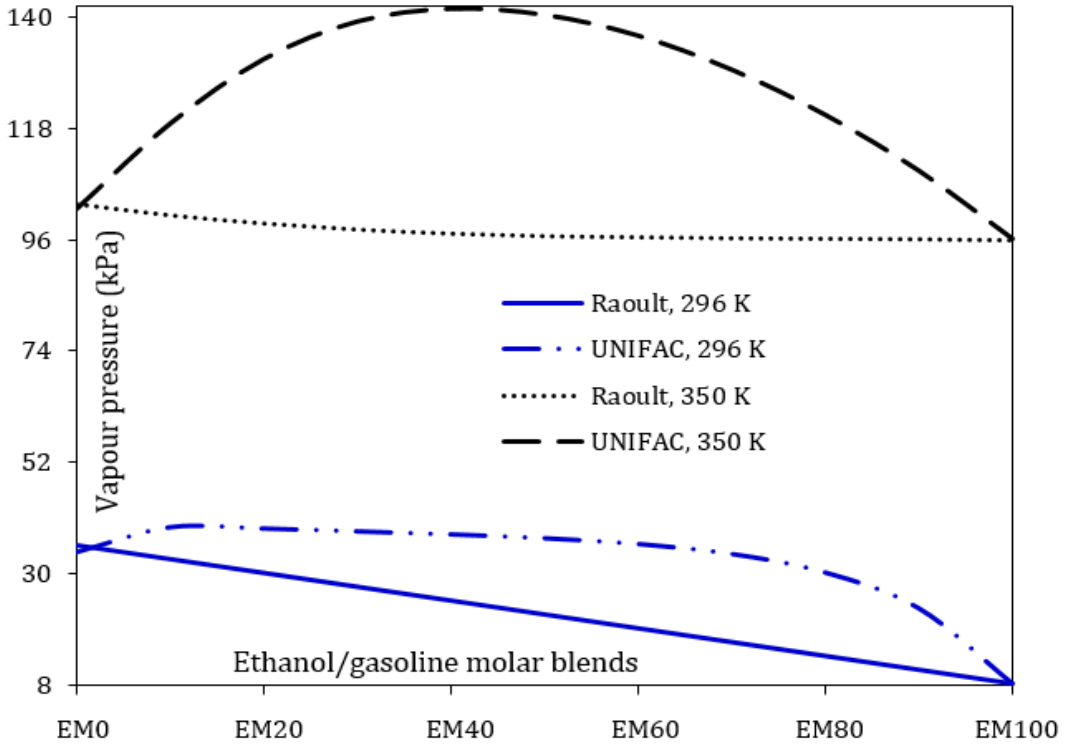

Figure 14. Total vapour pressure of various ethanol/gasoline molar blends (EM0–EM100), predicted by Raoult's law and the UNIFAC model at $T = 296$ K and 350 K.

As can be seen from Figure 14, the multi-component ACs have significant impact on the predictions of the total vapour pressure of ethanol/gasoline blends. For low ethanol molar fractions, breaks in the hydrogen bonds lead to a reduction in the inter-molecular forces [144]. This leads to an increase in the total vapour pressure. For high ethanol molar fractions, however, this pressure decreases as the contribution of the hydrogen bonds becomes important [144]. These predictions agree with those inferred from the experimental results presented in [143,145,146] (see Figure 13).

The heating and evaporation of blended ethanol/gasoline fuel droplets was also investigated using the same operating conditions as in Section 4.2 but taking into account the impacts of non-unity ACs. The evolutions of droplet surface temperatures T_s and radii R_d versus time for various initial ethanol molar fractions (EM85, EM50, EM20 and EM5) are shown in Figure 15. In this figure, the results predicted by four models are compared. The first one (labelled 'Ethanol/iso-octane') is based on the transient UNIFAC model to predict

the ACs for a binary mixture, in which gasoline fuel is approximated with iso-octane. The second one (labelled 'Raoult') is based on the assumption that the AC is equal to one, taking into account the full composition (21 components) of ethanol/gasoline fuel blend. The third model (labelled 'Steady UNIFAC') is based on the steady-state UNIFAC model, in which the ACs are predicted based on the initial liquid fuel composition (21 components of gasoline and ethanol fuels) and temperature. In the fourth model (labelled 'Transient UNIFAC'), the ACs are calculated based on the surface compositions and temperatures at each time-step.

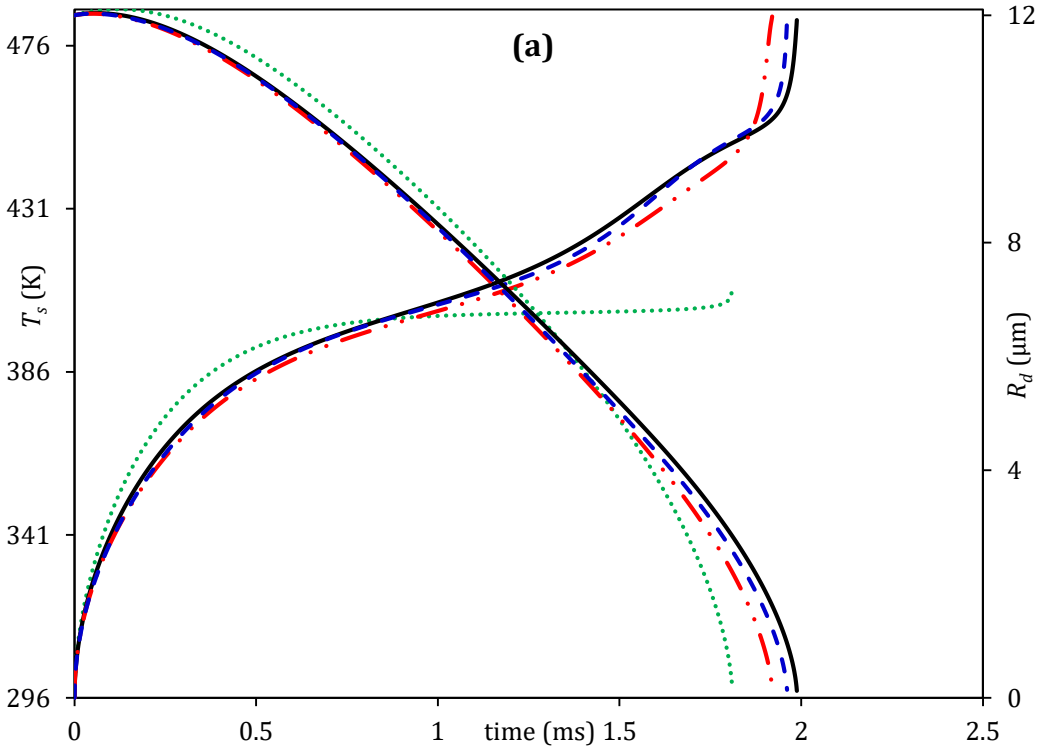

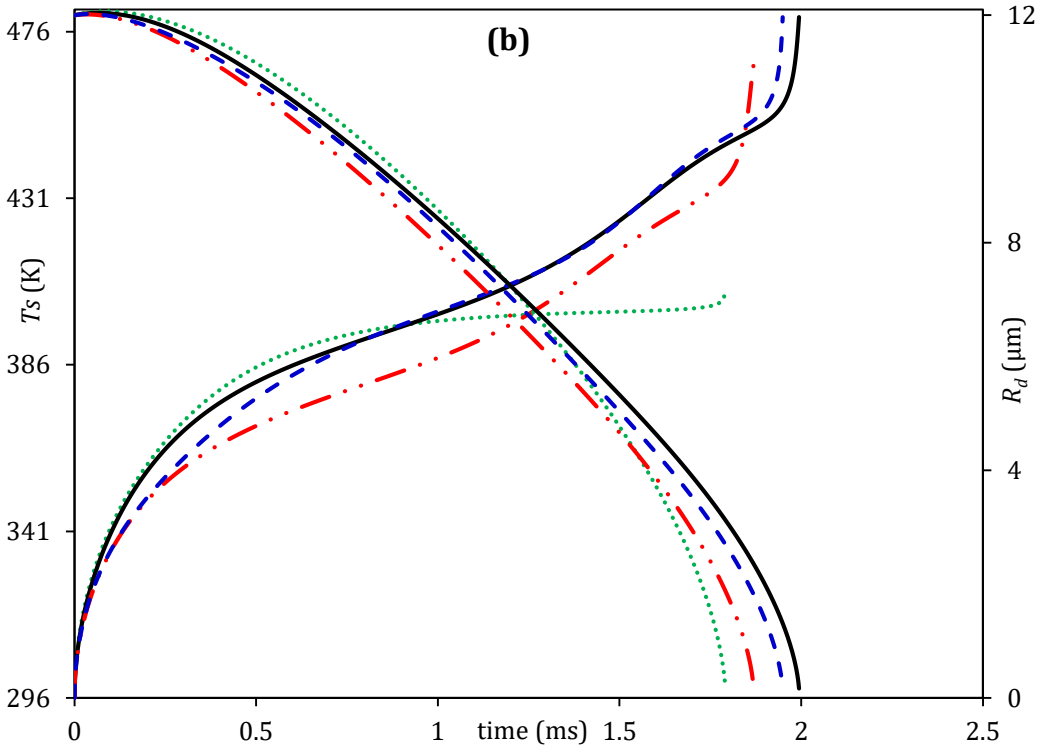
(b)
476
431
386
341
296
Ts (K)
12
8
4
0
Rd (µm)
0
0.5
1
time (ms)
1.5
2
2.5

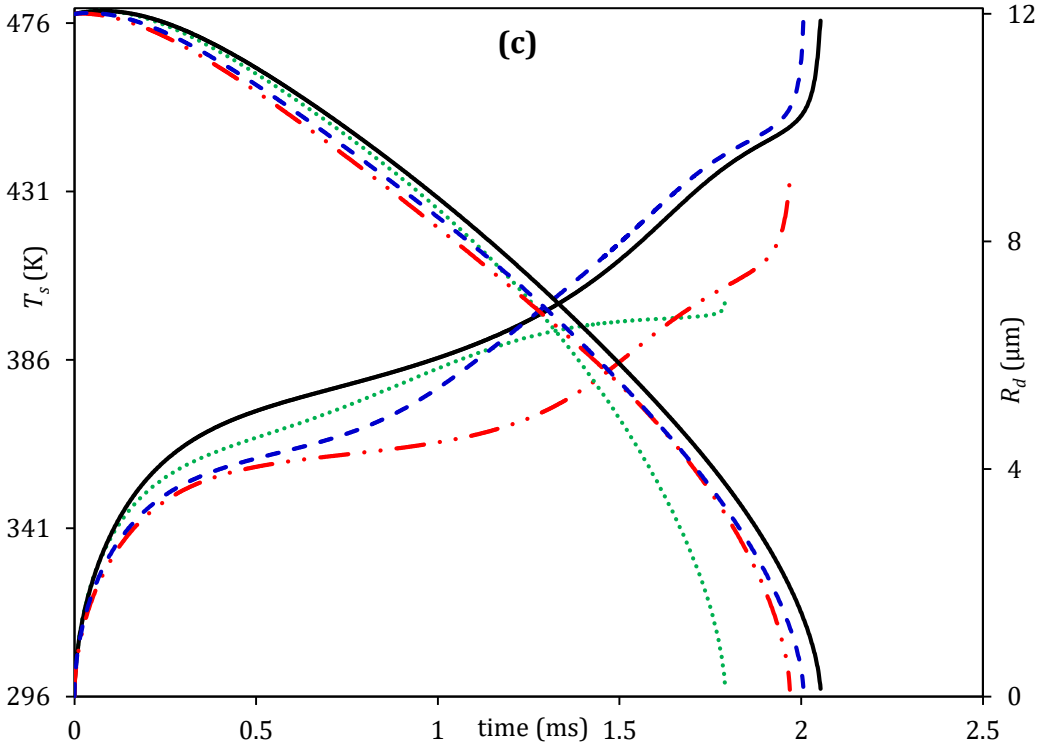
(c)
476
431
386
341
296
Ts (K)
12
8
4
0
Rd (µm)
0
0.5
1
time (ms)
1.5
2
2.5

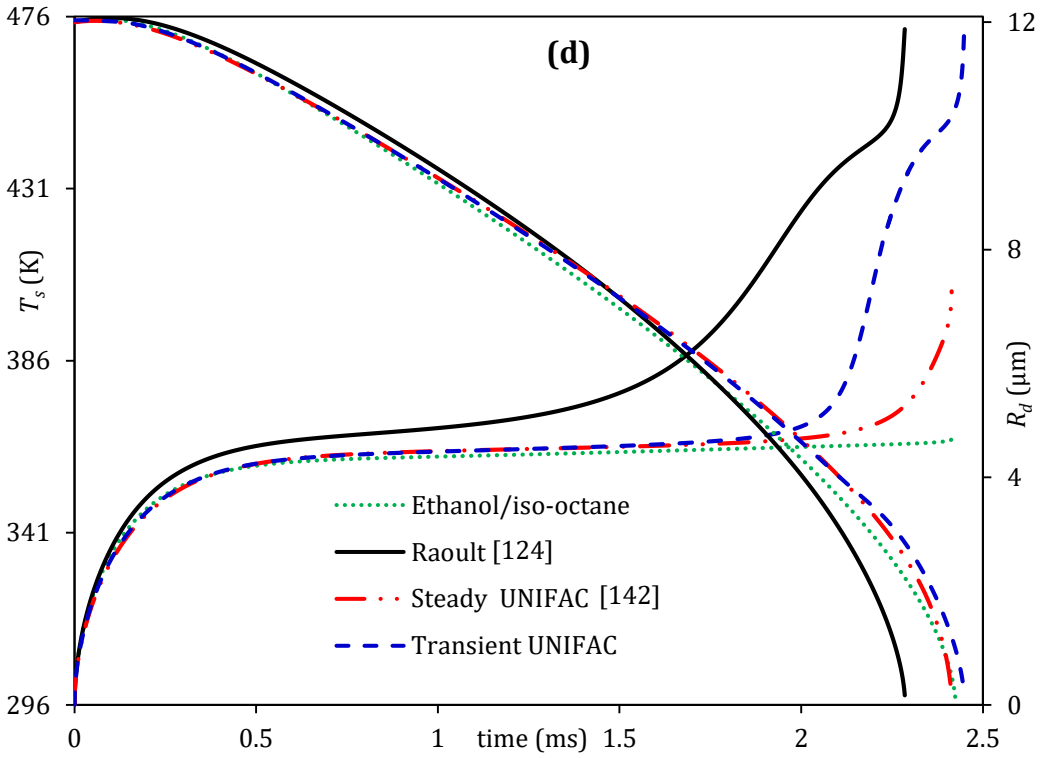

Figure 15. Droplet surface temperatures and radii versus time for EM5 (a), EM20 (b), EM85 (c) and EM85 (d) blends for various approaches to calculating the total vapour pressures at droplet surfaces.

As can be seen in Figure 15, the predicted droplet lifetimes and surface temperatures strongly depend on the type of model used to estimate the ACs. The approximation of gasoline by a single component (iso-octane) leads to significant underpredictions of droplet surface temperatures and lifetimes. These underpredictions can be as much as 22.6% and 10.7% for droplet surface temperatures and lifetimes, respectively. The predictions of droplet lifetimes using the steady-state UNIFAC model show reasonable agreement with those predicted using the transient UNIFAC model (ACs are calculated using the molar fractions of components and droplet surface temperatures at each time step). The latter two models, however, predict rather different droplet surface temperatures. Using the steady-state UNIFAC model can lead to about 14.7% error in the prediction of droplet surface temperatures, compared to those predicted using the transient approach. This is related to high dependency of the ACs on the liquid molar fractions at the surface of the droplet. The accuracy of the transient UNIFAC model is illustrated in comparison to the experimental

data, as in Figure 13. Assuming a steady UNIFAC model gives similar trends to those in Figure 14 where the vapour pressure shows linear relationship with the fuel fractions. The assumption of unity ACs leads to underpredicted ethanol/gasoline droplet lifetimes by up to 6.7%, compared with those predicted using the transient UNIFAC model. A significant impact of ACs on droplet heating and evaporation can be attributed to the fact that ethanol and gasoline fuels form blends which are far from ideal due to the high polarity of ethanol [140,145]. Hence, Raoult's law is not recommended for predicting the vapour pressures of such blends.

The droplet lifetimes and surface temperatures for various volume fractions of ethanol/gasoline fuel blends and their differences compared to E0 (pure gasoline), taking into account the multi-component ACs, are presented in Table 7. The following volume fractions of the components were considered: E0, E5, E20, E30 E50 and E85 (EX refers to a mixture of X% volume fraction of ethanol and (100-X) % volume fraction of gasoline).

Table 7. The impact of ethanol/gasoline fuel blends on estimated droplet lifetimes (in ms) and surface temperatures (in K) taking into account transient multi-component ACs $\left(\text{Diff }\% = \frac{|\text{lifetime}, T_{s\,\text{Blend}} - \text{lifetime}, T_{s\,\text{E0}}|}{\text{lifetime}, T_{s\,\text{E0}}} \times 100\right)$.

blend	lifetime	Diff %	T_s	Diff %
E0	1.968	-	483.7	-
E5	1.954	0.71	482.0	0.35
E20	1.964	0.20	478.2	1.14
E30	2.031	3.20	476.0	1.59
E50	2.241	13.9	475.5	1.70
E85	2.563	30.2	471.4	2.54

As can be seen from Table 7, in contrast to the results presented in Section 4.2, the droplet lifetimes of E5 and E20 are shorter than those of E0. This is attributed to the higher total vapour pressure of the mixture (calculated using the transient ACs) than predicted in

Section 4.2. In Tables 8 and 9, the results of droplet lifetimes and surface temperatures, obtained using Raoult's law and the transient UNIFAC model for E0–E85 blends, are compared. As these tables show, the errors in calculating droplet lifetimes and surface temperatures, using Raoult's law, can reach up to 5.7% and 0.4%, respectively.

Table 8. The estimated errors in prediction of droplet lifetimes (in ms) based on Raoult's law compared to the case where the transient UNIFAC approach is used $\left(\text{error \% } (\boldsymbol{\varepsilon}\ \%) = \frac{|\text{lifetime}_{\text{UNIFAC}} - \text{lifetime}_{\text{Raoult}}|}{\text{lifetime}_{\text{UNIFAC}}} \times 100\right)$.

blend	lifetime, UNIFAC	lifetime, Raoult	$\boldsymbol{\varepsilon}$ %
E0	1.968	1.988	1.02
E5	1.954	1.989	1.79
E20	1.964	2.021	2.90
E30	2.031	2.058	1.33
E50	2.241	2.156	3.79
E85	2.563	2.418	5.66

Table 9. The estimated errors in prediction of droplet surface temperatures (in K) based on Raoult's law compared to the case where the transient UNIFAC approach is used $\left(\text{error \% } (\boldsymbol{\varepsilon}\ \%) = \frac{|T_{s\ \text{UNIFAC}} - T_{s\ \text{Raoult}}|}{T_{s\ \text{UNIFAC}}} \times 100\right)$.

blend	T_s, UNIFAC	T_s, Raoult	$\boldsymbol{\varepsilon}$ %
E0	483.7	483.2	0.10
E5	482.0	481.5	0.11
E20	478.2	478.2	0.00
E30	476.0	476.8	0.17
E50	475.5	473.6	0.40
E85	471.4	473.1	0.36

4.4. Summary of Chapter 4

The previously suggested model (Discrete Multi-Component Model (DMCM)) was applied for droplet heating and evaporation of gasoline, ethanol and their blends. The DMCM took

into account the temperature gradient, recirculation, and species diffusion inside droplets. In contrast to all previous studies, the DMCM was improved to take into account the impact of the radiative temperature and the impact of the vapour-liquid equilibrium on the droplet heating and evaporation. The effects of ambient conditions (ambient pressure, ambient temperature and radiative temperature), and ethanol/gasoline fuel blend ratios on multi-component fuel droplet heating and evaporation were investigated. The ambient pressures, gas and radiative temperatures, and ethanol/gasoline fuel ratios are considered in the ranges 3–30 bar, 400–650 K, 1000–2000 K, and 0% (pure gasoline)–100% (pure ethanol), respectively.

Results revealed that gasoline fuel had less evaporation time than ethanol under realistic gasoline engine conditions. It was found that he evaporation time always increased with increasing the ethanol fraction on the expense of gasoline fraction. The droplet surface temperature for gasoline, however, was significantly higher than that of ethanol. For pure ethanol, the predicted droplet surface temperature was 24.3% lower, and lifetime 33.9% higher, than that for gasoline fuel under the same conditions. Taking into account radiation decreased the gasoline fuel droplet evaporation times by up to 28.6%, and those of ethanol fuel droplets by up to 21.8%, compared to the cases where radiation was ignored.

The universal quasi-chemical functional–group activity coefficient model was used to predict the ACs of the blended ethanol and gasoline fuels approximated by 21 components. In contrast to previous studies, it was shown that droplet lifetimes predicted for pure gasoline were not always shorter than those predicted for ethanol/gasoline blends. They depended on the total vapour pressure of the mixture. Considering the ACs led to errors of up to 5.7% in droplet lifetime compared to the case where the ACs were ignored.

These findings proved the applicability of increasing the fractions of ethanol in gasoline and the possible use of the new blend for petrol engines without any modifications to meet the ongoing governmental regulations for reducing the GGE.

CHAPTER FIVE: Bio/Diesel-Fuel Blends

5.1. Overview

Diesel engines are, by far, the main power source of heavy duty vehicles and power generation systems because of their relatively high efficiencies [147]. Due to the common GGE (mainly carbon oxides and nitrogen oxides) associated with diesel engines, and its depletion as a fossil fuel, many investigations (e.g. [148–155]) have been carried out on the possible replacement of diesel fuel with blended fuels, such as ethanol, biodiesel and ethanol/gasoline (85% ethanol and 15% gasoline which is known as E85).

In this chapter, the possibility or replacing some of the diesel fractions by biodiesel and ethanol are investigated in terms of common physical and chemical characteristics, such as droplet heating and evaporation, Cetane Number (CN), viscosity and heating value. Also, the impacts of the maximal radiative temperatures and non-ideal behaviour of the vapour-liquid equilibrium are investigated. The impact of reducing the number of components on the predictions accuracy and CPU time is also investigated in this Chapter.

5.2. Biodiesel/Diesel Fuel Blends

The most used biofuel, in specific fractions in diesel fuel, is biodiesel due to relatively close CN and density to those of the diesel fuel. Compared to fossil fuel, biodiesel fuel has several advantages: it has less CO_2 emissions, higher flash point, and it is cost effective; in addition, the blend of biodiesel/diesel fuels can be used in diesel engines with minimal/no modifications [149,150]. According to the U.S. Environmental Protection Agency Tier I and Tier II standards (see [5] for details), Fatty Acid Methyl Ester (FAME) biodiesel types produced over the last decade pass the testing requirements for health effects [156].

5.2.1. Fuel compositions

The commercial diesel fuel used in the present work conforms to standard European Union fuel (EN590), formed of 98 hydrocarbons represented by 6 hydrocarbon groups and 3 characteristics components which are $C_{19}H_{34}$ (tricycloalkane), $C_{13}H_{12}$ (diaromatic), and $C_{14}H_{10}$ (phenanthrene). Molar fractions of various components in this fuel are presented in Table 10 [60].

Table 10. Molar fraction (%) of diesel fuel components.

Carbon no	alkanes	cycloalkanes	bicycloalkanes	alkylbenzenes	indanes & tetralines	naphthalenes
C8	0.308	-	-	0.497	-	-
C9	3.032	-	-	3.2357	-	-
C10	5.0541	0.6408	0.6926	5.3584	1.3157	1.9366
C11	3.163	1.8745	1.0524	0.9492	1.3632	2.5290
C12	2.6156	1.6951	0.9753	1.9149	1.1951	1.4012
C13	2.5439	1.2646	0.6611	0.6873	1.0652	0.7692
C14	2.6497	1.3633	0.5631	0.6469	0.8406	0.4879
C15	3.1646	1.2353	0.4314	0.4782	0.7051	0.3843
C16	2.6579	1.0449	0.4921	0.4564	0.6684	0.2854
C17	2.8605	1.0162	0.6529	0.4204	0.5598	0.2072
C18	3.2403	1.2848	0.6554	0.5234	0.5357	0.2358
C19	3.5296	1.3566	0.9901	0.3226	0.3403	0.2151
C20	2.2338	0.9961	0.1965	0.2848	0.3227	0.2256
C21	1.443	0.5374	0.0935	0.2032	0.1638	-
C22	0.799	0.304	0.0701	0.0969	0.0781	-
C23	0.3972	0.109	0.0488	0.0494	-	-
C24	0.1903	0.0755	0.0234	0.0473	-	-
C25	0.0997	0.0445	0.0169	-	-	-
C26	0.0425	0.0214	-	-	-	-
C27	0.0309	0.0155	-	-	-	-
Total %	40.65	14.88	7.62	16.17	9.15	8.68

The other 3 components considered were $C_{19}H_{34}$ (represents the tricycloalkane group (with molar fraction of 0.015647)), $C_{13}H_{12}$ (represents the diaromatic group (with molar fraction

of 0.01224)) and $C_{14}H_{10}$ (represents the phenanthrene group (with molar fraction of 0.006577)).

Twenty-two types of biodiesel fuels were blended with diesel using the authors' solver to investigate their heating and evaporation processes. These are: Tallow Methyl Ester (TME), Lard Methyl Ester (LME), Butter Methyl Ester (BME), Coconut Methyl Ester (CME), Palm Kernel Methyl Ester (PMK), Palm Methyl Ester (PME), Safflower Methyl Ester (SFE), Peanut Methyl Ester (PTE), Cottonseed Methyl Ester (CSE), Corn Methyl Ester (CNE), Sunflower Methyl Ester (SNE), Soybean Methyl Ester (SME), Rapeseed Methyl Ester (RME), Linseed Methyl Ester (LNE), Tung Methyl Ester (TGE), Hemp-oil Methyl Ester, produced from Hemp seed oil in Ukraine (HM1), Hemp-oil Methyl Ester, produced in European Union (HM2), Canola seed methyl ester (CAN), Waste cooking-oil Methyl Ester (WCO), Camelina methyl ester (CML), Jatropha methyl ester (JTR) and Yellow grease methyl ester (YGR). Four fractions of biodiesel/diesel blends were investigated; these are 5% biodiesel with 95% diesel fuels (B5), 20% biodiesel with 80% diesel fuels (B20), 50% biodiesel with 50% diesel fuels (B50), pure biodiesel (B100) and pure diesel fuels (B0). The molar fractions of these biodiesel fuels are illustrated in Tables 11 and 12.

Table 11. Biodiesel fuel compositions (:0,1,2,3,4 refer to the number of double bonds in the component's structure) [63].

Methyl esters	Biodiesel Fuels										
	TME	LME	BME	CME	PMK	PME	SFE	PTE	CSE	CNE	SNE
C8:0	-	-	5.2	6.0	2.6	-	-	-	-	-	-
C10:0	-	-	2.8	8.0	4.0	-	-	-	-	-	-
C12:0	0.2	-	3.4	50.0	50.0	0.3	-	-	-	-	-
C14:0	2.5	1.0	11.0	15.0	17.0	1.3	-	0.5	2.0	1.0	-
C15:0	-	-	-	-	-	-	-	-	-	-	-
C16:0	27.9	26.0	31.7	9.0	8.0	45.1	5.2	8.0	19.0	9.0	5.9
C17:0	-	-	-	-	-	-	-	-	-	-	-
C18:0	23.0	14.0	10.8	3.0	1.7	4.5	2.2	4.0	2.0	2.5	4.2
C20:0	0.4	-	0.4	-	1.5	0.4	-	7.0	-	-	1.4
C22:0	0.4	-	0.4	-	1.5	0.2	-	7.0	-	-	1.4
C24:0	-	-	-	-	-	-	-	-	-	-	-
C16:1	2.5	2.8	2.4	-	0.4	0.2	-	1.5	-	1.5	-
C17:1	-	-	-	-	-	-	-	-	-	-	-
C18:1	40.0	44.0	26.3	7.0	12.0	38.4	76.4	49.0	31.0	40.0	18.5
C20:1	0.3	2.0	1.0	-	-	-	-	-	2.5	1.0	-
C22:1	0.3	2.0	1.0	-	-	-	-	-	2.5	1.0	-
C24:1	-	-	-	-	-	-	-	-	-	-	-
C18:2	2.0	8.0	3.0	2.0	1.3	9.2	16.2	23.0	41.0	44.0	68.3
C20:2	-	-	-	-	-	-	-	-	-	-	-
C18:3	-	-	0.6	-	-	0.2	-	-	-	-	0.3
C20:3	-	-	-	-	-	-	-	-	-	-	-
C18:4	-	-	-	-	-	-	-	-	-	-	-
Others	0.5	0.2	-	-	-	0.2	-	-	-	-	-

Table 12. Biodiesel fuel compositions (continued).

Methyl esters	Biodiesel Fuels										
	TGE	HM1	SME	LNE	HM2	CAN	WCO	RME	CML	JTR	YGR
C8:0	-	-	-	-	-	-	-	-	-	-	-
C10:0	-	-	-	-	-	-	-	-	-	-	-
C12:0	-	-	-	-	-	-	0.2	-	0.4	0.1	0.2
C14:0	-	-	0.3	0.2	-	-	0.7	-	2.6	0.3	0.8
C15:0	-	-	-	-	-	-	-	-	-	-	0.1
C16:0	3.6	6.6	10.9	6.2	6.5	4.5	15.7	4.9	5.8	14.3	16.0
C17:0	-	0.2	-	-	-	0.1	0.2	-	-	0.1	0.1
C18:0	2.6	2.1	4.4	0.6	2.5	2.0	6.1	1.7	2.7	5.9	6.9
C20:0	-	0.5	0.4	-	0.9	0.6	0.4	0.6	1.3	0.2	0.3
C22:0	13.1	0.3	-	-	-	0.4	0.4	-	0.9	0.2	0.4
C24:0	-	0.2	-	-	-	0.2	0.3	-	0.7	2.5	0.2
C16:1	-	0.3	-	-	-	0.4	0.7	-	-	1.0	0.9
C17:1	-	-	-	-	-	-	-	-	-	-	0.1
C18:1	10.1	11.9	24.0	18.0	11.9	59.7	42.8	26.6	15.9	38.9	43.2
C20:1	0.8	0.3	-	-	0.9	1.5	0.6	-	13.7	0.1	0.5
C22:1	-	0.2	-	-	-	0.4	0.2	22.3	2.9	0.1	0.1
C24:1	-	0.2	-	-	-	-	-	0.8	0.2	0.1	4.3
C18:2	13.8	56.6	52.8	16.0	54.7	20.8	29.4	24.8	16.0	34.8	24.3
C20:2	-	-	-	-	-	-	-	-	1.4	-	-
C18:3	51.6	20.6	7.2	59.0	20.1	9.4	2.0	9.7	33.8	0.3	1.1
C20:3	-	-	-	-	-	-	-	-	0.8	-	-
C18:4	-	-	-	-	-	-	-	-	-	-	0.5
Others	4.4	-	-	-	2.5	-	0.3	8.6	0.9	1.1	-

The properties of diesel and biodiesel are illustrated in Appendices D and E, respectively. The liquid and vapour diffusion coefficients are provided in Appendix F. The average values

of the liquid properties were estimated based on appropriate formulae as illustrated in Appendix G.

5.2.2. Impacts of biodiesel/diesel fuel blends

The Discrete Multi Component Model (DMCM) was facilitated for the analysis of heating and evaporation of biodiesel/diesel fuel droplets of initial radius $R_{do} = 12$ μm and temperature $T_o = 360$ K. The droplet was moving at $U_d = 10$ m.s^{-1} in still air of pressure and temperature equal to $p_g = 30$ bar and $T_g = 800$ K, respectively. The evolutions of droplet surface temperatures (T_s) and radii (R_d) for B0, B5, B20, B50, B80, and B100 fuels of twenty-two types of biodiesel fuels were analysed. Typical results from these analyses are presented in Figures 16 and 17.

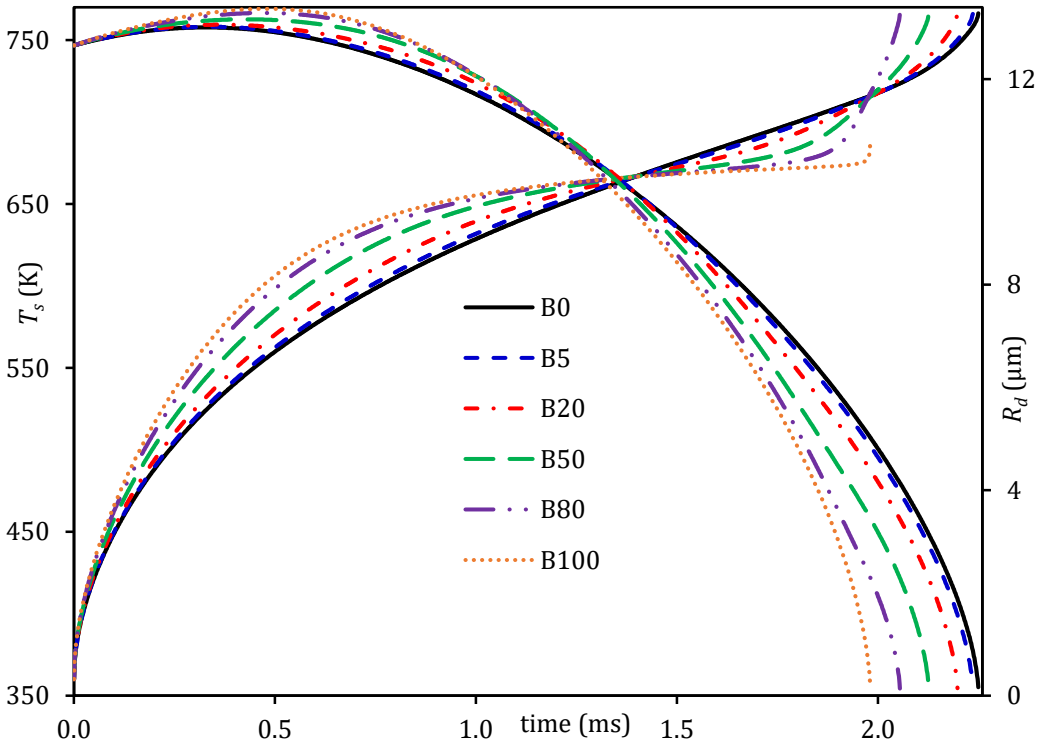

Figure 16. Droplet surface temperatures and radii versus time for various SME/diesel fuel blends.

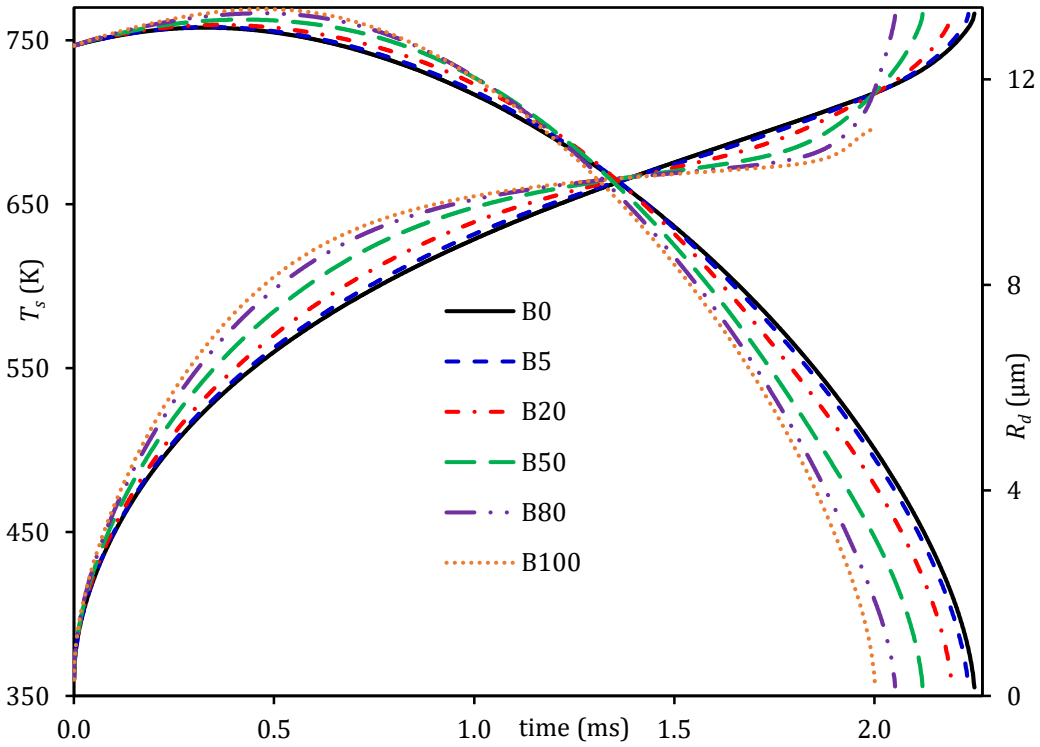

Figure 17. Droplet surface temperatures and radii versus time for various WCO/diesel fuel blends.

In Figures 16 and 17, one can see that increasing the fraction of biodiesel fuel from B5 to B100 has a noticeable effect on the evolution of T_s and R_d for both SME and WCO fuels. The predicted droplet surface temperature of B100 is higher than that of B5 during the initial heating period. This is attributed to a sudden increase in biodiesel fuel density, compared with a relatively small increase in diesel fuel density. According to [73], the increase in droplet surface temperature can enhance the droplet break-up process due to the decrease in droplet surface tension (droplet's surface tension decreases with increasing the its surface temperature). The droplet lifetimes of SME and WCO biodiesel fuels blended with B0 fuel and their deviations from those predicted for B0 fuel (2.25ms) are presented in Table 13.

Table 13. Estimation of the droplet lifetimes (in ms) of biodiesel/diesel blends and their differences compared with B0 droplet lifetime (2.25 ms), $\left(\text{Diff }\% = \frac{\text{lifetime}_{B0} - \text{lifetime}_{\text{blend}}}{\text{lifetime}_{B0}}\right) \times 100$.

Blends	Biodiesel Fuels			
	SME		WCO	
	Lifetime	Diff %	Lifetime	Diff %
B5	2.236	0.62	2.237	0.57
B20	2.198	2.31	2.194	2.49
B50	2.127	5.47	2.121	5.73
B80	2.055	8.67	2.052	8.80
100	1.981	11.96	2.002	11.02

As can be seen from Table 13, the droplet lifetime for B100 (SME) fuel is 12% less than that for B0. This reduction does not exceed 0.7% for the B5 fuel blend for the same fuel. Also, the droplet lifetime of the WCO biodiesel fuel droplet is noticeably close to that of the SME droplet; it is 12% and 0.7% shorter for the B100 and B5 blends, respectively. The deviation in droplet lifetimes for B100 of both SME and WCO may not be ignored in most engineering applications; for B5 it can be tolerated in some engineering applications.

A full illustration of the droplet lifetime results for the other 20 types of biodiesel fuels are shown in Table 14. The droplet lifetimes of 20 types of biodiesel fuels mixtures with diesel fuel and their differences from the one predicted for B0 (2.25ms) are presented in this table.

Table 14. Estimation of biodiesel and biodiesel/diesel fuel droplets lifetimes (in ms) and their differences compared with those of B0 fuel (2.25 ms).

Biodiesel fuels	B100		B50		B20		B5	
	Lifetime	Diff %	Lifetime	Diff %	Lifetime	Diff %	Lifetime	Diff %
TME	1.967	12.6	2.102	6.6	2.184	2.9	2.232	0.80
LME	1.995	11.3	2.114	6.0	2.190	2.7	2.234	0.71
BME	1.943	13.6	2.089	7.2	2.180	3.1	2.232	0.80
CME	1.765	21.6	2.036	9.5	2.166	3.7	2.229	0.93
PMK	1.846	18.0	2.050	8.9	2.169	3.6	2.230	0.89
PME	1.944	13.6	2.097	6.8	2.183	3.0	2.232	0.80
SFE	1.980	12.0	2.122	5.7	2.195	2.4	2.235	0.67
PTE	2.052	8.8	2.138	5.0	2.199	2.3	2.236	0.62
CSE	2.014	10.5	2.128	5.4	2.197	2.4	2.236	0.62
CNE	2.002	11.0	2.128	5.4	2.197	2.4	2.236	0.62
SNE	2.011	10.6	2.132	5.2	2.200	2.2	2.237	0.58
RME	2.131	5.3	2.188	2.8	2.222	1.2	2.242	0.36
LNE	1.991	11.5	2.141	4.8	2.206	2.0	2.239	0.49
TGE	2.085	7.3	2.160	4.0	2.211	1.7	2.240	0.44
HME1	2.022	10.1	2.138	5.0	2.203	2.1	2.237	0.58
HME2	1.994	11.4	2.135	5.1	2.202	2.1	2.238	0.53
CAN	2.014	10.5	2.130	5.3	2.199	2.3	2.236	0.62
CML	2.064	8.3	2.153	4.3	2.209	1.8	2.239	0.49
JTR	2.047	9.0	2.133	5.2	2.198	2.3	2.236	0.62
YGR	2.077	7.7	2.149	4.5	2.203	2.1	2.237	0.58

As can be seen from Table 14, the droplet lifetime for B100 of RME fuel is 6% less than that of B0. This reduction does not exceed 0.4% for the B5 fuel blend for the same fuel. Also, droplet lifetime of TGE biodiesel fuel droplet is noticeably close to that of B0 droplet; it is less than 8% and 0.5% for B100 and B5 mixtures, respectively. The maximum difference in droplet lifetimes for these fuels is up to 21. 6% (B100 CME), which cannot be sacrificed in

any engineering application, and it is always higher than 5.29% (RME) compared to B0, which may be tolerated in some limited engineering applications.

Several past studies (see [64,73] for example) analysed the heating and evaporation of B0 fuel droplets, and compared with the results of biodiesel/diesel blends. For instance, in [64], the droplet lifetime for B100 of WCO was shown to be 11% less than that of B0. While in [73], the droplet lifetime for B100 of SME fuel was shown to be 6 % less than that for B0. In this study, too similar trends were predicted for the same fuels. This prediction, however, was different for the other types of biodiesel fuel presented in this work. For example, the B100 droplet lifetimes for CME and PMK biodiesel fuels showed deviations of 21.6% and 18%, respectively, from that of B0 fuel.

A general trend shows that droplets' lifetimes of all 22 types of B5 biodiesel/diesel blends that are used in this study deviate with less than 1% from the one predicated for B0 droplets. This concludes the possibility of labelling biodiesel/diesel blends fuel pumps, with up to about 5% biodiesel concentration, without modifying the automotive system is achievable. For some fuel blends (for example B20 RME, TGE, LNE, and HME1), this deviation (up to 2%) is still relatively negligible to mix higher biodiesel concentrations (for example, 20% biodiesel and 80% diesel fuels) without losing the main feature of these processes (i.e. droplet lifetime).

The difference in vapour pressures and enthalpies of evaporation between hydrocarbons and methyl esters is the main reason for the influence of biodiesel fuel fractions on the heating and evaporation of diesel fuel droplets. For instance, when increasing the biodiesel fractions, the droplet surface temperature tends to reach a plateau during the evaporation process, which is similar to the case of single component model (see [113]). Additionally, the significance of such behaviour can change depending on the input parameters and ambient conditions.

5.2.3. Impacts of ambient conditions

In contrast to the findings in [60,64,73], where the radiative effects on the evaporation of droplets are shown to be negligible, the current analysis provides interesting updates to previous findings. In the model used in this research, the full composition of biodiesel/diesel fuel is considered, but with a simplified radiation model. The results of investigations under a range of diesel engine injection conditions, accounting for different radiation temperatures of B0 – B100 fuel blends (based on SME and WCO biodiesel fuels), are presented in Figures 18 and 19, and Tables 15.

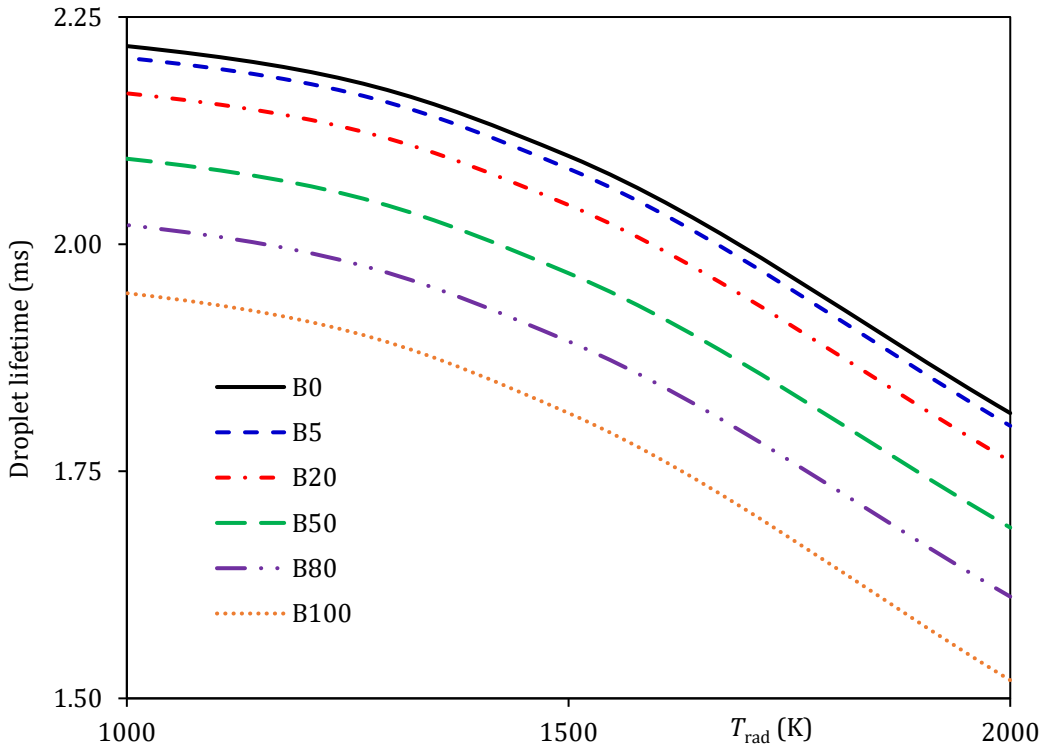

Figure 18. The estimated droplet lifetimes versus radiation temperatures T_{rad} for B0 – B100 SME/diesel fuel blends.

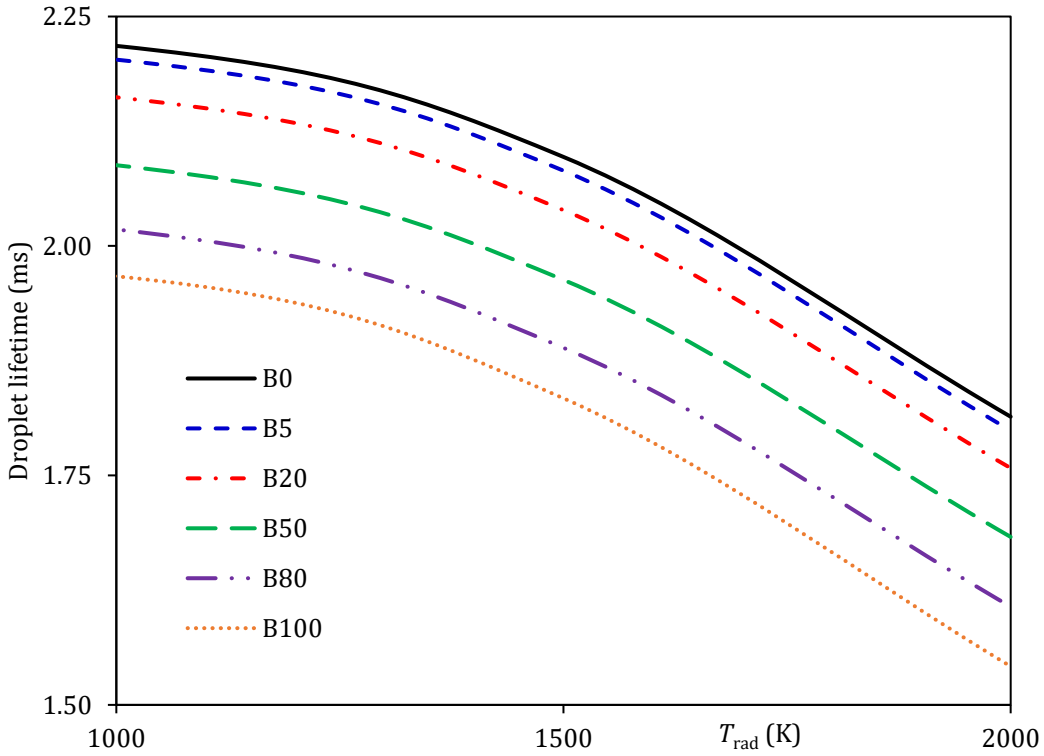

Figure 19. The estimated droplet lifetimes versus radiation temperatures T_{rad} for B0 – B100 WCO/diesel fuel blends.

Table 15. The blended fuel droplet lifetimes (in ms) under radiative effects and their estimated differences for the case when radiation is ignored, $\left(\text{Diff }\% = \frac{\text{lifetime}_{\text{no rad}} - \text{lifetime}_{\text{rad}}}{\text{lifetime}_{\text{no rad}}} \times 100\right)$.

Blends		No radiation	T_{rad}= 1000 K		T_{rad}= 1500 K		T_{rad} = 2000 K	
		time	time	Diff %	time	Diff %	time	Diff %
WCO	B0	2.250	2.218	1.42	2.097	6.80	1.814	19.38
	B5	2.237	2.203	1.52	2.082	6.93	1.799	19.54
	B20	2.198	2.162	1.64	2.039	7.23	1.758	20.02
	B50	2.127	2.091	1.70	1.963	7.71	1.683	20.87
	B80	2.052	2.016	1.75	1.889	7.94	1.607	21.69
	B100	2.002	1.964	1.89	1.834	8.40	1.542	22.97
SME	B0	2.250	2.218	1.42	2.097	6.80	1.814	19.38
	B5	2.236	2.204	1.43	2.083	6.84	1.800	19.50
	B20	2.198	2.166	1.46	2.043	7.05	1.761	19.88
	B50	2.127	2.094	1.55	1.968	7.48	1.688	20.64
	B80	2.055	2.021	1.65	1.893	7.88	1.612	21.56
	B100	1.981	1.946	1.77	1.814	8.43	1.520	23.27

As evident from Figures 18 and 19, the impact of radiation becomes more significant at high radiation temperatures. For instance, droplet lifetime is reduced by 19.4% and up to 23.3% for B0 and B100, respectively, when the radiation temperature is 2000 K. From the results presented in Table 15, the impact of radiative temperature on droplet lifetimes is seen to increase as the biodiesel fraction increases.

The effect of in-cylinder pressures and temperatures on the estimated droplet lifetimes for B0 – B100 fuel blends is presented in Figures 20-23. As follows from Figures 20 and 21, increasing ambient pressure at ambient temperature 800 K leads to a reduction in estimated droplet lifetimes with similar trends for all SME/diesel and WCO/diesel fuel blends. This effect is attributed to the fact that higher ambient pressure leads to increased gas density and a faster evaporation rate. Similar trends are observed for the impact of ambient temperatures on droplet lifetimes at ambient pressure $p_g = 30$ bar, as shown in Figures 22 and 23.

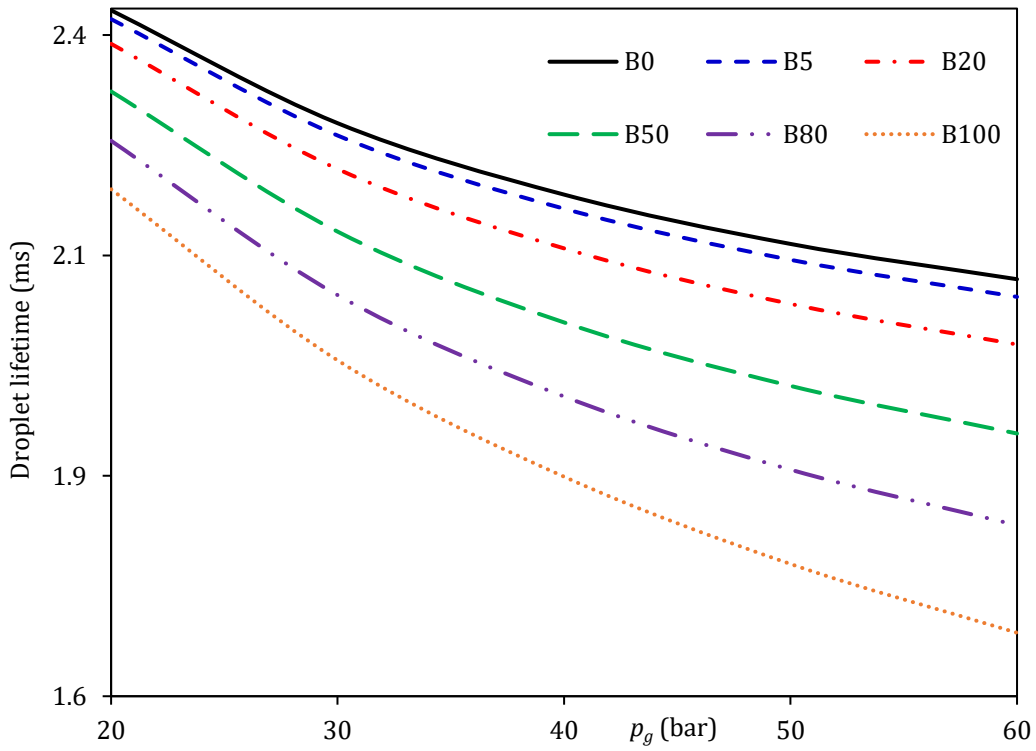

Figure 20. The impact of ambient pressures on droplet lifetimes for B0 – B100 of SME/diesel fuel blends at $T_g = 800$ K.

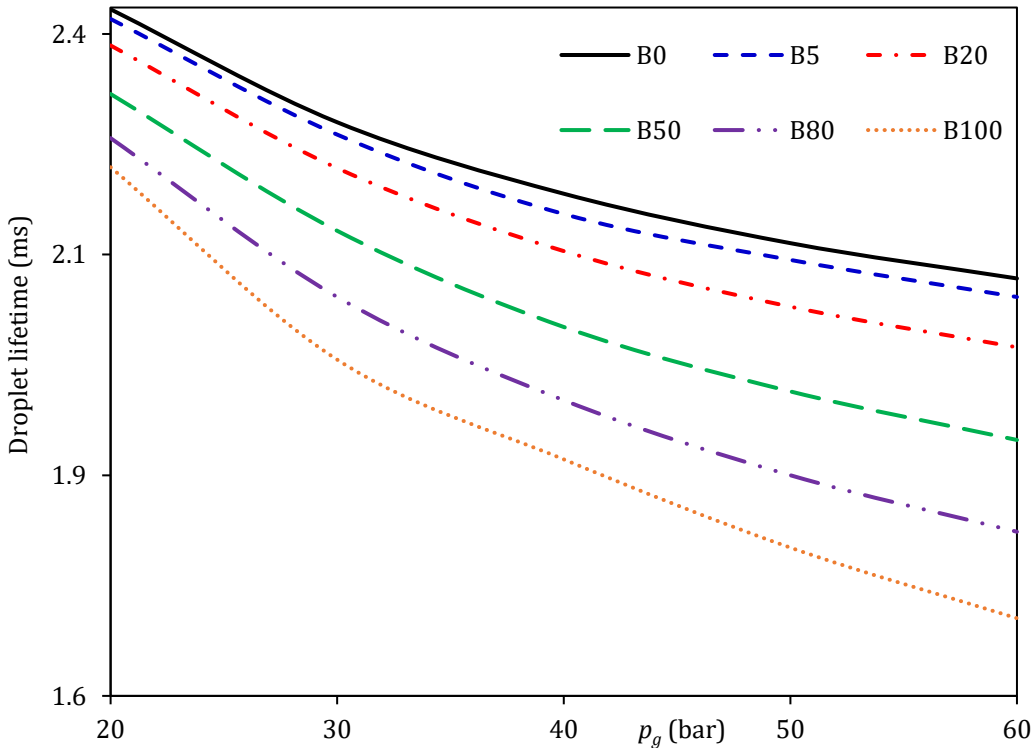

Figure 21. The impact of ambient pressures on droplet lifetimes for B0 – B100 of WCO/diesel fuel blends at $T_g = 800$ K.

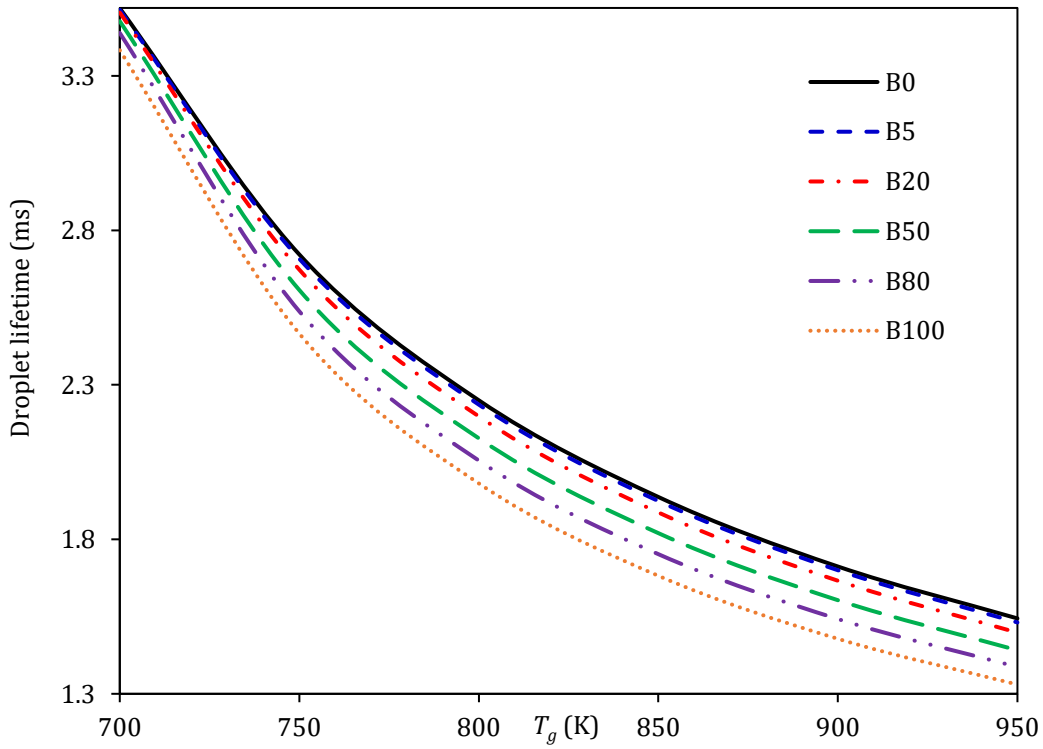

Figure 22. The impact of ambient temperatures on droplet lifetimes for B0 – B100 of SME/diesel fuel blends at $p_g = 30$ bar.

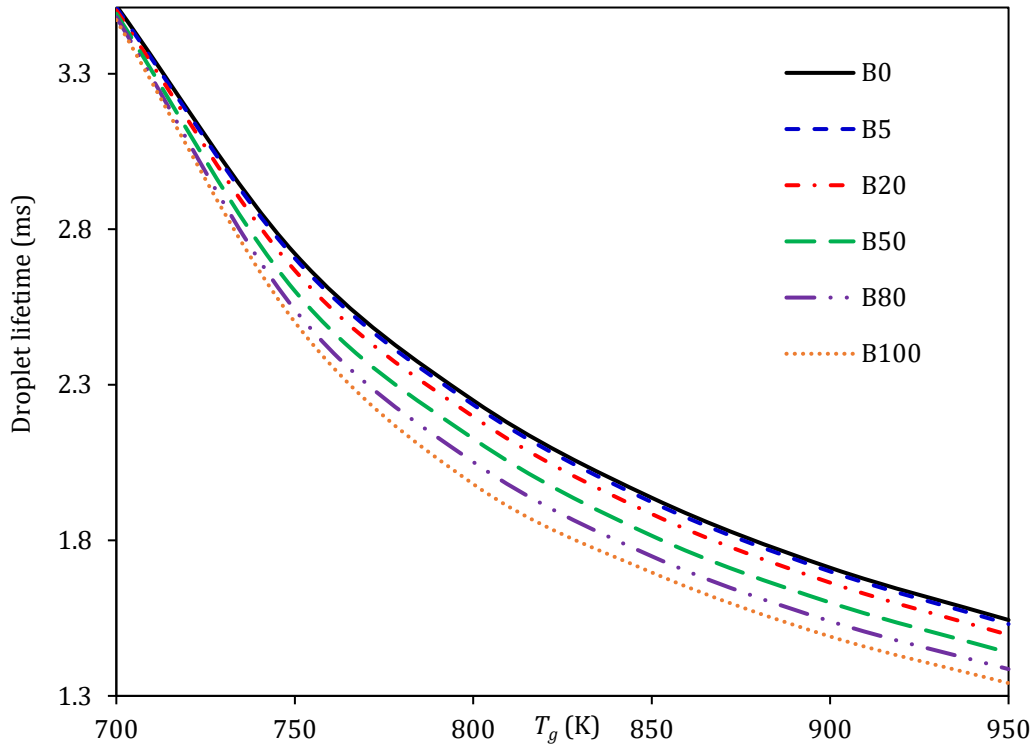

Figure 23. The impact of ambient temperatures on droplet lifetimes for B0 – B100 of WCO/diesel fuel blends at p_g = 30 bar.

As can be seen from Figures 22 and 23, ambient temperatures have a noticeable impact on reducing droplet lifetimes for all biodiesel/diesel fuel blends. Increasing the ambient temperature leads to a reduction in the liquid density and an increase in the vapour pressure. Thus, the evaporation rate increases. The full evolution of B0 fuel droplet radii and surface temperatures, presented in Figures 20-23, are shown in Figures F1 and F2 in Appendix F.

To summarise the findings, an increase in the radiative temperature, ambient pressure, or ambient temperature, leads to a faster evaporation of biodiesel/diesel fuel droplets, regardless of their blending fractions. The differences in droplet lifetimes for various biodiesel/diesel fractions are clearly observed for high ambient temperature and pressure. This can be attributed to the impact of these high conditions on the thermodynamic and transport properties. For instance, the partial vapour pressure of each individual component is proportional to the total ambient pressure. The influence of ambient pressure

on other properties, such as density, viscosity, specific heat capacity, latent heat of evaporation and thermal conductivity, depend on the ambient temperature.

5.3. E85-Diesel Fuel Blends

Ethanol and ethanol/gasoline mixtures have been shown to be suitable for blending with diesel fuels [147,157]. It is known that mixtures with up to 85% diesel and 15% ethanol are used in standard diesel engines without significant impacts on these engines [9]. Also, it has been reported in [10] that ethanol can be blended with diesel fuel at up to 20% ethanol. For higher fractions of ethanol, additives may become essential to attain the needed miscibility in order to stabilise the blend, control the phase separation, and attain the required cetane number [9,148,153,158–160].

The most common blend of diesel fuel is not pure ethanol but E85 fuel (E85 refers to 85% ethanol and 15% gasoline) [147,157,159,161]. The addition of 15% gasoline to ethanol is commonly used to improve the low temperature properties of the mixture and the cold start in diesel engines [159,162]. The results of experimental research, provided in [159], have shown that the presence of E85 in diesel fuel leads to a noticeable reduction in nitrogen oxides. This mixture, however, has also led to a noticeable increase in the ignition delay and an increase in the production of carbon monoxides. The combustion temperature decreases with increasing the E85-diesel fuel fraction, and the brake efficiency slightly increases for higher E85-diesel fuel fractions [159]. These effects, however, need to be treated cautiously; for instance, the addition of 20% E85 can lead to up to 16% increase in nitrogen oxides [159].

So far, the research on E85-diesel fuel blends has focused on the physical properties, exhaust toxic emissions and ignition of this fuel [147,157,159,161]. The impact of such blends, accounting for full fuel compositions, and their detailed species chemical structure and properties, on droplet heating and evaporation has not been studied anywhere in the

literature to the best of the author's knowledge. In this section, the analysis of Section 4.3 is generalised to the case of blended E85-diesel droplets, using the DMCM and Multi-Dimensional Quasi-Discrete Model (MDQDM). Note that, the composition of diesel fuel used in this section is same as that used in Section 5.2.

5.3.1. Model validation

The results of the application of the DMCM to investigate the evaporation of diesel fuel were validated against experimental data and verified against the results of other numerical simulations [163,164]. In these papers, diesel fuel was approximated by the following components (based on their mass fractions): 8% toluene (C_7H_8), 11% decane ($C_{10}H_{22}$), 21% dodecane ($C_{12}H_{26}$), 27% tetradecane ($C_{14}H_{30}$), 17% hexadecane ($C_{16}H_{34}$), and 16% octadecane ($C_{18}H_{38}$). Droplets with initial diameters of 0.86 mm (for ambient gas temperature $T = 523$ K), and 0.84 mm (for ambient gas temperature $T = 723$ K) with an initial temperature of 300 K were suspended at the tip of a quartz fibre [164]. The droplet relative velocities in a chamber with ambient pressure of 1 atm were 0.3 m/s. The ETC/ED models were used in [163]. Note that the authors of the latter paper state that 'the droplet temperature and composition were assumed to be uniform', which would contradict their claim that they used the ETC/ED models. It is believed that this was a typo and they were referring to the droplet surface temperature and composition.

The time evolutions of the normalised squared droplet diameters, predicted using the DMCM, were compared with the numerical results presented in [163] and experimental data provided in [164]. The results of the comparison are shown in Figure 24. As follows from this figure, the predictions from the author's computational solver are close to the numerical and experimental data.

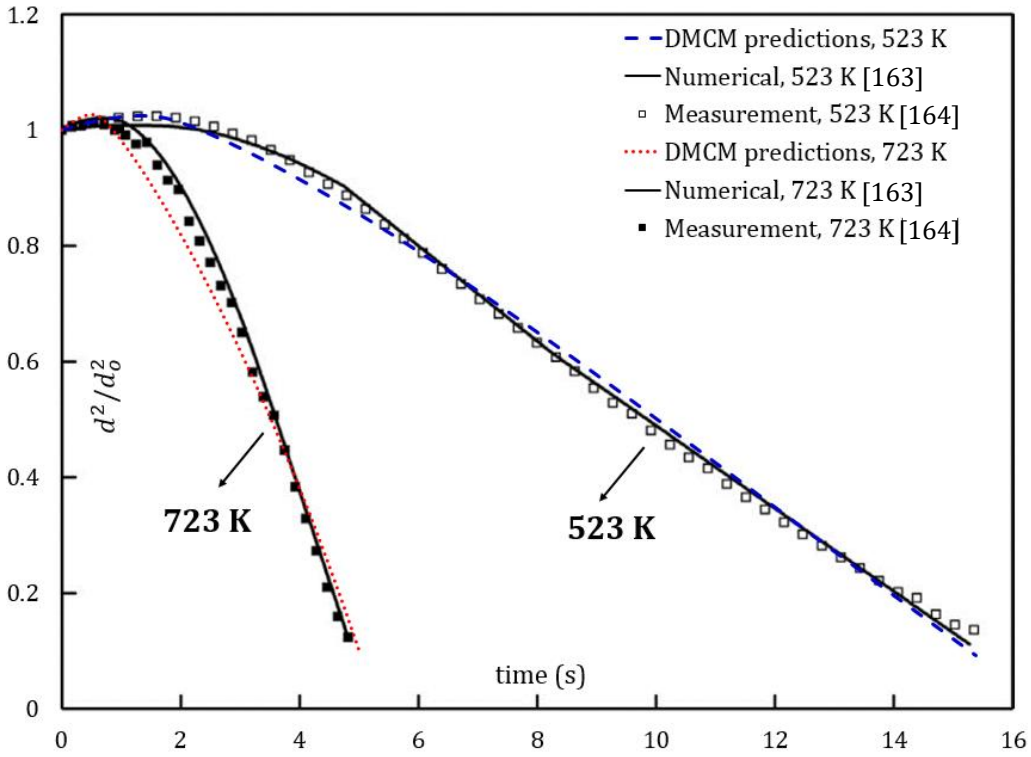

Figure 24. Normalised squared diameters of diesel fuel (represented by 6 components) droplets versus time [163,164].

5.3.2. Predictions of the DMCM

The impacts of various volume fractions of E85-diesel fuel blends on droplet heating and evaporation were investigated using the DMCM, where the contribution of 98, 119 and 21 components were considered for the full number of components (i.e. without any approximation or ignoring any components) of pure diesel, 4 mixtures of E85-diesel blends and pure E85, respectively, as shown in Tables 4 and 10. The following volume fractions of E85-diesel fuels were considered: pure diesel, E85-5 (5% E85 and 95% diesel), E85-20 (20% E85 and 80% diesel), E85-50 (50% E85 and 50% diesel), and E85. The partial vapour pressures of the components of the blended fuel were calculated taking into account the non-unity ACs for up to 119 components using the UNIFAC model. The same ambient conditions and input parameters, used in Section 5.2, were used in this section. The time evolution of droplet radii (R_d) and surface temperatures (T_s) for various E85-diesel fuel blends are shown in Figures 25 and 26, respectively.

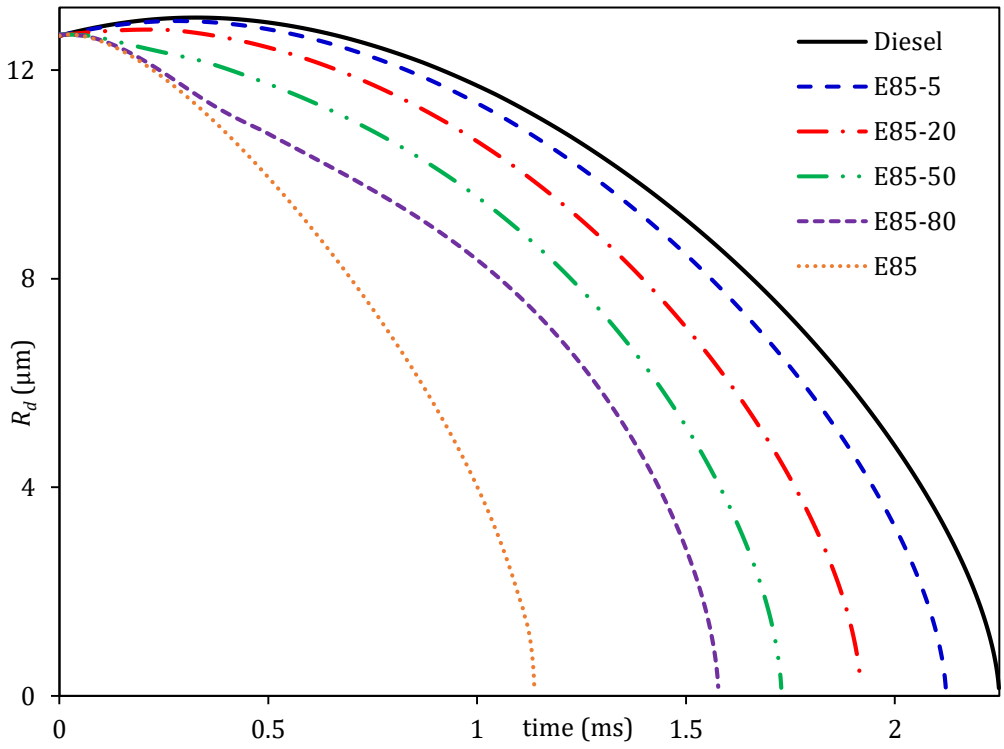

Figure 25. Droplet radii versus time for various E85-diesel blends.

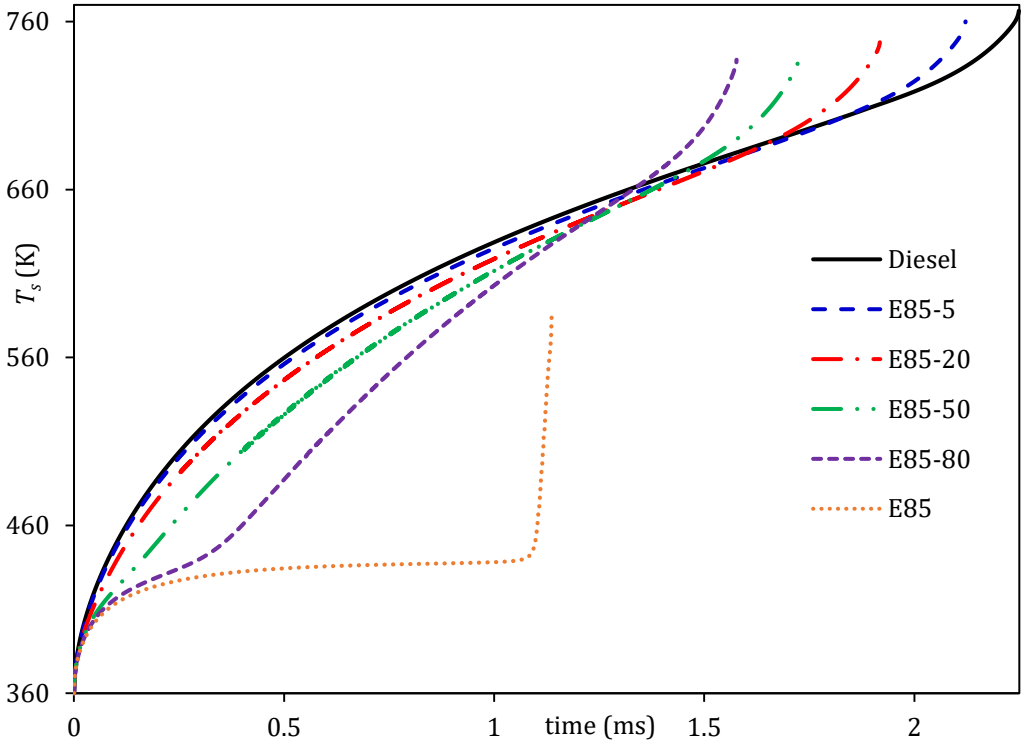

Figure 26. Droplet surface temperatures versus time for various E85-diesel blends.

As follows from Figure 25, droplet lifetime for pure diesel is longer than that for any blend. It decreases as the E85 fraction increases. The difference in droplet lifetime for E85-5 compared to pure diesel is 5.7%. This difference reaches 49.5% for pure E85. This significant reduction in droplet lifetime is ascribed to the fact that E85 is more volatile than pure diesel and has a saturation vapour pressure of 107 KPa (at $T = 360$ K). It is worth noting here that it is only 2.3 kPa for the pure diesel at the same temperature.

As can be seen from Figure 26, droplet surface temperature decreases with increasing E85 volume fractions. For E85-5, it is up to 0.78% less than that of pure diesel. This reduction is as high as 3.4% for E85-50 and reached 23.4% for pure E85. This difference is attributed to the fact that the heat capacity of ethanol is noticeably higher than that of diesel fuel. In agreement with the previous studies, droplet surface temperatures do not show plateau profiles due to the diffusion of components in droplets [73,165].

The temperature distribution inside the droplet is shown in Figure 27 at time instants 0.02, 0.3, 0.5 and 1 ms. As can be seen from the figure, the temperature difference between the droplet centre and its surface can reach up to 9.2 %. The results shown in Figure 27 should be treated with care for the case of non-zero droplet relative velocities, since the ETC/ED models were primarily developed for prediction of the average surface temperatures and species mass fractions in moving droplets.

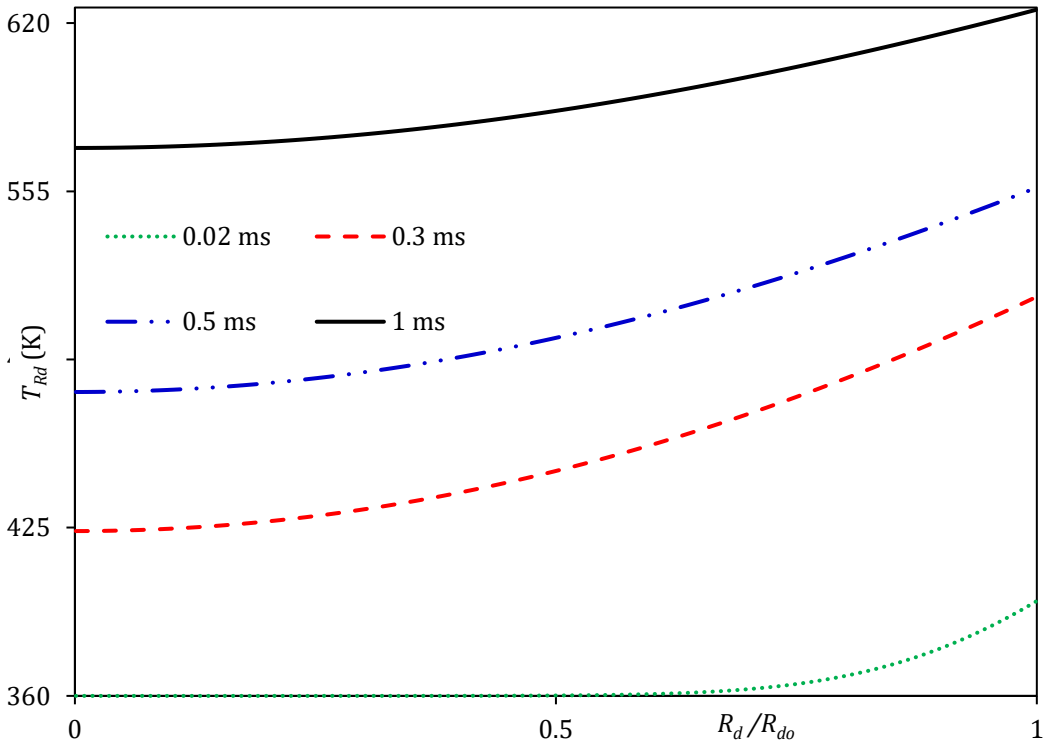

Figure 27. Temperature inside droplet versus normalised distance from the centre of droplet for E85-5 blend at time instants 0.02, 0.3, 0.5 and 1 ms.

The distillation characteristics of E85-5 and pure E85, estimated using the ETC/ED models are presented in Figure 28. The ambient conditions for these cases are same as the cases in Figures 25-27. As can be seen from the figure, the percentage volume recovered as distillate, for pure E85, starts at $T = 403$ K and ends (100% recovered) at $T = 440$ K, which is less than the average boiling point of pure E85 at $p = 30$ bar. For the E85-5 mixture, the percentage volume recovered starts at $T = 438$ K and ends at $T = 760$ K. The sudden increase in droplet surface temperature without any volume recovered, for the latter mixture, is ascribed to the fact that the lighter components (E85) are evaporated and the remaining are only the diesel components which start evaporating at $T = 584$ K. This behaviour is similar to that observed in [140]. Such behaviour cannot be predicted if the ETC/ED models were not used.

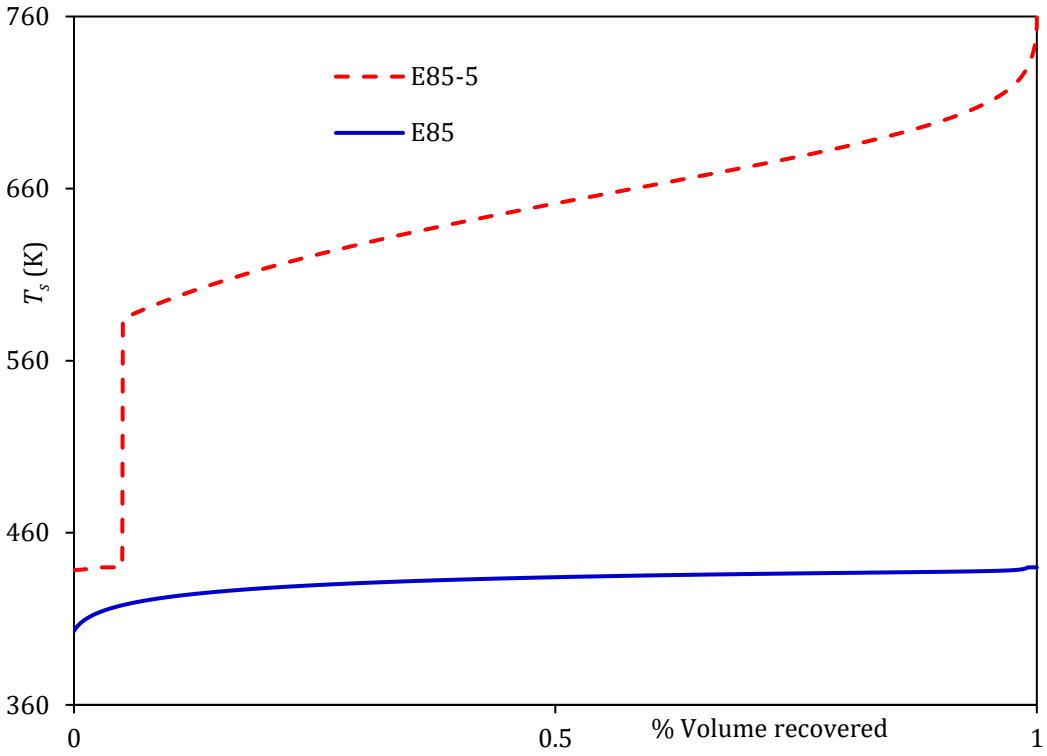

Figure 28. Droplet surface temperature versus percentage volume recovered as distillate for E85-5 and pure E85 using the ETC/ED models.

To assess the impact of the non-ideality of the liquid phase on the estimated droplet lifetimes and surface temperatures, a comparison between the results based on the two activity coefficients (the unity and UNIFAC) for E85-5 and E85-20 fuel blends is shown in Figure 29. One can see from this figure that the droplet lifetime predicted, using the UNIFAC model, is about 3.6% shorter than that based on the assumption of a unity activity coefficient. This is attributed to the fact that the non-ideal mixture entails a higher vapour pressure, due to the presence of ethanol, compared to the ideal mixture. Hence, the faster evaporation rates and shorter droplet lifetimes. Although the impact of the ACs on droplet lifetime was too small, causing only up to 3.6% shorter droplet lifetime, these had significant impacts on vapour pressure with up to 29% high vapour pressure when considering the impacts of ACs (see Figure 14, Chapter 4).

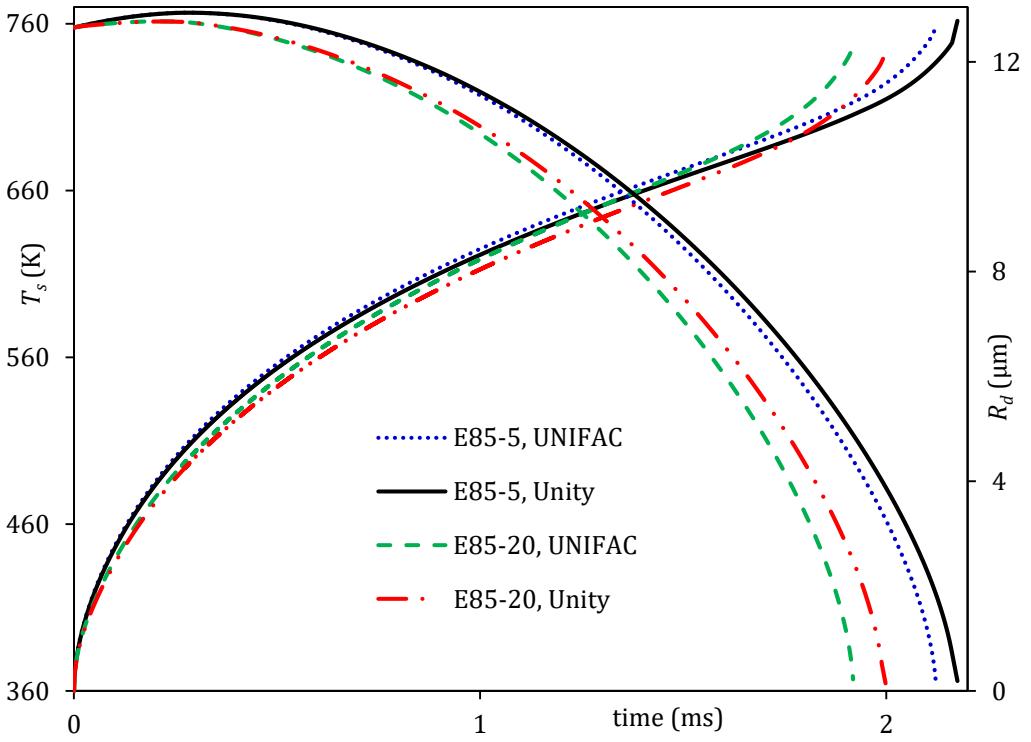

Figure 29. Evolution of droplet radii and surface temperatures for E85-5 and E85-20 blends.

The time evolution of nine selected (out of 119) species mass fractions for E85-5 blend is shown in Figure 30. The selected components are: $C_{10}H_{22}$, $C_{19}H_{40}$, $C_{27}H_{56}$ (the alkane group), $C_{20}H_{40}$, $C_{27}H_{54}$ (the cycloalkane group), $C_{12}H_{18}$, $C_{24}H_{42}$ (the alkylbenzene group), C_8H_{18} (iso-octane in gasoline) and C_2H_5OH (ethanol). As evident from the figure, the mass fractions of the lighter components in the blend (e.g., C_2H_5OH, C_8H_{18} and $C_{10}H_{22}$) decrease monotonically with time, while the mass fractions of the intermediate components initially increase at the expense of lighter components and then decrease with time. The mass fractions of heavy components ($C_{27}H_{56}$ and $C_{27}H_{54}$) increase until they become the dominant ones, although they have very small fractions initially.

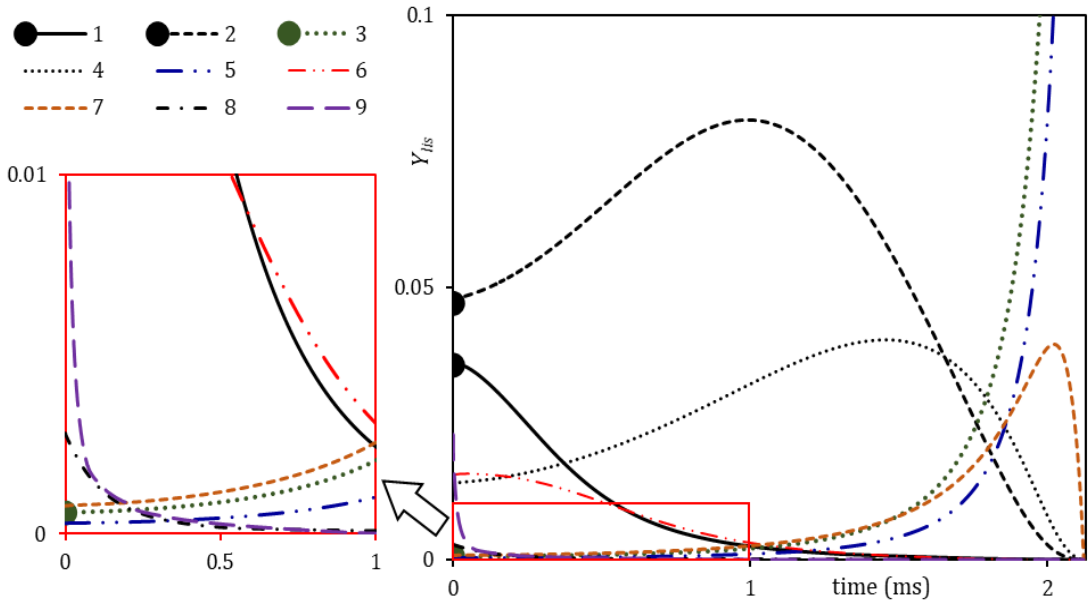

Figure 30. The plots of surface mass fractions Y_{lis} of 9 representative components of the E85-5 blend versus time. The plots for the following components are shown: $C_{10}H_{22}$ (1), $C_{19}H_{40}$ (2), $C_{27}H_{56}$ (3), $C_{20}H_{40}$ (4), $C_{27}H_{54}$ (5), $C_{12}H_{18}$ (6), $C_{24}H_{42}$ (7), C_8H_{18} (8) and C_2H_5OH (9).

5.3.3. Predictions of the MDQDM

The MDQDM was also used to analyse E85-5 droplets. The input parameters and ambient conditions were the same as those used for the analysis based on the DMCM. The impacts of various approximations of 119 components of E85-5 blends on the predictions of droplet radii and surface temperatures are shown in Figures 31 and 32, respectively. These approximations are: 90, 63, 45, 20 and 16 C/QC (see Table H in Appendix H for details).

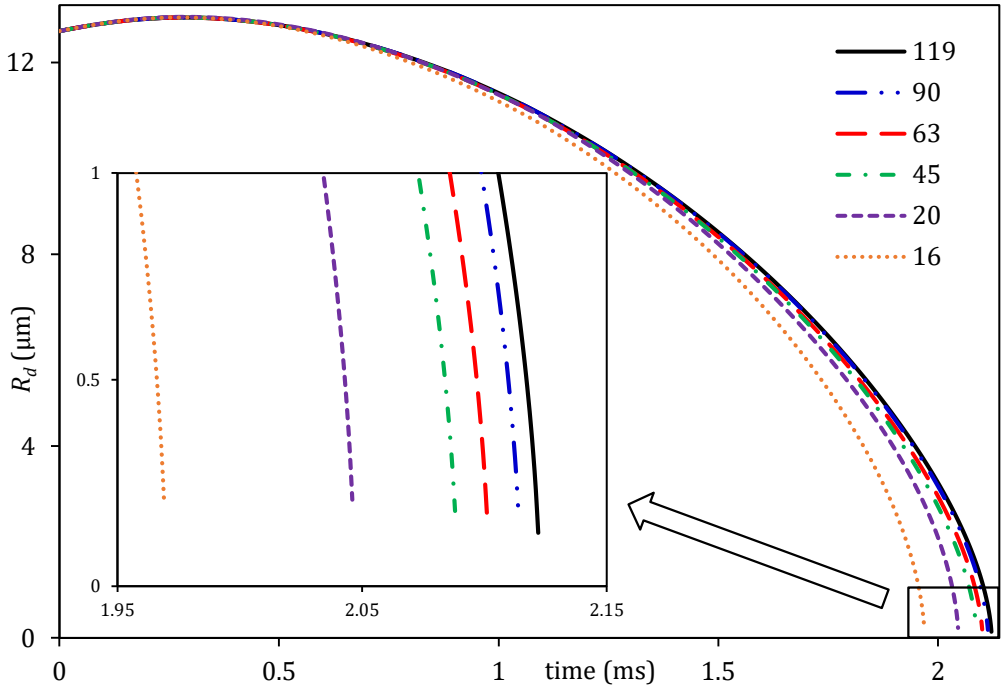

Figure 31. Droplet radii versus time for six approximations of E85-5: 119 components using the DMCM, and 90, 63, 45, 20 and 16 C/QC (numbers near the curves) using the MDQDM.

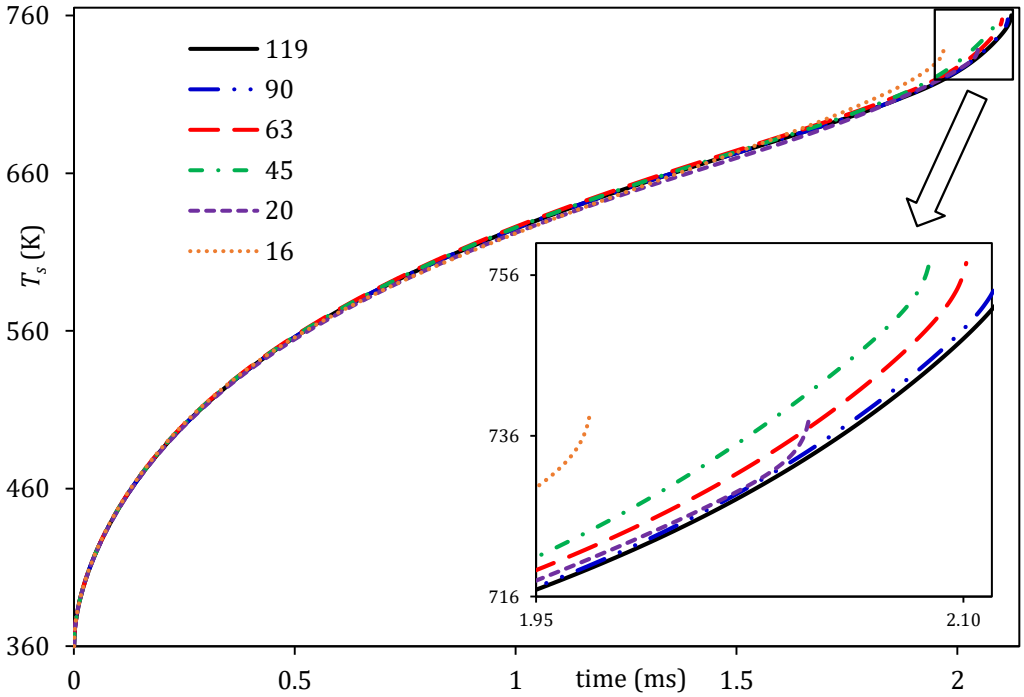

Figure 32. Droplet surface temperatures versus time for six approximations of the E85-5 blend: 119 components using the DMCM, and 90, 63, 45, 20, and 16 C/QC (numbers near the curves) using the MDQDM.

As can be seen from Figures 31 and 32, the errors in droplet lifetimes and surface temperatures predicted by the model using 90 C/QC are 0.38% and up to 0.26%, respectively, compared with those predicted using the DMCM taking into account the contributions of all components. These errors increase to 0.99% and up to 0.39% for droplet lifetimes and surface temperatures, respectively, when the blend is approximated by 63 C/QC. They further increase to 7.16% for droplet lifetime and up to 2.90% for the droplet surface temperature, when 16 C/QC were used. It should be noted that the less % difference, the better, as this means the reduction model is accurate and the original number of components can be represented by less components to save the computational time. These errors are rather large for many engineering applications. At the same time, it was found that the approximation of the blend by 20 C/QC underpredicts the droplet lifetimes and surface temperatures by up to 3.58% and up to 2.90%, respectively, which is acceptable in most engineering applications.

The computational efficiency of the MDQDM is illustrated in Table 16. For example, the approximation of 119 E85-5 components by 20 components/quasi components reduces CPU time by up to 82.7%. The workstation used is fitted with i5-3337U, dual Core, 8 GB RAM, and 1.80 GHz processor. The time step was set as 1 μs.

Table 16. The impact of reducing the number of components on CPU time (in sec) $\left(\text{Diff }\% = \frac{|\text{CPU time}_{(C/QC)} - \text{CPU time}_{119}|}{\text{CPU time}_{119}} \times 100\right)$.

number of C/QC	CPU time	Diff %
119	1816	-
90	1360	25.1
63	955	47.4
45	687	62.2
20	314	82.7
16	247	86.4

It should be noted that these results were produced using the analysis presented in this thesis. However, the estimated time for produced the same results using conventional CFD tools is almost impossible to predict, as the computational time is expected to be much longer and dependent on the computer simulation capacity.

5.4. Ethanol/Biodiesel/Diesel Fuel Blends

As stated in Section 5.3, blending higher fraction of ethanol with diesel requires some additives to attain the needed miscibility in order to stabilise the blend, control the phase separation, and attain the required cetane number. Therefore, researchers have started to add some agents to stabilise the mixture and attain the required CN [148,166]. Dimethyl ether is one of such agent for suitable CN booster when it is mixed with diesel, as it has a CN of greater than 55 [167]. However, it is believed that this component cannot be used in diesel engines effectively due to its lower values of MW, boiling point, and density, which make it evaporate much faster than the components of diesel fuel. Among other different agents, biodiesel is a chemically-convenient additive to mix with ethanol/diesel fuel (E/D) blend [168].

The most recent studies conducted have focused on the ethanol/biodiesel/diesel (EBD) fuel blend. For instance, Kwanchareon et al. [148] studied the GGE and the CN of this fuel blend. The presence of biodiesel in EBD blend resulted in a significant reduction in the Carbon monoxide (CO) and Hydrocarbons (HC) emissions of internal combustion engines (ICE) compared to the E/D blend. In [151], the solubility of EBD blend was investigated at two different temperatures, which showed that the solubility of ethanol increased when increasing the temperature. Beatrice et al. [169] studied the influence of blending 10% biodiesel, 20% ethanol, and 70% diesel fuels on ICE performance. In the latter study, the smoke and Nitrogen Oxides (NO_X) emissions were found to be significantly less than those of pure diesel. The impact of EBD blend on emissions was investigated experimentally in

[170], where results showed that the EBD blend had lower NO_X emissions compared to those of pure diesel. In similar other studies [171–175], the EBD blend was CN-richer and its combustion produced less NO_X emissions than diesel combustion. According to [168,176], up to 25% of biodiesel and 10% of ethanol could be blended with diesel effectively.

In a brief summary, previous studies on EBD blends only focused on the solubility, toxic emissions, heating value and CN of these blends. The impact of such blends on droplet heating and evaporation, with consideration to full fuel compositions, has not been investigated anywhere in the literature to the best of author's knowledge. In this section, the new key findings are the investigation into mixing different fractions of EBD blends with consideration of their droplet lifetimes and surface temperatures, viscosities, CN and heating value.

5.4.1. Heating and evaporation

The heating and evaporation of EBD blends were investigated using the DMCM and same ambient conditions and input parameters as in Sections 5.2 and 5.3, taking into account the UNIFAC model for the predictions of ACs of 106 components of the EBD blends. The biodiesel fuel was represented by SME in this study. The evolutions of droplet radii are shown in Figure 33, and their surface temperatures are presented in Figure 34.

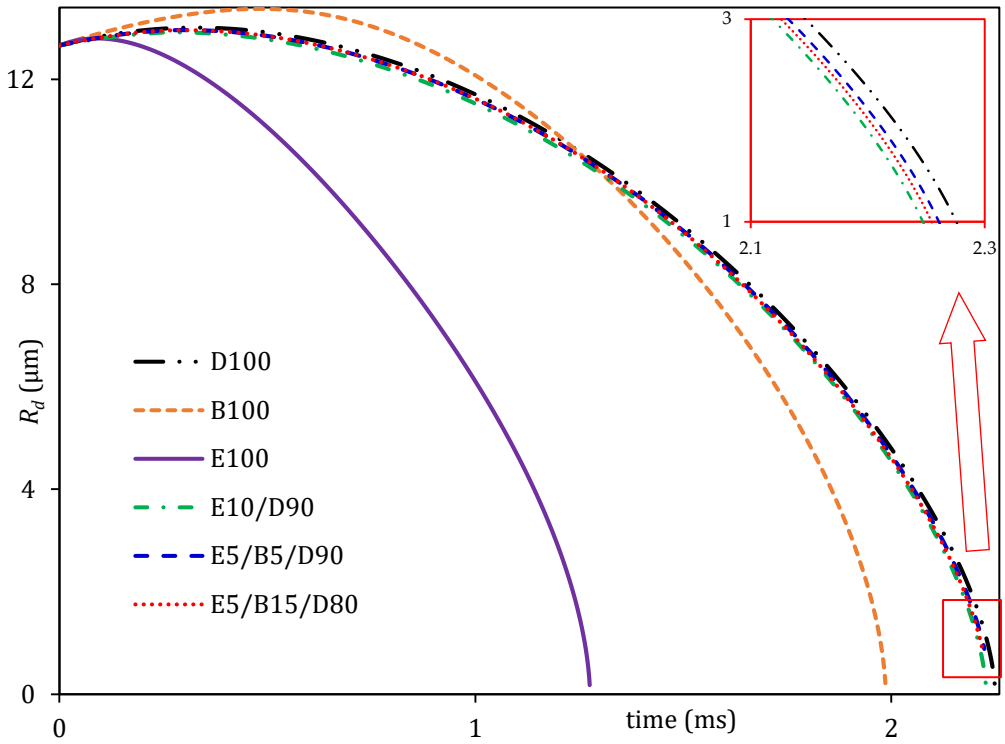

Figure 33. The evolution of droplet radii for pure diesel (indicated as D100), pure biodiesel (indicated as B100), pure ethanol (indicated as E100), and three different EBD blends.

As presented in Figure 33, the droplet lifetime decreases as the fractions of biodiesel, ethanol, or both fuels increase at the expense of diesel fuel. This decrease is 0.7% when a blend of E5/B5/D90 is used, and further decreases by 0.9% when 10% of ethanol is mixed with 90% of diesel. This reduction reaches up to 1.2% when the total fraction of biofuels was 20% (15% biodiesel and 5% ethanol). Predictions show that pure biodiesel and pure ethanol have 11.7% and 43.3% less droplet lifetime than pure diesel respectively. This shorter droplet lifetime is ascribed to the fact that ethanol and biodiesel had higher vapour pressures than diesel, which make them evaporate faster than pure diesel.

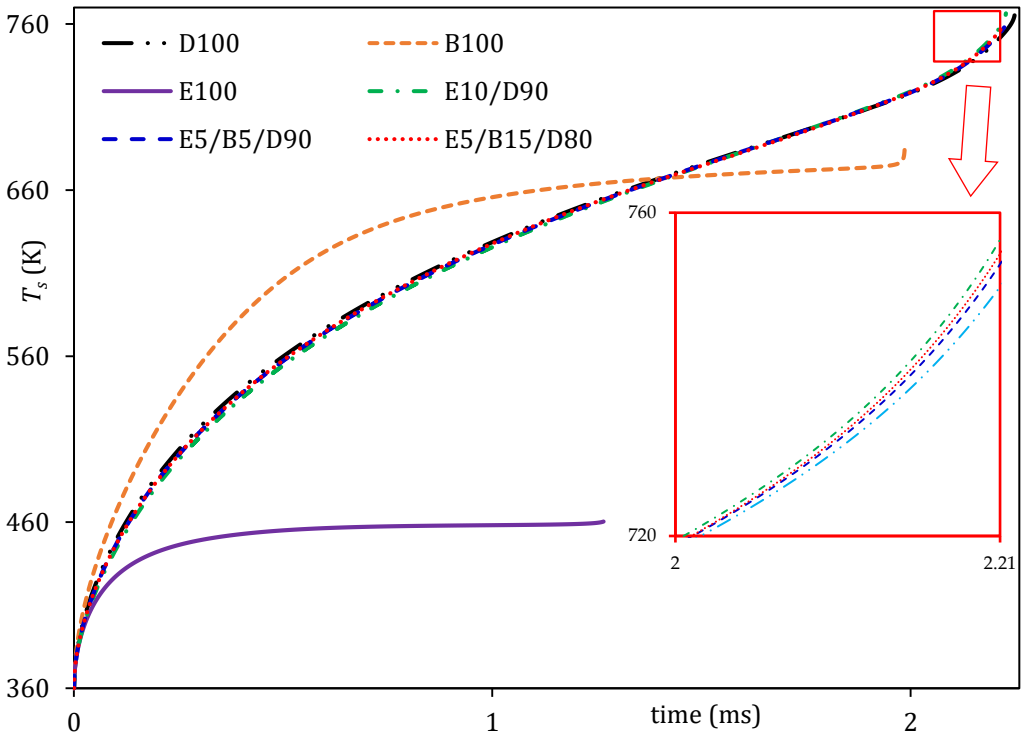

Figure 34. The evolution of droplet surface temperatures for the same fuels and their blends as in Figure 40.

Droplet surface temperature decreases with increasing biofuels fractions (Figure 34). A reduction of up to 0.5% is predicted for the E5/B5/D90 blend compared to the pure diesel. This decrease reaches up to 1% for the E5/B15/D80 blend. However, the reduction is significant for pure biodiesel and pure ethanol, which are up to 10.6% and 39.4%, respectively, compared to pure diesel. This is attributed to their higher heat of capacity, as components with higher heat capacity have lower temperature rise. The very negligible differences between diesel fuel and its blends are obtained for single droplet. For real applications which include a polydisperse spray, these differences can be tolerated further (i.e. up to 5% differences can be acceptable, as a result of the higher uncertainties on the droplet size). That makes the suggested blends in this chapter broadly acceptable in relevant engineering applications.

5.4.2. Cetane number and viscosity

In order to further illustrate the feasibility of mixing different fractions of biofuels with diesel, some important characteristics were investigated. CN is one of the most important characteristics of diesel fuel, as it measures the combustion quality of diesel fuel [75]. The presence of ethanol in diesel results in a reduction in its CN and viscosity, which is another important property that influences the quality of atomization and combustion [174,177]. Therefore, biodiesel fuel was used to compensate the decrease in the aforesaid two properties [166]. The impact of biodiesel fuel on the CN of ethanol/diesel blends was predicted using the formula suggested in [178]. The CN of pure diesel fuel (CN_D) was predicted using the formula suggested in [179], as follows:

$$CN_D = \frac{\sum_i v_i \beta_i CN_i}{\sum_i v_i \beta_i}. \quad (36)$$

For each species group, v_i is the total volume fraction, β_i is the blending parameter, and CN_i is the cetane number of that group. The CN number for each component is inferred from [179,180,84,181]. It should be emphasised that the n-alkanes and iso-alkanes groups were merged together in [60] to form one group due to their similar physical properties. For the predictions of the CN, however, these two groups were considered separately due to the impact of varying component structures (straight chain or branched) on the CN. The predictions of the CN_D, using Equation (36), is presented in Table 17. Note that the last three groups of diesel fuel, presented in [60], have been ignored due to their small fractions (1.56%, 1.224%, and 0.66%).

Table 17. The volume fractions and parameters of each group of diesel fuel and their predicted CN.

Groups	v_i	β_i
n-alkanes	15.94	0.5212
iso-alkanes	31.32	7.3717
cycloalkanes	15.99	0.0727
bicycloalkanes	7.53	0.0727
aromatics	12.84	3.1967
tetralines	10.39	3.1967
naphthalenes	5.97	0.0727
$CN_D = 54.5$		

The CN number of each component present in biodiesel fuel was predicted using the formula suggested in [182], which is based on the carbon number of the component and the number of double-bonds existing in each component. Then, the following formula (Equation 37), suggested in [183], was used for the predictions of the CN of biodiesel fuel (CN_B). Note that CN_B depends on molecular structure. Methyl lineolate ($C_{19}H_{34}O_2$), for instance, has very low CN (23). Based on this, not all types of biodiesel can compensate for the reduction of CN caused by ethanol. However, SME fuel has small fractions of methyl lineolate which make it an appropriate fuel to boost the CN_B of the blend.

$$CN_B = 1.068 \sum(CN_i y_i) - 6.747, \quad (37)$$

where CN_i and y_i are the CN number and mass fraction, respectively, of component i in the biodiesel fuel.

The CN of the EBD blend was predicted using the formula proposed in [178] and compared with the volume fraction mixing rule for the predictions of CN of EBD blends [184]. The latter formula proposed in [178] illustrates that each 1 vol. % of ethanol causes a decrease in CN by 0.6 units which will be well compensated by 0.55 units for each 1 vol. % of biodiesel.

The impact of different fractions of ethanol and biodiesel on the CN of the EBD blend is shown in Table 18.

Table 18. Predicted CN of biodiesel, diesel, ethanol, and their blends.

EBD vol.%	CN [184]	CN [178]
D100	54.5	54.5
B100	56.4	56.4
E100	8.0	8.0
E10/D90	49.8	48.6
E5/B5/D90	52.3	54.4
E5/B15/D90	52.5	55.0

Zöldy [178] suggested a correlation to predict the viscosity of EBD blends based on several experimental measurements [178]. Such an approach may not be enough to predict the viscosity of the analysed blends. A more rigorous approach will need to be considered to predict the viscosity of a blend of species with different structures. Therefore, the UNIFAC–VISCO method was used, which is described as [129]:

$$\ln \mu_m = \sum_i x_i \ln(\mu_i V_i) - \ln V_m + \frac{\Delta^* g^{EC}}{RT} + \frac{\Delta^* g^{RC}}{RT}, \quad (38)$$

where μ_m is the mixture viscosity and μ_i is the viscosity of i^{th}component, respectively. V_m and V_i are the volumes of the mixture and i^{th}component, respectively, $\frac{\Delta^* g^{EC}}{RT} = \sum_i x_i \ln\frac{\Phi_i}{X_i} + \frac{z}{2}\sum_i x_i q_i \ln\frac{\theta_i}{\Phi_i}$, and $\frac{\Delta^* g^{ER}}{RT} = -\sum_i x_i \ln \gamma_i^{*R}$. All the terms and parameters appearing in Equation (38) and their related terms are the same as those for the UNIFAC model (see Chapter 3 for more details). The application of Equation (38) for the predictions of the EBD viscosity is summarised in Table 19.

Table 19. Predicted viscosity (at $T = 40$ °C) of biodiesel, diesel, ethanol, and their blends.

EBD vol.%	μ_m (cP)
D100	3.51
B100	3.59
E100	0. 81
E10/D90	3.27
E5/B5/D90	3.46
E5/B15/D80	3.44

As can be seen from Tables 18 and 19, the addition of 15% biodiesel and 5% ethanol results in up to 0.2% and 2% reduction in the CN and viscosity, respectively, compared to pure diesel, which can be sacrificed in diesel engines. In fact, the presence of biodiesel compensates the reduction in the CN and viscosity caused by ethanol, as the E10/D90 blend has approximately 10.8% and 7% less CN and viscosity, respectively, compared to pure diesel.

5.4.3. Heating value

The impact of biodiesel and ethanol additions on the heating value (HV) of diesel was predicted for different EBD blends using the following formula [185]:

$$\mathrm{HV}_{\mathrm{blend}} = (v_B \mathrm{HV}_D \rho_D + v_B \mathrm{HV}_B \rho_B + v_E \mathrm{HV}_E \rho_E)/\rho_{\mathrm{blend}}, \quad (39)$$

where $\mathrm{HV}_D, \mathrm{HV}_B$, and HV_E refer to the heating values (in MJ/kg) of diesel, biodiesel, and ethanol respectively; and v_D, v_B, and v_E refer to the volume fractions of diesel, biodiesel, and ethanol respectively. ρ_D, ρ_B, ρ_E, and ρ_{blend} refer to the densities of diesel, biodiesel, ethanol, and their blend, respectively. The solution to Equation (39) was compared to the experimental data of [148], and presented in Figure 42 (see Table 20 for the blends in x-axis of Figure 35).

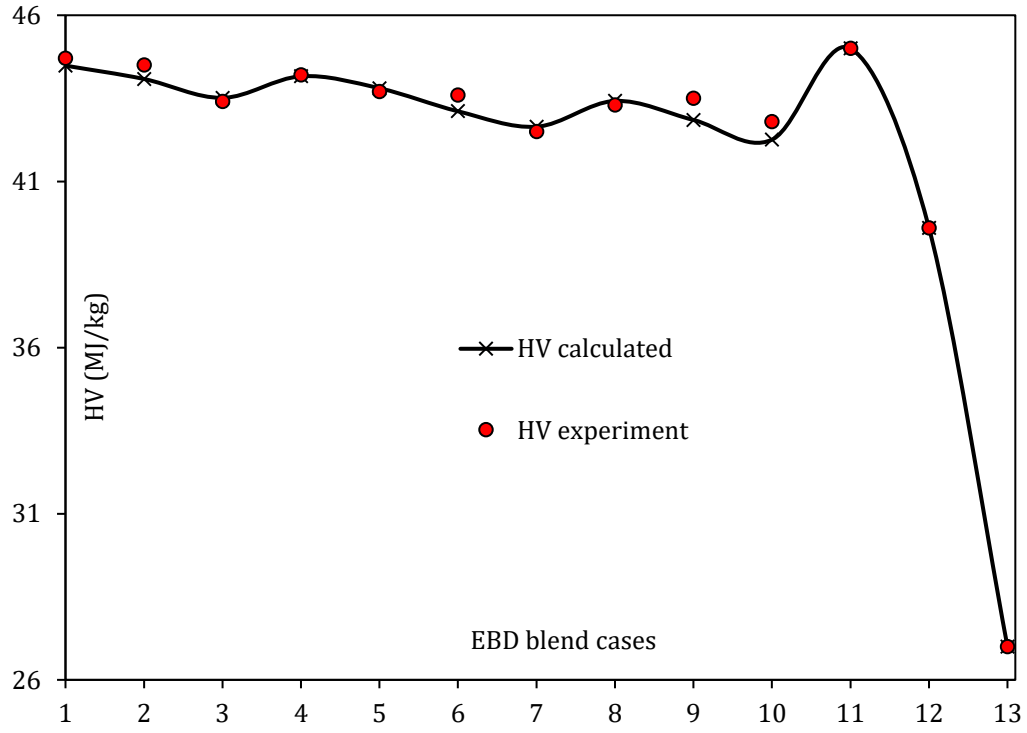

Figure 35. The predicted heating value, experimentally measured in [148], for ethanol, biodiesel, diesel, and their blends. The x-axis blend cases are illustrated in Table 20.

Table 20. The cases of EBD blends used in Figure 35.

Sample	%D	%B	%E
1	90	10	0
2	90	5	5
3	90	0	10
4	85	15	0
5	85	10	5
6	85	5	10
7	85	0	15
8	80	15	5
9	80	10	10
10	80	5	15
11	100	0	0
12	0	100	0
13	0	0	100

As shown in Figure 42, the predicted HVs are in agreement with the experimental data. The HV of ethanol (case 13) is very low due to its small structure. The addition of biodiesel has compensated the reduction in HV caused by ethanol. For instance, E10/D90 (case 3) has 3% less HV compared to pure diesel, while E5/B5/D90 has only 0.5 less HV compared to pure diesel. Predictions shows that the targeted blend (E5/B15/B80) has 2.2% less HV compared to pure diesel, which can be tolerated in diesel engines.

5.5. Summary of Chapter 5

In this chapter, the discrete multi-component model was applied for diesel, 22 types of biodiesel and their blends, E85-diesel blends and ethanol/biodiesel/diesel blends under conditions representative of diesel engines. Moreover, the Multi-Dimensional Quasi-Discrete Model (MDQDM) was applied for E85-diesel blend. Approximations were made for the universal quasi-chemical functional–group activity coefficient model in order to include some functional groups of diesel fuel that their non-ideal vapour-liquid equilibrium characteristics were not available in literature. The impact of the ambient pressures, gas and radiative temperatures on two selected types of biodiesel fuel (SME and WCO), diesel and their blends was analysed. Ambient pressures and temperatures, and radiative temperatures in the ranges 20-60 bar, 700-950 K, and 1000-2000k, respectively, were considered. Finally, the effect of ethanol and biodiesel on the CN and heating value of diesel fuel was studied.

In contrast to previous studies, it was shown that droplet evaporation time and surface temperature predicted for B100 were not always close to those predicted for pure diesel fuel, but were dependent on the biodiesel fuel type and ambient conditions. The impact of radiation on opaque droplet lifetimes was shown to be significant, leading to about 19.4% and 23.3% faster evaporation for B0 and B100, respectively, compared to the case where radiation is ignored.

For E85-diesel blend, results showed that high fractions of E85-diesel fuel blends had a significant impact on the evolutions of droplet radii and surface temperatures. For instance, droplet lifetime and surface temperature for a blend of 50 vol. % E85 and 50 vol. % diesel were 23.2% and up to 3.4% less than those of pure diesel fuel, respectively. The application of the MDQD model led to a saving of up to 86.4% of CPU time when reducing the 119 components to 16 C/QC without a sacrifice to the main features of the model. Under the same ambient conditions, the temperature difference between the droplet centre and its surface reached up to 9.2 %.

Ultimately, for ethanol/biodiesel/diesel blend, it was observed that a mixture of up to 15% biodiesel, 5% ethanol, and 80% diesel fuels had led to small variations in droplet lifetime, CN, viscosity, and heating value of pure diesel, with less than 1.2%, 0.2%, 2%, and 2.2% reduction in those values, respectively.

All the presented findings of increasing the biofuel fraction in the diesel fuel, using the models presented in Chapter 3, confirmed the possibility of using higher biofuel fractions than those currently proposed in the UK market for instance (up to 7% in diesel fuel). It can be concluded from this chapter that the currently allowed fraction can be increased to 20%. This finding can have noticeable impact on reducing the GGE.

CHAPTER SIX: Complex Fuel Surrogates

6.1. Overview

This chapter presents a new approach to the formulation of fuel surrogates in application to gasoline, diesel, and their biofuel blends (including blends of biodiesel/diesel and ethanol/gasoline). This new approach, described as a 'Complex Fuel Surrogates Model (CFSM)', is based on a modified version of the Multi-Dimensional Quasi-Discrete Model (MDQDM).

There are two types of surrogates, namely, physical and chemical surrogates. Physical surrogates are used to match the processes preceding the onset of combustion (droplet heating and evaporation); while chemical surrogates are used to match the combustion characteristics of fuels. To the best of the author's knowledge, there has not been any study on formulating surrogates for bio-fossil fuel blends to match both the physical and chemical characteristics of these fuels.

In this work, the aim is to predict fuel surrogates that can be used for the simulation of processes preceding and exceeding the onset of ignition. Some of the combustion characteristics are also predicted using the formulated surrogates in order to investigate their ability to represent the real fuel.

6.2. The Complex Fuel Surrogates Model

The CFSM is also based on the analytical solutions of the heat and mass transfer equation. This model is essentially a modified version of the MDQDM. In the latter model, QC are generated within each hydrocarbon and methyl-ester groups. These components have non-integer carbon numbers (see [73,186] for more details). It is not possible to formulate the physical surrogates of each fuel using these QC, because they cannot be measured experimentally for validation purposes. Furthermore, they cannot be implemented into commercial CFD codes for the prediction of combustion characteristics; since the chemical

mechanisms of the vast majority of these QC are not available. To address these issues, in this chapter, a modified version of the MDQDM is proposed which would be able to generate actual components (with integer carbon numbers) that can be utilised to analyse, design and development of broad range of engineering applications by means of numerical simulations. The model is described as a 'Complex Fuel Surrogates Model' (CFSM), and primarily designed to generate actual components (with rounding half-up to the nearest integer carbon numbers) and formulate fuel surrogates.

The carbon number of each Approximate Discrete Component (ADC) generated by the CFSM can be introduced as [187]:

$$n_{im} = \left[\frac{\sum_{am}^{bm}(n_{im}\, Y_{im})}{\sum_{am}^{bm} Y_{im}}\right] \tag{40}$$

where m refers to the hydrocarbon group number in the fuel, n is the carbon number of the i^{th} component in group m, Y is the mass fraction of the i^{th} component in group m. In contrast to the original MDQDM (where the QC carbon number is a non-integer value, see Equation (6) in [60]), the nearest integer of the carbon number is determined from Equation (40). Also, in contrast to the MDQDM, the mass fractions Y_{im} are used (instead of the molar fractions) to calculate the ADC group averaged carbon number n_{im}. These mass fractions are used to demonstrate the importance of heavy components on the expense of less important (lighter) ones for the prediction of droplet lifetime. For example, alkanes (the heaviest group) make up to 44.53% of diesel mass fractions (only 41.48% diesel molar fractions), which dominates the fuel composition on the expense of lighter components – such as naphthalenes with up to 7.46% mass fractions (9% molar fractions) and alkylbenzenes with up to 13.62% mass fractions (16.75 molar fractions).

The integer ADC are generated within each group, where am and bm are the start and end counted components of the grouped species, respectively; and am for the second grouped components is $bm_{\text{old}+1}$. For example, a typical diesel fuel has 9 groups of hydrocarbons in

which the group of alkanes contains 20 components. To reduce these 20 alkane components to 4 components, each row of 5 components (sub-group) is grouped to form an ADC. The ADC carbon numbers of each sub-group of alkanes are determined as:

$$\left.\begin{aligned} n_{(1-5)m} &= \left[\frac{\sum_{i=5}^{i=1}(n_{im}\,Y_{im})}{\sum_{i=5}^{i=1} Y_{im}}\right] \\ n_{(6-10)m} &= \left[\frac{\sum_{i=10}^{i=6}(n_{im}\,Y_{im})}{\sum_{i=10}^{i=6} Y_{im}}\right] \\ n_{(11-15)m} &= \left[\frac{\sum_{i=15}^{i=11}(n_{im}\,Y_{im})}{\sum_{i=15}^{i=11} Y_{im}}\right] \\ n_{(16-20)m} &= \left[\frac{\sum_{i=20}^{i=16}(n_{im}\,Y_{im})}{\sum_{i=20}^{i=16} Y_{im}}\right] \end{aligned}\right\} \quad (41)$$

The mathematical expressions for the formulation of fuel surrogates, presented so far, are based on the numbers of carbon atoms and mass fractions of species. In this study, the formulation of fuel surrogates based on the latter two key parameters bridges the gap between the physical and chemical properties predicted by the formulated surrogates.

6.3. Diesel Fuel Surrogates

The diesel fuel surrogates were formulated using the CFSM, and their physical characteristics were compared with those predicted using MDQDM and Discrete Multi Component Model (DMCM). An example of the QC generated using the MDQDM and the ADC generated using the CFSM is presented in Table 21, where the 98 components of diesel fuel were replaced with 6 QC and 6 ADC.

Table 21. Quasi-Components (QC) and Approximate Discrete Components (ADC), representing the groups of species in diesel fuel.

Group	Molar fractions (%)	QC	Mass fractions (%)	ADC
n-alkane	41.48	$C_{14.763}H_{31.526}$	44.53	$C_{16}H_{34}$
cycloalkane	15.41	$C_{15.364}H_{30.728}$	17.05	$C_{17}H_{34}$
bi-cycloalkane	7.89	$C_{14.743}H_{27.486}$	8.29	$C_{16}H_{30}$
alkylbenzene	16.75	$C_{11.726}H_{17.452}$	13.62	$C_{13}H_{20}$
tetraline	9.48	$C_{13.832}H_{19.664}$	9.05	$C_{15}H_{22}$
naphthalene	8.99	$C_{12.392}H_{12.784}$	7.46	$C_{13}H_{14}$

The evolutions of droplet surface temperatures and radii (Figure 36) predicted using the MDQDM and CFSM were compared with those predicted for the full compositions of diesel fuel using the DMCM. These computations were performed using the identical ambient conditions and input parameters as outlined in Chapter 5. The results clearly show that the CFSM model improves these predictions when compared to those predicted using the MDQDM.

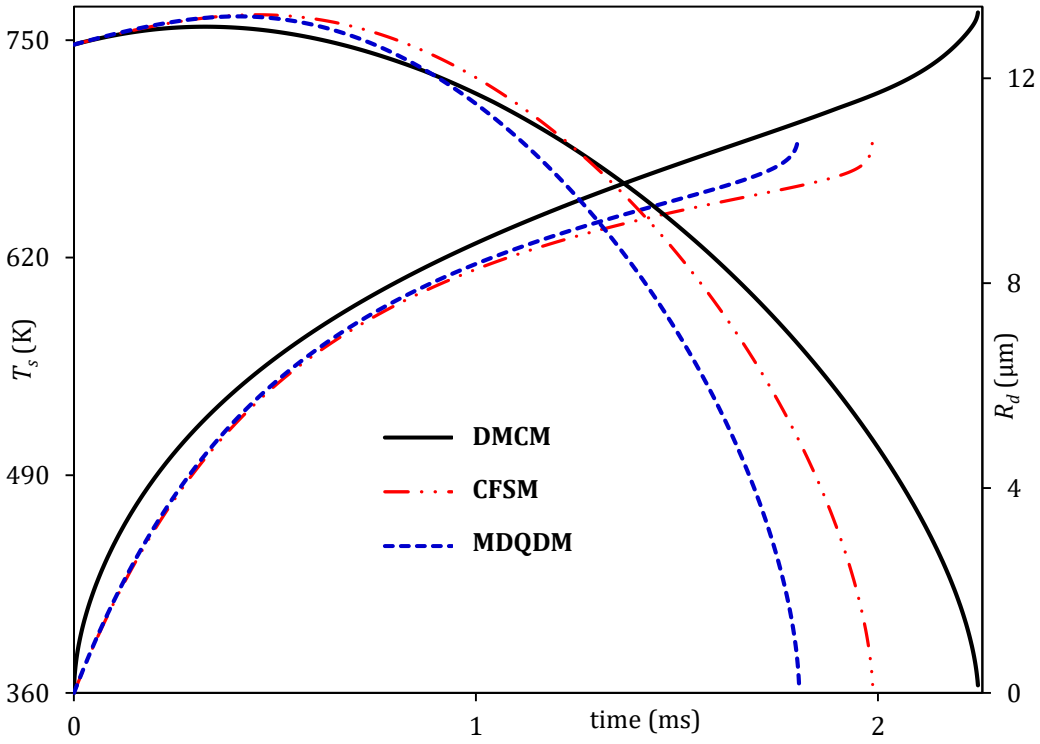

Figure 36. Evolution of droplet surface temperatures and radii predicted for the full compositions of diesel fuel (98 components) using DMCM, 6 approximate discrete components using CFSM, and 6 quasi-components using MDQDM.

Figure 36 shows the improvement in the evolutions of droplet radii and surface temperatures achieved through the CFSM compared to the MDQDM. Other chemical and physical properties of individual species can also be examined. As presented in Appendices B, C, E and F, all properties are carbon number dependant and they can be calculated whether the carbon number is integer or non-integer (i.e. for QC). For example, the average density of the 6 QC fuel presented in Table 21 is 762 kg. m^{-3} which deviates by 7.9% from the real diesel fuel. For 6 ADC, however, the average density is 801.5 kg. m^{-3} which deviates by only 3.1% from the full composition of diesel fuel.

A detailed comparison between the MDQDM and CFSM was made at different time instants. The droplet radii and surface temperatures variations with the numbers of C/QC and ADC were predicted using the MQDQM and CFSM at four different time instances ($t = 0.5$ ms, $t = 1$ ms, $t = 1.5$ ms and $t = 2$ ms), and the comparative plots are presented in Figures 37-40. The ambient and the input parameter values were maintained as in Chapter 5.

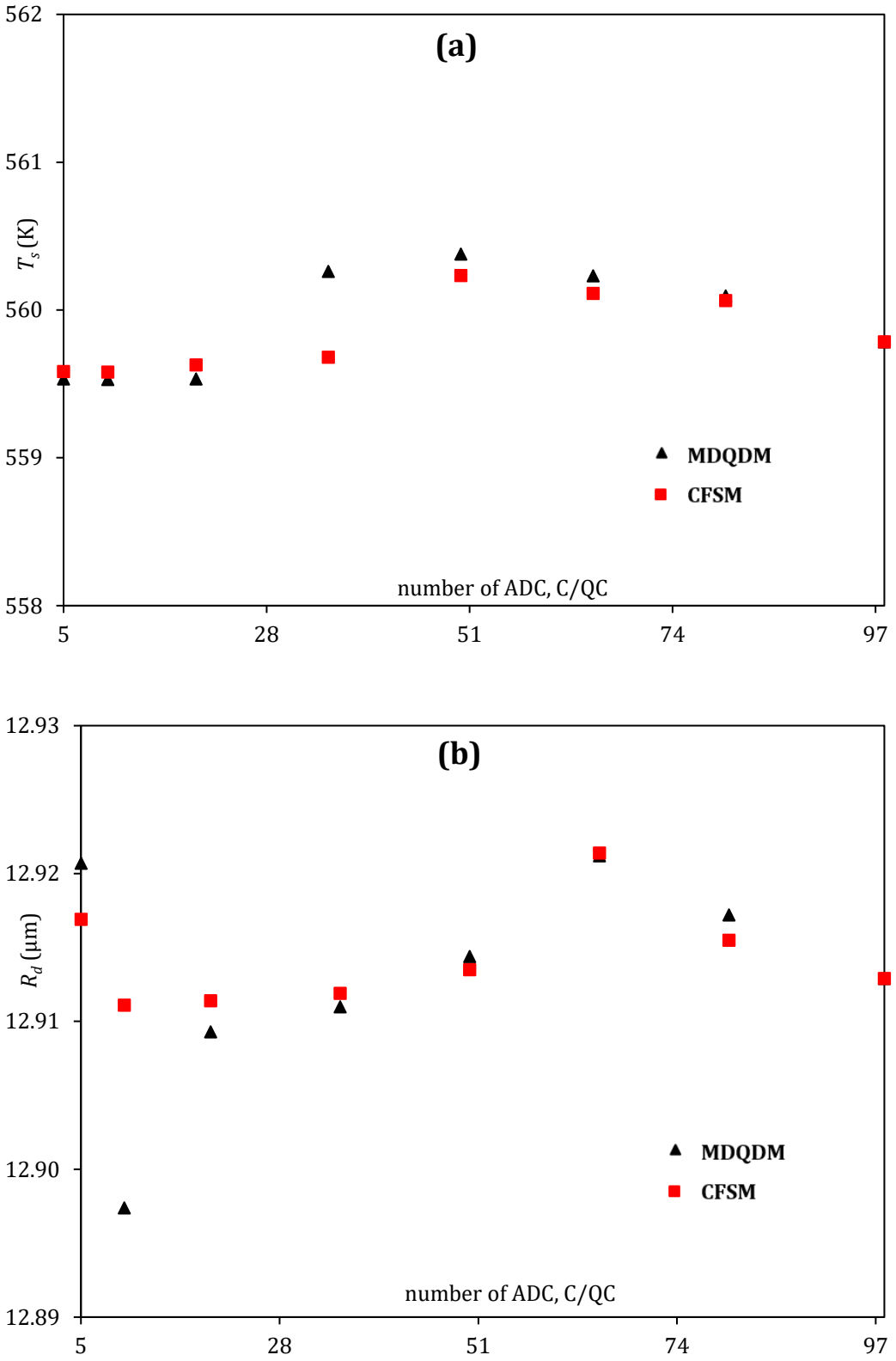

Figure 37. The values of droplet surface temperatures (a) and radii (b) versus ADC and C/QC at time instant 0.5 ms.

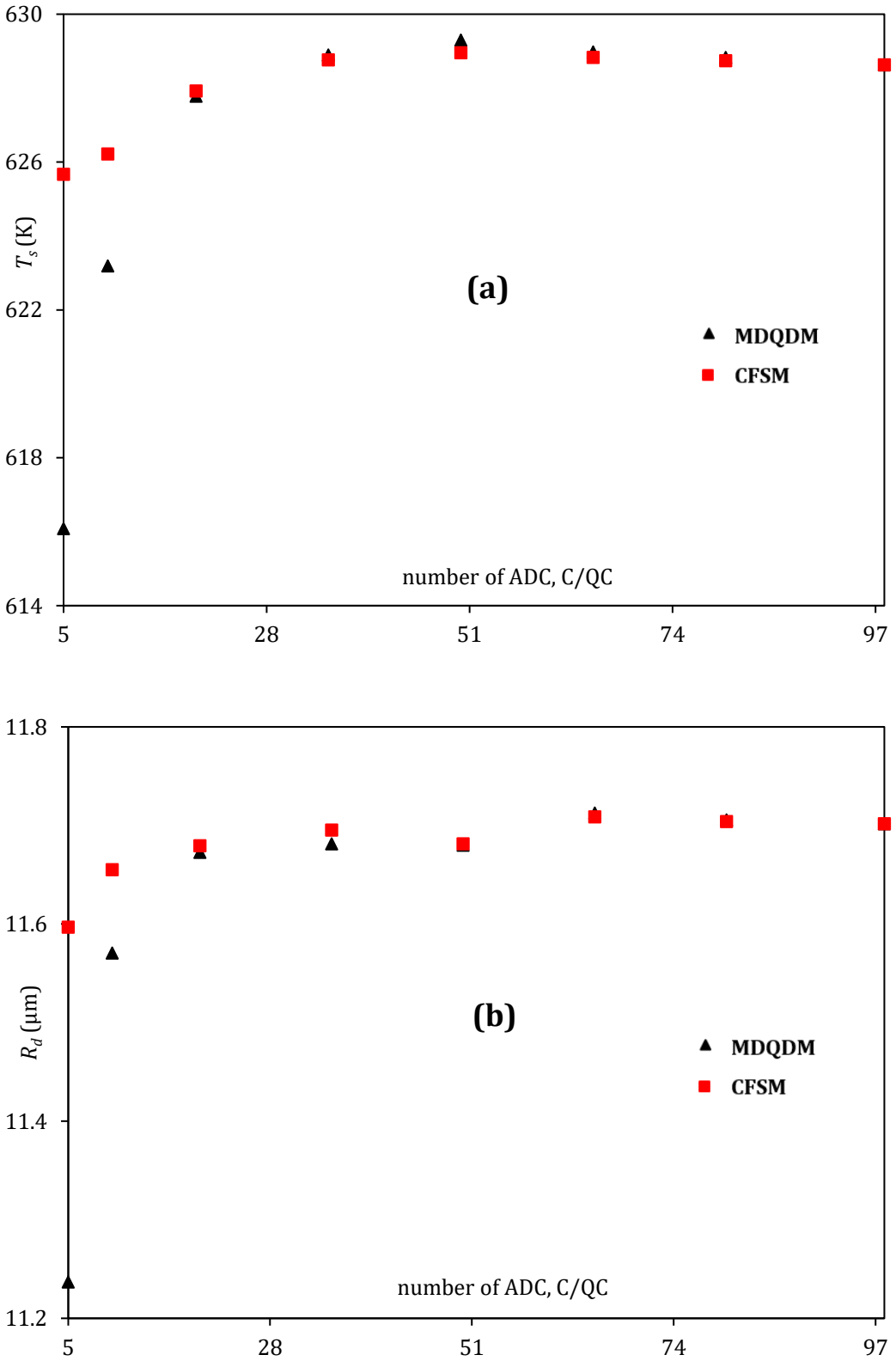

Figure 38. The values of droplet surface temperatures (a) and radii (b) versus ADC and C/QC at time instant 1 ms.

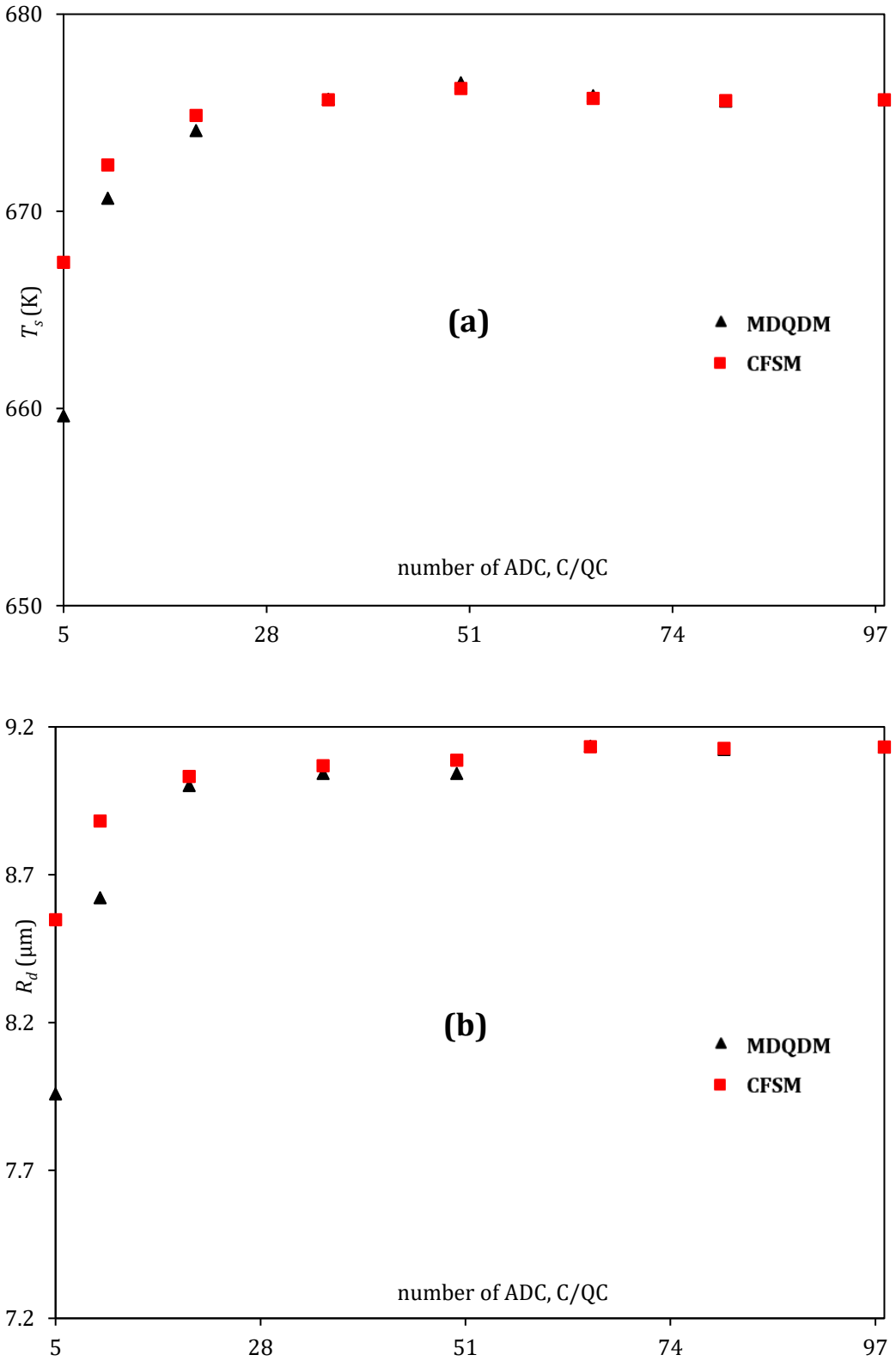

Figure 39. The values of droplet surface temperatures (a) and radii (b) versus ADC and C/QC at time instant 1.5 ms.

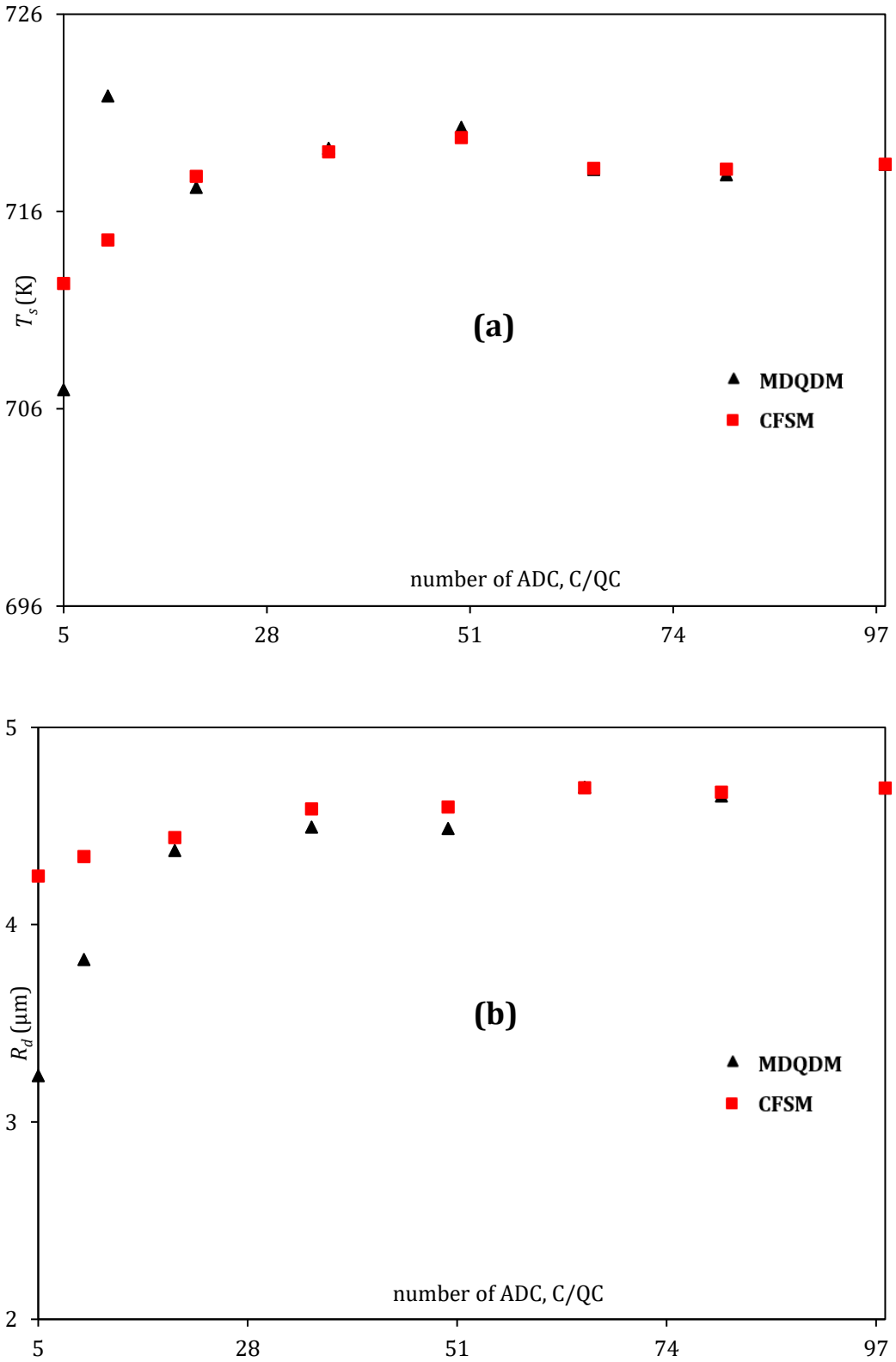

Figure 40. The values of droplet surface temperatures (a) and radii (b) versus ADC and C/QC at time instant 2 ms.

As can be seen from Figures 37-40, the predictions of CFSM are generally better than those obtained using the MDQDM especially with the small numbers (≤10) of ADC and C/QC. The predictions of the CFSM for droplet radii and surface temperatures when the full composition of diesel fuel (98 components) is approximated by 10 ADC are reasonably close to those predicted using the DMCM with up to 4% errors. The results presented in Figures 37-40 confirm the previous trends inferred from Figure 36.

Although the diesel droplet heating and evaporation using the CFSM are verified, the selection of ADC in this model is still based on trial and error. Hence, this model still requires experienced end-users to run it. The impact of the trial and error on the predicted droplet surface temperatures and radii are noticeable in Figure 37 – where the new approximation of the full composition of diesel fuel with the range 50-75 ADC overpredicts these results. Some fluctuations are observed in at different time instants (e.g., Figure 40) where those approximations can overpredict or underpredict the results of the 98 components. A universal algorithm is undoubtedly needed for the selection of QC or ADC to minimise such uncertainty. In the current work, however, the primary aim was to formulate fuel surrogates that match the real physical and chemical characteristics of their fuels.

The chemical and physical characteristics of the formulated surrogate were further investigated using the CFSM (Sur1) and two other surrogates from literatures (Sur2 [188] and Sur3 [189]). The predictions of these surrogates were compared to the full composition of diesel fuel obtained from [186]. Table 22 summarises the molar fraction of the formulated surrogate (Sur1) and the other two surrogates from the literature (Sur2, Sur3).

Table 22. The molar fractions of the three surrogates (Sur1, Sur2, and Sur3) of diesel fuel.

Component	Chemical formula	Molar fractions (%)		
		Sur1	Sur2 [188]	Sur3 [189]
n-hexadecane	$C_{16}H_{34}$	42.89	41.3	0.88
iso-cetane	$C_{16}H_{34}$	-	36.8	7.48
n-butylcyclohexane	$C_{10}H_{20}$	-	-	29.66
n-pentylcyclododecane	$C_{17}H_{34}$	16.43	-	-
bi-cyclohexane	$C_{12}H_{24}$	-	-	25.26
bi-cycloocatne	$C_{16}H_{30}$	7.88	-	-
toluene	C_7H_8	-	-	10.94
heptylbenzene	$C_{13}H_{20}$	13.12	-	-
decalin	$C_{10}H_{18}$	-	-	25.78
1-dimethyl-4-iso-propyltetralin	$C_{15}H_{22}$	8.72	-	-
naphthalene	$C_{11}H_{10}$	-	21.9	-
1-methyl-2-ethyl-naphthalene	$C_{13}H_{14}$	10.95	-	-

The diesel fuel droplet lifetimes were investigated for the full composition of fuel, using the DMCM and the three surrogates (Sur1, Sur2 and Sur3), the evolutions of which are illustrated in Figure 41. The ambient and the input parameter values were again maintained as in Chapter 5 apart from the droplet initial temperature which was assumed to be equal to $T_{do} = 296$ K.

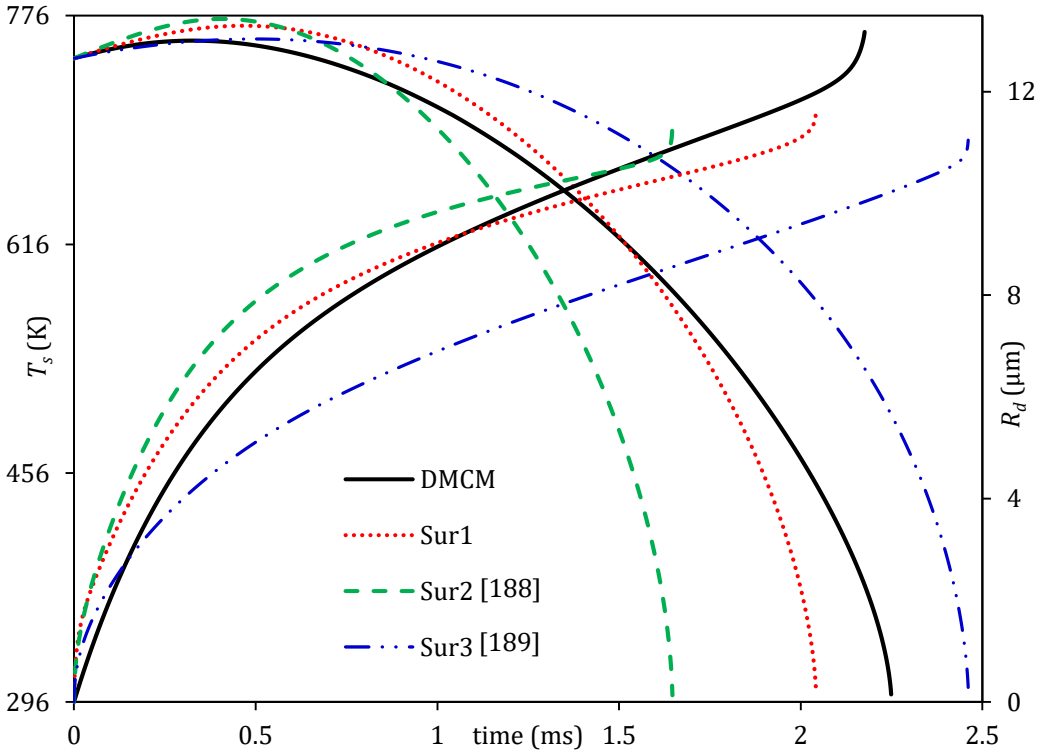

Figure 41. Evolutions of droplet surface temperatures and radii for the full compositions of diesel fuel and the 3 surrogates (Sur1, Sur2 and Sur3).

From Figure 41, the evolutions of the droplet radii of Sur1 are of reasonably close with those predicted for the full compositions of diesel, where it underpredicts the droplet's lifetime by up to 6.8%. The predictions of Sur2 (inferred from [188]) and Sur3 (inferred from [189]) however, were found to result in the errors of 26.8% and 8.4%, respectively while predicting the droplet lifetime. Also, the droplet surface temperatures are underpredicted by 7.3%, 8.4%, and 9.9% using Sur1, Sur2 and Sur3 respectively. These errors were estimated in comparison to the same reference values obtained for the full composition of diesel fuel using the DMCM.

To further understand the suitability of the suggested surrogates to represent diesel fuel, the Cetane Number (CN) was calculated for these surrogates. In the original composition of diesel fuel presented in [60], n-alkanes and iso-alkanes were merged together into one group due to their similar thermodynamic and transport properties. For the calculation of CN however, these two groups were treated individually in the current analysis, due to their

different CN values with various component structures – normal (straight chains) or isomers (branched chains) [190]. In addition, the viscosities of the two suggested surrogates were also compared to the full compositions of diesel fuel. The viscosity was predicted using the UNIFAC–VISCO method [129]. The predictions of the CNs and the viscosities of the formulated surrogate, using the CFSM (Sur1), and the other two surrogates (Sur2 and Sur3), were compared to those calculated for the full compositions of diesel fuel as shown in Table 23.

Table 23. The CNs and viscosities (in cP) of diesel fuel and its three surrogates (Sur1, Sur2 and Sur3).

Fuel	CN	Error (%)	Viscosity	Error (%)
diesel	54.5	-	4.516	-
Sur1	53.3	2.2	4.442	1.6
Sur2 [188]	39.8	27.0	4.483	0.8
Sur3 [189]	60.1	10.3	3.35	26.2

As can be seen from Table 23, Sur1 mimics the CN of diesel fuel with an error of less than 3%. Also, Sur1 and Sur2 closely match the viscosity for the full composition of diesel fuel, with errors of only 1.6% and 0.8%, respectively. Despite a close agreement on the prediction of viscosity, it is evident from these results (Figure 48 and Table 23), that the Sur2 model predictions were found to record significant errors, beyond the acceptable limit. This is ascribed to the fact that Sur2 (composed of 3 components) is dominated by alkanes (78.1%, as shown in Table 22), ignoring the fair contributions of other hydrocarbons. Considering the importance of physical and chemical features of fuel surrogates (droplet's lifetime and temperature, CN and viscosity), Sur1 is relatively the best surrogate group to represent diesel fuel, compared to the other two surrogates (Sur 2 and Sur3).

6.4. Gasoline Fuel Surrogates

The droplet surface temperature and lifetime for the full composition of gasoline FACE C were predicted in Section 4.2, assuming Raoult's law was valid. In Section 4.3, the impact of activity coefficient on the vapour-liquid equilibrium for this fuel was accounted for. In this section, a comparison is made for the physical and chemical features of the full composition of fuel obtained from [71,124], the formulated surrogates using the CFSM (Sur4), and the two suggested surrogates (Sur5 and Sur6) inferred from [31,80]. Table 24 illustrates the molar fraction of the three surrogates.

Table 24. The molar fractions of the three surrogates (Sur4, Sur5 and Sur6) of gasoline fuel.

Component	Molar fractions (%)		
	Sur4	Sur5 [31]	Sur6 [80]
n-butane	-	17.0	18.4
n-pentane	29.184	-	-
n-heptane	-	11.0	12.5
n-undecane	0. 022	-	-
iso-pentane	10.737	8.0	5.0
iso-heptane	-	5.0	4.7
iso-octane	55.231	56.0	54.6
iso-decane	0.483	-	-
toluene	-	3.0	4.8
iso-propylbenzene	4.343	-	-

Initially, the droplet surface temperatures and lifetimes were predicted using DMCM using the conditions and input parameters stated in Chapter 4. The predicted evolutions of droplet radii and surface temperatures for the full compositions and the three surrogates are presented in Figure 42.

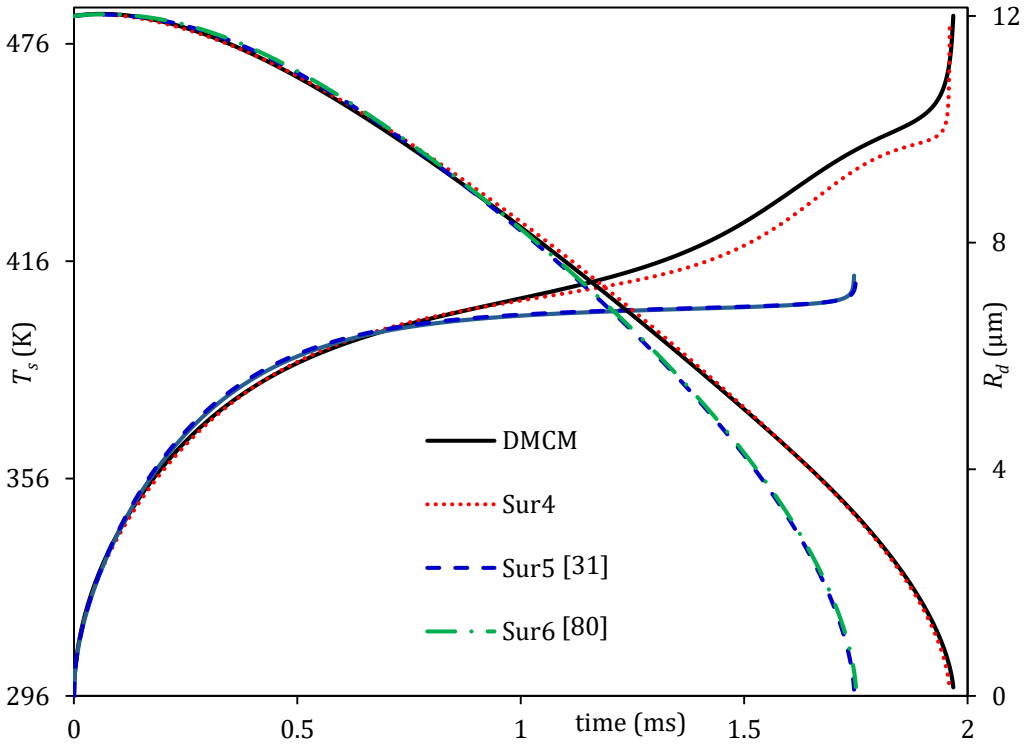

Figure 42. Evolutions of droplet radii and surface temperatures for the full compositions of gasoline and its 3 suggested surrogates: Sur4 (derived using the CFSM), Sur5 (inferred from [31]) and Sur6 (inferred from [80]).

As shown in Figure 42, the predictions of Sur4 droplet surface temperatures and radii using the CFSM vary only by 0.71% and 0.41%, respectively, when compared to those predicted for the full composition of the same fuel using the DMCM. At the same time, the use of the Sur5 and Sur6 surrogates underpredicts the droplet lifetimes and surface temperatures by up to 15% and 11.3%, respectively.

The densities and vapour pressures of the three fuel surrogates (Sur4, Sur5 and Sur6) and the full composition were calculated under the same input parameters and transient conditions of the droplet. The density of each component was predicted using the data inferred from [191]. The linear blending of volume fractions was used to make up the density of the mixture. The vapour pressure was calculated using the set of expressions provided in [129] for each component. The modified Raoult's law, using the UNIFAC model, was used to determine the partial vapour pressure of each component. The predicted values

of densities and vapour pressures for the full composition of fuel and the three fuel surrogates (Sur4, Sur5 and Sur6) are presented in Table 25.

Table 25. The calculated vapour pressures (in kPa) and densities (in $kg \cdot m^{-3}$) for gasoline fuel and its surrogates (Sur4, Sur5 and Sur6) at 296 K.

Fuel	Vapour pressure	Error (%)	Density	Error (%)
gasoline	34.25	-	682.3	-
Sur4	35.77	4.4	680.8	0.22
Sur5 [31]	54.49	59.1	680.3	0.29
Sur6 [80]	52.41	53.0	683.3	0.15

As evident from Table 25, the densities of all three surrogates are found to be in close agreement with that predicted for the full composition of gasoline fuel. However, the vapour pressures of the two surrogates, Sur5 and Sur6 (inferred from [31,80]), are found to be significantly different from those calculated for the full composition of gasoline fuel, showing errors of up to 59.1% and 53%, respectively. These large errors produced by Sur5 and Sur 6 surrogates were expected, because these surrogates were originally developed to match the RON, H/C and MW ignoring the physical characteristics of fuel (e.g., droplet lifetime and vapour pressure). These characteristics were predicted using Sur4, resulted in an error of only 4.4%, when compared to the results from DMCM.

The RON, MW and H/C ratio were compared to those of the full composition of gasoline FACE C. According to [192], the flame speed and the diffusivity of the real fuel can be matched using a suggested surrogate when the H/C ratio and the MWs are matched. Also, the ignition time delays of the fuel and its surrogates can be matched when their RONs are in good agreement [31]. The H/C ratios were predicted for the suggested surrogates using the following relationship [80]:

$$\frac{H}{C} = \frac{\sum_i^n X_i(N_{Hi})}{\sum_i^n X_i(N_{Ci})}, \tag{42}$$

where X_i, N_{Ci}, H_{Ci} are the molar fraction, number of carbon atoms, and number of hydrogen atoms respectively, of their i^{th} component. The RON of Sur4 is predicted using the following relationship [193]:

$$\mathrm{RON} = \frac{\sum_i v_i \beta_i \mathrm{ON_i}}{\sum_i v_i \beta_i}, \tag{43}$$

where v_i is the volume fraction of component i, β_i is a parameter value for each hydrocarbon group and $\mathrm{ON_i}$ is the octane number of component i. Equation 43 can be used for the predictions of RON and MON by using the appropriate β_i. The MW was calculated using the linear blending of the molar fractions. The values of RON, MW and the H/C ratio of the full composition fuel and the three surrogates are shown in Table 26. It should be emphasised that the RON, predicted in [31,80] for Sur5 and Sur6, were based on the linear molar blending rule and not on detailed hydrocarbon groups. As can be seen from this table, the suggested surrogate matches the three aforesaid properties with negligible deviation compared to the full composition of FACE C gasoline fuel.

Table 26. The RONs, H/C ratios and MWs (in $\mathrm{g \cdot mole^{-1}}$) of gasoline fuel and its surrogates.

Fuel	RON	H/C	MW
gasoline	84.7	2.27	97.2
Sur4	85.8	2.24	97.8
Sur5 [31]	85.3	2.25	98.4
Sur6 [80]	85.3	2.23	98.1

6.5. Blended Ethanol/Gasoline Surrogates

The predictions of the droplet heating and evaporation of biodiesel, ethanol, ethanol/gasoline blends and biodiesel/diesel blends are investigated in [41,43,124,134,194,195]. Due to ongoing efforts in research communities worldwide in increasing the fraction of biofuels in the baseline fuel and to comply with some of the recent governmental regulations (for instance, the UK Department for Transport announced in

April 2018 that the government was aiming to double the use of biofuel from its current 4.9% to 9.75% by 2020), the formulation of bio-fossil fuel blend surrogates is essential to study the feasibility of increasing the biofuel fractions.

The ethanol/gasoline fuel surrogate was generated using the input parameters and ambient conditions and input parameters described in Chapter 4. The UNIFAC model was considered for all functional groups in this section (without any approximation) due to the significant non-ideality of ethanol/gasoline blends. The impact of ethanol addition on droplet lifetime and surface temperature of gasoline fuel was presented in Chapter 4. In this study, the impact of ethanol on the RON and the densities was investigated and compared to those of pure gasoline. In addition, the predictions of all the aforementioned characteristics were computed by the suggested fuel surrogate and compared to the full composition of fuel. The RONs and the densities of different fractions of ethanol/gasoline blends are shown in Table 27.

Table 27. The RONs and densities (in $kg \cdot m^{-3}$) of ethanol/gasoline fuel blends.

Fuel	RON	Density
gasoline	85.8	680.4
E5	87.7	685.7
E20	92.7	701.7
E50	100	773.8
E85	106	770.1
E100	108	787.2

Results indicates that the addition of ethanol can be sacrificed in gasoline engines by up to 20% due to the minor deviations in RON and density (which were 8% and 3%, respectively) when compared to pure gasoline. According to the findings in Chapter 4 and in the current work, ethanol can be blended with gasoline by up to 20% without any engine modifications. Based on these findings, the E20 is used for the surrogate formulation of the

ethanol/gasoline blend. The molar fractions of the suggested surrogate, using the CFSM and the surrogate suggested in [196], are shown in Table 28.

Table 28. The molar fractions of E20 surrogates (Sur7 and Sur8).

Component	Molar fractions (%)	
	Sur7	Sur8 [196]
n-hexane	18.13	-
n-heptane	-	11.82
iso-pentane	6.64	-
iso-octane	34.17	25.28
iso-decane	2.99	-
toluene	-	25.81
iso-propylbenzene	3.1	-
ethanol	38.13	37.08

The evolutions of the droplet radii and surface temperatures predicted by the author's formulated fuel surrogate (Sur7), the surrogate suggested in the literature (Sur8 [196]) and the full composition of the E20 blend, are shown in Figure 43.

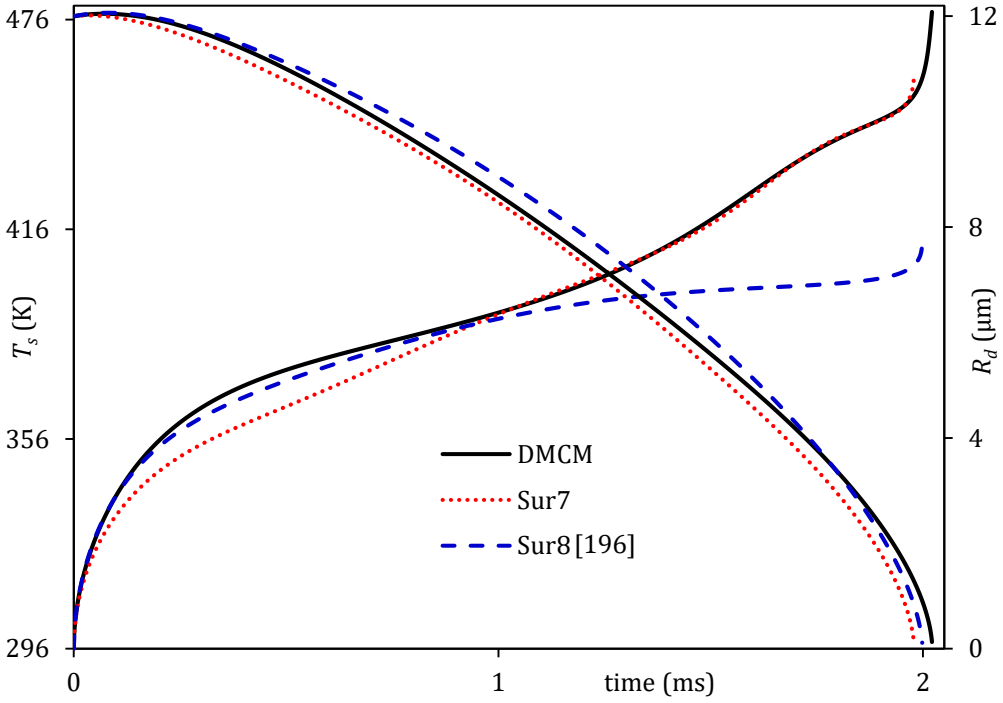

Figure 43. Evolution of the droplet radii and surface temperatures for the full compositions of E20 and the two surrogates (Sur7 and Sur8).

The predictions reveal that the suggested surrogate (Sur7) is in a good agreement with the full composition of E20. The predicted errors in droplet lifetime and surface temperature are up to 2.1% and 4%, respectively, compared to the same results predicted using the DMCM. Similarly, a negligible deviation in droplet lifetime, compared to the full composition of gasoline, is observed for Sur8 (the surrogate inferred from [196]). However, using Sur8 shows a significant deviation in the droplet surface temperature with up to 14%. The RON, H/C and MW were studied to examine the ability of the two surrogates by means of fuel representation, as shown in Table 29.

Table 29. The RONs, H/C ratios and MWs (in $g \cdot mole^{-1}$) of gasoline fuel and its surrogates.

Fuel	RON	H/C	MW
E20	92.5	2.23	78.22
Sur7	95.3	2.24	79.54
Sur8 [196]	96.4	2.25	81.59

The RONs, H/C ratios and MWs predicted by the two surrogates show a good agreement with those predicted by the full composition of gasoline fuel.

6.6. Blended Biodiesel/Diesel Surrogate

The feasibility of adding biodiesel fuel to diesel at different fractions has been highlighted in many studies (e.g., see [73]). According to the latest renewable fuel statistics report by the UK Department for Transport, 80% of the biodiesel produced in the UK was from used cooking oil, which accounts for around 115 million litres [197]. Therefore, biodiesel/diesel surrogate is commonly based on the blend of WCO biodiesel and diesel [198]. To the best of the author knowledge, there is insufficient literature about the surrogates of WCO and its diesel blends. The impact of biodiesel addition on droplet lifetime and surface temperature was presented in [73].

In this study, the impact of biodiesel on the CN was investigated and compared to that of pure diesel. The CN, predicted by different biodiesel/diesel blends using the expression provided in Chapter 5 which is based on the linear blending of volume fractions, is shown in Table 30.

Table 30. The CNs of biodiesel/diesel fuel blends.

Fuel	CN
diesel	54.5
B5	54.8
B10	55.1
B20	55.8
B50	57.7
B100	60.9

Following a recent finding by the author in [195], biodiesel can be blended with diesel by up to 10% without a need for engine modification. In this section, the same ambient conditions and input parameters as in Chapter 5 were used to generate surrogates of B10 (10% vol. biodiesel and 90% vol. diesel fuel blend). The formulated surrogate was compared with the full composition of B10. The molar fractions of the formulated surrogate are shown in Table 31. The original composition of WCO biodiesel fuel was inferred from [50].

Table 31. The molar fractions of the B10 surrogate (Sur9).

Component	Chemical formula	Molar fractions (%)
n-hexadecane	$C_{16}H_{34}$	38.60
n-pentylcyclododecane	$C_{17}H_{34}$	14.79
bi-cycloocatne	$C_{16}H_{30}$	7.09
heptylbenzene	$C_{13}H_{20}$	11.81
1-dimethyl-4-isopropyltetralin	$C_{15}H_{22}$	7.85
1-methyl-2-ethylnaphthalene	$C_{13}H_{14}$	9.86
1-methyl-oleate	$C_{19}H_{36}O_2$	5.85
1-methyl-linoleate	$C_{19}H_{34}O_2$	4.15

The WCO fuel consists of 8 saturated components (making 24.1% of the fuel), 4 unsaturated components with one double bond (making 44.4% of the fuel) and 2 unsaturated components with two double bonds (making 31.5% of the fuel). According to total fraction of each group, the dominant two groups are those with unsaturated methyl esters, hence unsaturated components (1-methyl-oleate, and 1-methyl-linoleate) were chosen to represent WCO in B10 fuel blend.

The droplet radii and surface temperatures were predicted for the suggested surrogate (Sur9) and compared with the full composition of B10 blends, using the DMCM as shown in Figure 44. The surrogate's droplet lifetime and temperature are underpredicted by up to 7.1% and 8.7%, compared with the full composition of B10. These underpredictions can be tolerated in some engineering applications.

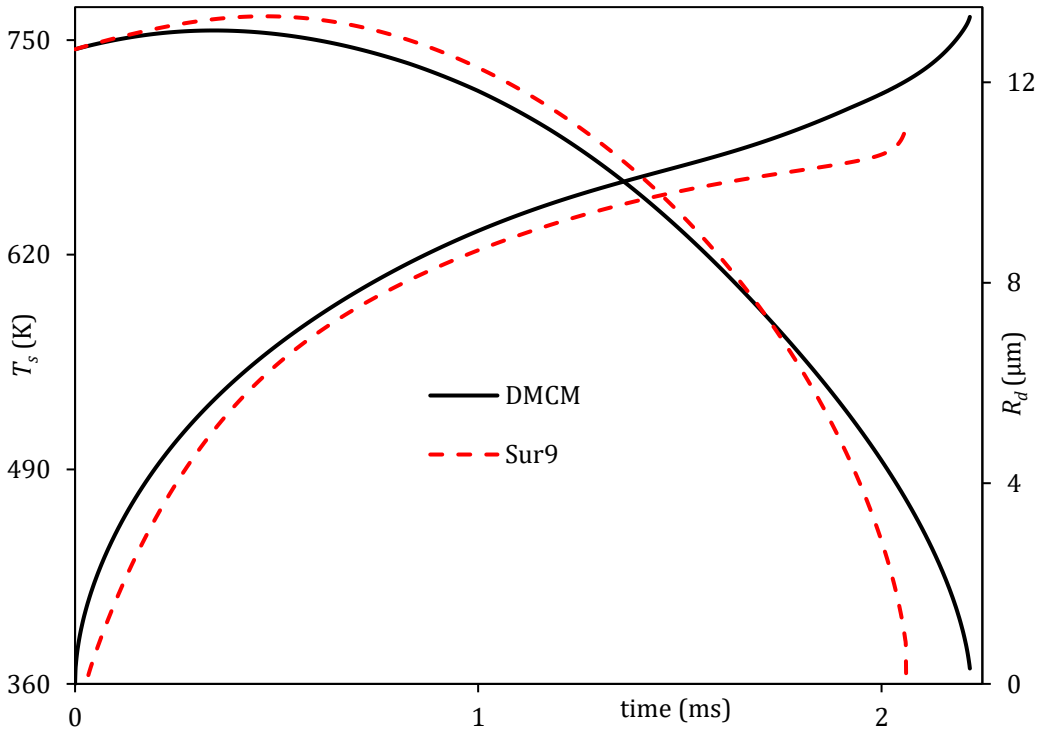

Figure 44. Evolutions of droplet radii and surface temperatures for the full compositions of B10 and a suggested surrogate. The same ambient conditions and model as in the case shown in Figure 41 were used.

The CN (predicted by the surrogate) was also compared to the full composition of B10. The CN of Sur9 (53.9) shows a reasonable agreement with that of the full composition of B10 (55.1). Therefore, based on the verifications for droplet's lifetime and surface temperature and CN, the formulated surrogate for the B10 blend (Sur9) has closely matched the characteristics of the full composition for the blend.

6.7. Summary of Chapter 6

A new approach to the formulation of fuel surrogates in application to gasoline, diesel, and their biofuel blends (including blends of biodiesel/diesel and ethanol/gasoline) was suggested. This new approach, described as a 'Complex Fuel Surrogates Model (CFSM)', was based on a modified version of the multi-dimensional quasi-discrete Model. The new approach was aimed to reduce the full composition of fuel to a much smaller number of components based on their mass fractions to formulate fuel surrogates.

The mathematical expressions for the formulation of fuel surrogates are based on the numbers of carbon atoms of components and their mass fractions and not on targeting certain physical or chemical properties during the formulation of surrogates. It was found that these two targeted characteristics were substantial for matching the final physical and chemical properties of the full components of fuels.

The formulated surrogates for gasoline and blended ethanol/gasoline fuels matched the data from the full compositions of the same fuels for droplet lifetime, surface temperature, density, vapour pressure, H/C ratio, molar weight and research octane number, using the CFSM. Also, the Cetane number and viscosity of diesel and biodiesel/diesel blends were mimicked by their suggested surrogates.

The findings can be used for the development of detailed combustion model using the formulated surrogates. The importance of the CFSM can be more significant in application to fuel blends in order to fully understand the influence of these blends and maximise their uses for road vehicles.

CHAPTER SEVEN: Auto-Selection of Quasi-Components of Fuel Blends

7.1. Overview

A new algorithm for the auto-selection of Components/Quasi-Components (C/QC) in the Multi-Dimensional Quasi-Discrete Model (MDQDM) is suggested and applied to the analysis of fuel droplet heating and evaporation in this chapter. The suggested approach is utilised for the maximum number of components to assess its functionality. The heating and evaporation predictions as well as the computational time of the new approach are compared to those of the Discrete Multi Component Model (DMCM) and the original MDQDM.

The component generated by the MDQDM have non-integer carbon number (called QC) which cannot be used for the prediction of the combustion characteristics due to the unavailability of the chemical mechanisms for such components. Efforts were made to reduce the number of components of different fuels through the generation of component with integer carbon number (so-called 'Approximate-Discrete Components (ADC)') representative components as investigated in Chapter 6. This was achieved through the suggestion of a CFSM which was based on the modified version of the MDQDM. The CFSM was used for the formulation of fuel surrogates in application to gasoline, diesel and their biofuel blends. In the MDQDM and CFSM, the choice of the QC and ADC was based on trial and error, which required experienced end-users (i.e. not directly implementable into commercial CFD codes). In response to this problem, the development and application of a new algorithm for the auto-selection of C/QC is achieved. The model is described as ''Transient Multi-Dimensional Quasi-Discrete Model (TMDQDM)''. The importance of this new approach is that the generated C/QC are provided through a universal algorithm based on the transient (rather than initially decided) contributions of each group of species. The

model can be generalised to be a transient multi-dimensional approximate-discrete model (i.e. transient model with ADC). The proposed model can be applicable to any fuel type and mixtures with least user-interventions, which makes it directly implementable into CFD codes. Also, in contrast to MDQDM, the TMDQDM is aimed to improve the predicted droplet lifetimes and temperatures.

7.2. The Transient Multi-Dimensional Quasi-Discrete Model

The TMDQDM is based on the original MDQDM, assuming that all processes are spherically symmetric. The droplet movement relevant to ambient gas (air) is considered, using the ETC/ED models.

In contrast to the original application of the MDQDM, the new algorithm does not require direct user involvement in the selection of C/QC. Changes in the number of C/QC are allowed during the process of droplet heating and evaporation. A flowchart for the new algorithm is shown in Figure 45. Initially (t=0), the number of components is taken equal to the total number of components (i.e. the DMCM is used for the prediction of droplet heating and evaporation). Then, during the evaporation process, the formation of C/QC is allowed within each group of hydrocarbons, as in the conventional MDQDM. In contrast to the conventional MDQDM, the number of QC/QC within each group is not pre-selected by the user but is determined by the code at each time-step.

The new algorithm allows automatic reduction of the number of C/QC from their initial number to a smaller number, which is determined by the algorithm at specific time-steps. The mass fraction of group i at a certain time-step (G_i) increases or decreases compared with its value in the previous time-step $\left(G_{i_{\mathrm{old}}}\right)$. The species mass fractions are more sensitive to transient effects than their molar fractions; hence, their use in this model to calculate G_i [199]:

$$G_i = \sum_{n=1}^{N_i} Y_{ni}, \tag{44}$$

where Y_{ni} are the mass fractions of individual species n in group i and N_i is the total number of species in the same group i (in the case of Diesel fuel, $N_i \leq 20$ for all groups). The change in G_i is estimated as:

$$\Delta G_i = \frac{\left|G_i - G_{i_{\text{old}}}\right|}{G_i}. \tag{45}$$

If ΔG_i is greater than an *à priori* chosen small number K (in our current analysis, $K = 0.1$), the number of C/QC within each group (N_i) is reduced from the previous number $\left(N_{i_{\text{old}}}\right)$ by a certain factor F:

$$N_i = \left\lceil F\, N_{i_{\text{old}}} \right\rceil, \tag{46}$$

where F is assumed equal to 0.75, $\lceil\ \rceil$ indicates rounding up or down to the nearest integer (e.g. $\lceil 7.5 \rceil = 8$ and $\lceil 7.4 \rceil = 7$). The value of F can be chosen in accordance to the requirement of model. For small values, the reduction in number of components will be fast (i.e. CPU efficient model), but the solution accuracy will be sacrificed. In a compromise between the two important features, in this analysis, the number $F = 0.75$ is proposed using trial-and-error.

The QC in the developed algorithm are formed of the components with the smallest molar fractions in any group i. The selection is based on reverse collation of components to accommodate merging the least contributing components in that group first, starting with the components with the largest carbon numbers (usually the smallest molar fractions) and ending up with the components with the smallest carbon numbers, and usually the highest molar contributions. The number of C/QC selected to form the new QC is taken equal to $\lceil N_i/2 \rceil$. In the case where $\lceil N_i/2 \rceil$ is an even number, the QC are formed of each 2 components in the group of components with the largest carbon numbers. If $\lceil N_i/2 \rceil$ is an odd number, however, then the nearest component that is not selected is added to this

group to form an even number of components and each two C/QC in this group are merged to form a new QC. For example, in the case of the alkanes, which include 20 of 98 Diesel fuel components, at the initial stage ($N_{i_{\text{old}}} = 20$), $N_i = \lceil 0 \cdot 75 \times 20 \rceil = 15$ C/QC after the first reduction of the number of components. The first 10 components remain unchanged, and the remaining 10 components form 5 QC (each 2 components form 1 QC). Thus, the averaged carbon numbers of these 5 alkane QC are determined as:

$$\left.\begin{aligned}
\bar{n}_{(11-12)_{\text{alk}}} &= \left\lfloor \frac{\sum_{j=12}^{j=11} n_j X}{\sum_{j=12}^{j=11} X_j} \right\rfloor \\
\bar{n}_{(13-14)_{\text{alk}}} &= \left\lfloor \frac{\sum_{j=14}^{j=13} n_j X_j}{\sum_{j=14}^{j=13} X_j} \right\rfloor \\
\bar{n}_{(15-16)_{\text{alk}}} &= \left\lfloor \frac{\sum_{j=16}^{j=15} n_j X_j}{\sum_{j=16}^{j=15} X_j} \right\rfloor \\
\bar{n}_{(17-18)_{\text{alk}}} &= \left\lfloor \frac{\sum_{j=18}^{j=17} n_j X_j}{\sum_{j=18}^{j=17} X_j} \right\rfloor \\
\bar{n}_{(19-20)_{\text{alk}}} &= \left\lfloor \frac{\sum_{j=20}^{j=19} n_j X_j}{\sum_{j=20}^{j=19} X_j} \right\rfloor
\end{aligned}\right\}. \tag{47}$$

Similarly, if a certain group contains 11 components, these reduce to $N_i = \lceil 0 \cdot 75 \times 11 \rceil = 8$. The first 5 components remain unchanged, while the last 6 components form 3 QC – distributed as 2 components each, following the same procedure as shown in (6). The speed of change in mass fractions of certain species or groups is influenced by their high evaporation rates, which indicates the need to reduce their C/QC representation in the fuel composition. When the reduction in group mass fractions G_i is small (i.e. $\Delta G_i \leq K$), the code uses the previous number of C/QC, $N_{i_{\text{old}}}$ (i.e. $F = 1$).

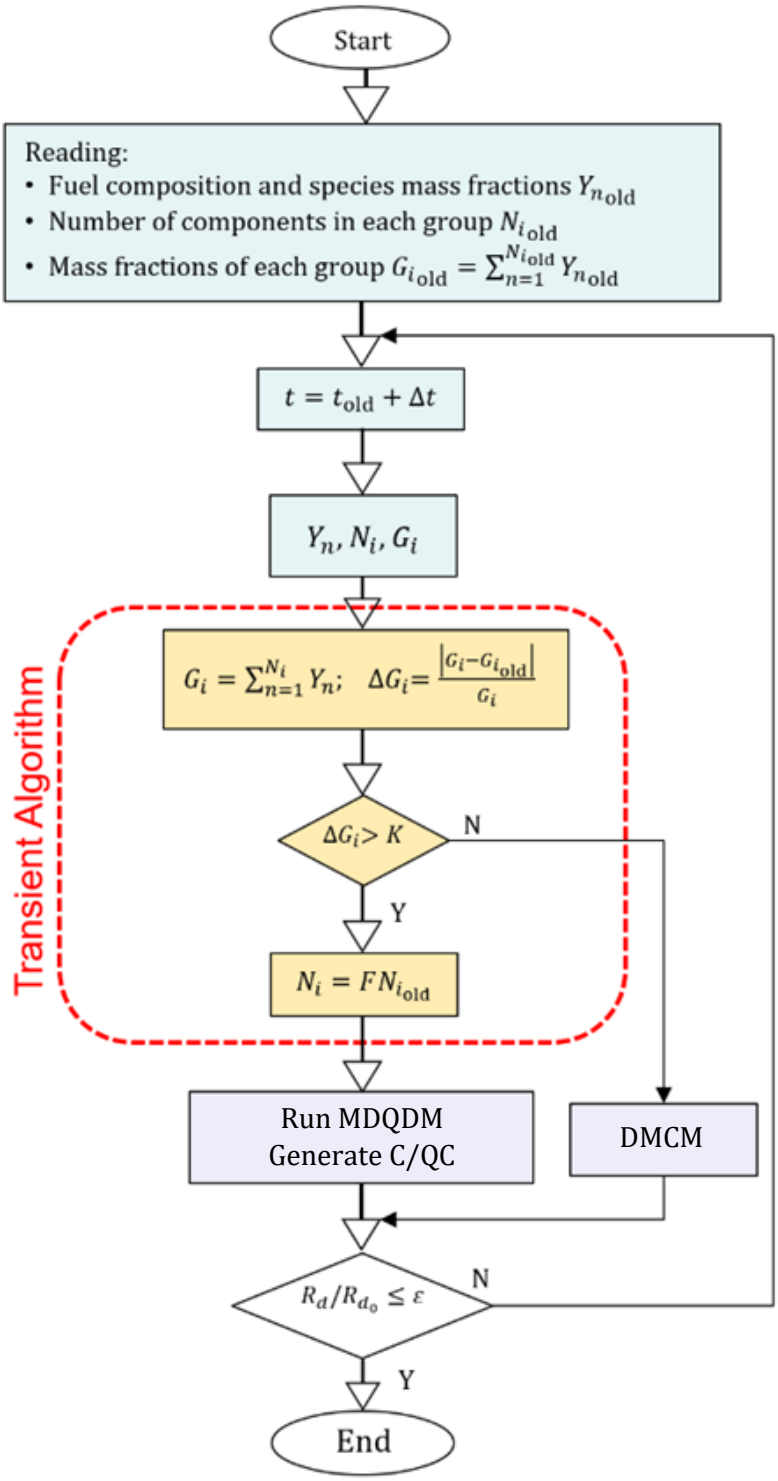

Figure 45. Flowchart of the new algorithm, where the minimum change in mass fraction ratio $K = 0.1$, reduction factor $F = 0.75$ and the minimum ratio of droplet radii $\varepsilon = 10^{-6}$.

In the new algorithm, users can define the minimum number of C/QC. This option is built into the final stage of the algorithm when further auto-reduction in the number of C/QC is blocked after this number reaches a certain minimum value. For example, if the minimum

number of C/QC is defined by the end-user as '10 C/QC' and the remaining number of C/QC is '15', the auto-reduction will lead to 11 C/QC ($\lceil 0.75 \times 15 \rceil$). However, the further reduction of 11 C/QC, following the algorithm, would lead to less than 10 C/QC. Hence, '11 C/QC' will auto-reduce to '10 C/QC' only.

The new algorithm can lead to a compromise between the accuracy of the DC model and the computational speed of the original MDQD model.

The model will be applied for the E85-diesel fuel blends. As stated in Chapter 5, the blending ethanol with hydrocarbons form a highly non-ideal mixture, therefore, the multi-component universal quasi-chemical functional group activity coefficients model is combined with the new model to accurately predict the vapour-liquid equilibrium.

7.3. E85-Diesel Fuel Blend

The model was applied for E85-diesel blends as this blend has the highest number of components to the best of the author's knowledge, and it is important that the proposed model is applied for the highest possible number of components to examine its significance for the predictions of droplet lifetimes and surface temperatures. The same volume fractions of E85-diesel fuel blends, and ambient conditions and input parameters as set out in Chapter 5 were considered, apart from the initial droplet temperature which was taken to be equal to $T_o = 298$ K. The evolution of different fractions of E85-diesel fuel droplet radii and surface temperatures predicted using the DMCM, MDQDM and TMDQDM are shown in Figures 46-55.

In Figure 46, five cases are shown: the contributions of all 98 components are accounted for, using the DMCM (indicated as DMCM (98)); the 98 components are approximated with 15 C/QC using the MDQDM (indicated as MDQDM (15)); the 98 components are reduced to 15 C/QC using the TMDQDM (indicated as TMDQDM (98-15)); the 98 components are approximated with 10 C/QC using the MDQDM (indicated as MDQDM (10)); and the 98

components are reduced to 10 C/QC using the TMDQDM (indicated as TMDQDM (98-10)). As can be seen from the figure, the TMDQDM 98-15 comes the closest in predicting the droplet evolution and lifetime, when compared with those predicted using the DMCM. This is followed by the TMDQD 98-10. Note that the results of the DMCM is always used as a reference as it includes the total number of components and it has been validated for different fuels in Chapters 4 and 5.

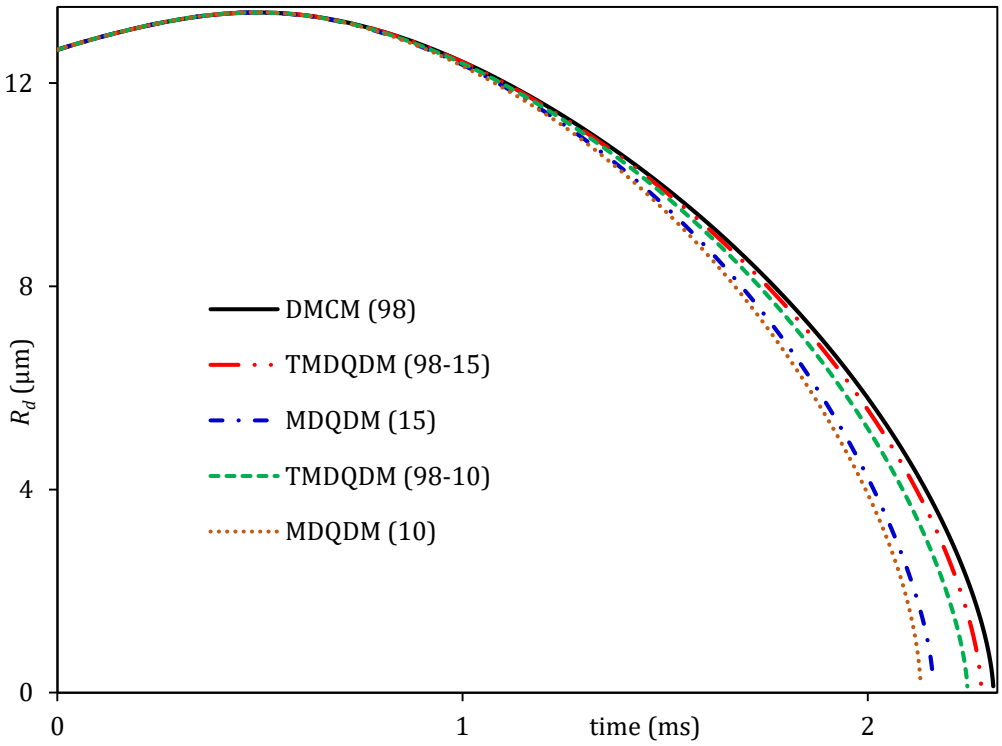

Figure 46. Evolutions of droplet radii versus time for 98 components of pure diesel fuel using the DMCM and two approximations of the original MDQDM and MDQDM with the new transient algorithm (indicated as TMDQDM).

The reduction of the number of components to 15 using the TMDQDM underpredicts the droplet lifetime by only 1.3% compared to the DMCM. The approximation of the full composition by 15 C/QC using the MDQDM, however, underpredicts the droplet lifetime by 6.5%. The underprediction is further increased when the number of C/QC is reduced to 10. The underprediction is 2.8% using the TMDQDM and 7.8% using the MDQDM. As expected, the same trends are present for the droplet surface temperatures (Figure 47).

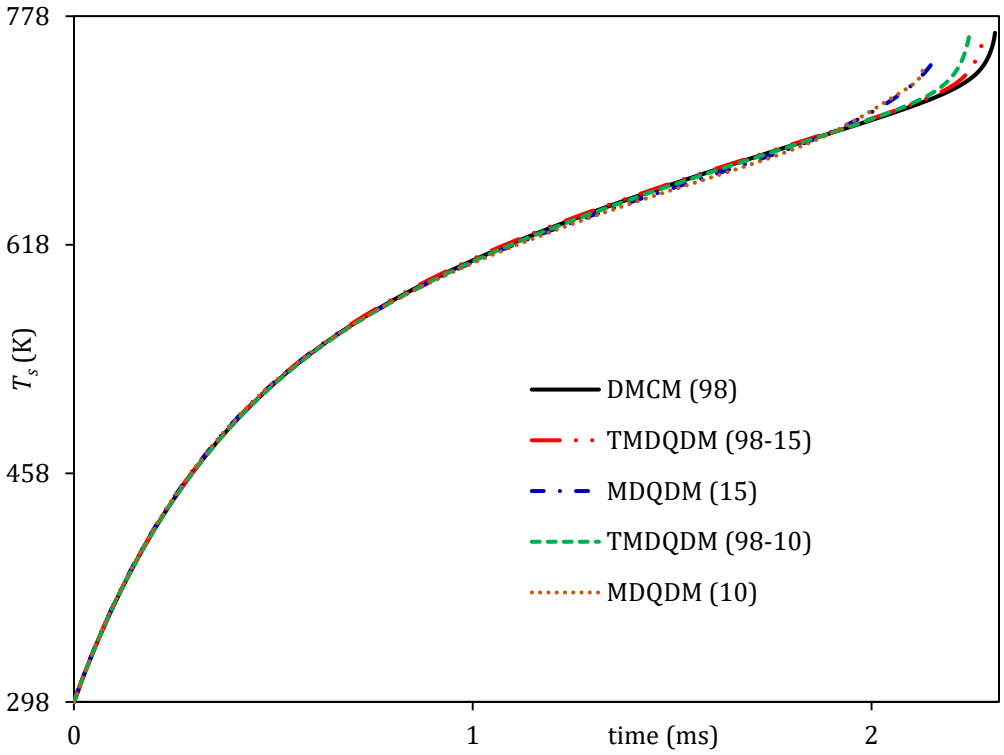

Figure 47. Evolution of droplet surface temperatures of pure diesel fuel using the DMCM, original MDQDM and the MDQDM with the new transient algorithm (indicated as TMDQDM).

The evolutions of droplet radii and surface temperatures were predicted for the contributions of all 119 components of E85-diesel blends, using the same models as in Figures 46 and 47 (see Figures 48-55). Similar to Figures 46 and 47, both the droplet lifetimes and surface temperatures show the nearest agreement between the results predicted by the MDQDM with the new algorithm (119-20) and DMCM.

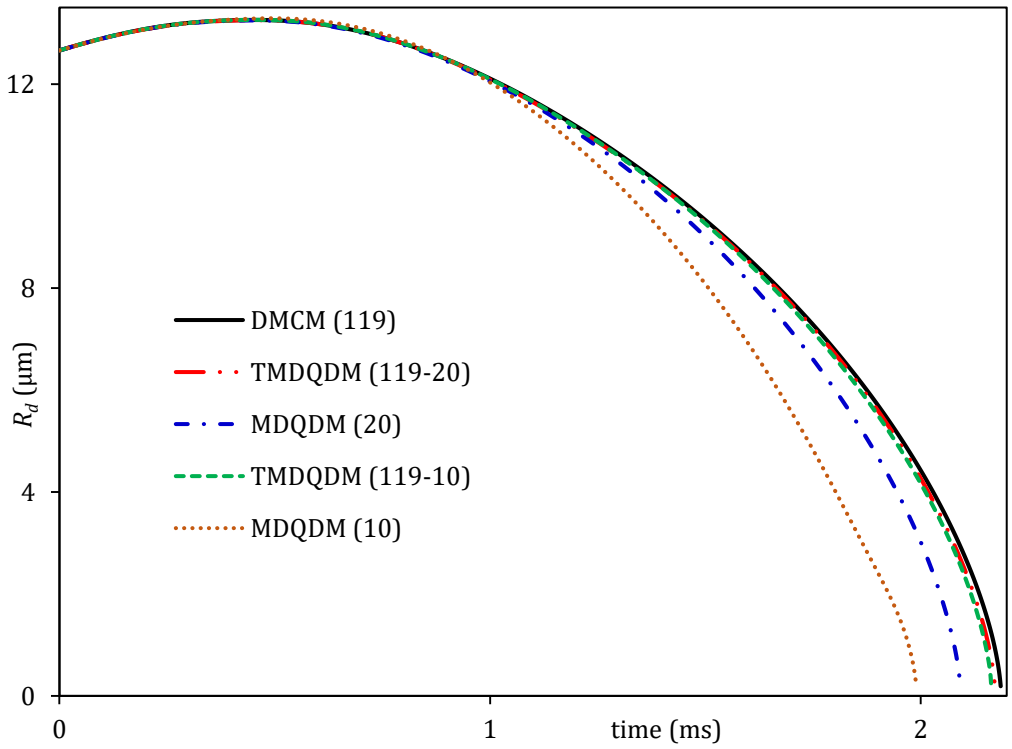

Figure 48. Evolutions of droplet radii versus time for 119 components for E85-5 (95% diesel and 5% E85) using the DMCM and two approximations of the original MDQDM and MDQDM with the new transient algorithm (indicated as TMDQDM).

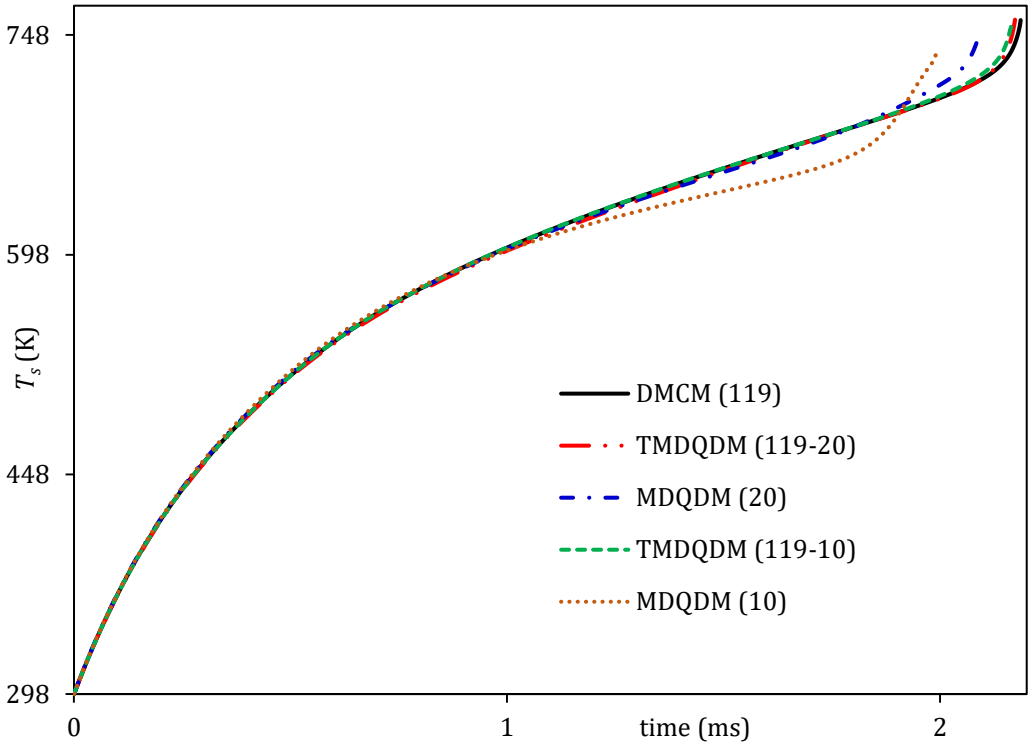

Figure 49. Evolution of droplet surface temperatures versus time for 119 components for E85-5 (95% diesel and 5% E85) using the DMCM, original MDQDM and the MDQDM with the new transient algorithm (indicated as TMDQDM).

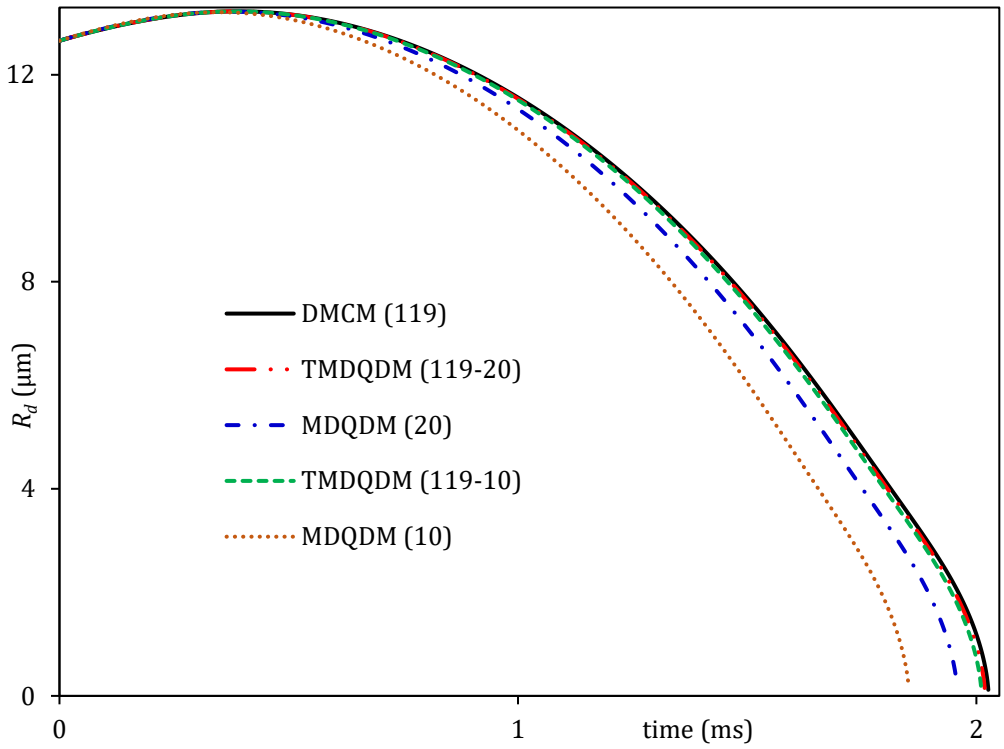

Figure 50. Evolutions of droplet radii versus time for 119 components for E85-20 (80% diesel and 20% E85) using the DMCM and two approximations of the original MDQDM and MDQDM with the new transient algorithm (indicated as TMDQDM).

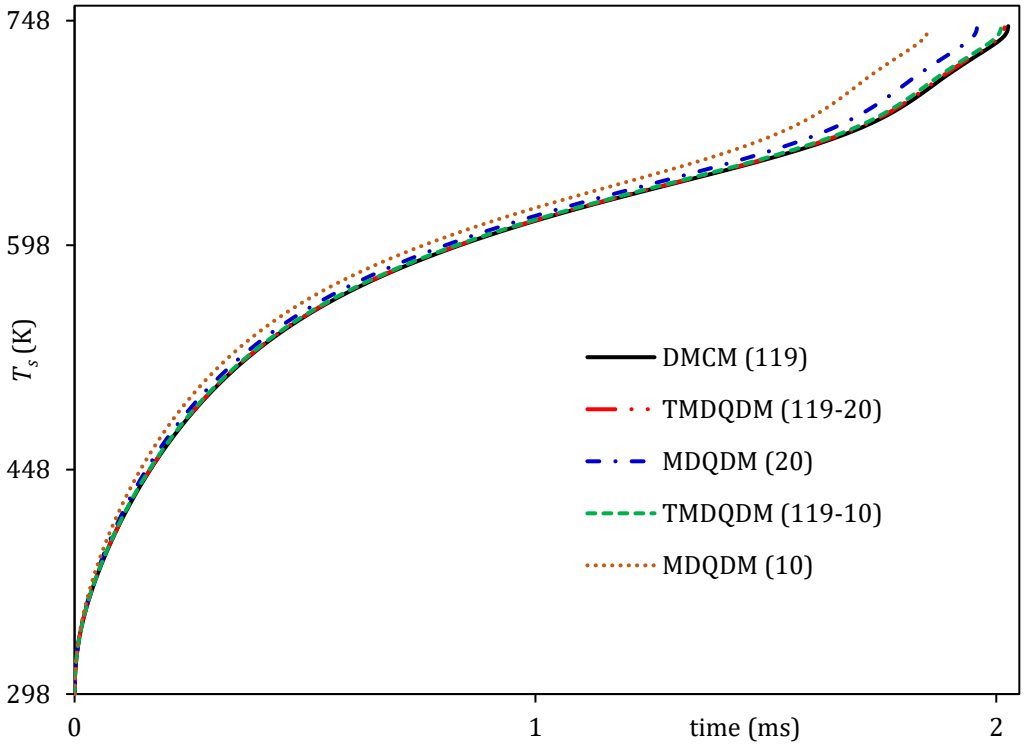

Figure 51. Evolution of droplet surface temperatures versus time for 119 components for E85-20 (80% diesel and 20% E85) using the DMCM, original MDQDM and the MDQDM with the new transient algorithm (indicated as TMDQDM).

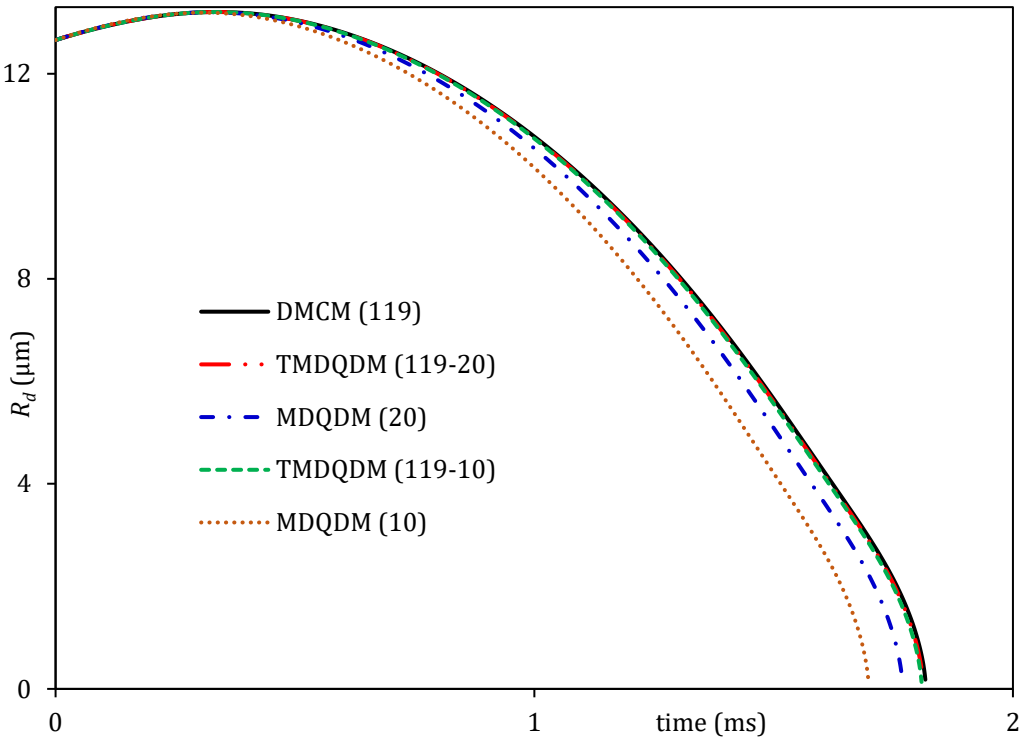

Figure 52. Evolutions of droplet radii versus time for 119 components for E85-50 (50% diesel and 50% E85) using the DMCM and two approximations of the original MDQDM and MDQDM with the new transient algorithm (indicated as TMDQDM).

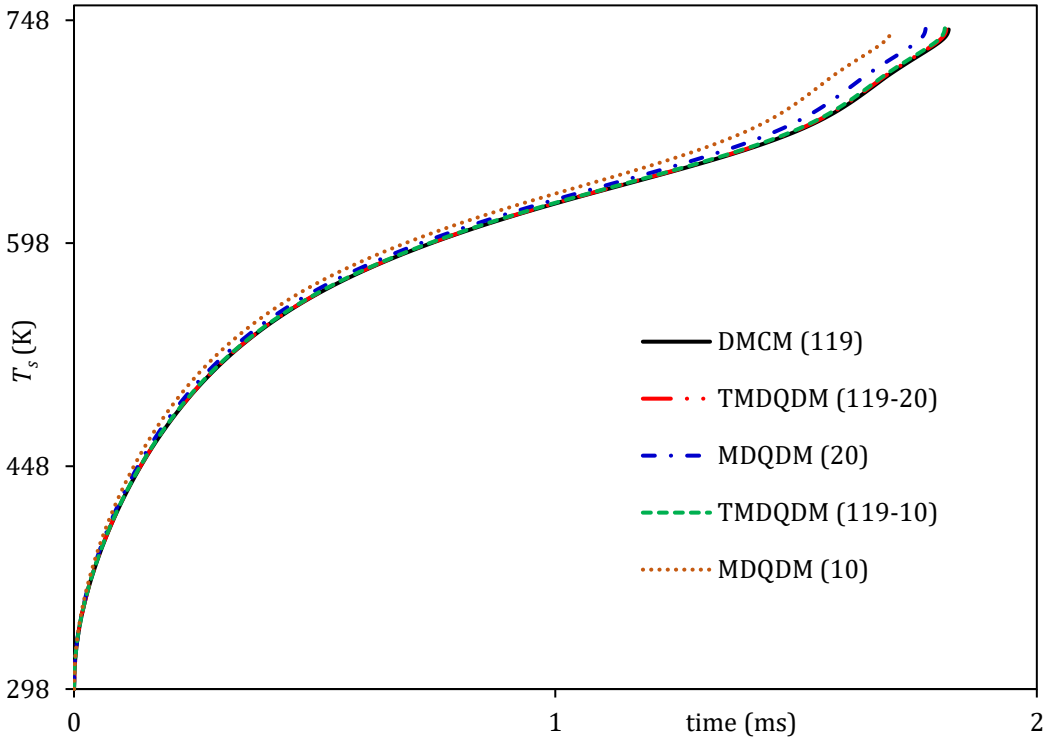

Figure 53. Evolution of droplet surface temperatures versus time for 119 components for E85-50 (50% diesel and 50% E85) using the DMCM, original MDQDM and the MDQDM with the new transient algorithm (indicated as TMDQDM).

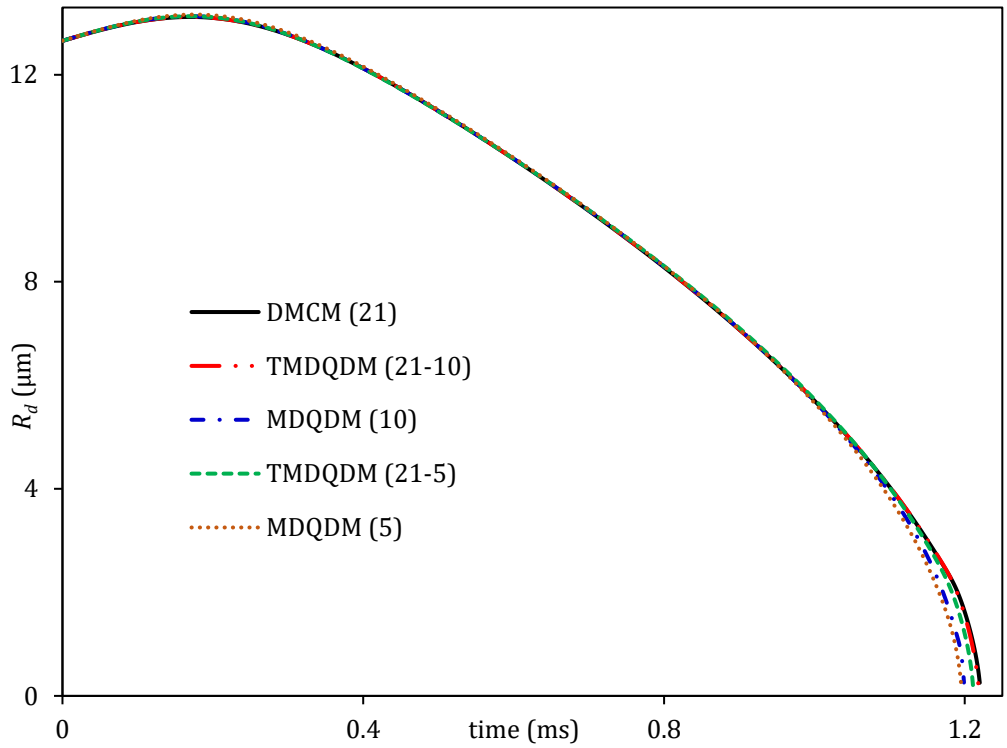

Figure 54. Evolutions of droplet radii versus time for 21 components for E85 (100% E85) using the DMCM and two approximations of the original MDQDM and MDQDM with the new transient algorithm (indicated as TMDQDM).

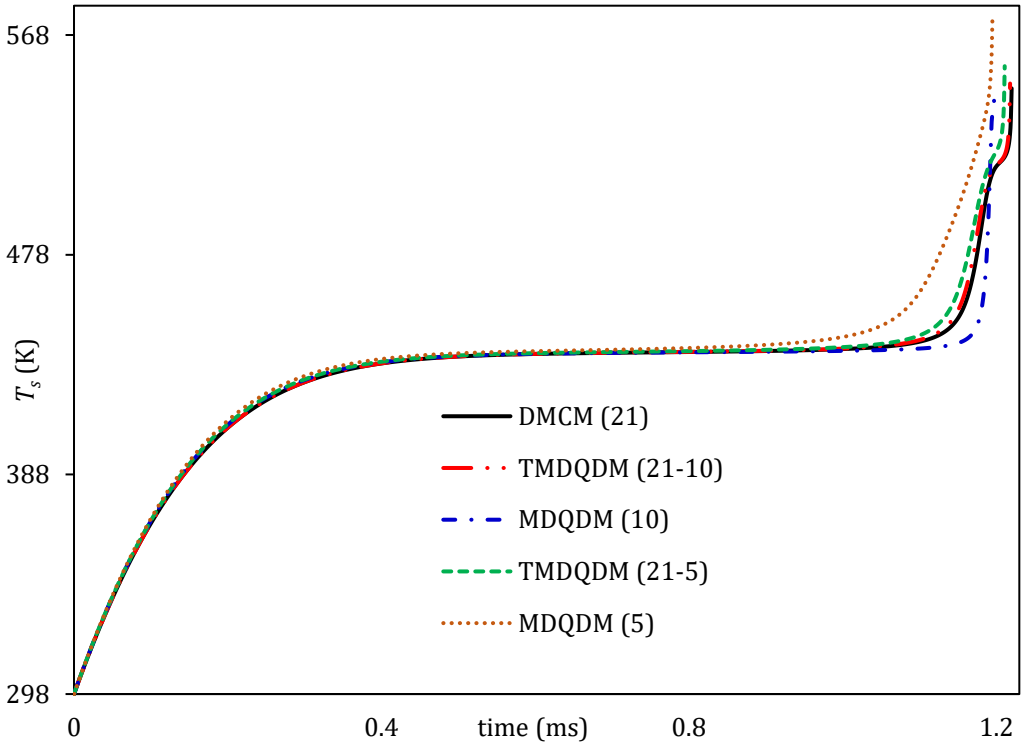

Figure 55. Evolutions of droplet surface temperature versus time for 21 components for E85 (100% E85) using the DMCM and two approximations of the original MDQDM and MDQDM with the new transient algorithm (indicated as TMDQDM).

The predicted droplet lifetimes for various E85-diesel fuel blends are illustrated in Table 32, using the original MDQDM and the one with the new algorithm and the errors compared to the DMCM.

Table 32. Droplet lifetimes (ms) of various E85/diesel blends, predicted using the MDQDM with the new algorithm implemented into it (TMDQD) and the original MDQDM, and the errors ($\boldsymbol{\varepsilon}\% = (\text{time}_{\text{DMCM}} - \text{time}_{\text{model}}) \times 100/\text{time}_{\text{DMCM}}$) of their predictions compared to the predictions using the DMCM.

Model	diesel	ε%	E85-5	ε%	E85-20	ε%	E85-50	ε%	E85	ε%
DMCM	2.31	-	2.186	-	2.026	-	1.817	-	1.22	-
TMDQD(20)	2.28	1.3	2.173	0.41	2.018	0.40	1.812	0.28	-	-
MDQD(20)	2.16	6.4	2.092	4.12	1.96	3.36	1.769	2.64	-	-
TMDQD(10)	2.25	2.77	2.164	0.82	2.01	0.79	1.809	0.44	1.218	0.16
MDQD(10)	2.13	7.75	1.99	8.8	1.85	8.59	1.698	6.55	1.99	1.17
TMDQD(5)	-	-	-	-	-	-	-	-	1.211	0.74
MDQD(5)	-	-	-	-	-	-	-	-	1.195	2.05

As can be seen from Table 32, the droplet lifetimes and the prediction errors of both models decrease with increasing the E85/diesel fuel blend ratios in most cases. The MDQDM with the new algorithm, however, shows better predictions of droplet lifetimes for all fuel blends than the original MDQDM. For instance, reducing the number of components of E85 fuel (21) to 5 using the MDQDM with the new algorithm leads to underprediction of the droplet lifetime by up to 0.74%. In the case of the original MDQDM this error increases up to 2.05%. In all IC engines, the whole processes preceding the onset of combustion (physical delay) within their idle speed range are typically (2– 6 ms) [200–202]. In such a short time, the accuracy in droplet lifetimes is crucial and hence, the use of TMDQD model for simulating these processes can be invaluable in such applications and conditions.

The values of droplet surface temperatures and radii versus the number of C/QC predicted using both versions of the MDQDM based algorithms are shown in Figure 56. These results are estimated for the E85-5 fuel blend, composed of 119 components, at time instants $t =$

0.3 ms, $t = 0.5$ ms, $t = 1$ ms, $t = 1.5$ ms and $t = 2$ ms. The values of the numbers of C/QC used by the TMDQD algorithm were fixed at these time instants and are shown as triangles. Note that in the TMDQD algorithm the full composition of fuel is auto-reduced to different numbers of C/QC at different time instants. In the case of the original MDQDM, the number of C/QC is pre-defined for each separate code run.

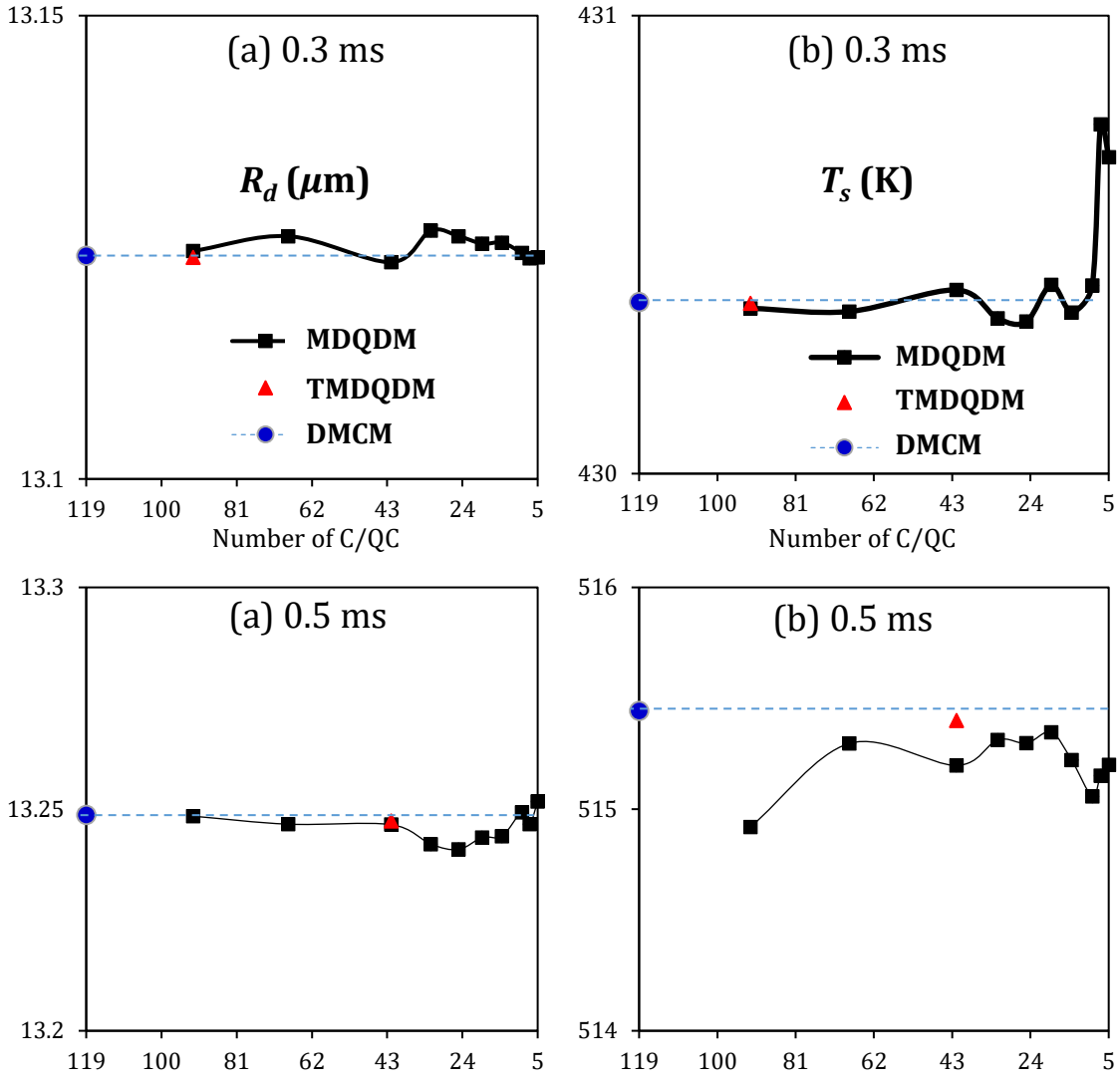

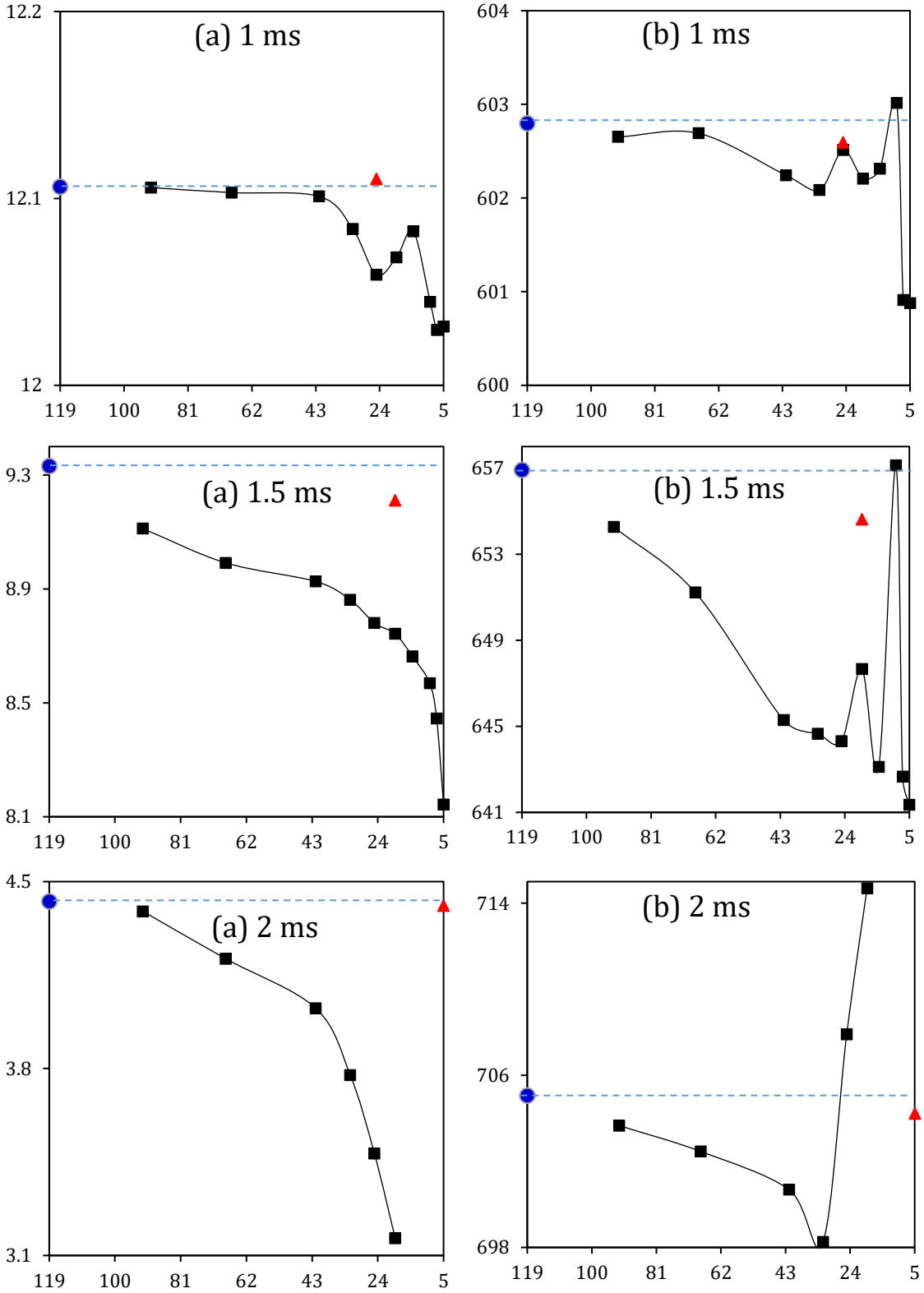

Figure 56. Droplet radii in μm (a) and surface temperatures in K (b) versus the numbers of C/QC predicted by the TMDQD algorithm (▲), the DMCM (●) and the original MDQDM (■) at time instants (0.3 ms, 0.5 ms, 1 ms, 1.5 ms and 2 ms) for various numbers of C/QC.

As can be seen from Figure 56, the predictions of the TMDQD algorithm for droplet surface temperatures and radii are generally more consistent with the DMCM predictions than those predicted using the original MDQDM. Note that the predictions of both approaches are closer at the early stages of heating and evaporation (up to 0.5 ms) than at the later times. The predictions of the original MDQDM show fluctuations in droplet radii and surface temperatures for small numbers of C/QC. This is attributed to the fact that the reduction in the number of C/QC in the original MDQDM is based on trial-and-error, which requires experienced end-users and makes it difficult to implement this approach into CFD codes. Note that the fluctuations predicted by the original MDQDM become less visible at later evaporation times ($\geq$ 1 ms), when the lighter (volatile) components have mostly evaporated. At times close to the evaporation time (>1.5 ms), the original MDQDM fails to predict the droplet surface temperatures and radii accurately. The deviation becomes more noticeable for small numbers of C/QC in the MDQDM.

As expected, the improvement in the modelling capacity of TMDQDM comes at a price, and it is on the expense of its computational time, as shown in Figure 57 (for E85-5 fuel blend).

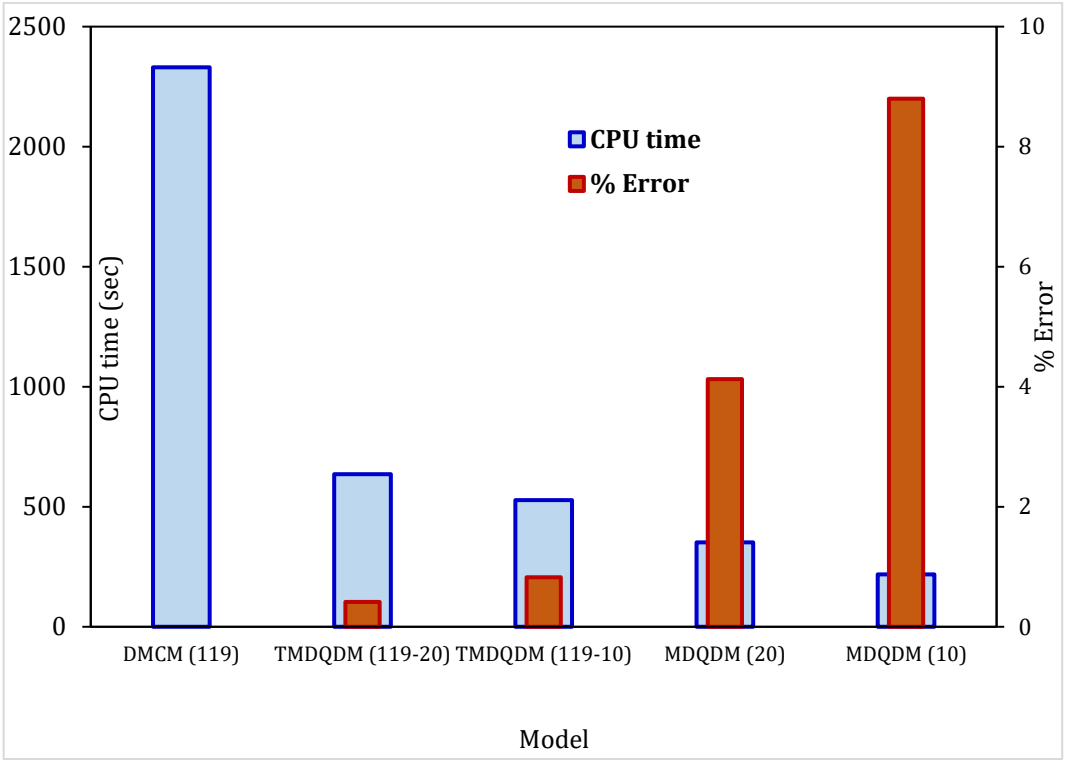

Figure 57. CPU time (wide bars) and errors (narrow bars) of various modelling approaches, compared with the prediction of the DMCM for three modelling approaches as error %=100 $\times$(time$_{DMCM}$-time$_{model}$)/time$_{DMCM}$, for E85-5 fuel blend.

In Figure 57, a noticeable improvement in TMDQDM predictions is made, in comparison to the same results predicted using the original MDQDM, but on the expense of computational time. This finding can justify the importance of using MDQDM where CPU efficiency is more important than accuracy in some engineering applications. However, the TMDQDM proposed in this research thesis is a compromise when both prediction accuracy and CPU efficiency are needed for these predictions.

The CPU time of all fuel blends using the three models and their time savings are illustrated in Table 33. From that table and Table 32, it can be concluded that the importance of the TMDQDM is presented when the actual droplet lifetime is around 2 ms or greater. For the case of pure E85, the TMDQDM underpredicts the droplet lifetime by 0.738, while the MDQDM underpredicts the droplet lifetime by 2.094 (for the case of 21-5 and 5, respectively). On the other hand, the TMDQDM saved 53.92% and the MDQDM saved 74.18% of the CPU time compared to the DMCM. In conclusion, the MDQDM is still sufficient

to be used when the droplet lifetime is less than 2 ms, although this lifetime does not exist for a droplet in any automotive system as droplet lifetimes for ICE are in the range of 2-6 ms.

Table 33. CPU time (in sec) required for each blend using two approximations of the TMDQDM and MDQDM and their saved time compared to the DMCM.

Model	CPU time (sec) and their time savings (T.S.%) compared to DMCM									
	diesel	T.S.%	E85-5	T.S.%	E85-20	T.S.%	E85-50	T.S.%	E85	T.S.%
DMCM	2511	-	2331	-	2177	-	1985	-	306	-
TMDQDM(20)	789	68.6	635	65.03	537	75.33	488	75.42	-	-
MDQDM(20)	428	82.9	351	80.67	427	80.39	363	81.71	-	-
TMDQDM(10)	698	72.2	528	70.93	480	77.95	421	78.79	158	48.4
MDQDM(10)	329	86.9	218	88	306	85.94	261	86.85	107	65.03
TMDQDM(5)	-	-	-	-	-	-	-	-	141	53.92
MDQDM(5)	-	-	-	-	-	-	-	-	79	74.18

7.4. Summary of Chapter 7

A Transient Multi-Dimensional Quasi-Discrete Model (TMDQDM) was suggested for the analysis of fuel droplet heating and evaporation. The model was a generalised approach for dealing with a broad range of fuel blends and compositions. It was based on the previously suggested Multi-Dimensional Quasi-Discrete Model (MDQDM). In contrast to the MDQDM, the new model (TMDQDM) took into account the transient contributions of all groups of hydrocarbons, aiming for higher accuracy of the selected quasi-components than those produced using the original MDQDM. The associated effects of transient fuel compositions on the droplet lifetimes were numerically investigated for several mixtures of E85 (85% ethanol and 15% gasoline) and diesel fuels. It was shown that using the new TMDQDM approach could reduce the full compositions of all analysed E85-diesel mixtures from 119 components to 10 components/quasi-components with up to 0.82% errors in predicted droplet lifetimes. These predictions were relatively more accurate than those predicted using the previously suggested MDQDM – which gave up to 8.8% errors. The CPU time

needed to run this model was up to 79% less than that needed using the full composition of fuel. However, this was not the best CPU efficient approach compared with the time saving of the MDQDM (88%) less than using the full fuel composition. Overall, in this age of continuing advancement on computation resources, the slightly increased computational expense is more than offset by the improved accuracy offered by the new model.

CHAPTER EIGHT: Combustion of Fuel Surrogate

8.1. Overview

In this chapter, surrogate for kerosene fuel is formulated using the model presented in Chapter 6. The formulated surrogate is then compared with the kerosene surrogate provided in the commercial CFD software tool ANSYS-Fluent. The suggested surrogate is examined in terms of heating and evaporation using the implemented CFSM into ANSYS-Fluent via the User-Defined Function (UDF). Finally, the ignition time delay of the suggested surrogate is predicted and compared to those of the fuel composition of kerosene and ANSYS kerosene suggested surrogate.

8.2. Surrogate Formulation

The Complex Fuel Surrogate Model (CFSM), which has been discussed and presented in detail in earlier chapter (Chapter 6), was used for the formulation of kerosene surrogate. The composition of the full kerosene is shown in Table 34.

Table 34. Molar fractions of kerosene fuel, inferred from [203,204].

Carbon no	n-alkanes	iso-alkanes	cycloalkanes/olefins	alkylbenzenes	naphtobenzenes	diaromatics
C7	0.19	0.23	0.17	0.09	-	-
C8	0.19	0.39	0.63	0.61	-	-
C9	0.49	1.72	2.38	1.56	0.22	-
C10	0.70	4.09	5.83	2.72	1.06	0.09
C11	0.75	5.33	6.93	2.19	1.81	0.25
C12	1.15	6.67	7.40	3.00	3.48	0.3
C13	0.87	5.06	4.49	2.91	0.9	0.06
C14	0.89	5.14	3.78	1.74	0.24	-
C15	0.57	5.63	1.67	0.35	-	-
C16	0.05	2.11	0.74	-	-	-
C17	-	-	0.48	-	-	-
Total %	5.84	36.09	34.52	15.16	7.70	0.7

The composition shown in Table 34 was investigated in terms of heating and evaporation using the DMCM. The CFSM was then used to generate a surrogate for the kerosene fuel. The CFSM was limited for 2 Approximate-Discrete Components (ADC) (i.e. the generated surrogate consisted of two components only). This limit in the number of components was because the generated surrogate was later used for combustion studies using detailed chemical mechanisms. The two generated ADC were iso-decane ($C_{10}H_{22}$) and cyclododecane ($C_{12}H_{24}$), with fractions of 0.534 and 0.466, respectively. These two components with their fractions represent the suggested surrogate for kerosene. In Table 34, one can see that these two components represent two groups of the highest molar fractions (iso-alkanes and alkylbenzene). Therefore, the CFSM has generated iso-decane (not n-decane) among the dominant species in kerosene fuel. The evolutions of droplet diameter for the suggested surrogate, using the CFSM, were compared with the predictions of the Multi-Dimensional Quasi-Discrete Model (MDQDM) and DMCM (Figure 58). For this comparison, a single droplet was considered using a typical GTE conditions. The initial droplet diameter and temperature were 100 μm and 375 K, respectively. The ambient gas temperature and pressure were 800 K and 4 bar respectively.

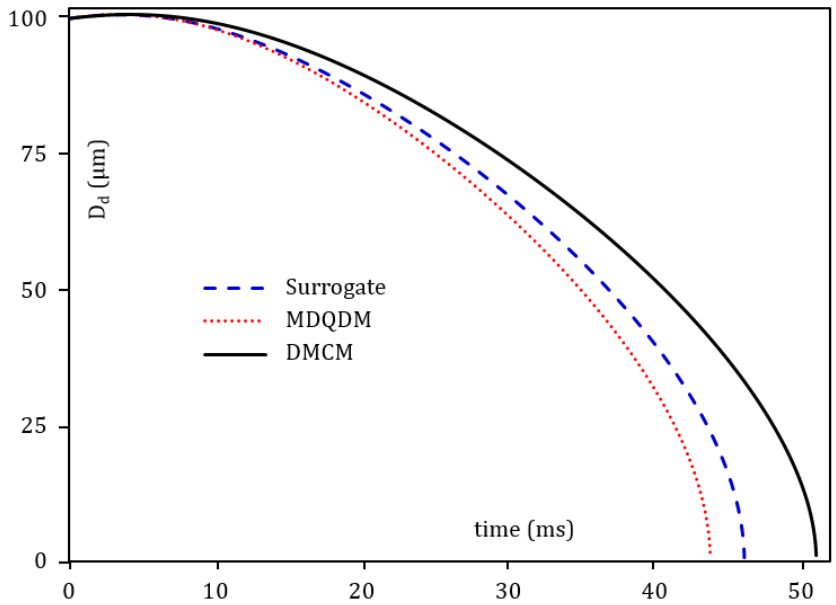

Figure 58. The droplet evaporation versus time for kerosene using the DMCM, MDQDM and surrogate (CFSM).

Compared to the full composition, the suggested surrogate shows 7.6% deviation. This deviation can be well reduced if only one extra component was considered for the surrogate. For the implementation and combustions studies, however, this deviation is acceptable in order to maintain no more than two components.

8.3. Implementation of DMCM

The main reason behind the implementation of the DMCM model into ANSYS-Fluent is due to the fact that the latter software tool does not take into account several factors for the droplet heating and evaporation, e.g. temperature gradient, diffusion of species, and internal recirculation inside moving droplets. Instead, it is based on the assumption that all these factors can be ignored. The reasons behind these simplifications were discussed in Chapter 2. The work presented in [57] was the first work of its kind to investigated the implementation of the droplet heating and evaporation model for the simulation of ICE full-cycle. The work of [57] was for mono-component. This work was then generalised in [205] to the case of binary-components in which the diffusion of species were also considered, combined with the temperature gradient inside the droplet. The latter work, however, was conducted for cooling evaporation in which the droplet was left in the ambient for evaporation. Furthermore, no full evaporation was observed.

In this proof of concept work, the thesis finding of CFSM was implemented into a commercial CFD code with an attempt to simulate the combustion processes in a GTE. Such an approach is the first of its kind for any former literature work. A detailed analysis of the heating and evaporation of the generated kerosene fuel surrogate was implemented into the 3D CFD model [206]. The implemented heating and evaporation model takes into account the temperature gradient, species diffusion and recirculation inside droplets. This was done via the implementation of the DMCM into ANSYS-Fluent using the UDF. The heating and evaporation were assumed to take place in a can type combustor. The

computational domain and polyhedral mesh used for the hydrodynamic model are shown in Figure 59. The generated mesh consisted of 262,255 cells with a cell volume range of 0.0057647 – 470 mm^3 and face cell area range of 0.014 – 8 mm^2.

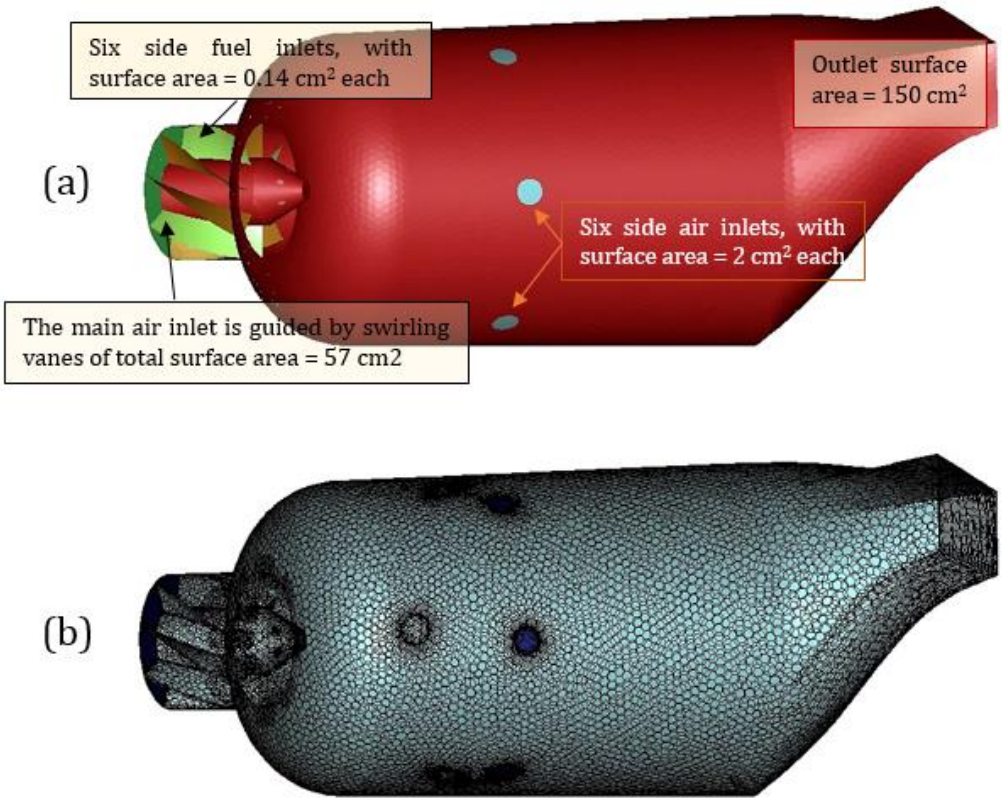

Figure 59. The can combustor geometry, showing (a) the internal walls of the system, and (b) the polyhedral mesh, used in the CFD simulation. The cell volume range is 0.0057647 – 470 mm^3, the face cell area range is 0.014 – 8 mm^2, and the total number of cells is 262,255.

Pressure-based solver with a realizable $\kappa - \varepsilon$ turbulence model was used for the hydrodynamic region with enhanced wall treatment taking into account the effect of curvature. The domain pressure and velocity were coupled in a quasi-transient manner. The following modelling set-up was made: standard for pressure and first order upwind for the momentum, the turbulent kinetic energy, dissipation rate, progress variable, mean mixture fraction, mixture fraction variance and progress variable variance. Four thousand iterations were set for the numerical residuals.

The droplet lifetime predicted by the new ANSYS CFD model was assessed in comparison to the original in-house code for a 100 μm diameter droplet moving into stationary air at $U_d = 1\ \mathrm{m.s^{-1}}$. The initial fuel temperature was $T_o = 375\ \mathrm{K}$ under the ambient air temperature and pressure of $T_g = 800\ \mathrm{K}$ and $p_g = 4\ \mathrm{bar}$, respectively. In Figure 60, the evolution of droplet diameter with time is presented using three approaches: 1) the results predicted by standard ANSYS-Fluent software using constant properties; 2) the results predicted by ANSYS-Fluent and transient properties of fuel components using the UDF, but without the CFSM; and 3) ANSYS-Fluent results with full implementation of the CFSM and transient thermodynamic and transport properties.

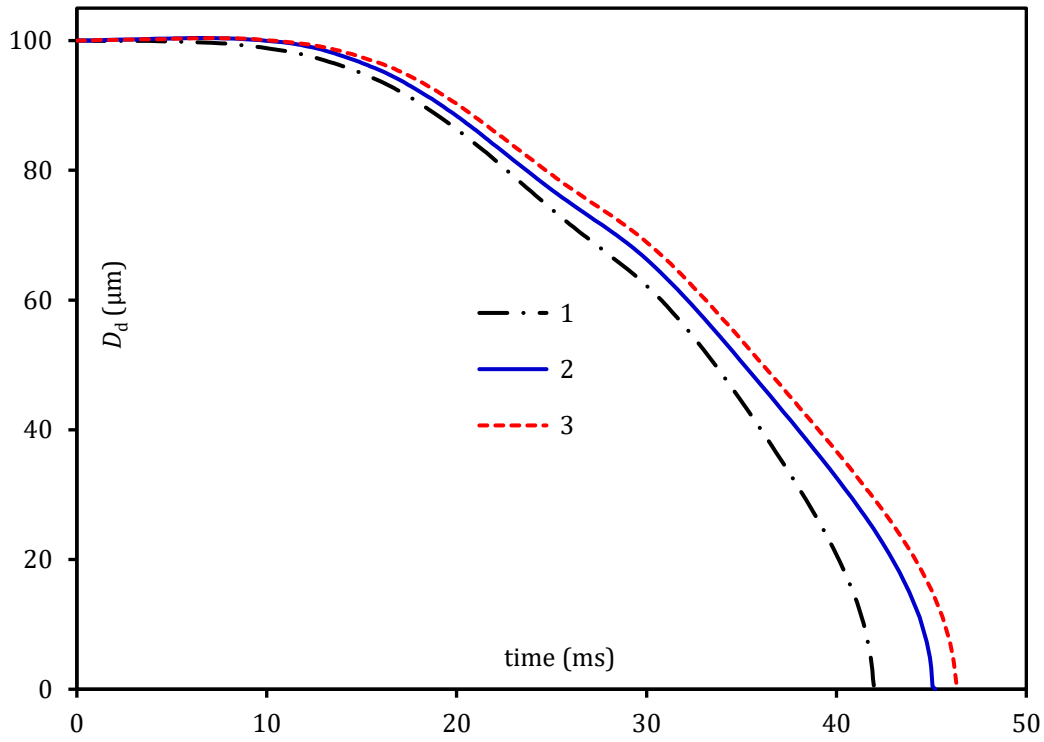

Figure 60. The evolutions of droplet diameter using the three modelling approaches: 1 refers to Standard ANSYS-Fluent results, with constant properties, 2 refers to ANSYS-Fluent results, with in-house properties using UDF, and 3 refers to ANSYS-fluent results incorporating the CFSM using UDF.

As follows from Figure 60, the incorporation of the DMCM into ANSYS-Fluent leads to prediction of up to 10.4% longer evaporation times compared to the case when the standard ANSYS-Fluent model is used.

A contour of the droplet evaporation inside the can combustor is shown in Figure 61. As can be seen from that figure, all droplets are injected at a diameter of 100 μm, and all these droplets are evaporated at around a distance of 40% of the injection point.

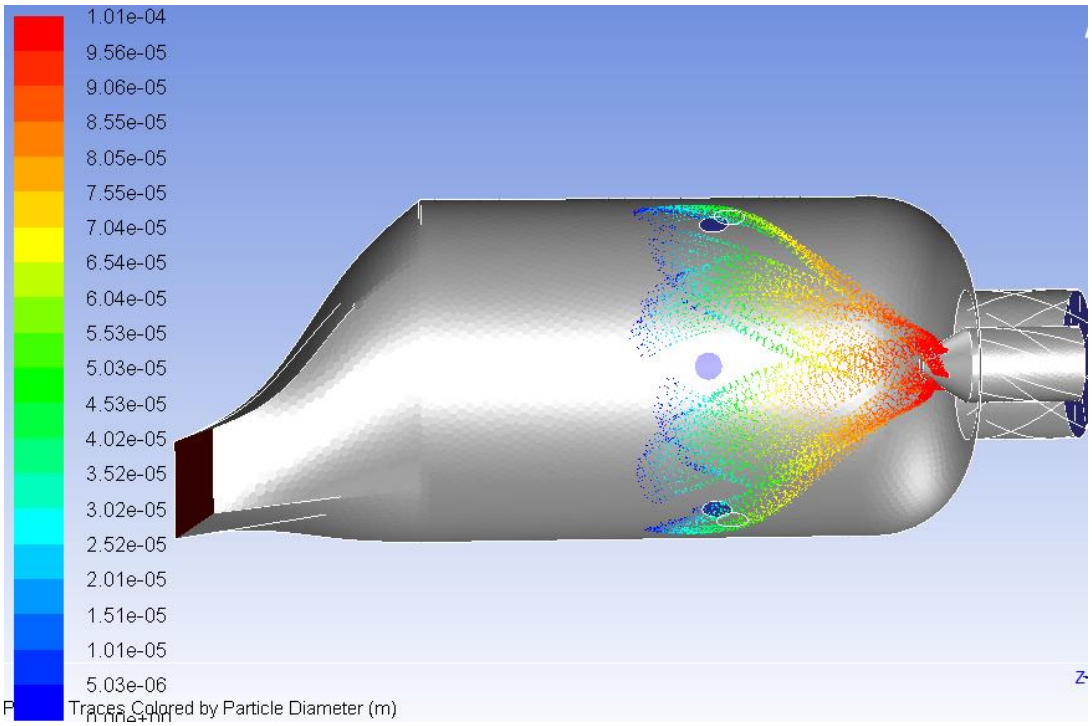

Figure 61. Profile of droplet diameter starting from the injection until the full evaporation.

The results validating ANSYS-Fluent simulation that incorporated the new model is presented in Figure 62. The validation was done by comparing the computed results with experimental data reported in the literature [207]. This was based on a kerosene droplet with initial diameter 1.8 mm and initial temperature 298 K. The droplet was exposed to an air flow rate of 20 L/min at 0.1 MPa ambient pressure. As can be seen from Figure 62, there is a general agreement between the numerical results and experimental data. In CFSM analyses, the effect of thermal swelling on droplet heating and evaporation was taken into account. Some discrepancies, however are presented when comparing numerical to experimental results. The major one is that the full evaporation is not achieved for the experimental measurements. This is attributed to measurement uncertainty [207].

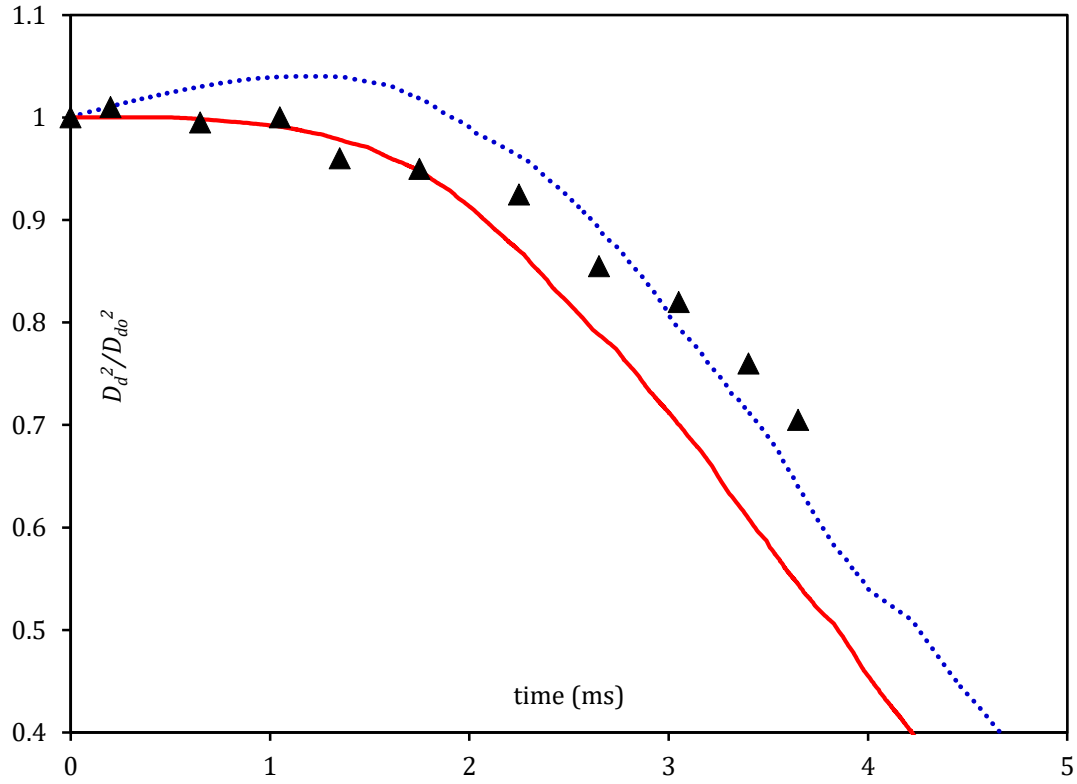

Figure 62. The validation of the models for the normalised squared droplet diameters predicted by the standard ANSYS-Fluent (solid curve), and ANSYS-Fluent incorporating the CFSM (dotted curve), using data reported in [207] (bold triangles) for kerosene fuel.

8.4. Combustion and Ignition Time Delay

The combustion characteristics of the suggested surrogate (53.4% iso-decane and 46.6% cyclododecane) was also compared with the simulated results of a suggested kerosene surrogate in ANSYS. The latter surrogate consists of one hypothetical component ($C_{12}H_{23}$) which does not exist in real life. The combustion of the surrogates was investigated based on the partially premixed combustion model. A co-axial air-blast atomizer was used with primary and secondary air and fuel mass flowrates of 0.15, 0.025 and 0.003 kg/s, respectively.

The thermodynamic state of the species in the flame is described using the Flamelet Generated Manifold (FGM) model. In the FGM model, a detailed mechanism of reactants and products is required to describe the combustion reactions. Flamelet structures were imported from an external file generated in ANSYS CHEMKIN tool. The combustion

mechanism of iso-decane and cyclododecane (components of the suggested surrogate) were imported from [208]. The chemical mechanism of iso-decane and cyclododecane were merged together using ANSYS CHEMKIN tool. The resulting chemical mechanism of the two components, included 194 species and 1459 reactions. The equations of the adiabatic premixed flame are converted from physical-space to the reaction-progress space. These equations are [89,170, 209]:

$$\rho \frac{\partial Y_k}{\partial t} + \frac{\partial Y_k}{\partial c} \dot{\omega}_c = \rho \chi_c \frac{\partial^2 Y_k}{\partial c^2} + \dot{\omega}_k \tag{48}$$

$$\rho \frac{\partial T}{\partial t} + \frac{\partial T}{\partial c} \dot{\omega}_c = \rho \chi_c \frac{\partial^2 T}{\partial c^2} - \frac{1}{c_p} \sum_k h_k \dot{\omega}_k + \frac{\rho \chi_c}{c_p} \left(\frac{\partial c_p}{\partial c} + \sum_k c_{p,k} + \frac{\partial Y_k}{\partial c} \right) \frac{\partial T}{\partial c} \tag{49}$$

where Y_k is the mass fraction of species k, t is time (in s), $\dot{\omega}_k$ (in mol.L^{-1}.s^{-1}) is the reaction rate of species k, ρ (in kg.m^{-3}) is the density, h_k is the enthalpy (in kJ.mol^{-1}), and c_p is the specific heat capacity (in kJ.kg^{-1}.K^{-1}). χ_c is the scalar dissipation which is expressed as [89,170, 209]:

$$\chi_c(f, c) = \chi_{max} \exp\left[-2 \left(erfc^{-1}\left(\frac{f}{f_{sto}} \right) \right)^2 \right] . \exp\left[-2 \left(erfc^{-1}(2c) \right)^2 \right] \tag{50}$$

where f is the mixture fraction and f_{sto} is the stoichiometric mixture fraction.

After importing the flamelet, the compositions and temperature of the fuel and oxidizer streams were specified. Compositions of the fuel were the same as those presented in Section 8.2 and the temperatures presented in Table 35. The flamelet was numerically described using the advanced default control options of Ansys-Fluent. These control options include initial Fourier number, Flourier number multiplier, relative error tolerance, absolute error tolerance, flamelet convergence tolerance and maximum integration time. The default values for the size of flamelet (32), maximum number of flamelet (10) and scalar

dissipation of each flame (0.01 s^{-1}) were used in this CFD model. Additionally, the probability density function was created which acted as a lookup table in the final calculations. Furthermore, the FGM model was fully defined and the combustion chemistry has been preprocessed.

Table 35. The input parameters used for the combustion simulation.

Parameter	Value	Unit
Primary injection air velocity	10	m/s
Secondary injection air velocity	6	m/s
Fuel mass flowrate	0.003	Kg/s
Ambient pressure	4	Bar
Air temperature	293	K
Fuel temperature	375	K
Oxidation temperature	800	K

The NO_x species are calculated in Ansys-Fluent via solving the mass transport equation which accounts for the diffusion, convection, formation and consumption of all species. The transport equation can be expressed as [89,170, 209]:

$$\frac{\partial}{\partial t}\left(\rho Y_{NO_X}\right) + \nabla.\left(\rho \vec{V} Y_{NO_x}\right) = +\nabla.\left(\rho \mathcal{D} \nabla Y_{NO_x}\right) + S_{NO_x} \quad (51)$$

where $\mathcal{D}$ is the effective diffusion coefficient and S_{NO_x} is a source term.

As can be seen from Figure 63, the entrainment of air flow enhances the oxidation of the mixture (suggested surrogate and air) with charge from the dilution holes. The NO_X, and CO_2 are at a relatively low level, indicating well diluted fuel leading to complete combustion.

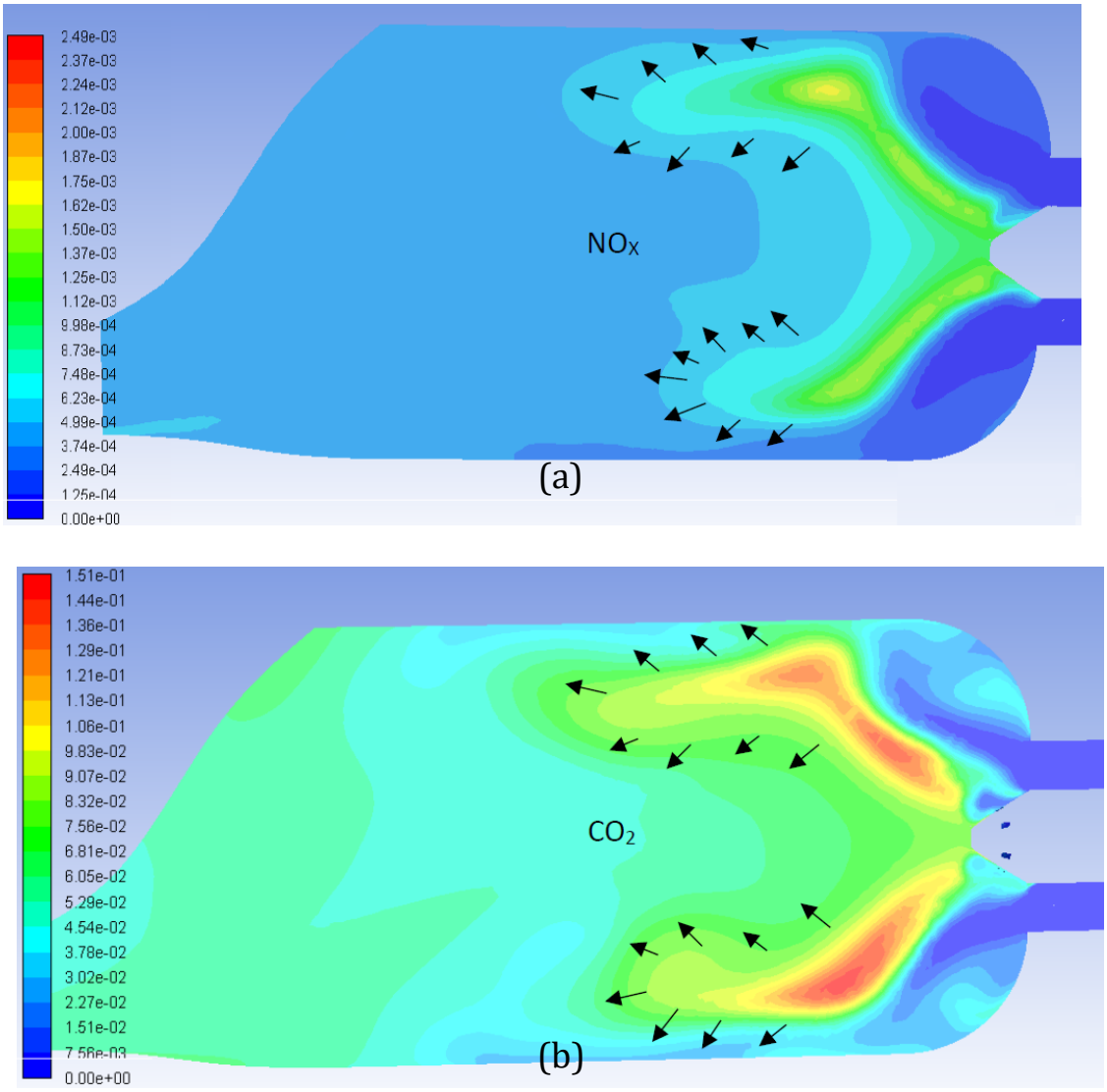

Figure 63. The species distribution (dimensionless mass fraction), (a) NO_X and (b) CO_2, at the symmetry plane of the combustion chamber using the suggested kerosene surrogate (53.4% iso-decane and 46.6% cyclododecane). Black arrows show the species diffusion from the high concentration content to the lower concentration content.

Further illustrations of the combustion species formation inside the can combustor, and at various sections along its length are provided in Figure 64.

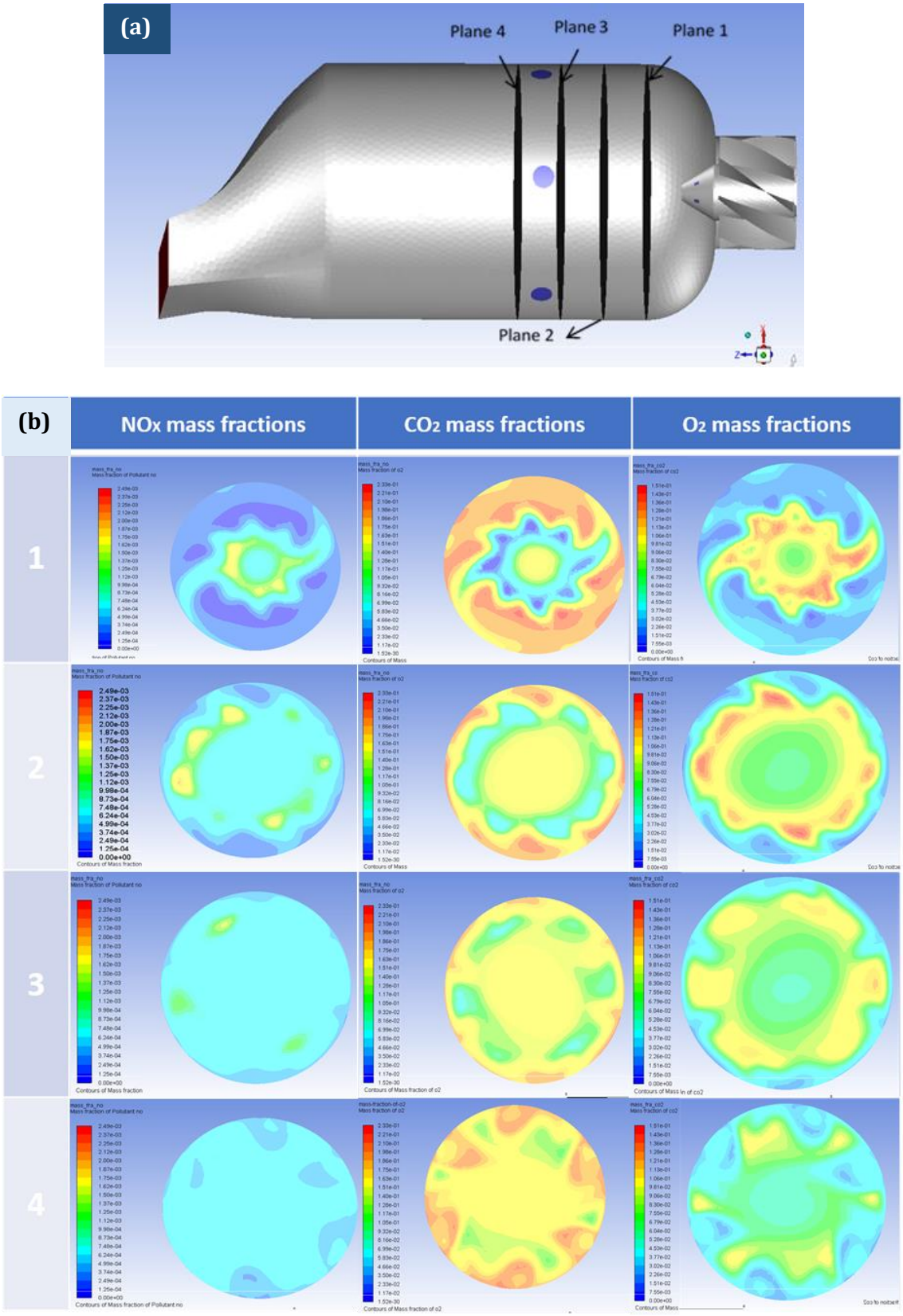

Figure 64. Species formation and distribution across the can combustor at four planes, showing (a) the four planes along the combustor, and (b) the profile contours for the four planes.

The above results were obtained for the suggested surrogate. The species distributions were also obtained for ANSYS kerosene surrogate. The distribution of NO_X, and CO_2 are shown in Figure 65. Compared to Figure 63, it can be seen that the implementation of the detailed combustion chemistry of the suggested kerosene surrogate leads to lower NO_X, and CO_2. This is because the combustion chemistry of the ANSYS kerosene surrogate does not include a detailed species generated as a result of the combustion process. Instead, it includes 20 species only (N_2, O_2, $C_{12}H_{23}$, CO, CO_2, H_2O, H_2, C, OH, CH_4, H, O, HO_2, H_2O_2, HCO, CHO, NO, HOCO, C_2H_6 and HCOOH). Hence, the mass fractions of NO_X, and CO_2 are higher than those of the suggested surrogate (using the CFSM) with the detailed combustion chemistry.

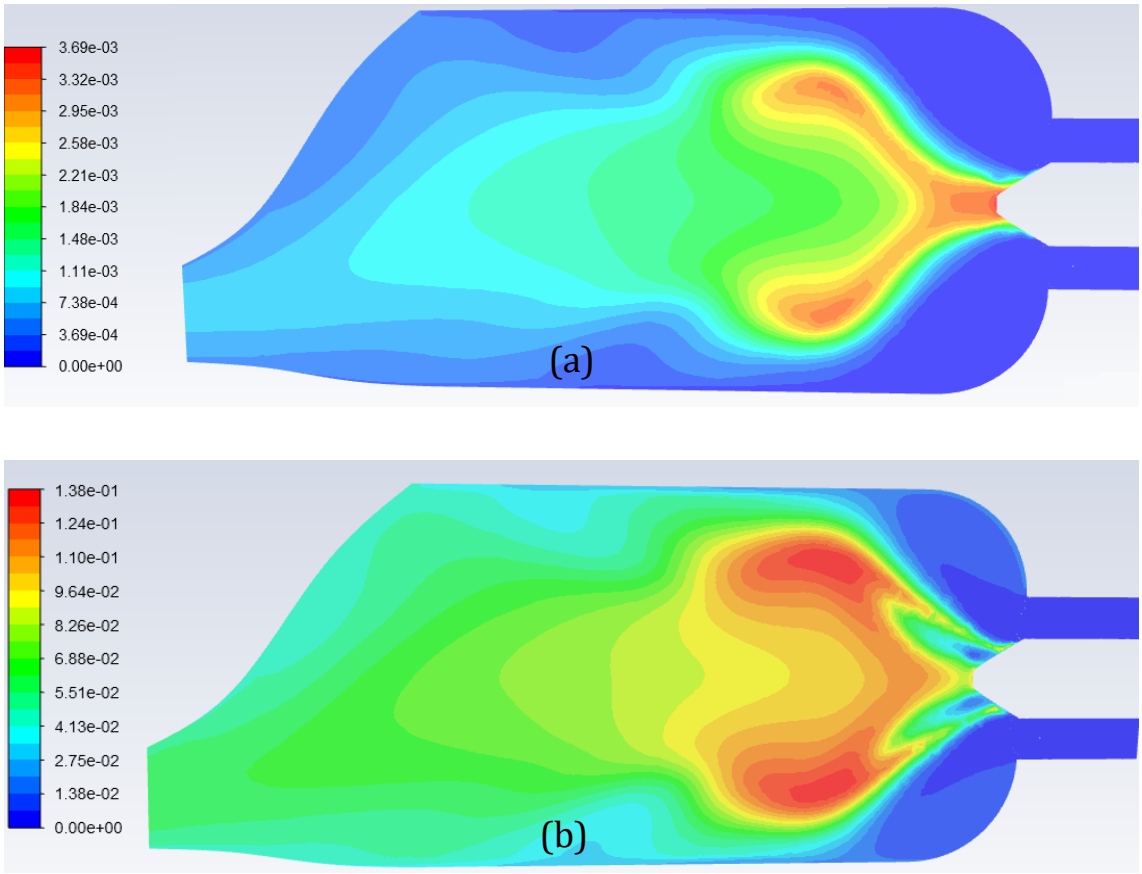

Figure 65. The species distribution, (a) NO_X and (b) CO_2, at the symmetry plane of the combustion chamber using ANSYS kerosene surrogate ($C_{12}H_{23}$).

The Thermodynamic characteristics of the combustion process of the suggested surrogate and ANSYS surrogate are presented in Table 36. Noticeable difference between the two surrogates is observed. The thermodynamic characteristics of ANSYS surrogate are always higher because, in average, this surrogate is heavier than the suggested surrogate.

Table 36. Thermodynamic characteristics of the combustion process

Parameter	ANSYS surrogate	Suggested surrogate
Total reaction heat (MJ.kg^{-1})	-4.99E+02	-4.03E+02
Internal Energy (MJ.kg^{-1})	3.11E+04	3.05E+04
Total enthalpy at the outlet (MJ.kg^{-1})	3.48E+02	3.41E+02
Evaporation enthalpy (MJ.kg^{-1})	-1.61	-1.473

The ignition time delays of kerosene surrogates were estimated at different combustion temperatures, pressures and equivalence ratios. The Arrhenius relationships of ignition time delay suggested in [99], for RP-3 kerosene, was used for the suggested surrogate (53.4% iso-decane and 46.6% cyclododecane) using the appropriate activation energy. The relationships can be expressed as [209]:

$$\tau_{\text{ign}} = 4.719 \times 10^{-3} P^{-0.72} \phi^{1.27} \exp\left(\frac{Ea}{RT}\right) \quad (52)$$

where P is the pressure in Pa, ϕ is the equivalence ratio (fuel/air ratio), Ea is the activation energy which is 134.68 kJ. mol^{-1}, R is the universal gas constant in kJ. mol^{-1}. K and T is the oxidation temperature in K.

The ignition time delay of the suggested kerosene surrogate was compared to the full composition of kerosene fuel. The ignition time delay of the latter one was estimated based on a modified form of the Arrhenius relationships (using the appropriate activation energy), recommended for a multi-component kerosene of n-decane, n-dodecane, isocetane,

methylcyclohexane and toluene with a molar fraction of 14%, 10%, 30%, 36%, 10%, respectively. Further details on this expression can be found in [209]:

$$\tau_{\text{ign}} = 6.824 \times 10^{-3} P^{-0.71} \phi^{1.59} \exp\left(\frac{Ea}{RT}\right) \quad (53)$$

The Ea for the kerosene fuel is 132.8 kJ. mol^{-1}.

A comparison between the ignition time delay of the full composition of kerosene fuel and the two surrogates (suggested surrogate and ANSYS surrogate) was conducted (Figure 66). The analysis was conducted at pressure of 4 bar, equivalence ratio of 1 and oxidation temperature range of 1000-1500 K. The prediction of the ignition time delays of the fuel and its suggested surrogate are very close at the high oxidation temperature. However, a significant difference is noticed at low oxidation temperature. To improve the predictions of the ignition time delay at low oxidation temperature, surrogate with higher number of components is possibly needed. The ignition time delay of the surrogate suggested in ANSYS deviates significantly from that of the full composition of kerosene fuel. The main reason behind that deviation is that the activation energy of ANSYS surrogate is noticeably low (118 kJ/mole).

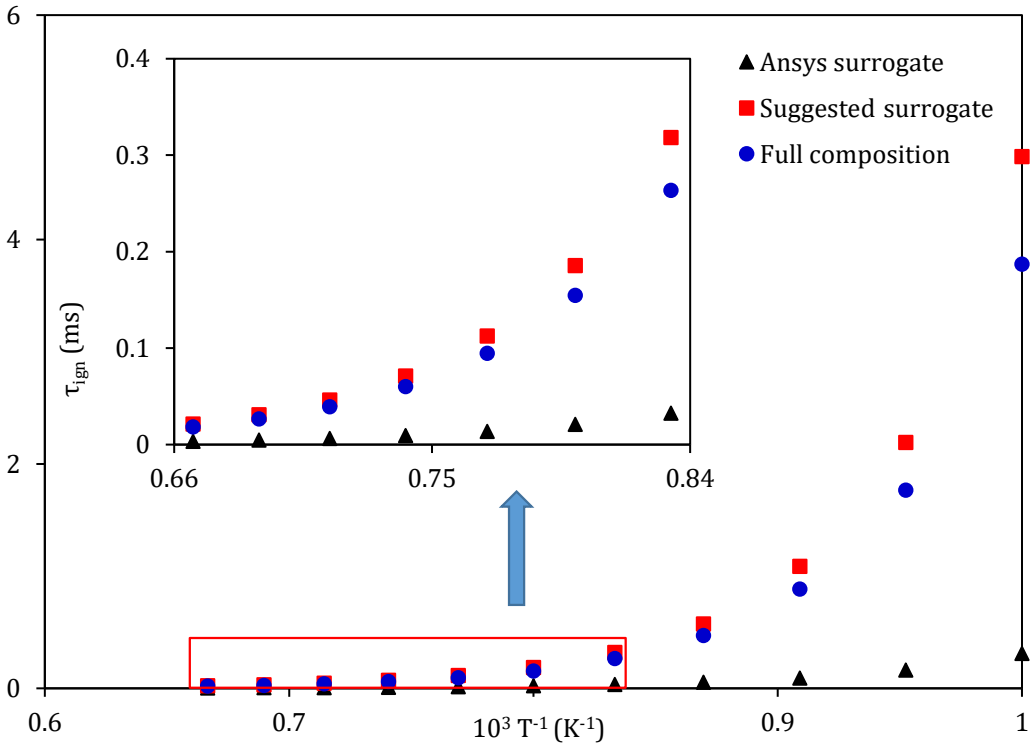

Figure 66. Ignition time delay of the full composition of kerosene fuel and its surrogates (suggested surrogate and Ansys surrogate) at pressure of 4 bar and equivalence ratio of 1.

The ignition time delays of the suggested kerosene were estimated, using equation 52, at different pressures and equivalence ratios. For the predictions of the ignition time delays, a range of 1000-1500 K oxidation temperature was chosen. The impact of equivalence ratio on the ignition time delays is shown in Figures 67 and 68. It can be seen from these figures that the ignition time delay increases with increasing the equivalence ratio. Moreover, it increases with decreasing the oxidation temperature. The impact of pressure, at three different equivalence ratios, is illustrated in Figures 69-71. It is obvious that the ignition time delay decreases with increasing the pressure for all equivalence ratios.

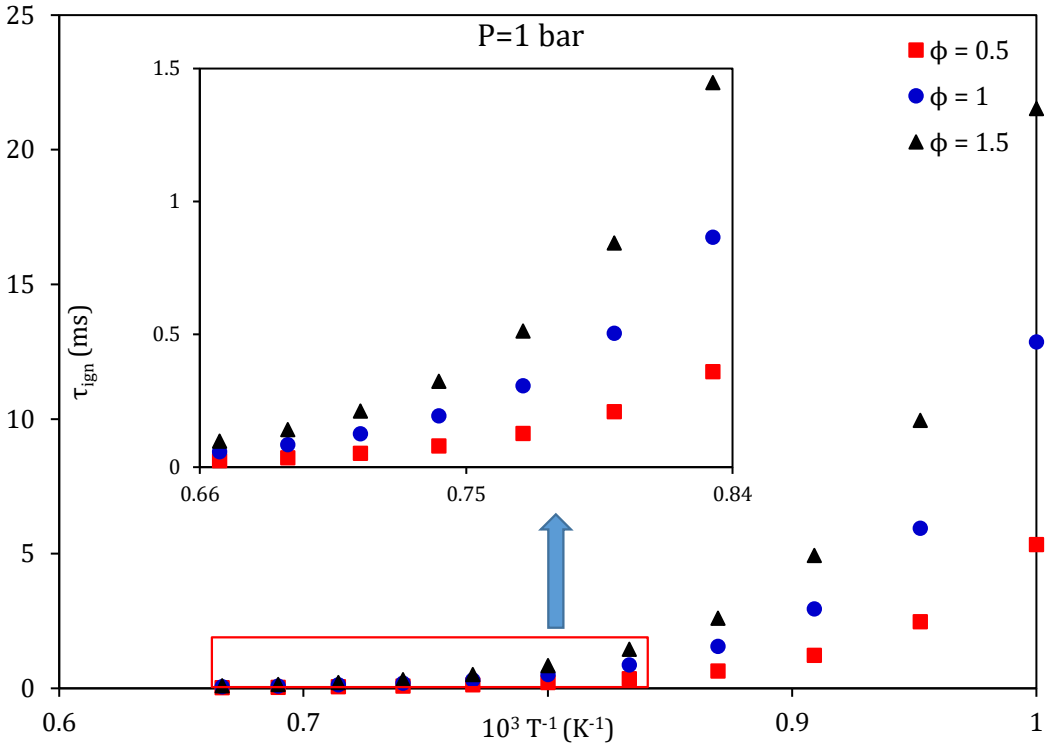

Figure 67. Ignition time delay of the proposed kerosene surrogate at different equivalence ratios and pressure of 1 bar.

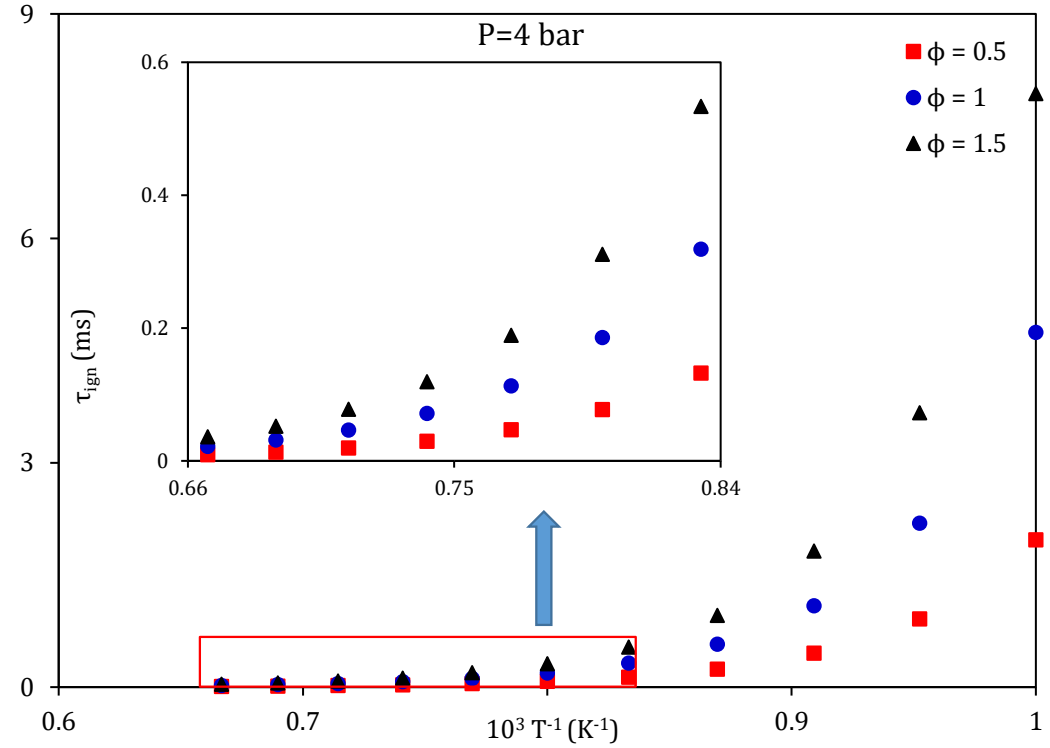

Figure 68. Ignition time delay of the proposed kerosene surrogate at different equivalence ratios and pressure of 4 bar.

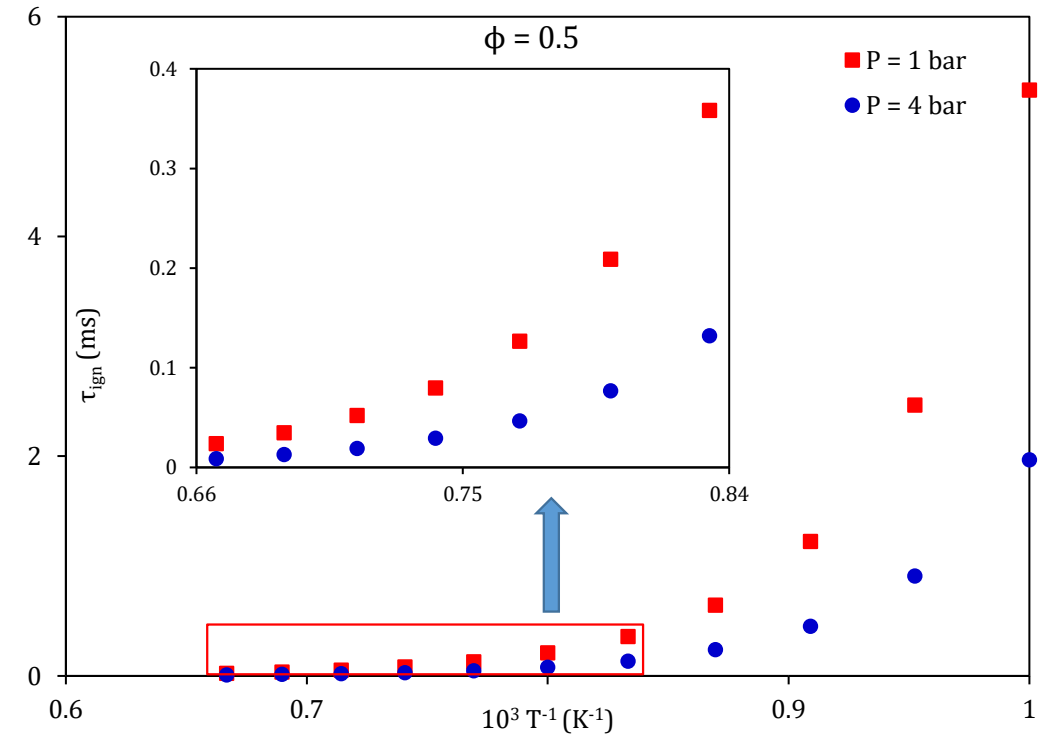

Figure 69. Ignition time delay of the proposed kerosene surrogate at different pressures and equivalence ratio of 0.5.

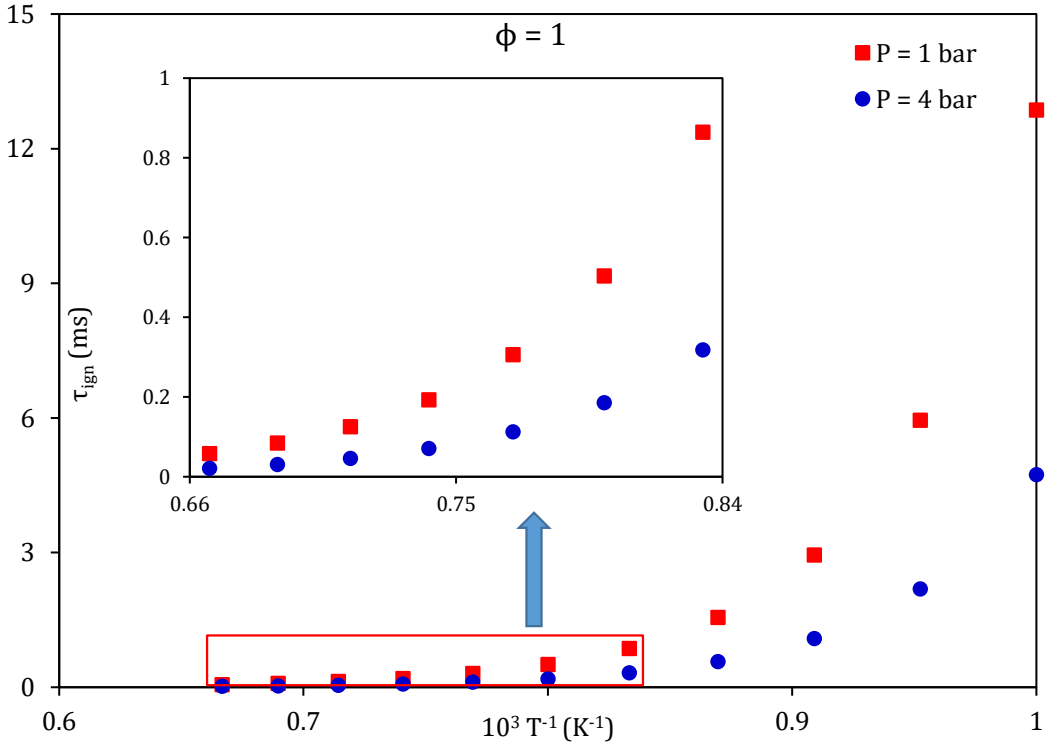

Figure 70. Ignition time delay of the proposed kerosene surrogate at different pressures and equivalence ratio of 1.

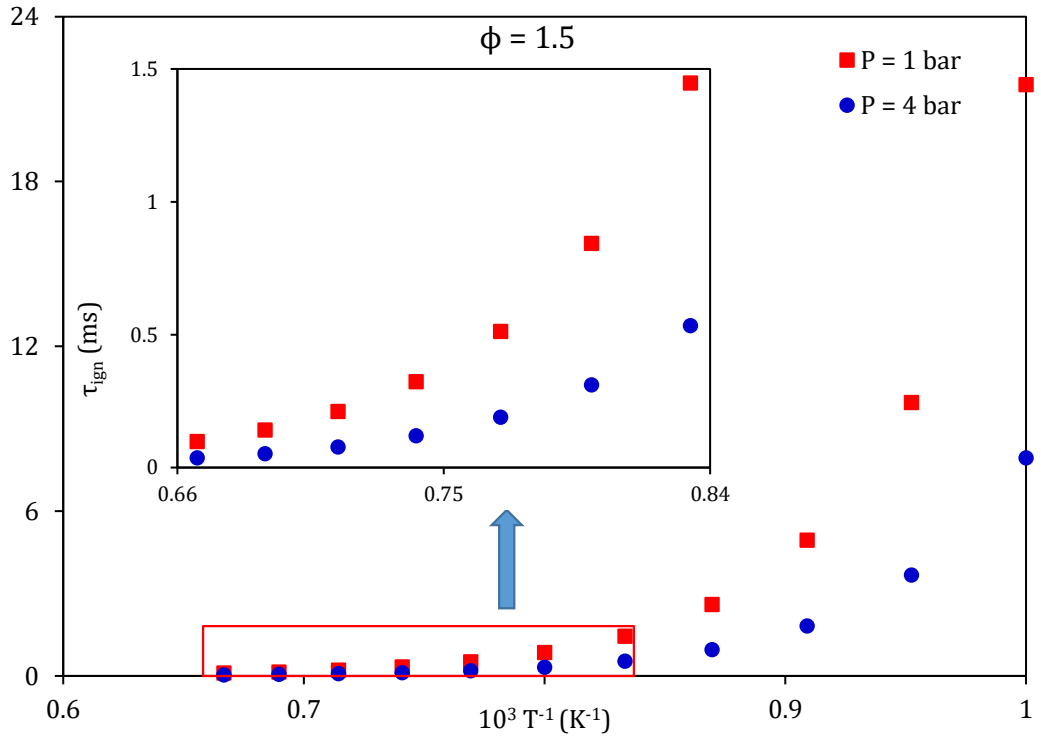

Figure 71. Ignition time delay of the proposed kerosene surrogate at different pressures and equivalence ratio of 1.5.

Based on the results obtained above, one can say that formulated surrogates should include higher number of components (not only two as suggested) in order to improve the predictions accuracy. This vision can be true to a limited extent, based on the fact that the chemical mechanisms are compatible for a wider range of components. Generally speaking, if a certain fuel is represented by at least two components with reasonable component fraction, these two components can reproduce certain characteristics of that fuel with a negligible deviation. For example, representing kerosene fuel by n-hexadecane only will overpredict its evaporation time, while the evaporation time will be underpredicted if the kerosene fuel is represented by n-octane only. Therefore, using a mixture of the two components with appropriate distribution to their mass fractions may solve the problem. This will also reduce the computational cost significantly. Based on these justifications, the suggested surrogate, generated by the CFSM, consisted of two components in this chapter.

8.5. Summary of Chapter 8

In this chapter, the Complex Fuel Surrogate Model (CFSM) was used to generate surrogate for kerosene fuel. A heating and evaporation model including the suggest surrogate was then implemented into ANSYS-Fluent for 3D simulation. The combustion of the suggested surrogate was also investigated based on partially premixed combustion model. The chemical mechanism of 194 species with 1459 reactions was implemented into the CFD code. The ignition time delay of the suggested surrogate was compared to those of the surrogate suggested by ANSYS and the full composition of kerosene fuel.

Results revealed that the customised version of ANSYS-Fluent including the implemented model showed close agreement with experimental data. This was attributed to the physics inside droplet that the implemented model considered which were the temperature gradient, recirculation and mainly species diffusion. The generated surrogate, using the CFSM, showed closer predictions for the ignition time delay to the full composition of kerosene fuel than that of the surrogate suggested by ANSYS.

It was demonstrated through simulations in this chapter that surrogate of at least two components can capture the actual characteristics of the real fuel if there was an appropriate distribution to the mass fraction of these two components. This will have substantial influence in terms of the computational efficiency.

The improvements of the accuracy of commercial computational software tools, with the implementation of the models presented in this thesis, are the key significance of this chapter. The findings showcase the importance of the introduced models, mainly those in Chapters 6 and 7, to a real example of engineering application.

CHAPTER NINE: Conclusions and Recommendations

This chapter outlines the main concluding remarks from the research undertaken in this thesis and sets out the recommendations to progress the research further in future.

9.1. Conclusions

In line with the global demand to reduce the greenhouse gas emissions (GGE), a detailed research programme was formulated and conducted to assess the feasibility of increasing the fraction of biofuel in the baseline fuel (diesel and gasoline) with the main aim of reducing GGE; various processes associated with the combustion mechanism were also considered.

This work investigated the heating, evaporation and some of the combustion characteristics of pure fuels (gasoline, diesel and kerosene) and blended fuels (ethanol/gasoline, biodiesel/diesel and ethanol/biodiesel/diesel). Previously developed models, including the Discrete Multi-Component Model (DMCM) and the Multi-Dimensional Quasi-Discrete Model (MDQDM), were generalised to take into account some important factors such as the activity coefficient and radiative temperature. The previously developed models were also modified, and their new versions were examined for improving the predictions and CPU time and formulating fuel surrogates.

The impacts of ambient conditions, including pressure and ambient and radiative temperatures, and fractions of ethanol in ethanol/gasoline fuel blends, on droplet heating and evaporation were investigated. The DMCM was used for the analysis as it took into account all the number of components existed in the ethanol/gasoline fuel blends. The full composition of gasoline FACE C fuel, transient diffusion of species, recirculation, and temperature gradient inside droplets were accounted for, using the Effective Thermal Conductivity/Effective Diffusivity (ETC/ED) models. All processes inside the droplet were

assumed to be spherically symmetric. The model was validated against relevant experimental data.

The analysis focused on ethanol/gasoline fuel blends with 0%, 5%, 20%, 50%, 85% and 100% molar fractions of ethanol, and it was shown that the droplet lifetime for pure gasoline fuel was the smallest, but its maximal droplet surface temperature was the largest. The droplet lifetime increased with increasing ethanol molar fraction, leading to a difference of 33.9% between pure gasoline fuel and pure ethanol results under the same conditions. Also, the predicted ethanol droplet surface temperature was shown to be up to 24.3% lower than that predicted for gasoline fuel. This was attributed to the fact that ethanol has lower boiling and critical temperatures, but higher liquid density and lower saturated vapour pressure than gasoline fuel.

It was concluded that the addition of ethanol to gasoline fuel made the fuel less volatile. Increasing the radiative temperature, ambient pressure, or ambient temperature, led to a faster evaporation of ethanol/gasoline droplets regardless of their blending fractions at temperatures greater than 400 K. At low ambient temperature (400 K), however, increasing the ambient pressure led to longer droplet lifetimes.

The DMCM was also applied for the ethanol/gasoline fuel blend but by considering the Activity Coefficient (AC). The Universal Quasi-Chemical Functional–group AC (UNIFAC) model was used to predict the activity coefficients of the components of blended ethanol/gasoline (21 components) fuels. It was found that the droplet lifetimes for the blends were not always shorter compared with those for pure gasoline droplets. It was shown that the application of the model using Raoult's law (AC=1) could lead to up to 5.7% errors in estimated droplet lifetimes for ethanol/gasoline blends, compared to the predictions of the same model using the transient UNIFAC approach.

The DMCM was also used to analyse the heating and evaporation of blended biodiesel/diesel fuel droplets using twenty-two types of biodiesel fuels. The effect of

increasing biodiesel fuel concentration on the evolutions of droplet surface temperatures and evaporation times was clearly illustrated in this research. The predicted B5 (5% biodiesel and 95% diesel) fuel droplet lifetimes for the 22 types of biodiesel fuel were only 1% less than that of pure diesel fuel. The RME biodiesel fuel droplet were observed to have lifetimes close to that of pure diesel fuel, where their predicted lifetimes for B5 and B100 (100% biodiesel) droplets were up to 0.4% and 6%, respectively, less than the one estimated for pure diesel fuel droplet.

The impacts of ambient conditions, including pressure, temperature, and radiative temperatures, on droplet heating and evaporation were also investigated using the DMCM. The analysis was specifically focused on the SME and the WCO biodiesel fuel. It was observed that increasing the radiative temperature, ambient pressure, and ambient temperature always led to a faster evaporation of biodiesel/diesel fuel droplets.

The DMCM and MDQDM were applied for the predictions of heating and evaporation of blended E85-diesel (E85 refers to 85% ethanol and 15% gasoline) fuel droplets. In the MDQDM, a large number of components was replaced with a much smaller number of Components/Quasi-Components (C/QC). This model was developed to address the issue when the number of components exceeds several dozen which makes the DMCM computationally expensive. The UNIFAC model was combined with MDQDM to improve the predictions of the vapour-liquid equilibrium. The MDQDM was also based on the ETC/ED models to solve the heat transfer and species diffusion equations.

It was shown that E85-diesel blended fuel droplets had shorter lifetimes than those of pure diesel. Higher fractions of E85 resulted in up to 49.5% shorter droplet lifetimes and up to 23.4% lower droplet surface temperatures than those of pure diesel. Such a significant impact of high E85-diesel fractions was thought to be due to the differences in their saturated vapour pressure.

In the case of the E85-5 blend, the assumption of an ideal-mixture with a unity activity coefficient (i.e. Raoult's law is valid) was shown to lead to overprediction of droplet lifetimes by up to 3.6%, compared to the case when the UNIFAC activity coefficient was used.

It was shown that replacing 119 components of the blended fuel with 20 C/QC reduced the CPU time by up to 83% with less than 3.6% and 2.9% underpredicted droplet lifetimes and surface temperatures, respectively, compared to the prediction of the model accounting for all the 119 components.

The feasibility of mixing different fuel fractions of biodiesel and ethanol with diesel in terms of heating and evaporation characteristics, Cetane Number (CN), viscosity, and heating value were also investigated using the DMCM and other mathematical correlations. Predictions revealed that the presence of biodiesel at the expense of ethanol (e.g., 5% biodiesel and 5% ethanol, instead of only 10% of ethanol) compensated the reduction in droplet lifetime, surface temperature, CN, viscosity, and even the heating value. It was found that a blend of 15% biodiesel, 5% ethanol, and 80% diesel fuels led to less than 1.2%, 0.2%, 2%, and 2.2% reduction in droplet lifetime, CN, viscosity and heating value, respectively, compared to those of pure diesel fuel. It was concluded that the presence of biofuels with up to 20% in diesel fuel can be used in engines designed for pure diesel with minimal, or no any design modifications.

A new approach was developed for the formulation of fuel surrogates using based on a modified version of the MDQDM, described as a 'Complex Fuel Surrogates Model' (CFSM). In this new approach, the aim was to generate actual components (with integer carbon numbers) instead of QC. These components called Approximate Discrete-Components (ADC). The CFSM was verified against the DMCM, in application to the full compositions of gasoline and diesel fuels and their ethanol/gasoline and biodiesel/diesel blends. The other important purpose of the CFSM was broaden the usefulness of the model for future implementation into commercial CFD codes and experimental validations. The physical and

chemical properties of the formulated surrogates (Sur1 for diesel, Sur4 for gasoline, Sur7 for E20, and Sur9 for B10) were compared to the full compositions of each fuel.

The physical and chemical characteristics of the formulated surrogates were computed. These included the evolutions of droplet radii and surface temperatures, vapour pressures, H/C, research octane numbers for gasoline and ethanol/gasoline fuels, and cetane numbers for diesel and biodiesel/diesel fuels. The same physical and chemical verifications were applied to the fuel surrogates recommended in literature (noting that the surrogates of B10 have not been presented anywhere in literature to the best of the author knowledge). The chemical and physical behaviours of the four suggested surrogates were in reasonably close agreements with those predicted for the full compositions of their fuels, exceeding the relative predictions of these fuels provided by the surrogates suggested in literature. For example, in the case of gasoline fuel the literature alternatives to the surrogate suggested in this research exposed the predicted droplet lifetimes to errors of up to 26.8% and the predicted vapour pressure to errors of up to 59.1%. The usefulness of the introduced CFSM was verified for the formulation of surrogates in application to a broad range of fuel compositions.

Although the droplet heating and evaporation of the formulated surrogates using the CFSM were predicted and compared to those when considering the total number of components in fuel, the selection of ADC in this model was based on trial and error to match some required characteristics of fuels. Hence, this model still requires experienced end-users to run it. The impact of the trial and error on the predicted droplet surface temperatures and radii were noticeable in some predictions. For instance, the new approximation of the full composition of diesel fuel with the range 50-75 ADC overpredicted the results of the DMCM. Some fluctuations were observed at varying time instants.

In response to that, a novel approach was proposed for the auto-selection of components in the MDQDM. The model was used for the analysis of fuel droplet heating and evaporation.

As in the original MDQDM suggested earlier, the large number of fuel components were reduced to a much small number of C/QC. In contrast to the original MDQD model, these were auto-updated within algorithmic time-steps to consider the transient diffusions of species for the selection of quasi-components. Hence, the implementation of new algorithm was described as 'transient' with the 'TMDQDM' acronym.

The new (TMDQD) model was analysed in application to a wide range of E85 and diesel fuel blend and compared to the previously introduced MDQDM in terms of accuracy and computational competency. Results revealed that that using the new TMDQDM approach could reduce the full compositions of all analysed E85-diesel mixtures from 119 components to 10 C/QC with up to 1.82% errors in predicted droplet lifetimes and temperatures. These predictions were consistently more accurate than those predicted using the previously suggested MDQDM – which gives up to 8.8% errors. The CPU time needed to run this model was 79% less than that needed using the full composition of fuel. However, this was not the best CPU efficient approach since the time saving of the MDQDM was 88% less than of when using the full fuel composition. None the less, this slight increase in computing resource was more than offset by the improvement in the accuracy of prediction.

The final part of this research involved formulation of kerosene fuel surrogate using the CFSM. The model was implemented into ANSYS-Fluent, via the user-defined function. The heating and evaporation of the surrogate using the implemented model was compared to the standard simulation of heating and evaporation using ANSYS-Fluent. The combustion of the proposed surrogate was investigated using ANSYS-Fluent and incorporating a detailed combustion mechanism for the proposed surrogate. The ignition time delay of the suggested surrogate was compared to the full composition of the kerosene fuel using Arrhenius relationship. It was shown that a customised version of ANSYS-Fluent incorporating the DMCM led to predictions that were closer to experimental data than the predictions of the

conventional ANSYS-Fluent code. It was noticed that the implementation of the detailed combustion chemistry of the proposed kerosene surrogate led to lower predictions of the NO_X, and CO_2 compared to the case of the ANSYS-Fluent surrogate. The prediction of the ignition time delays of the fuel and its surrogate were very close at high oxidation temperature $T > 1200$ K.

To sum up, the study has developed advanced models for the modelling of heating and evaporation process as well as some other important characteristics such as octane number, heating value, hydrogen/carbon ratio and cetane number. This has been done in line with the current shifting from pure fossil fuels and those with up to 5% biofuels to 10% and more (For instance, using E20 instead of E5 in on road vehicles). The developed models will be opening up new possibilities for much higher blends than those currently existed in the fuel processing industry, broader engine types (including GTE), and wider market consumption with less GGE. The thesis' findings revealed that up to 30% of biofuel can be blended with fossil fuel and used in petrol and diesel engines with minimal modifications to these engines. The feasibility of implementation of our models in GTE is performed, with application to the full combustion process of that engine using three-dimensional CFD model.

9.2. Recommendations

Despite the good progress in developing the CFSM and TMDQDM and their usefulness in generating fuel surrogates and improving the predictions of heating and evaporation, some important processes were ignored in these models. All the modelled processes were based on the assumption that all processes were spherically symmetric. Shapes of some droplets in ICE applications, however, are far from sphericity. All modelled droplets were isolated without considering the impact of interaction between droplet. The developed models were based on the on the hydrodynamic approximation without considering the kinetic region. The impact of moving interface, as a result of the evaporation, on droplet heating and

evaporation was not considered. The impact of radiation on droplet heating and evaporation was investigated based on the assumption that the droplet is a black body. Most droplet are grey with emissivity of less than 1.

Based on the aforementioned facts and other important points, the following suggestions could be explored:

- Non-spherically symmetric droplet can be modelled using the DMCM. This, however, needs to a new analytical solution to the heat and mass transfer equations.
- The impact of radiation of the heating and evaporation of a semi-transparent droplet needs to be modelled. This requires the measurements of wavelengths of all components that needed to be considered when modelling the droplet heating and evaporation.
- The impact of species diffusion with time on the preignition process should be considered. This is important as it demonstrates, for instance, why automotive fuel has more fraction of the lighter components in the Winter.
- The implementation of the heating and evaporation model into a CFD code can be improved by considering multi-components instead of binary mixture.
- Although the kinetic region is difficult to be introduced for fuels contained tens of components, it may be practical to be introduced when modelling fuel surrogates (up to 5 components).

References

[1] Kalghatgi G. Is it really the end of internal combustion engines and petroleum in transport? Applied Energy 2018;225:965–74. https://doi.org/10.1016/j.apenergy.2018.05.076.

[2] Kalghatgi G, Levinsky H, Colket M. Future transportation fuels. Progress in Energy and Combustion Science 2018;69:103–5. https://doi.org/10.1016/j.pecs.2018.06.003.

[3] Ali O, Mamat R, Najafi G, Yusaf T, Safieddin Ardebili S. Optimization of Biodiesel-Diesel Blended Fuel Properties and Engine Performance with Ether Additive Using Statistical Analysis and Response Surface Methods. Energies 2015;8:14136–50. https://doi.org/10.3390/en81212420.

[4] Qasim M, Ansari TM, Hussain M. Combustion, Performance, and Emission Evaluation of a Diesel Engine with Biodiesel Like Fuel Blends Derived From a Mixture of Pakistani Waste Canola and Waste Transformer Oils. Energies 2017;10:1023. https://doi.org/10.3390/en10071023.

[5] EPA U. US Environmental Protection Agency 2014. http://www.epa.gov/ (accessed November 15, 2017).

[6] Masum BM, Masjuki HH, Kalam MA, Rizwanul Fattah IM, Palash SM, Abedin MJ. Effect of ethanol–gasoline blend on NOx emission in SI engine. Renewable and Sustainable Energy Reviews 2013;24:209–22. https://doi.org/10.1016/j.rser.2013.03.046.

[7] Pure European Renewavle Ethanol n.d. https://epure.org/ (accessed January 5, 2020).

[8] Alternative Fuels Data Center. U.S. Department of Energy: Energy Efficiency and Renewable Energy n.d. http://www.afdc.energy.gov (accessed February 12, 2017).

[9] Torres-Jimenez E, Jerman MS, Gregorc A, Lisec I, Dorado MP, Kegl B. Physical and chemical properties of ethanol–diesel fuel blends. Fuel 2011;90:795–802. https://doi.org/10.1016/j.fuel.2010.09.045.

[10] Padala S, Woo C, Kook S, Hawkes ER. Ethanol utilisation in a diesel engine using dual-fuelling technology. Fuel 2013;109:597–607. https://doi.org/10.1016/j.fuel.2013.03.049.

[11] Al Qubeissi M. Heating and Evaporation of Multi-Component Fuel Droplets. Stuttgart: WiSa; 2015.

[12] Department for Transport, UK. New regulations to double the use of sustainable renewable fuels by 2020 13/042018. https://www.gov.uk/government/news/new-regulations-to-double-the-use-of-sustainable-renewable-fuels-by-2020 (accessed February 22, 2019).

[13] Eller D. Trump administration gives final approval for year-round E15 use 2019. https://eu.desmoinesregister.com/story/money/agriculture/2019/05/31/trump-administration-approves-year-round-e-15-use-biofuels-ethanol/1297055001/ (accessed August 16, 2019).

[14] The CFD Development of Non-premixed Dual Fuel Combustion Diesel Engine injected by High-pressure Gas in the Cylinder Chamber 2019. https://www.archie-west.ac.uk/projects/computational-fluid-dynamics/the-cfd-development-of-non-premixed-dual-fuel-combustion-diesel-engine-injected-by-high-pressure-gas-in-the-cylinder-chamber/.

[15] Agarwal AK, Dhar A, Gupta JG, Kim WI, Choi K, Lee CS, et al. Effect of fuel injection pressure and injection timing of Karanja biodiesel blends on fuel spray, engine performance, emissions and combustion characteristics. Energy Conversion and Management 2015;91:302–14. https://doi.org/10.1016/j.enconman.2014.12.004.

[16] Sirignano WA. Fluid Dynamics and Transport of Droplets and Sprays. Cambridge, U.K: Cambridge University Press; 2010.

[17] Stojkovic BD, Sick V. Evolution and impingement of an automotive fuel spray investigated with simultaneous Mie/LIF techniques: Appl Phys B 2001;73:75–83. https://doi.org/10.1007/s003400100598.

[18] Ott LS, Smith BL, Bruno TJ. Composition-Explicit Distillation Curves of Waste Lubricant Oils and Resourced Crude Oil: A Diagnostic for Re-Refining and Evaluation. American Journal of Environmental Sciences 2010;6:523–34. https://doi.org/10.3844/ajessp.2010.523.534.

[19] Smith BL, Bruno TJ. Advanced Distillation Curve Measurement with a Model Predictive Temperature Controller. Int J Thermophys 2006;27:1419–34. https://doi.org/10.1007/s10765-006-0113-7.

[20] Abdel-Qader Z, Hallett WLH. The role of liquid mixing in evaporation of complex multicomponent mixtures: modelling using continuous thermodynamics. Chemical Engineering Science 2005;60:1629–40. https://doi.org/10.1016/j.ces.2004.10.015.

[21] Zhu G-Sh, Reitz RD. A model for high-pressure vaporization of droplets of complex liquid mixtures using continuous thermodynamics. International Journal of Heat and Mass Transfer 2002;45:495–507. https://doi.org/10.1016/S0017-9310(01)00173-9.

[22] Davidson DF, Shao JK, Choudhary R, Mehl M, Obrecht N, Hanson RK. Ignition delay time measurements and modeling for gasoline at very high pressures. Proceedings of the Combustion Institute 2018. https://doi.org/10.1016/j.proci.2018.08.032.

[23] Sazhina EM, Sazhin SS, Heikal MR, Babushok VI, Johns RJR. A Detailed Modelling of the Spray Ignition Process in Diesel Engines. Combustion Science and Technology 2000;160:317–44. https://doi.org/10.1080/00102200008935806.

[24] Sazhin SS, Krutitskii PA. A Conduction Model for Transient Heating of Fuel Droplets. proceedings of the 3rd ISAAC Congress, River Edge, NJ: World Scientific; 2003, p. 1231–40.

[25] Hallett WLH, Legault NV. Modelling biodiesel droplet evaporation using continuous thermodynamics. Fuel 2011;90:1221–8. https://doi.org/10.1016/j.fuel.2010.11.035.

[26] Saha K, Abu-Ramadan E, Li X. Multicomponent evaporation model for pure and blended biodiesel droplets in high temperature convective environment. Applied Energy 2012;93:71–9. https://doi.org/10.1016/j.apenergy.2011.05.034.

[27] Sazhin SS, Elwardany A, Krutitskii PA, Castanet G, Lemoine F, Sazhina EM, et al. A simplified model for bi-component droplet heating and evaporation. International Journal of Heat and Mass Transfer 2010;53:4495–505. https://doi.org/10.1016/j.ijheatmasstransfer.2010.06.044.

[28] Sazhin SS. Droplets and Sprays. London: Springer; 2014.

[29] Sazhin SS. Modelling of fuel droplet heating and evaporation: Recent results and unsolved problems. Fuel 2017;196:69–101. https://doi.org/10.1016/j.fuel.2017.01.048.

[30] Elwardany AE, Sazhin SS, Im HG. A new formulation of physical surrogates of FACE A gasoline fuel based on heating and evaporation characteristics. Fuel 2016;176:56–62. https://doi.org/10.1016/j.fuel.2016.02.041.

[31] Sarathy SM, Kukkadapu G, Mehl M, Wang W, Javed T, Park S, et al. Ignition of alkane-rich FACE gasoline fuels and their surrogate mixtures. Proceedings of the Combustion Institute 2015;35:249–57. https://doi.org/10.1016/j.proci.2014.05.122.

[32] Zhang L, Kong S-Ch. Modeling of multi-component fuel vaporization and combustion for gasoline and diesel spray. Chemical Engineering Science 2009;64:3688–96. https://doi.org/10.1016/j.ces.2009.05.013.

[33] Keller P, Bader A, Hasse C. The influence of intra-droplet heat and mass transfer limitations in evaporation of binary hydrocarbon mixtures. International Journal of Heat and Mass Transfer 2013;67:1191–207. https://doi.org/10.1016/j.ijheatmasstransfer.2013.08.104.

[34] Chauveau C, Halter F, Lalonda A, Gokalp I. AN EXPERIMENTAL STUDY ON THE DROPLET VAPORIZATION: EFFECTS OF HEAT CONDUCTION THROUGH THE SUPPORT FIBER, Italy: ILASS 2008; 2008.

[35] Kitano T, Nishio J, Kurose R, Komori S. Effects of ambient pressure, gas temperature and combustion reaction on droplet evaporation. Combustion and Flame 2014;161:551–64. https://doi.org/10.1016/j.combustflame.2013.09.009.

[36] Dirbude S, Eswaran V, Kushari A. Droplet vaporization modeling of rapeseed and sunflower methyl esters. Fuel 2012;92:171–9. https://doi.org/10.1016/j.fuel.2011.07.030.

[37] Morin C, Chauveau C, Gökalp I. Droplet vaporisation characteristics of vegetable oil derived biofuels at high temperatures. Experimental Thermal and Fluid Science 2000;21:41–50. https://doi.org/10.1016/S0894-1777(99)00052-7.

[38] Kitano T, Nishio J, Kurose R, Komori S. Evaporation and combustion of multicomponent fuel droplets. Fuel 2014;136:219–25. https://doi.org/10.1016/j.fuel.2014.07.045.

[39] Banerjee R. Numerical investigation of evaporation of a single ethanol/iso-octane droplet. Fuel 2013;107:724–39. https://doi.org/10.1016/j.fuel.2013.01.003.

[40] Keller, Peter, Hasse, Christian. The influence of non-ideal thermodynamics on the evaporation of alcohol/alkane-LIF tracer sprays, 26th-ILASS – Europe 2014 Conference; 2014.

[41] Bader A, Keller P, Hasse C. The influence of non-ideal vapor–liquid equilibrium on the evaporation of ethanol/iso-octane droplets. International Journal of Heat and Mass Transfer 2013;64:547–58. https://doi.org/10.1016/j.ijheatmasstransfer.2013.04.056.

[42] Govindaraju PB, Ihme M. Group contribution method for multicomponent evaporation with application to transportation fuels. International Journal of Heat and Mass Transfer 2016;102:833–45. https://doi.org/10.1016/j.ijheatmasstransfer.2016.06.079.

[43] Járvás G, Kontos J, Hancsók J, Dallos A. Modeling ethanol–blended gasoline droplet evaporation using COSMO-RS theory and computation fluid dynamics. International Journal of Heat and Mass Transfer 2015;84:1019–29. https://doi.org/10.1016/j.ijheatmasstransfer.2014.12.046.

[44] Keller P, Knorsch T, Wensing M, Hasse C. Experimental and numerical analysis of iso-octane/ethanol sprays under gasoline engine conditions. International Journal of Heat and Mass Transfer 2015;84:497–510. https://doi.org/10.1016/j.ijheatmasstransfer.2015.01.011.

[45] Yi P, Long W, Jia M, Feng L, Tian J. Development of an improved hybrid multi-component vaporization model for realistic multi-component fuels. International Journal of Heat and Mass Transfer 2014;77:173–84. https://doi.org/10.1016/j.ijheatmasstransfer.2014.05.008.

[46] Ghose P, Patra J, Datta A, Mukhopadhyay A. Effect of air flow distribution on soot formation and radiative heat transfer in a model liquid fuel spray combustor firing kerosene. International Journal of Heat and Mass Transfer 2014;74:143–55. https://doi.org/10.1016/j.ijheatmasstransfer.2014.03.001.

[47] El-Asrag HA, Braun M. Effect of turbulence non-isotropy modeling on spray dynamics for an evaporating Acetone spray jet. International Journal of Multiphase Flow 2015;68:100–20. https://doi.org/10.1016/j.ijmultiphaseflow.2014.10.009.

[48] Borghesi G, Mastorakos E. Spontaneous ignition of isolated n -heptane droplets at low, intermediate, and high ambient temperatures from a mixture-fraction perspective. Combustion and Flame 2015;162:2544–60. https://doi.org/10.1016/j.combustflame.2015.03.003.

[49] Sánchez F, Kaiser AS, Zamora B, Ruiz J, Lucas M. Prediction of the lifetime of droplets emitted from mechanical cooling towers by numerical investigation. International Journal of Heat and Mass Transfer 2015;89:1190–206. https://doi.org/10.1016/j.ijheatmasstransfer.2015.06.014.

[50] Wongsarivej P, Tanthapanichakoon W. A model for a non-uniform spray evaporator taking into account the effect of non-isothermal polydisperse droplets. International Journal of Heat and Mass Transfer 2015;90:1170–7. https://doi.org/10.1016/j.ijheatmasstransfer.2015.07.035.

[51] Helgans B, Richter DH. Turbulent latent and sensible heat flux in the presence of evaporative droplets. International Journal of Multiphase Flow 2016;78:1–11. https://doi.org/10.1016/j.ijmultiphaseflow.2015.09.010.

[52] Nguyen D, Soria J, Honnery D. Efficiency of the lumped parameter concept and the role of liquid properties in modelling microdroplet evaporation. Fuel 2016;166:86–95. https://doi.org/10.1016/j.fuel.2015.10.097.

[53] Rehman HL, Weiss J, Seers P. Effect of heat conduction on droplet life time and evaporation rate under forced convection at low temperatures. Experimental Thermal and Fluid Science 2016;72:59–66. https://doi.org/10.1016/j.expthermflusci.2015.10.030.

[54] Azami MH, Savill M. Modelling of spray evaporation and penetration for alternative fuels. Fuel 2016;180:514–20. https://doi.org/10.1016/j.fuel.2016.04.050.

[55] Zhou T, Ye T, Zhu M, Zhao M, Chen J. Effect of droplet diameter and global equivalence ratio on n -heptane spray auto-ignition. Fuel 2017;187:137–45. https://doi.org/10.1016/j.fuel.2016.09.030.

[56] Gao P, Zhou X, Cheng B, Zhang D, Zhou G. Study on heat and mass transfer of droplet cooling in ultrasound wave. International Journal of Heat and Mass Transfer 2017;107:916–24. https://doi.org/10.1016/j.ijheatmasstransfer.2016.11.002.

[57] Rybdylova O, Al Qubeissi M, Braun M, Crua C, Manin J, Pickett LM, et al. A model for droplet heating and its implementation into ANSYS Fluent. International Communications in Heat and Mass Transfer 2016. https://doi.org/10.1016/j.icheatmasstransfer.2016.05.032.

[58] Sazhin SS, Al Qubeissi M, Kolodnytska R, Elwardany AE, Nasiri R, Heikal MR. Modelling of biodiesel fuel droplet heating and evaporation. Fuel 2014;115:559–72. https://doi.org/10.1016/j.fuel.2013.07.031.

[59] Yi P, Long W, Jia M, Tian J, Li B. Development of a quasi-dimensional vaporization model for multi-component fuels focusing on forced convection and high temperature conditions. International Journal of Heat and Mass Transfer 2016;97:130–45. https://doi.org/10.1016/j.ijheatmasstransfer.2016.01.075.

[60] Sazhin SS, Al Qubeissi M, Nasiri R, Gun'ko VM, Elwardany AE, Lemoine F, et al. A multi-dimensional quasi-discrete model for the analysis of Diesel fuel droplet heating and evaporation. Fuel 2014;129:238–66. https://doi.org/10.1016/j.fuel.2014.03.028.

[61] Ra Y, Reitz RD. A vaporization model for discrete multi-component fuel sprays. International Journal of Multiphase Flow 2009;35:101–17. https://doi.org/10.1016/j.ijmultiphaseflow.2008.10.006.

[62] Al Qubeissi M, Kolodnytska R, Sazhin SS. Biodiesel fuel droplets: modelling of heating and evaporation processes. 25th European Conference on Liquid Atomization and Spray Systems, vol. 4 (CD), Crete, Greece: 2013.

[63] Al Qubeissi M, Sazhin SS, Crua C, Turner J, Heikal MR. Modelling of biodiesel fuel droplet heating and evaporation: effects of fuel composition. Fuel 2015;154:308–18. https://doi.org/10.1016/j.fuel.2015.03.051.

[64] Al Qubeissi M, Sazhin SS. Blended biodiesel/Diesel fuel droplet heating and evaporation. vol. DHE-01, Brighton, UK: 2016, p. 179.

[65] Zhang L, Kong S-Ch. Vaporization modeling of petroleum–biofuel drops using a hybrid multi-component approach. Combustion and Flame 2010;157:2165–74. https://doi.org/10.1016/j.combustflame.2010.05.011.

[66] Elwardany A, Badra J, Sim J, Khurshid M, Sarathy M, Im H. Modeling of Heating and Evaporation of FACE I Gasoline Fuel and its Surrogates, 2016. https://doi.org/10.4271/2016-01-0878.

[67] Chen L, Li G, Fang B. Droplet evaporation characteristics of aviation kerosene surrogate fuel and butanol blends under forced convection. International Journal of Multiphase Flow 2019;114:229–39. https://doi.org/10.1016/j.ijmultiphaseflow.2019.03.012.

[68] Sazhin SS, Elwardany AE, Sazhina EM, Heikal MR. A quasi-discrete model for heating and evaporation of complex multicomponent hydrocarbon fuel droplets. International Journal of Heat and Mass Transfer 2011;54:4325–32. https://doi.org/10.1016/j.ijheatmasstransfer.2011.05.012.

[69] Elwardany AE, Sazhin SS. A quasi-discrete model for droplet heating and evaporation: Application to Diesel and gasoline fuels. Fuel 2012;97:685–94. https://doi.org/10.1016/j.fuel.2012.01.068.

[70] Elwardany AE, Sazhin SS, Farooq A. Modelling of heating and evaporation of gasoline fuel droplets: A comparative analysis of approximations. Fuel 2013;111:643–7. https://doi.org/10.1016/j.fuel.2013.03.030.

[71] Al Qubeissi M, Sazhin SS, Turner J, Begg S, Crua C, Heikal MR. Modelling of gasoline fuel droplets heating and evaporation. Fuel 2015;159:373–84. https://doi.org/10.1016/j.fuel.2015.06.028.

[72] Al Qubeissi M, Sazhin SS, de Sercey G, Crua C. Multi-dimensional quasi-discrete model for the investigation of heating and evaporation of Diesel fuel droplets. 26th European Conference on Liquid Atomization and Spray Systems, vol. ABS-135 (CD), Bremen, Germany: University of Bremen; 2014.

[73] Al Qubeissi M, Sazhin SS, Elwardany AE. Modelling of blended Diesel and biodiesel fuel droplet heating and evaporation. Fuel 2017;187:349–55. https://doi.org/10.1016/j.fuel.2016.09.060.

[74] Sarathy SM, Farooq A, Kalghatgi GT. Recent progress in gasoline surrogate fuels. Progress in Energy and Combustion Science 2018;65:67–108. https://doi.org/10.1016/j.pecs.2017.09.004.

[75] Pitz WJ, Mueller ChJ. Recent progress in the development of diesel surrogate fuels. Progress in Energy and Combustion Science 2011;37:330–50. https://doi.org/10.1016/j.pecs.2010.06.004.

[76] Mati K, Ristori A, Gaïl S, Pengloan G, Dagaut P. The oxidation of a diesel fuel at 1–10atm: Experimental study in a JSR and detailed chemical kinetic modeling. Proceedings of the Combustion Institute 2007;31:2939–46. https://doi.org/10.1016/j.proci.2006.07.073.

[77] Herbinet O, Pitz WJ, Westbrook CK. Detailed chemical kinetic mechanism for the oxidation of biodiesel fuels blend surrogate. Combustion and Flame 2010;157:893–908. https://doi.org/10.1016/j.combustflame.2009.10.013.

[78] Westbrook CK, Naik CV, Herbinet O, Pitz WJ, Mehl M, Sarathy SM, et al. Detailed chemical kinetic reaction mechanisms for soy and rapeseed biodiesel fuels. Combustion and Flame 2011;158:742–55. https://doi.org/10.1016/j.combustflame.2010.10.020.

[79] Lin R, Tavlarides LL. Thermophysical properties needed for the development of the supercritical diesel combustion technology: Evaluation of diesel fuel surrogate models. The Journal of Supercritical Fluids 2012;71:136–46. https://doi.org/10.1016/j.supflu.2012.08.003.

[80] Ahmed A, Goteng G, Shankar VSB, Al-Qurashi K, Roberts WL, Sarathy SM. A computational methodology for formulating gasoline surrogate fuels with accurate physical and chemical kinetic properties. Fuel 2015;143:290–300. https://doi.org/10.1016/j.fuel.2014.11.022.

[81] Kabil I, Sim J, Badra JA, Eldrainy Y, Abdelghaffar W, Mubarak Ali MJ, et al. A surrogate fuel formulation to characterize heating and evaporation of light naphtha droplets. Combustion Science and Technology 2018;190:1218–31. https://doi.org/10.1080/00102202.2018.1444037.

[82] Pati A, Gierth S, Haspel P, Hasse C, Munier J. Strategies to Define Surrogate Fuels for the Description of the Multicomponent Evaporation Behavior of Hydrocarbon Fuels, 2018. https://doi.org/10.4271/2018-01-1692.

[83] Kang D, Fridlyand A, Goldsborough SS, Wagnon SW, Mehl M, Pitz WJ, et al. Auto-ignition study of FACE gasoline and its surrogates at advanced IC engine conditions. Proceedings of the Combustion Institute 2018. https://doi.org/10.1016/j.proci.2018.08.053.

[84] Qian Y, Yu L, Li Z, Zhang Y, Xu L, Zhou Q, et al. A new methodology for diesel surrogate fuel formulation: Bridging fuel fundamental properties and real engine combustion characteristics. Energy 2018;148:424–47. https://doi.org/10.1016/j.energy.2018.01.181.

[85] Sazhina EM, Sazhin SS, Heikal MR, Marooney CJ. The Shell autoignition model: applications to gasoline and diesel fuels. Fuel 1999;78:389–401. https://doi.org/10.1016/S0016-2361(98)00167-7.

[86] Sileghem L, Alekseev VA, Vancoillie J, Van Geem KM, Nilsson EJK, Verhelst S, et al. Laminar burning velocity of gasoline and the gasoline surrogate components iso-octane, n-heptane and toluene. Fuel 2013;112:355–65. https://doi.org/10.1016/j.fuel.2013.05.049.

[87] Su M, Chen CP. Heating and evaporation of a new gasoline surrogate fuel: A discrete multicomponent modeling study. Fuel 2015;161:215–21. https://doi.org/10.1016/j.fuel.2015.08.048.

[88] Chang Y, Jia M, Li Y, Liu Y, Xie M, Wang H, et al. Development of a skeletal mechanism for diesel surrogate fuel by using a decoupling methodology. Combustion and Flame 2015;162:3785–802. https://doi.org/10.1016/j.combustflame.2015.07.016.

[89] Ji C, Dames E, Wang YL, Wang H, Egolfopoulos FN. Propagation and extinction of premixed C5–C12 n-alkane flames. Combustion and Flame 2010;157:277–87. https://doi.org/10.1016/j.combustflame.2009.06.011.

[90] Ranzi E, Frassoldati A, Grana R, Cuoci A, Faravelli T, Kelley AP, et al. Hierarchical and comparative kinetic modeling of laminar flame speeds of hydrocarbon and oxygenated fuels. Progress in Energy and Combustion Science 2012;38:468–501. https://doi.org/10.1016/j.pecs.2012.03.004.

[91] Ji C, Dames E, Wang H, Egolfopoulos FN. Propagation and extinction of benzene and alkylated benzene flames. Combustion and Flame 2012;159:1070–81. https://doi.org/10.1016/j.combustflame.2011.10.017.

[92] Cox RA, Cole JA. Chemical aspects of the autoignition of hydrocarbon□air mixtures. Combustion and Flame 1985;60:109–23. https://doi.org/10.1016/0010-2180(85)90001-X.

[93] Tanaka S, Ayala F, Keck JC. A reduced chemical kinetic model for HCCI combustion of primary reference fuels in a rapid compression machine. Combustion and Flame 2003;133:467–81. https://doi.org/10.1016/S0010-2180(03)00057-9.

[94] Ra Y, Reitz RD. A combustion model for multi-component fuels using a physical surrogate group chemistry representation (PSGCR). Combustion and Flame 2015;162:3456–81. https://doi.org/10.1016/j.combustflame.2015.05.014.

[95] Yu J, Ju Y, Gou X. Surrogate fuel formulation for oxygenated and hydrocarbon fuels by using the molecular structures and functional groups. Fuel 2016;166:211–8. https://doi.org/10.1016/j.fuel.2015.10.085.

[96] Abdul Jameel AG, Naser N, Issayev G, Touitou J, Ghosh MK, Emwas A-H, et al. A minimalist functional group (MFG) approach for surrogate fuel formulation. Combustion and Flame 2018;192:250–71. https://doi.org/10.1016/j.combustflame.2018.01.036.

[97] Koniavitis P, Rigopoulos S, Jones WP. Reduction of a detailed chemical mechanism for a kerosene surrogate via RCCE-CSP. Combustion and Flame 2018;194:85–106. https://doi.org/10.1016/j.combustflame.2018.04.004.

[98] Yan Y, Liu Y, Fang W, Liu Y, Li J. A simplified chemical reaction mechanism for two-component RP-3 kerosene surrogate fuel and its verification. Fuel 2018;227:127–34. https://doi.org/10.1016/j.fuel.2018.04.092.

[99] Liu J, Hu E, Zeng W, Zheng W. A new surrogate fuel for emulating the physical and chemical properties of RP-3 kerosene. Fuel 2020;259:116210. https://doi.org/10.1016/j.fuel.2019.116210.

[100] Sazhin SS. Advanced models of fuel droplet heating and evaporation. Progress in Energy and Combustion Science 2006;32:162–214. https://doi.org/10.1016/j.pecs.2005.11.001.

[101] Tonini S, Cossali GE. An exact solution of the mass transport equations for spheroidal evaporating drops. International Journal of Heat and Mass Transfer 2013;60:236–40. https://doi.org/10.1016/j.ijheatmasstransfer.2013.01.001.

[102] Zubkov VS, Cossali GE, Tonini S, Rybdylova O, Crua C, Heikal M, et al. Mathematical modelling of heating and evaporation of a spheroidal droplet. International Journal of Heat and Mass Transfer 2017;108:2181–90. https://doi.org/10.1016/j.ijheatmasstransfer.2016.12.074.

[103] Lima DR, Farias SN, Lima AGB. Mass transport in spheroids using the Galerkin method. Braz J Chem Eng 2004;21:667–80. https://doi.org/10.1590/S0104-66322004000400016.

[104] Alassar RS. Forced Convection Past an Oblate Spheroid at Low to Moderate Reynolds Numbers. Journal of Heat Transfer 2005;127:1062–70. https://doi.org/10.1115/1.1999654.

[105] Volkov RS, Kuznetsov GV, Strizhak PA. Influence of droplet concentration on evaporation in a high-temperature gas. International Journal of Heat and Mass Transfer 2016;96:20–8. https://doi.org/10.1016/j.ijheatmasstransfer.2016.01.029.

[106] Tonini S, Cossali GE. A multi-component drop evaporation model based on analytical solution of Stefan–Maxwell equations. International Journal of Heat and Mass Transfer 2016;92:184–9. https://doi.org/10.1016/j.ijheatmasstransfer.2015.08.014.

[107] Sazhin SS, Shishkova IN, Al Qubeissi M. A self-consistent kinetic model for droplet heating and evaporation. International Journal of Heat and Mass Transfer 2016;93:1206–17. https://doi.org/10.1016/j.ijheatmasstransfer.2015.10.039.

[108] Carslaw HS. Conduction of Heat in Solids. 2nd ed. Oxford: New York: Clarendon Press; Oxford University Press; 1986.

[109] Kartashov EM. Analytical Methods in Heat Transfer Theory in Solids. Moscow: Vysshaya Shkola; 2001.

[110] Abramzon B, Sirignano WA. Droplet vaporization model for spray combustion calculations. International Journal of Heat and Mass Transfer 1989;32:1605–18. https://doi.org/10.1016/0017-9310(89)90043-4.

[111] Elwardany AE. Modelling of multi-component fuel droplets heating and evaporation. PhD thesis. University of Brighton, 2012.

[112] Abramzon B, Sazhin SS. Convective vaporization of a fuel droplet with thermal radiation absorption. Fuel 2006;85:32–46. https://doi.org/10.1016/j.fuel.2005.02.027.

[113] Elwardany AE, Gusev IG, Castanet G, Lemoine F, Sazhin SS. Mono- and multi-component droplet cooling/heating and evaporation: comparative analysis of numerical models. Atom Sprays 2011;21:907–31. https://doi.org/10.1615/AtomizSpr.2012004194.

[114] Sazhin SS, Al Qubeissi M, Xie J-F. Two approaches to modelling the heating of evaporating droplets. International Communications in Heat and Mass Transfer 2014;57:353–6. https://doi.org/10.1016/j.icheatmasstransfer.2014.08.004.

[115] Sazhin SS, Krutitskii PA, Abdelghaffar WA, Sazhina EM, Mikhalovsky SV, Meikle ST, et al. Transient heating of diesel fuel droplets. International Journal of Heat and Mass Transfer 2004;47:3327–40. https://doi.org/10.1016/j.ijheatmasstransfer.2004.01.011.

[116] Maqua C, Castanet G, Grisch F, Lemoine F, Kristyadi T, Sazhin SS. Monodisperse droplet heating and evaporation: Experimental study and modelling. International Journal of Heat and Mass Transfer 2008;51:3932–45. https://doi.org/10.1016/j.ijheatmasstransfer.2007.12.011.

[117] Sazhin SS, Elwardany AE, Krutitskii PA, Deprédurand V, Castanet G, Lemoine F, et al. Multi-component droplet heating and evaporation: Numerical simulation versus experimental data. International Journal of Thermal Sciences 2011;50:1164–80. https://doi.org/10.1016/j.ijthermalsci.2011.02.020.

[118] Continillo G, Sirignano WA. Unsteady, Spherically-Symmetric Flame Propagation Through Multicomponent Fuel Spray Clouds. In: Angelino G, Luca LD, Sirignano WA, editors. Modern Research Topics in Aerospace Propulsion, Springer New York; 1991, p. 173–98.

[119] Faeth GM. Evaporation and combustion of sprays. Progress in Energy and Combustion Science 1983;9:1–76. https://doi.org/10.1016/0360-1285(83)90005-9.

[120] Deprédurand V, Castanet G, Lemoine F. Heat and mass transfer in evaporating droplets in interaction: Influence of the fuel. International Journal of Heat and Mass Transfer 2010;53:3495–502. https://doi.org/10.1016/j.ijheatmasstransfer.2010.04.010.

[121] Spalding DB. Convective Mass Transfer: an Introduction. London: Edward Arnold Publ. Ltd; 1963.

[122] Sazhin SS, Abdelghaffar WA, Krutitskii PA, Sazhina EM, Heikal MR. New approaches to numerical modelling of droplet transient heating and evaporation. International Journal of Heat and Mass Transfer 2005;48:4215–28. https://doi.org/10.1016/j.ijheatmasstransfer.2005.04.007.

[123] Al Qubeissi M, Sazhin SS, Al-Esawi N. Models for automotive fuel droplets heating and evaporation, Universitat Politècnica València; 2017. https://doi.org/10.4995/ILASS2017.2017.4754.

[124] Al Qubeissi M, Al-Esawi N, Sazhin SS, Ghaleeh M. Ethanol/Gasoline Droplet Heating and Evaporation: Effects of Fuel Blends and Ambient Conditions. Energy & Fuels 2018;32:6498–506. https://doi.org/10.1021/acs.energyfuels.8b00366.

[125] Al Qubeissi M, Al-Esawi N, Sazhin SS. Droplets heating and evaporation: an application to diesel-biodiesel fuel mixtures, Universitat Politècnica València; 2017. https://doi.org/10.4995/ILASS2017.2017.4644.

[126] Al Qubeissi M, Al-Esawi N, Kolodnytska R. Atomization of Bio-Fossil Fuel Blends. In: Nageswara-Rao M, Soneji JR, editors. Advances in Biofuels and Bioenergy, InTech; 2018. https://doi.org/10.5772/intechopen.73180.

[127] Brenn G, Deviprasath LJ, Durst F, Fink C. Evaporation of acoustically levitated multi-component liquid droplets. International Journal of Heat and Mass Transfer 2007;50:5073–86. https://doi.org/10.1016/j.ijheatmasstransfer.2007.07.036.

[128] Reid RC, Prausnitz JM, Poling BE. The properties of gases and liquids. 4th ed. New York: McGraw-Hill; 1987.

[129] Poling BE, Prausnitz JM, O'Connell JP. The properties of gases and liquids. New York: McGraw-Hill; 2001.

[130] Bondi A. van der Waals Volumes and Radii. The Journal of Physical Chemistry 1964;68:441–51. https://doi.org/10.1021/j100785a001.

[131] Al-Esawi N, Al Qubeissi M, Sazhin SS, Whitaker R. The impacts of the activity coefficient on heating and evaporation of ethanol/gasoline fuel blends. International Communications in Heat and Mass Transfer 2018;98:177–82. https://doi.org/10.1016/j.icheatmasstransfer.2018.08.018.

[132] Teng ST, Williams AD, Urdal K. Detailed hydrocarbon analysis of gasoline by GC-MS (SI-PIONA). J High Resolution Chromat 1994;17:469–75. https://doi.org/10.1002/jhrc.1240170614.

[133] Sawyer RF. Trends in auto emissions and gasoline composition. Environ Health Perspect 1993;101:5–12.

[134] Corsetti S, Miles REH, McDonald C, Belotti Y, Reid JP, Kiefer J, et al. Probing the Evaporation Dynamics of Ethanol/Gasoline Biofuel Blends Using Single Droplet Manipulation Techniques. The Journal of Physical Chemistry A 2015;119:12797–804. https://doi.org/10.1021/acs.jpca.5b10098.

[135] Ma X, Jiang C, Xu H, Ding H, Shuai S. Laminar burning characteristics of 2-methylfuran and isooctane blend fuels. Fuel 2014;116:281–91. https://doi.org/10.1016/j.fuel.2013.08.018.

[136] Paxson FL. The last American frontier. Simon Publications LLC; 2001.

[137] Sazhin SS, Kristyadi T, Abdelghaffar WA, Begg S, Heikal MR, Mikhalovsky SV, et al. Approximate Analysis of Thermal Radiation Absorption in Fuel Droplets. Journal of Heat Transfer 2007;129:1246. https://doi.org/10.1115/1.2740304.

[138] Pitz WJ, Cernansky NP, Dryer FL, Egolfopoulos FN, Farrell JT, Friend DG, et al. Development of an Experimental Database and Chemical Kinetic Models for Surrogate Gasoline Fuels. Warrendale, PA: SAE International; 2007.

[139] Department for Transport. Introducing E10 Petrol 2020. https://www.gov.uk/government/consultations/introducing-e10-petrol (accessed June 17, 2020).

[140] Hallett WLH, Beauchamp-Kiss S. Evaporation of single droplets of ethanol–fuel oil mixtures. Fuel 2010;89:2496–504. https://doi.org/10.1016/j.fuel.2010.03.007.

[141] Pumphrey JA, Brand JI, Scheller WA. Vapour pressure measurements and predictions for alcohol–gasoline blends. Fuel 2000;79:1405–11. https://doi.org/10.1016/S0016-2361(99)00284-7.

[142] Al-Esawi N, Al Qubeissi M, Sazhin SS, Emekwuru N, Blundell MV. Impact of corrected activity coefficient on the estimated droplet heating and evaporation. Eleven International Conference on Thermal Engineering: Theory and Applications, Doha, Qatar: 2018.

[143] Kar K, Last T, Haywood C, Raine R. Measurement of Vapor Pressures and Enthalpies of Vaporization of Gasoline and Ethanol Blends and Their Effects on Mixture Preparation in an SI Engine. SAE International Journal of Fuels and Lubricants 2009;1:132–44.

[144] Banerjee R, Gopinath R. CFD Analysis to Study Evaporation of a Single Ethanol/Iso-Octane Binary Mixture Droplet, ASME; 2011, p. 2571–8. https://doi.org/10.1115/AJK2011-10033.

[145] Balabin RM, Syunyaev RZ, Karpov SA. Molar enthalpy of vaporization of ethanol–gasoline mixtures and their colloid state. Fuel 2007;86:323–7. https://doi.org/10.1016/j.fuel.2006.08.008.

[146] Oktavian R, Amidelsi V, Rasmito A, Wibawa G. Vapor pressure measurements of ethanol–isooctane and 1-butanol–isooctane systems using a new ebulliometer. Fuel 2013;107:47–51. https://doi.org/10.1016/j.fuel.2013.02.005.

[147] Sarjovaara T, Larmi M. Dual fuel diesel combustion with an E85 ethanol/gasoline blend. Fuel 2015;139:704–14. https://doi.org/10.1016/j.fuel.2014.09.049.

[148] Kwanchareon P, Luengnaruemitchai A, Jai-In S. Solubility of a diesel–biodiesel–ethanol blend, its fuel properties, and its emission characteristics from diesel engine. Fuel 2007;86:1053–61. https://doi.org/10.1016/j.fuel.2006.09.034.

[149] Pan K-L, Li J-W, Chen C-P, Wang C-H. On droplet combustion of biodiesel fuel mixed with diesel/alkanes in microgravity condition. Combustion and Flame 2009;156:1926–36. https://doi.org/10.1016/j.combustflame.2009.07.020.

[150] US Department of Energy: Energy Efficiency and Renewable Energy. Biodiesel Blends 2015. http://www.afdc.energy.gov/fuels/biodiesel_blends.html (accessed July 29, 2017).

[151] Silveira MB, do Carmo FR, Santiago-Aguiar RS, de Sant'Ana HB. Ab–diesel: Liquid–liquid equilibrium and volumetric transport properties. Fuel 2014;119:292–300. https://doi.org/10.1016/j.fuel.2013.11.022.

[152] US Department of Energy. Ethanol Blends 2017. https://www.eia.gov/energyexplained/index.php?page=biofuel_ethanol_use#tab2 (accessed April 20, 2018).

[153] Li D, Zhen H, Xingcai L, Wu-gao Z, Jian-guang Y. Physico-chemical properties of ethanol–diesel blend fuel and its effect on performance and emissions of diesel engines. Renewable Energy 2005;30:967–76. https://doi.org/10.1016/j.renene.2004.07.010.

[154] Chin J-Y, Batterman SA, Northrop WF, Bohac SV, Assanis DN. Gaseous and Particulate Emissions from Diesel Engines at Idle and under Load: Comparison of Biodiesel Blend and Ultralow Sulfur Diesel Fuels. Energy & Fuels 2012;26:6737–48. https://doi.org/10.1021/ef300421h.

[155] Liu X, Wang H, Yao M. Experimental and Modeling Investigations on Soot Formation of Ethanol, *n* -Butanol, 2,5-Dimethylfuran, and Biodiesel in Diesel Engines. Energy & Fuels 2017;31:12108–19. https://doi.org/10.1021/acs.energyfuels.7b01622.

[156] Yuan W, Hansen AC, Zhang Q. Predicting the physical properties of biodiesel for combustion modeling. Transactions of the ASAE 2003;46:1487–93. https://doi.org/10.13031/2013.15631.

[157] Tutak W. Bioethanol E85 as a fuel for dual fuel diesel engine. Energy Conversion and Management 2014;86:39–48. https://doi.org/10.1016/j.enconman.2014.05.016.

[158] Satgé de Caro P. Interest of combining an additive with diesel–ethanol blends for use in diesel engines. Fuel 2001;80:565–74. https://doi.org/10.1016/S0016-2361(00)00117-4.

[159] Tutak W, Lukács K, Szwaja S, Bereczky Á. Alcohol–diesel fuel combustion in the compression ignition engine. Fuel 2015;154:196–206. https://doi.org/10.1016/j.fuel.2015.03.071.

[160] He B-Q, Shuai S-J, Wang J-X, He H. The effect of ethanol blended diesel fuels on emissions from a diesel engine. Atmospheric Environment 2003;37:4965–71. https://doi.org/10.1016/j.atmosenv.2003.08.029.

[161] Curran S, Hanson R, Wagner R. Effect of E85 on RCCI Performance and Emissions on a Multi-Cylinder Light-Duty Diesel Engine, 2012. https://doi.org/10.4271/2012-01-0376.

[162] Jeuland N, Montagne X, Gautrot X. Potentiality of Ethanol As a Fuel for Dedicated Engine. Oil & Gas Science and Technology 2004;59:559–70. https://doi.org/10.2516/ogst:2004040.

[163] Ni Z, Han K, Zhao C, Chen H, Pang B. Numerical simulation of droplet evaporation characteristics of multi-component acetone-butanol-ethanol and diesel blends under different environments. Fuel 2018;230:27–36. https://doi.org/10.1016/j.fuel.2018.05.038.

[164] Ma X, Zhang F, Han K, Yang B, Song G. Evaporation characteristics of acetone–butanol–ethanol and diesel blends droplets at high ambient temperatures. Fuel 2015;160:43–9. https://doi.org/10.1016/j.fuel.2015.07.079.

[165] Sazhin SS, Al Qubeissi M, Heikal MR. Modelling of biodiesel and Diesel fuel droplet heating and evaporation. 15th International Heat Transfer Conference, vol. IHTC15-8936, Kyoto, Japan: Begellhouse; 2014. https://doi.org/10.1615/IHTC15.evp.008936.

[166] Pidol L, Lecointe B, Starck L, Jeuland N. Ethanol–biodiesel–Diesel fuel blends: Performances and emissions in conventional Diesel and advanced Low Temperature Combustions. Fuel 2012;93:329–38. https://doi.org/10.1016/j.fuel.2011.09.008.

[167] Kim HJ, Park SH. Optimization study on exhaust emissions and fuel consumption in a dimethyl ether (DME) fueled diesel engine. Fuel 2016;182:541–9. https://doi.org/10.1016/j.fuel.2016.06.001.

[168] Shahir SA, Masjuki HH, Kalam MA, Imran A, Fattah IMR, Sanjid A. Feasibility of diesel–biodiesel–ethanol/bioethanol blend as existing CI engine fuel: An assessment of properties, material compatibility, safety and combustion. Renewable and Sustainable Energy Reviews 2014;32:379–95. https://doi.org/10.1016/j.rser.2014.01.029.

[169] Beatrice C, Napolitano P, Guido C. Injection parameter optimization by DoE of a light-duty diesel engine fed by Bio-ethanol/RME/diesel blend. Applied Energy 2014;113:373–84. https://doi.org/10.1016/j.apenergy.2013.07.058.

[170] Fang Q, Fang J, Zhuang J, Huang Z. Effects of ethanol–diesel–biodiesel blends on combustion and emissions in premixed low temperature combustion. Applied Thermal Engineering 2013;54:541–8. https://doi.org/10.1016/j.applthermaleng.2013.01.042.

[171] Aydın F, Öğüt H. Effects of using ethanol-biodiesel-diesel fuel in single cylinder diesel engine to engine performance and emissions. Renewable Energy 2017;103:688–94. https://doi.org/10.1016/j.renene.2016.10.083.

[172] Noorollahi Y, Azadbakht M, Ghobadian B. The effect of different diesterol (diesel–biodiesel–ethanol) blends on small air-cooled diesel engine performance and its exhaust gases. Energy 2018;142:196–200. https://doi.org/10.1016/j.energy.2017.10.024.

[173] Tse H, Leung CW, Cheung CS. Investigation on the combustion characteristics and particulate emissions from a diesel engine fueled with diesel-biodiesel-ethanol blends. Energy 2015;83:343–50. https://doi.org/10.1016/j.energy.2015.02.030.

[174] Labeckas G, Slavinskas S, Mažeika M. The effect of ethanol–diesel–biodiesel blends on combustion, performance and emissions of a direct injection diesel engine. Energy Conversion and Management 2014;79:698–720. https://doi.org/10.1016/j.enconman.2013.12.064.

[175] Shahir SA, Masjuki HH, Kalam MA, Imran A, Ashraful AM. Performance and emission assessment of diesel–biodiesel–ethanol/bioethanol blend as a fuel in diesel engines: A review. Renewable and Sustainable Energy Reviews 2015;48:62–78. https://doi.org/10.1016/j.rser.2015.03.049.

[176] Mofijur M, Rasul MG, Hyde J, Azad AK, Mamat R, Bhuiya MMK. Role of biofuel and their binary (diesel–biodiesel) and ternary (ethanol–biodiesel–diesel) blends on internal combustion engines emission reduction. Renewable and Sustainable Energy Reviews 2016;53:265–78. https://doi.org/10.1016/j.rser.2015.08.046.

[177] Alptekin E, Canakci M. Characterization of the key fuel properties of methyl ester–diesel fuel blends. Fuel 2009;88:75–80. https://doi.org/10.1016/j.fuel.2008.05.023.

[178] Zöldy M. ETHANOL–BIODIESEL–DIESEL BLENDS AS A DIESEL EXTENDER OPTION ON COMPRESSION IGNITION ENGINES. TRANSPORT 2011;26:303–9. https://doi.org/10.3846/16484142.2011.623824.

[179] Ghosh P, Jaffe SB. Detailed Composition-Based Model for Predicting the Cetane Number of Diesel Fuels. Industrial & Engineering Chemistry Research 2006;45:346–51. https://doi.org/10.1021/ie0508132.

[180] Santana R, Do P, Santikunaporn M, Alvarez W, Taylor J, Sughrue E, et al. Evaluation of different reaction strategies for the improvement of cetane number in diesel fuels. Fuel 2006;85:643–56. https://doi.org/10.1016/j.fuel.2005.08.028.

[181] Creton B, Dartiguelongue C, de Bruin T, Toulhoat H. Prediction of the Cetane Number of Diesel Compounds Using the Quantitative Structure Property Relationship. Energy & Fuels 2010;24:5396–403. https://doi.org/10.1021/ef1008456.

[182] Lapuerta M, Rodríguez-Fernández J, de Mora EF. Correlation for the estimation of the cetane number of biodiesel fuels and implications on the iodine number. Energy Policy 2009;37:4337–44. https://doi.org/10.1016/j.enpol.2009.05.049.

[183] Tong D, Hu C, Jiang K, Li Y. Cetane Number Prediction of Biodiesel from the Composition of the Fatty Acid Methyl Esters. Journal of the American Oil Chemists' Society 2011;88:415–23. https://doi.org/10.1007/s11746-010-1672-0.

[184] Shinde S, Yadav SD. Theoretical Properties Prediction of Diesel-Biodiesel-DEE Blend as a Fuel for C.I. Engine With Required Modifications for Optimum Performance. International Journal of Current Engineering and Technology 2016;6:1562–7.

[185] Grabar IG, Kolodnytska RV, Semenov VG. Biofuel Based on Oil for Diesel Engines. Zhytomyr: ZDTU; 2011.

[186] Al-Esawi N, Al Qubeissi M, Whitaker R, Sazhin SS. Blended E85–Diesel Fuel Droplet Heating and Evaporation. Energy & Fuels 2019;33:2477–88. https://doi.org/10.1021/acs.energyfuels.8b03014.

[187] Al-Esawi N, Al Qubeissi M. A new approach to formulation of complex fuel surrogates. Fuel 2021;283:118923. https://doi.org/10.1016/j.fuel.2020.118923.

[188] Yu L, Mao Y, Li A, Wang S, Qiu Y, Qian Y, et al. Experimental and modeling validation of a large diesel surrogate: Autoignition in heated rapid compression machine and oxidation in flow reactor. Combustion and Flame 2019;202:195–207. https://doi.org/10.1016/j.combustflame.2019.01.012.

[189] Huang Z, Xia J, Ju D, Lu X, Han D, Qiao X, et al. A six-component surrogate of diesel from direct coal liquefaction for spray analysis. Fuel 2018;234:1259–68. https://doi.org/10.1016/j.fuel.2018.07.138.

[190] Al-Esawi N, Al Qubeissi M, Kolodnytska R. The Impact of Biodiesel Fuel on Ethanol/Diesel Blends. Energies 2019;12:1804. https://doi.org/10.3390/en12091804.

[191] Yaws CL. Transport properties of chemicals and hydrocarbons: viscosity, thermal conductivity, and diffusivity of C1 to C100 organics and Ac to Zr inorganics. Norwich, NY: William Andrew; 2009.

[192] Mannaa O, Mansour MS, Roberts WL, Chung SH. Laminar burning velocities at elevated pressures for gasoline and gasoline surrogates associated with RON. Combustion and Flame 2015;162:2311–21. https://doi.org/10.1016/j.combustflame.2015.01.004.

[193] Ghosh P, Hickey KJ, Jaffe SB. Development of a Detailed Gasoline Composition-Based Octane Model. Industrial & Engineering Chemistry Research 2006;45:337–45. https://doi.org/10.1021/ie050811h.

[194] Al Qubeissi M. Predictions of droplet heating and evaporation: An application to biodiesel, diesel, gasoline and blended fuels. Applied Thermal Engineering 2018;136:260–7. https://doi.org/10.1016/j.applthermaleng.2018.03.010.

[195] Al-Esawi N, Al Qubeissi M, Sazhin SS. The impact of fuel blends and ambient conditions on the heating and evaporation of diesel and biodiesel fuel droplets. International Heat Transfer Conference 16, Beijing, China: Begellhouse; 2018, p. 6641–8. https://doi.org/10.1615/IHTC16.mpf.020772.

[196] Qian Y, Liu G, Guo J, Zhang Y, Zhu L, Lu X. Engine performance and octane on demand studies of a dual fuel spark ignition engine with ethanol/gasoline surrogates as fuel. Energy Conversion and Management 2019;183:296–306. https://doi.org/10.1016/j.enconman.2019.01.011.

[197] Department for Transport. Renewable Fuel Statistics 2019 2019. https://www.gov.uk/government/collections/renewable-fuel-statistics (accessed September 20, 2019).

[198] Kuti OA, Sarathy SM, Nishida K. Spray combustion simulation study of waste cooking oil biodiesel and diesel under direct injection diesel engine conditions. Fuel 2020;267:117240. https://doi.org/10.1016/j.fuel.2020.117240.

[199] Al Qubeissi M, Al-Esawi N, Sazhin SS. Auto-selection of quasi-components/components in the multi-dimensional quasi-discrete model. Fuel 2021; In Press.

[200] Burden S, Tekawade A, Oehlschlaeger MA. Ignition delay times for jet and diesel fuels: Constant volume spray and gas-phase shock tube measurements. Fuel 2018;219:312–9. https://doi.org/10.1016/j.fuel.2018.01.113.

[201] Efthymiou P, Davy MH, Garner CP, Hargrave GK, Rimmer JET, Richardson D, et al. An optical investigation of a cold-start DISI engine startup strategy. Internal Combustion

Engines: Performance, Fuel Economy and Emissions, Elsevier; 2013, p. 33–52. https://doi.org/10.1533/9781782421849.1.33.

[202] Petrukhin NV, Grishin NN, Sergeev SM. Ignition Delay Time – an Important Fuel Property. Chem Technol Fuels Oils 2016;51:581–4. https://doi.org/10.1007/s10553-016-0642-0.

[203] Lissitsyna K, Huertas S, Quintero LC, Polo LM. PIONA analysis of kerosene by comprehensive two-dimensional gas chromatography coupled to time of flight mass spectrometry. Fuel 2014;116:716–22. https://doi.org/10.1016/j.fuel.2013.07.077.

[204] Poulton L, Rybdylova O, Zubrilin IA, Matveev SG, Gurakov NI, Al Qubeissi M, et al. Modelling of multi-component kerosene and surrogate fuel droplet heating and evaporation characteristics: A comparative analysis. Fuel 2020;269:117115. https://doi.org/10.1016/j.fuel.2020.117115.

[205] Rybdylova O, Poulton L, Al Qubeissi M, Elwardany AE, Crua C, Khan T, et al. A model for multi-component droplet heating and evaporation and its implementation into ANSYS Fluent. International Communications in Heat and Mass Transfer 2018;90:29–33. https://doi.org/10.1016/j.icheatmasstransfer.2017.10.018.

[206] Al Qubeissi M, Wang G, Al-Esawi N, Rybdylova O, Sazhin SS. CFD modelling of gas-turbine fuel droplet heating, evaporation and combustion, Nottingham, UK: 08/092019, p. 1–3.

[207] Wang F, Liu R, Li M, Yao J, Jin J. Kerosene evaporation rate in high temperature air stationary and convective environment. Fuel 2018;211:582–90. https://doi.org/10.1016/j.fuel.2017.08.062.

[208] Wang H, Hanson RK, Bowman CT, Davidson DF, Pitsch H, Tsang W, et al. A high-temperature chemical kinetic model of nalkane, cyclohexane, and methyl-, ethyl-, n-propyl and n-butyl-cyclohexane oxidation at high temperatures. JetSurF 2010;1.

[209] Franzelli B, Riber E, Sanjosé M, Poinsot T. A two-step chemical scheme for kerosene–air premixed flames. Combustion and Flame 2010;157:1364–73. https://doi.org/10.1016/j.combustflame.2010.03.014.

[210] Komkoua Mbienda AJ, Tchawoua C, Vondou DA, Mkankam Kamga F. Evaluation of Vapor Pressure Estimation Methods for Use in Simulating the Dynamic of Atmospheric Organic Aerosols. International Journal of Geophysics 2013;2013:e612375. https://doi.org/10.1155/2013/612375.

[211] Yaws CL. The Yaws handbook of vapor pressure: Antoine coefficients. Houston, Tex.: Gulf Pub.; 2007.

[212] García-Miaja G, Troncoso J, Romaní L. Excess properties for binary systems ionic liquid+ethanol: Experimental results and theoretical description using the ERAS model. Fluid Phase Equilibria 2008;274:59–67. https://doi.org/10.1016/j.fluid.2008.09.004.

[213] Deprédurand V. Approche expérimentale de l'évaporation de sprays de combustibles multicomposant. Vandoeuvre-les-Nancy, INPL; 2009.

[214] Sinnott RK. Chemical Engineering Design. 4th ed. Oxford: Elsevier Butterworth-Heinemann; 2005.

[215] Sih R, Armenti M, Mammucari R, Dehghani F, Foster NR. Viscosity measurements on saturated gas-expanded liquid systems—Ethanol and carbon dioxide. The Journal of Supercritical Fluids 2008;43:460–8. https://doi.org/10.1016/j.supflu.2007.08.001.

[216] Perry RH. Perry's Chemical Engineers' Handbook. 7th ed. McGraw-Hill; 1997.

[217] Aucejo A, Loras S, Muñoz R, Ordoñez LM. Isobaric vapor–liquid equilibrium for binary mixtures of 2-methylpentane+ethanol and +2-methyl-2-propanol. Fluid Phase Equilibria 1999;156:173–83. https://doi.org/10.1016/S0378-3812(99)00029-1.

[218] NIST. National Institute of Standards and Technology 2017. http://webbook.nist.gov/chemistry/fluid/ (accessed July 28, 2017).

[219] Petravic J. Thermal conductivity of ethanol. The Journal of Chemical Physics 2005;123:174503. https://doi.org/10.1063/1.2102867.

Appendix A. Thermodynamic Properties of Air

A.1. Density

A direct implementation of the density in kg. m^{-3} of air can be found using the ideal gas equation of state which can be generalised to take the nonideality of gas [11]:

$$\rho_{air} = \frac{p_g\, MW}{R\, T_r} \tag{A.1}$$

where p_g is the ambient pressure of gas in kPa, MW is the molar weight for air (18.015 kg. $kmol^{-1}$), R is the universal gas constant (8.314 kJ. $kmol^{-1}$. K^{-1}), T_r is the reference temperature (T_r (K) $= \frac{2}{3}\, T_s + \frac{1}{3} T_g$).

A.2. Specific heat capacity

The specific heat capacity of air in J. kg^{-1}. K^{-1} is approximated as [11]:

$$c_p = 1074.8 - 0.558\, T + 1.4 \times 10^{-3}\, T^2 - 1.1 \times 10^{-6}\, T^3 + 3.15 \times 10^{-10}\, T^4 \tag{A.2}$$

A.3. Viscosity

The dynamic viscosity of air in Pa. s is approximated as [11]:

$$\mu = 27.724 + 0.581\, T - 1.934 \times 10^{-4}\, T^2 \tag{A.3}$$

A.4. Thermal conductivity

The thermal conductivity of air in W. m^{-1}. K^{-1} is approximated as [11]:

$$k = 0.0036 + 0.0252\, \tilde{T} - 1.89 \times 10^{-3}\, \tilde{T}^2 \tag{A.4}$$

where $\tilde{T} = \frac{T}{300}$. The above expression is valid for the range of temperature $250\ \text{K} \leq T \leq 1200\ \text{K}$.

Appendix B. Thermodynamic Properties of Gasoline

All the thermodynamic properties of gasoline were inferred from [71] (apart from the saturated vapour pressure) as follows:

B.1. Boiling and critical temperatures and critical pressure

The dependences of boiling and critical temperatures and critical pressures on the carbon number (n) was approximated based on each hydrocarbon group as:

B.1.1. n-alkanes

$T_b = -1.1328n^2 + 45.02n + 111.68$ (K)

$T_c = -1.7679n^2 + 56.967n + 222.57$ (K)

$P_c = -0.0404n^3 + 1.2475n^2 - 14.239n + 79.185$ (bar)

B.1.2. iso-alkanes

$T_b = -1.1597n^2 + 44.011n + 107.75$ (K)

$T_c = -2.4511n^2 + 66.891n + 183.88$ (K)

$P_c = -0.0186n^3 + 0.459n^2 - 5.924n + 54.071$ (bar)

B.1.3. alkylbenzenes

$T_b = -1.4662n^2 + 46.596n + 136.63$ (K)

$T_c = 0.0257n^2 + 15.718n + 499.56$ (K)

$P_c = 0.7329n^2 - 17.615n + 131.36$ (bar)

B.1.4. naphthalenes, cycloalkanes and olefins

For naphthalene (C_9H_{10}), $T_b = 451.12$ K, $T_c = 684.9$ K, and $P_c = 39.5$ bar

For cycloalkane (C_8H_{16}), $T_b = 394.25$ K, $T_c = 586.99$ K, and $P_c = 29.57$ bar

For olefin (C_9H_{18}), $T_b = 420.02$ K, $T_c = 594$ K, and $P_c = 23.3$ bar

B.2. Liquid density

The liquid density (in kg. m^{-3}) was approximated using the following expression:

$$\rho = 10^3 A B^{-(1-T_r)^C} \quad \text{(B.2)}$$

The dependences of the coefficients A, B and C on the carbon number (n) was approximated based on each hydrocarbon group.

B.2.1. n-alkanes

$A = -0.000248n^2 + 0.0047n + 0.2137$

$B = 0.00003842n^2 - 0.0029866n + 0.282645$

$C = 0.00006352n^2 - 0.0001965n + 0.27969$

B.2.2. iso-alkanes

$A = -0.0009814n^2 + 0.01674n + 0.175683$

$B = -0.0007061n^2 + 0.0087363n + 0.249117$

$C = 0.00114457n^2 - 0.0087363n + 0.343958$

B.2.3. alkylbenzenes

For this hydrocarbon group, the coefficients A, B and C for the 4 components of this groups are shown in Table B.2.3.

Table B.2.3. The coefficients used in equation B.2 for the predictions of the liquid density of alkylbenzenes.

Component	n	A	B	C
C_8H_{10}	8	0.2876	0.26513	0.2741
C_9H_{12}	9	0.2692	0.24988	0.27454
$C_{10}H_{14}$	10	0.2769	0.25841	0.28838
$C_{11}H_{16}$	11	0.2758	0.26261	0.28571

B.2.4. naphthalenes, cycloalkanes and olefins

For the naphthalene, cycloalkane and olefin components, the coefficients A, B and C are shown in Table B.2.4.

Table B.2.4. The coefficients used in equation B.2 for the predictions of the liquid density of naphthalene, cycloalkane and olefin.

Component	A	B	C
naphthalene	0.3102	0.26114	0.0223
cycloalkane	0.26497	0.27385	0.28571
olefin	0.2391	0.25815	0.28571

B.3. Liquid viscosity

The liquid viscosity (in Pa. s^{-1}) was approximated using the following expression:

$$\mu = 10^{\left(a+\frac{b}{T}+cT+dT^2\right)^{-3}} \quad \text{(B.3)}$$

The coefficients a, b, c and d are provided for each hydrocarbon group.

B.3.1. n-alkanes

For this hydrocarbon group, the coefficients a, b, c and d are shown in Table B.3.1.

Table B.3.1. The coefficients used in equation B.3 for the predictions of the liquid viscosity of n-alkanes.

Component	n	a	b	c	d
n-butane	4	-4.6402	485	0.0134	-0.0000197
n-pentane	5	-7.1711	747	0.0217	-0.0000272
n-hexane	6	-5.0715	655	0.0123	-0.000015
n-decane	10	-6.0716	1020	0.0122	-0.0000119
n-dodecane	12	-7.0687	1263	0.013735	-0.0000122

B.3.2. iso-alkanes

For this hydrocarbon group, the coefficients a, b, c and d are shown in Table B.3.2.

Table B.3.2. The coefficients used in equation B.3 for the predictions of the liquid viscosity of iso-alkanes.

Component	n	a	b	c	d
C_4H_{10}	4	-1.8077	258.93	0.003021	-0.00000864
C_5H_{12}	5	-5.8089	706.6875	0.014813	-0.00001853
C_6H_{14}	6	-10.2364	1387.16	0.024213	-0.00002408
C_7H_{16}	7	-4.8431	641.43	0.011545	-0.00001374
C_8H_{18}	8	-10.2217	1423.586	0.024242	-0.00002336
C_9H_{20}	9	-4.2577	652.867	0.008355	-0.00000898
$C_{10}H_{22}$	10	-4.8378	782.643	0.009299	-0.00000938
$C_{11}H_{22}$	11	-4.2302	709.676	0.007402	-0.00000741

B.3.3. alkylbenzenes

For this hydrocarbon group, the coefficients a, b, c and d are shown in Table B.3.3.

Table B.3.3. The coefficients used in equation B.3 for the predictions of the liquid viscosity of alkylbenzenes.

Component	n	a	b	c	d
C_8H_{10}	8	-7.8805	1250	0.016116	-0.00001399
C_9H_{12}	9	-5.3013	897.655	0.009761	-0.00000886
$C_{10}H_{14}$	10	-4.3468	781.441	0.007281	-0.00000673
$C_{11}H_{16}$	11	-4.641	853.23	0.00785	-0.0000071

B.3.4. naphthalenes, cycloalkanes and olefins

For the naphthalene, cycloalkane and olefin components, the coefficients a, b, c and d are shown in Table B.3.4

Table B.3.4. The coefficients used in B.3 for the predictions of the liquid viscosity of naphthalene, cycloalkane and olefin.

Component	a	b	c	d
naphthalene	-7.3304	1330.6	0.012617	-0.0000086
cycloalkane	-4.2467	654.41	0.008539	-0.0000093
olefin	-6.5557	993.5	0.014232	-0.0000141

B.4. Liquid heat capacity

The liquid heat capacities (in $\mathrm{J.kg^{-1}.K^{-1}}$) of all hydrocarbon groups were approximated using the following expression:

$$c_l = A_1 + A_2T + A_3T^2 \quad \text{(B.4)}$$

The coefficients A_1, A_2 and A_3 for all hydrocarbon groups were estimated as follows:

$$A_1 = 4184\left(-1.17126 + (0.023722 + 0.024907\tilde{\rho})K_w + \frac{1.14982-0.046535K_w}{\tilde{\rho}}\right)$$

$$A_2 = 7531.2\left(10^{-4}(1 + 0.82463K_w) + 1.12172 - \frac{0.27634}{\tilde{\rho}}\right)$$

$$A_3 = 13556.16\left(10^{-8}(1 + 0.82463K_w) + 2.9027 - \frac{0.70958}{\tilde{\rho}}\right)$$

K_w is the Watson characterisation factor, estimated as $K_w = \frac{1.8T_b^{1/3}}{\tilde{\rho}}$, $\tilde{\rho}$ is the relative density as shown in Table B.4, and $T_r = \frac{T}{T_c}$.

Table B.4. The relative densities for each carbon number in each hydrocarbon group.

Component	n	$\tilde{\rho}$
n-alkanes	4	0.592
	5	0.631
	6	0.662
	10	0.737
	12	0.566
Iso-alkanes	4	0.620
	5	0.661
	6	0.391
	7	0.713
	8	0.729
	9	0.739
	10	0.743
	11	0.884
alkylbenzenes	8	0.884
	9	0.875
	10	0.872
	11	0.862
naphthalenes	9	0.969
cycloalkanes	8	0.771
olefins	9	0.733

B.5. Liquid thermal conductivity

The liquid thermal conductivities (in $\mathrm{W.m^{-1}.K^{-1}}$) of all hydrocarbon groups were estimated, using the Latini formula:

$$k = \frac{A(1-T_r)^{0.38}}{T_r^{1/6}} \qquad \text{(B.5.1)}$$

The coefficient A was estimated using the following expression:

$$A = \frac{A^* T_b^{\alpha}}{MW^{\beta} T_c^{\gamma}} \quad \text{(B.5.2)}$$

where MW is the molar weight in g. mol^{-1}. All other coefficients are shown in Table B.5 for all hydrocarbon groups.

Table B.5. The coefficients used in equation B.5.2 for the predictions of the liquid thermal conductivity of all hydrocarbon groups.

Component	A^*	α	β	γ
n/iso-alkanes	0.0035	1.2	0.5	0.167
alkylbenzenes	0.0346	1.2	1	0.167
naphthalenes	0.035	1.2	0.5	0.167
cycloalkanes	0.031	1.2	1	0.167
olefins	0.0361	1.2	1	0.167

B.6. Enthalpy of evaporation

The enthalpy of evaporation (in J. kg^{-1}) was estimated using the following expression:

$$L = A(1 - T_r)^B \times \frac{10^6}{MW} \quad \text{(B.6)}$$

The coefficients A and B are provided for each hydrocarbon group.

B.6.1. n-alkanes

For this hydrocarbon group, the coefficients A and B are shown in Table B.6.1.

Table B.6.1. The coefficients used in equation B.6 for the predictions of the enthalpy of evaporation of n-alkanes.

Component	n	A	B
n-butane	4	33.0198	0.377
n-pentane	5	39.8543	0.398
n-hexane	6	45.6100	0.401
n-decane	10	71.4282	0.451
n-dodecane	12	77.1658	0.407

B.6.2. iso-alkanes

For this hydrocarbon group, the coefficients A and B are shown in Table B.6.2.

Table B.6.2. The coefficients used in equation B.6 for the predictions of the enthalpy of evaporation of iso-alkanes.

Component	n	A	B
C_4H_{10}	4	31.95380	0.392
C_5H_{12}	5	37.68615	0.395
C_6H_{14}	6	42.32119	0.393
C_7H_{16}	7	46.95571	0.388
C_8H_{18}	8	49.32456	0.382
C_9H_{20}	9	56.10624	0.380
$C_{10}H_{22}$	10	59.25229	0.380
$C_{11}H_{22}$	11	65.11180	0.380

B.6.3. alkylbenzenes

For this hydrocarbon group, the coefficients A and B are shown in Table B.6.3.

Table B.6.3. The coefficients used in equation B.6 for the predictions of the enthalpy of evaporation of alkylbenzenes.

Component	n	a	B
C_8H_{10}	8	55.6060	0.3750
C_9H_{12}	9	59.9749	0.3853
$C_{10}H_{14}$	10	63.3265	0.3796
$C_{11}H_{16}$	11	65.2016	0.3800

B.6.4. naphthalenes, cycloalkanes and olefins

For the naphthalene, cycloalkane and olefin components, the coefficients A and B are shown in Table B.6.4

Table B.6.4. The coefficients used in B.6 for the predictions of the enthalpy of evaporation of naphthalene, cycloalkane and olefin.

Component	a	b
naphthalene	62.1067	0.42
cycloalkane	50.9505	0.38
olefin	61.7073	0.38

B.7. Saturated vapour pressure

The following expression, inferred from [128,129], was used for the estimation of the gasoline vapour pressure (in Pa)

$$\ln p^{\mathrm{sat}} = f^0(T_r) + \omega f^1(T_r) + \omega^2 f^2(T_r) \quad \text{(B.7.1)}$$

where

$$\omega = -\frac{\ln\frac{P_c}{1.01325} + f^o(T_{br})}{f^1(T_{br})} \quad \text{(B.7.2)}$$

$$f^o(T_r) = (-5.97616\,\tau + 1.29874\,\tau^{1.5} - 0.60394\,\tau^{2.5} - 1.06841\,\tau^5)/T_r \quad \text{(B.7.3)}$$

$$f^1(T_r) = (-5.03365\,\tau + 1.11505\,\tau^{1.5} - 5.41217\,\tau^{2.5} - 7.46628\,\tau^5)/T_r \quad \text{(B.7.4)}$$

$$f^2(T_r) = (-0.64771\,\tau + 2.41539\,\tau^{1.5} - 4.26979\,\tau^{2.5} + 3.25259\,\tau^5)/T_r \quad \text{(B.7.5)}$$

$\tau = 1 - T$.

Note that there was a mistake in the corresponding expression for p^{sat}, given in,[210] which was overlooked in [71]. For the range of temperatures used in the model of [71] (296 – 484 K), the error in the estimated pressure calculation in [210] could lead to overprediction of the droplet evaporation time by up to 150%.

Appendix C. Thermodynamic Properties of Ethanol

C.1. Boiling and critical points and liquid density

The boiling temperature, critical temperature, and critical pressure of ethanol (C_2H_6O) are 351.44 K, 516.25 K and 63.84 bar, respectively [211]. The following expression for the liquid density of ethanol was used in the current analysis [211]:

$$\rho = 1000\, AB^{-(1-T_r)^C}\ (\mathrm{kg.m^{-3}}), \tag{C.1}$$

where $A = 0.2657$, $B = 0.264$ and $C = 0.2367$. The results predicted by Equation (C.1) were compared with approximations suggested in [111] and validated against experimental data provided in [212], as shown in Figure C.1.

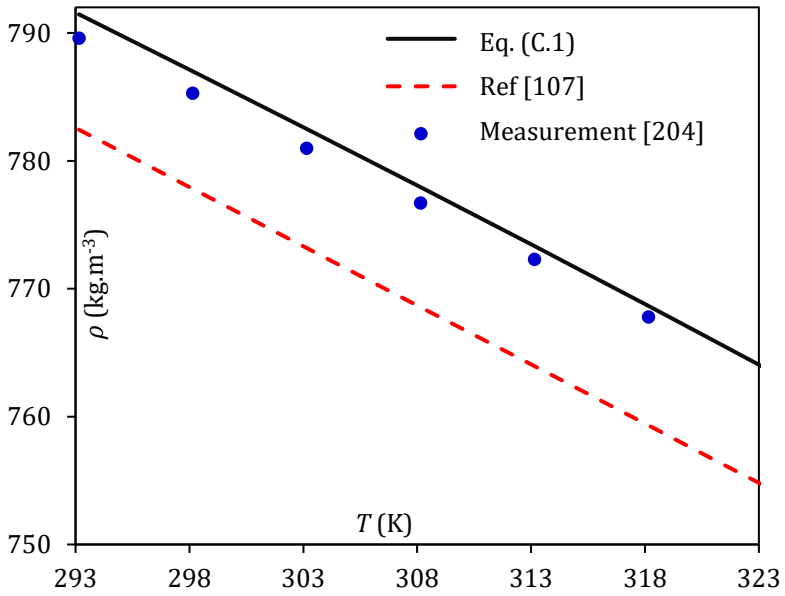

Figure C.1. Comparison of liquid density (ρ) estimated using Equation (C.1) with other approximations and experimental data.

C.2. Liquid viscosity

The following approximation for the liquid viscosity of ethanol was used in the thesis' analysis [111,213]:

$$\log_{10}\mu = \frac{686.64}{T} - 5.282 \quad (\mathrm{Pa.s}). \tag{C.2}$$

The results predicted by Equation (C.2) were compared with those inferred from [211,214] and experimental data provided in [215] as shown in Figure C.2.

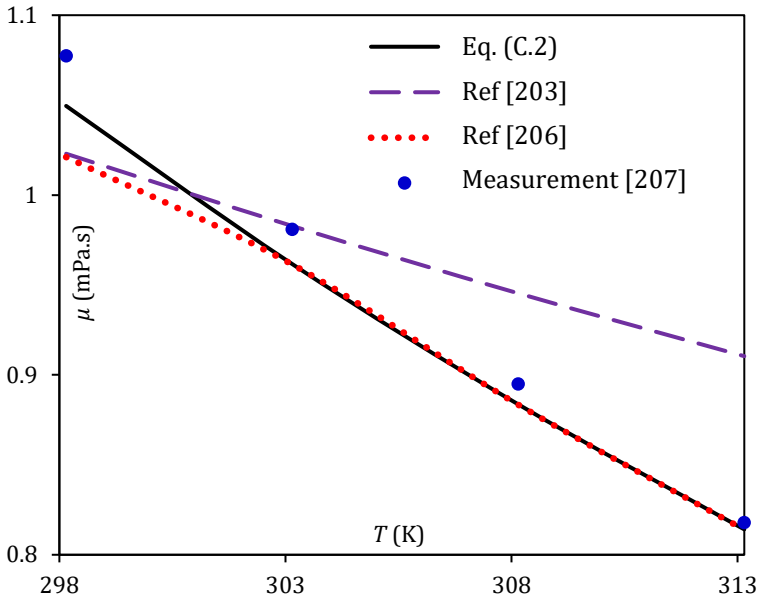

Figure C.2. Comparison of liquid viscosity (μ), estimated using Equation (C.2), with other approximations and experimental data.

C.3. Liquid heat capacity

The specific heat capacity was calculated using the following approximation [216]:

$$c_l = (A + BT + CT^2 + DT^3)/MW \quad (\mathrm{J\,.kg^{-1}.K^{-1}}), \tag{C.3}$$

where $A = 102640$, $B = -139.63$, $C = -0.03034$ and $D = 0.0020386$. Predictions of Equation (C.3) were compared with the approximations suggested in [111,211,213] and validated against experimental data provided in [212]. The results are shown in Figure C.3.

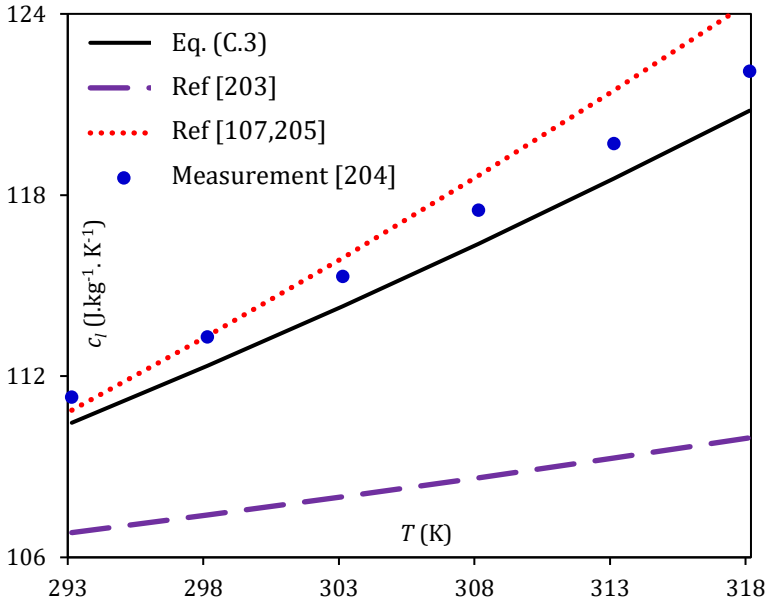

Figure C.3. Comparison of specific liquid heat capacity (c_l), predicted by Equation (C.3), with other approximations and experimental data.

C.4. Saturated vapour pressure

The saturated vapour pressure was estimated using the following approximation [111,213,214]:

$$\ln\left(\frac{p^{sat}}{133.3224}\right) = A - B/(C+T) \quad \text{(Pa)}, \tag{C.4}$$

where $A = 18.5242$, $B = 3578.91$ and $C = 50.5$. The predictions of Equation (C.4) were compared with the approximations suggested in [129,211] and experimental data provided in [217]. The results are shown in Figure C.4.

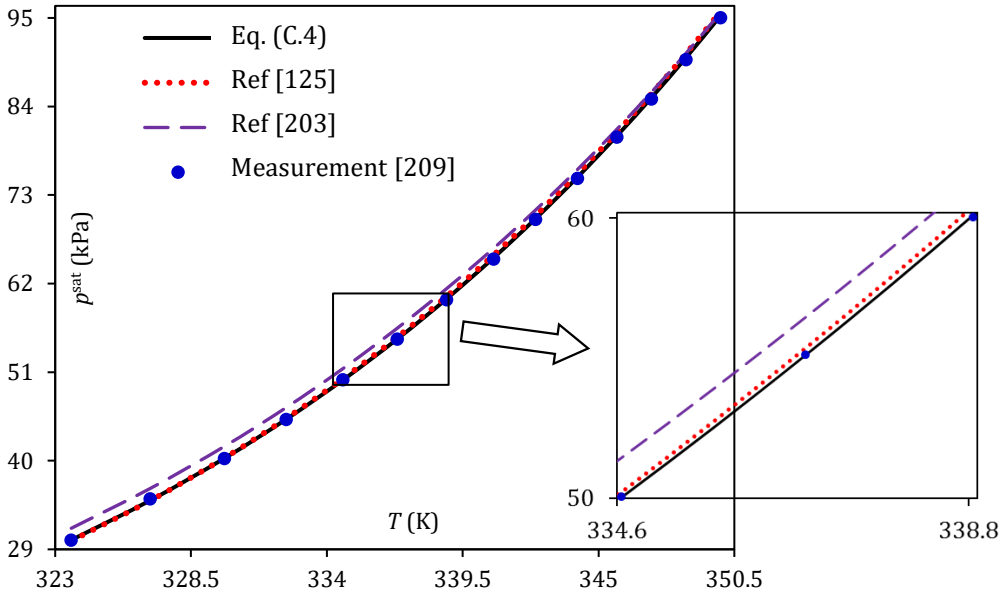

Figure C.4. Comparison of saturated vapour pressure (p^{sat}), predicted by Equation (C.4), with other approximations and experimental data.

C.5. Latent heat of evaporation

Latent heat of evaporation was estimated using the following approximation [111,213]:

$$L = 120910(T_c - T)^{0.38} \quad (\text{J.kg}^{-1}), \tag{C.5}$$

The predictions of Equation (C.5) were compared with the approximation suggested in [211] and experimental data provided in [218]. The results of this comparison are shown in Figure C.5.

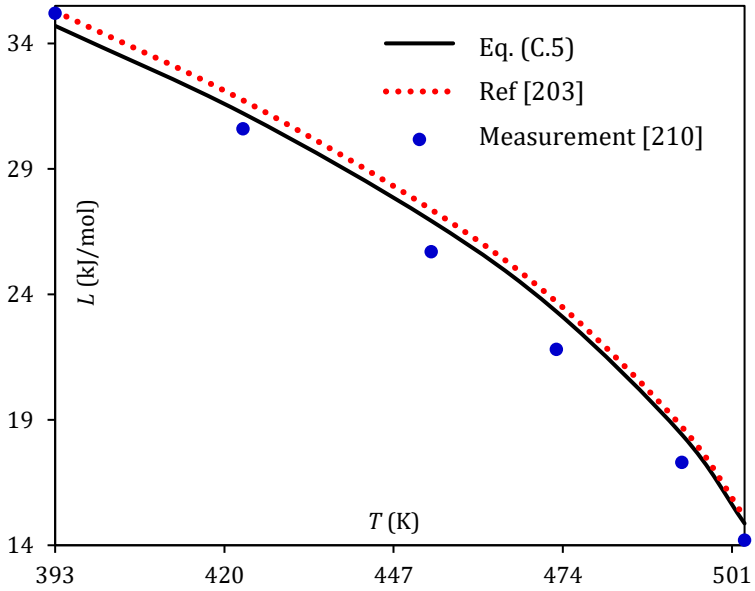

Figure C.5. Comparison of the latent heat of evaporation (L) inferred from Equation (C.5) with other approximations and experimental data.

C.6. Liquid thermal conductivity

Liquid thermal conductivity was estimated using the following approximation [211]:

$$k = A + BT + CT^2 \quad (\mathrm{W.m^{-1}.K^{-1}}), \tag{C.6}$$

where $A = 0.2245$, $B = -0.00005633$ and $C = -0.00000042178$. The results predicted by Equation (C.6) were compared with the estimations of thermal conductivity reported by other authors [111,213,216] and experimental data reported in [219]. The results of this comparison are shown in Figure C.6.

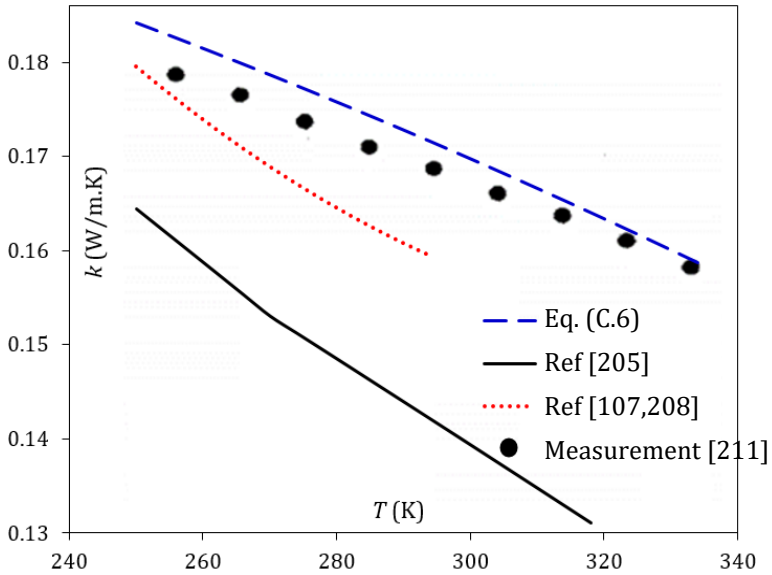

Figure C.6. Comparison of the liquid thermal conductivity estimated using Equation (C.6) with other.

Appendix D. Supporting Results of Chapter 4

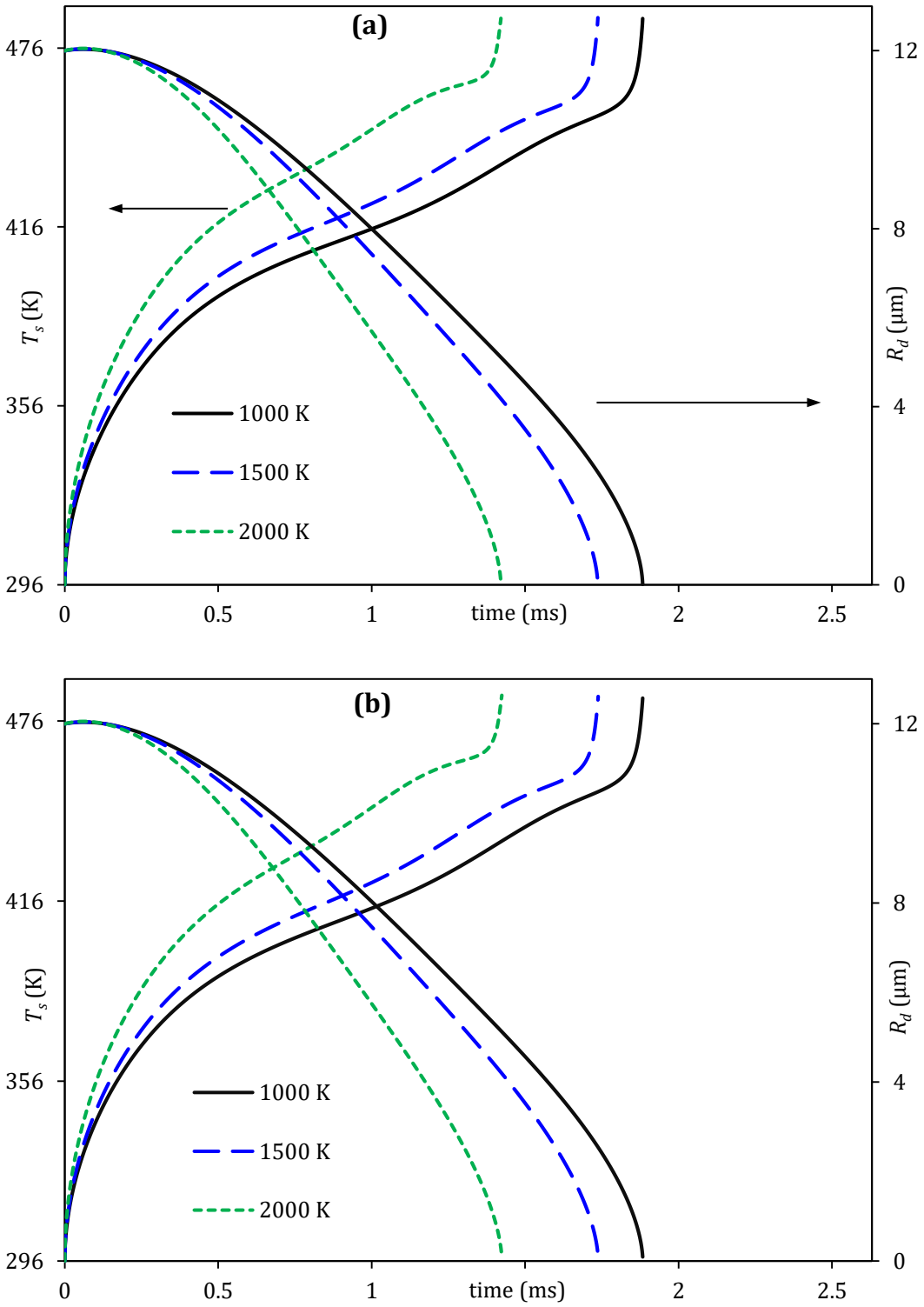

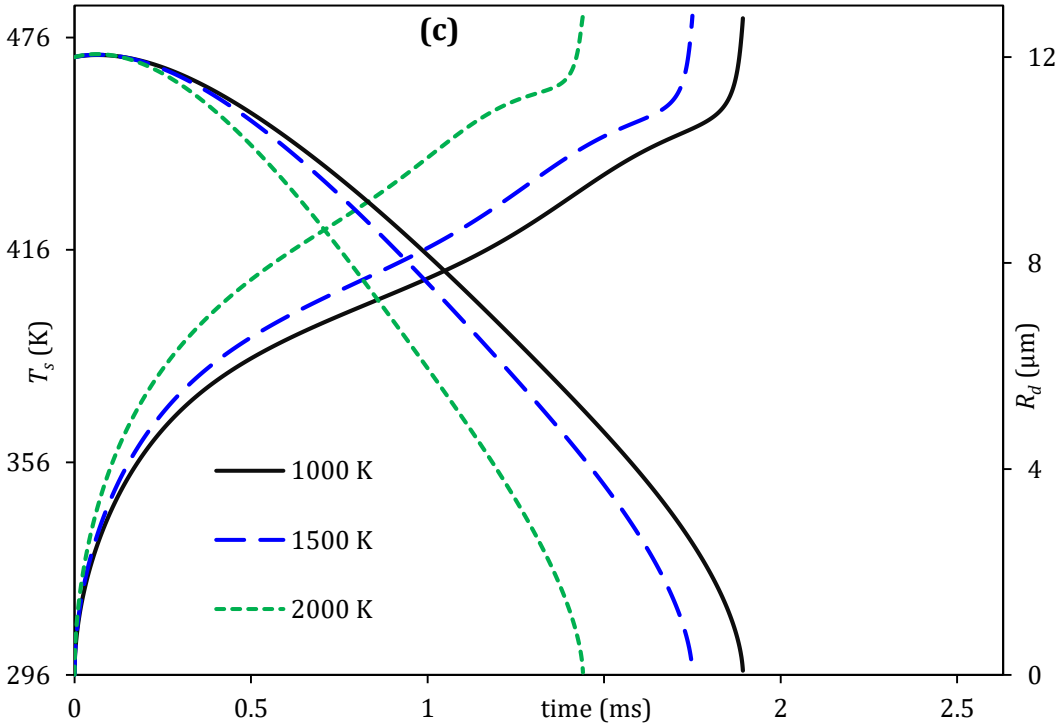
(c)
476
416
356
296
T_s (K)
12
8
4
0
R_d (μm)
0
0.5
1
time (ms)
2
2.5
1000 K
1500 K
2000 K

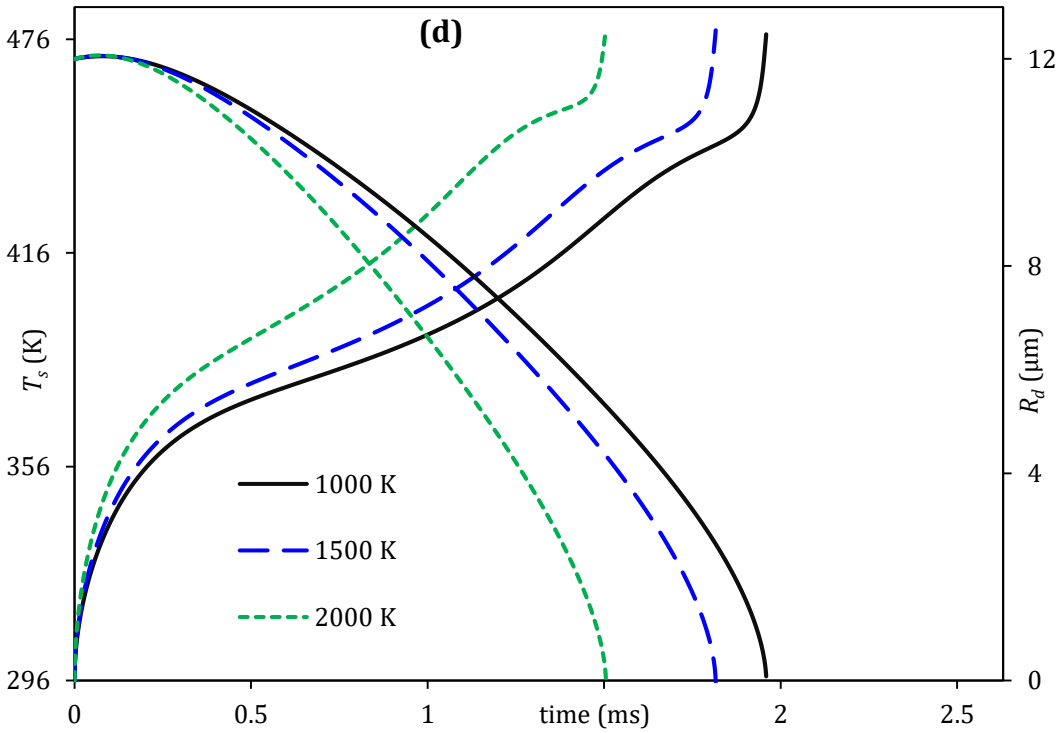
(d)
476
416
356
296
T_s (K)
12
8
4
0
R_d (μm)
0
0.5
1
time (ms)
2
2.5
1000 K
1500 K
2000 K

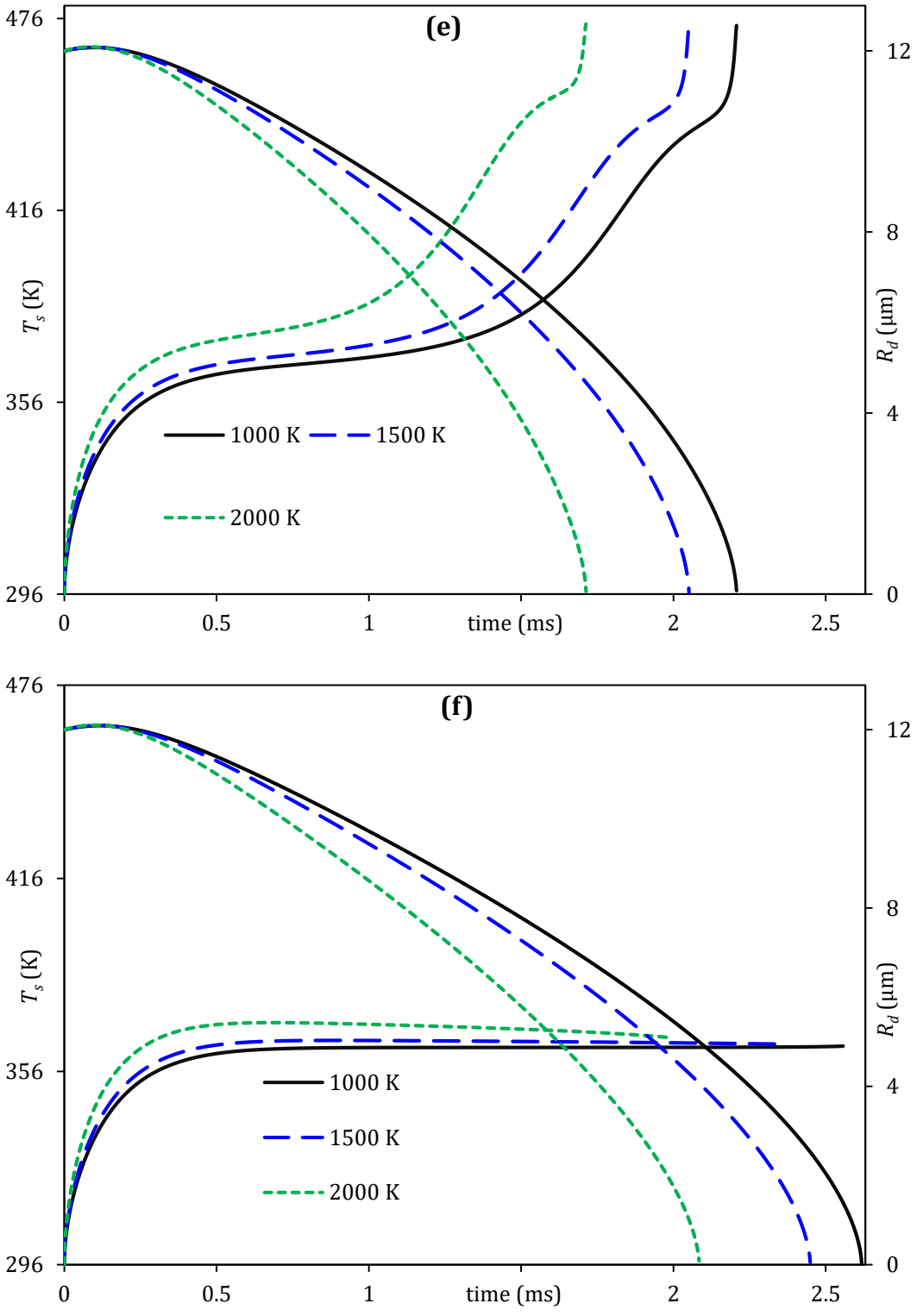

Figure D1. Effects of radiative temperatures (1000 K, 1500 K, and 2000 K) on droplet radii and surface temperatures for EM0 (a), EM5 (b), EM20 (c), EM50 (d), EM85 (e) and EM100 (f) blends.

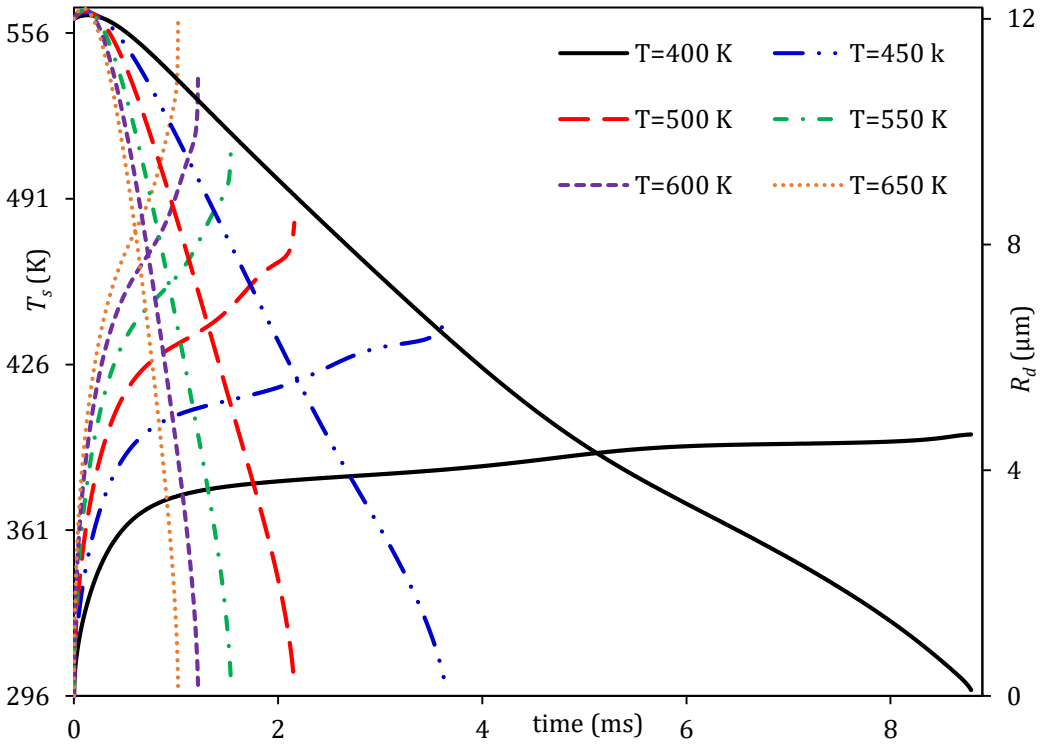

Figure D2. Impact of ambient temperatures on the evolution of droplet surface temperatures and radii for gasoline fuel at $p_g = 30$ bar.

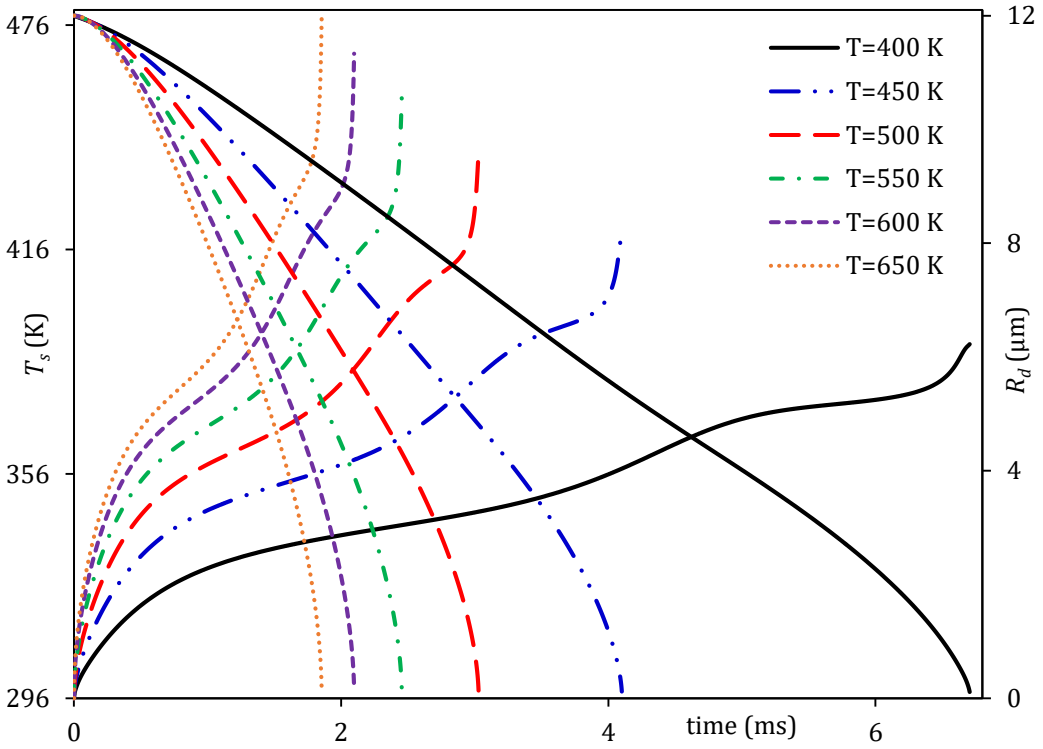

Figure D3. Impact of ambient temperatures on the evolution of droplet surface temperatures and radii for gasoline fuel at $p_g = 3$ bar.

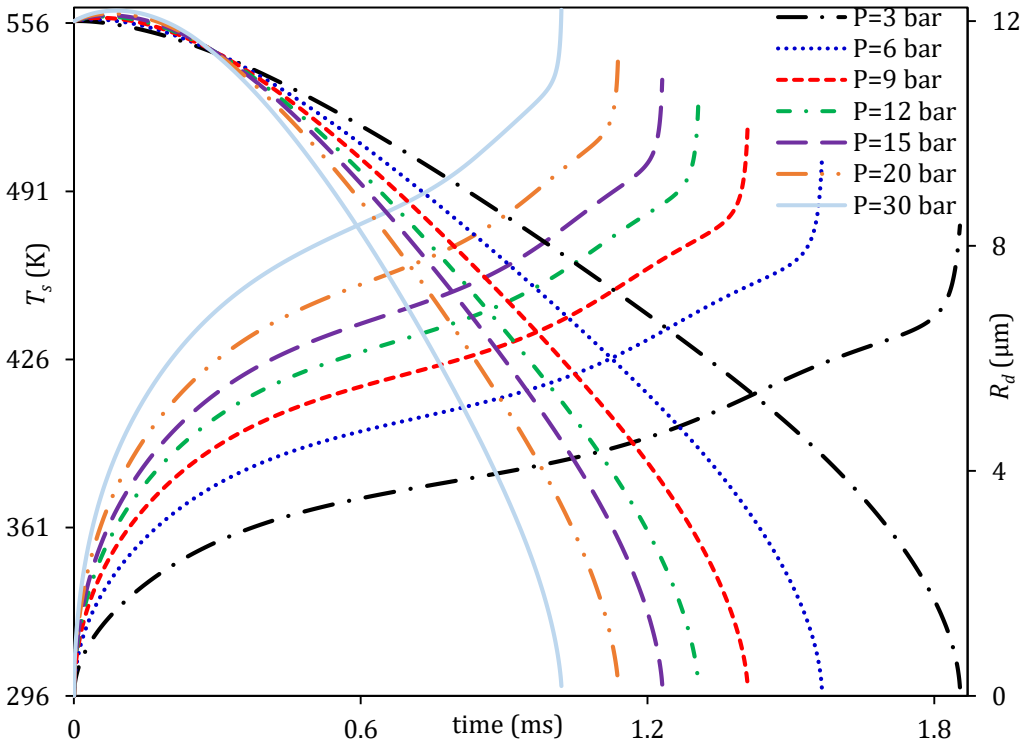

Figure D4. Impact of ambient pressures on the evolution of droplet surface temperatures and radii for gasoline fuel at $T_g = 650$ K.

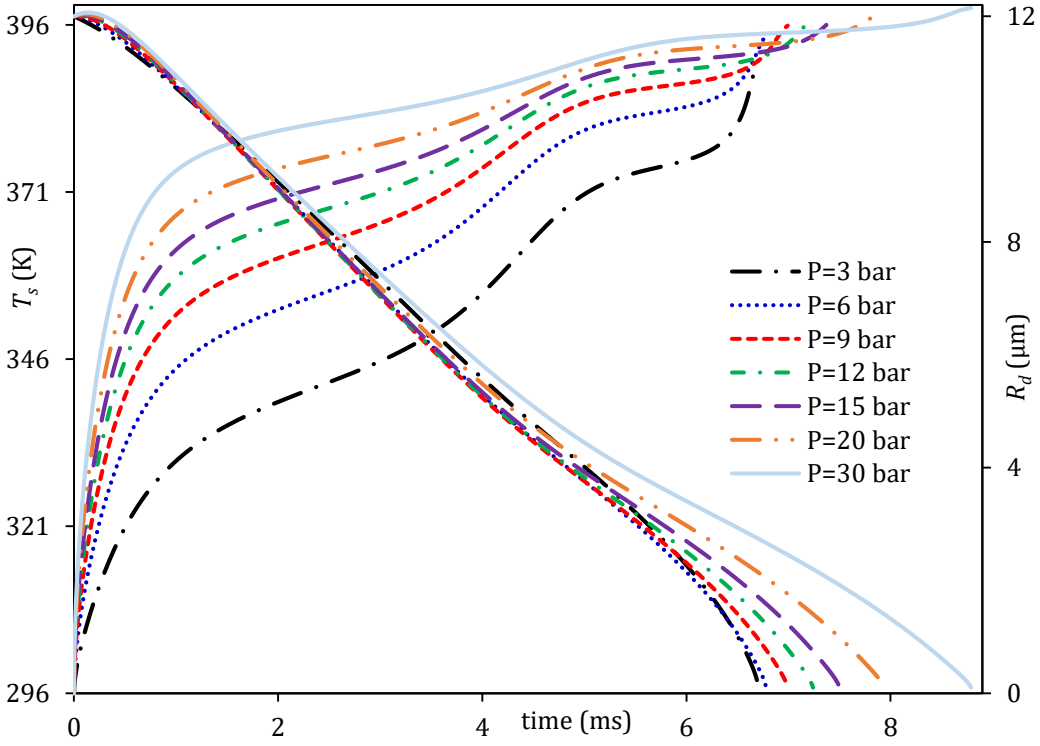

Figure D5. Impact of ambient pressures on the evolution of droplet surface temperatures and radii for gasoline fuel at $T_g = 400$ K.

Appendix E. Thermodynamic Properties of Diesel

All the thermodynamic properties of diesel were inferred from [60] as follows:

E.1. Boiling and critical temperatures

The dependences of boiling and critical temperatures on the carbon number (n) was approximated based on each hydrocarbon group as:

E.1.1. alkanes

$T_b = 0.020138n^3 - 1.404751n^2 + 44.9138n + 118.37237$ (K)

$T_c = 0.035337n^3 - 2.188372n^2 + 55.918666n + 242.30599$ (K)

E.1.2. cycloalkanes

$T_b = -0.4776n^2 + 32.312n + 176.51$ (K)

$T_c = 667$ (K) for $n \leq 10$

$T_c = 0.0125n^3 - 0.9002n^2 + 31.442n + 425.28$ (K) for $n > 10$

E.1.3. bicycloalkanes

$T_b = 217.41 \ln(n) - 32.662$ (K)

$T_c = 703.6$ (K) for n = 10

$T_c = 752.51$ (K) for n = 11

$T_c = 762.49$ (K) for n = 12

$T_c = 134.85 \ln(n) + 395.85$ (K) for $13 \leq n \leq 24$

$T_c = 833.34$ (K) for n = 25

E.1.4. alkylbenzenes

$T_b = -0.5252n^2 + 33.426n + 171.6$ (K)

$T_c = -0.4388n^2 + 27.408n + 427.89$ (K)

E.1.5. indanes and tetralines

$T_b = -0.3319n^2 + 25.894n + 249.21$ (K)

$T_c = 720.15$ (K) for n = 10

$T_c = -0.2486n^2 + 17.898n + 555.59$ (K) for $n > 10$

E.1.6. naphthalenes

$T_b = 15.218n + 350.37$ (K)

$T_c = 9.7878n + 655.14$ (K)

E.1.7. tricycloalkanes, diaromatics and phenanthrenes

tricycloalkanes: $T_b = 692.33$ (K) , $T_c = 937.25$ (K)

diaromatics: $T_b = 537.42$ (K) , $T_c = 760$ (K)

phenanthrenes: $T_b = 610$ (K) , $T_c = 869$ (K)

E.2. Liquid density

The liquid density (in kg. m^{-3}) was approximated using the following expression:

$$\rho = 10^3 A B^{-(1-T_r)^C} \quad \text{(E.2.1)}$$

Equation E.2.1 was used to estimate the densities of alkanes, cycloalkanes, bicycloalkanes and indanes and tetralines groups. The dependences of the coefficients A, B and C on the carbon number (n) was approximated based on each hydrocarbon group.

E.2.1. alkanes

$A = 0.00006196n + 0.234362$

$B = 0.000047157n^2 - 0.00237693n + 0.2768741$

$C = 0.00059704n + 0.2816916$

E.2.2. cycloalkanes

$A = 0.00003n^2 - 0.0016n + 0.278$

$B = 0.00003n^2 - 0.00237693n + 0.2823$

$C = 0.28571$

E.2.3. bicycloalkanes

$A = -0.0034n + 0.3231$ for $11 \leq n \leq 12$

$A = -0.0002n^2 - 0.0072n + 0.3529$ for $13 \leq n \leq 18$

$A = 5 \times 10^{-5}n^2 - 0.0032n + 0.3168$ for $13 \leq n \leq 18$

$B = -0.0031n + 0.3022$ for $11 \leq n \leq 12$

$B = -0.0003n^2 - 0.0278n + 0.4966$ for $13 \leq n \leq 18$

$B = 0.0004n^2 - 0.0179n + 0.4965$ for $13 \leq n \leq 18$

$C = 0.28571$

E.2.4. indanes and tetralines

$A = 0.0002n^2 - 0.0079n + 0.3622$

$B = 7 \times 10^{-5}n^3 + 0.0031n^2 - 0.0438n + 0.4608$ for $10 \leq n \leq 16$

$B = 7 \times 10^{-5}n^2 - 0.0025n + 0.2908$ for $17 \leq n \leq 20$

$C = 0.2677$ for $n = 10$

$C = 0.28571$ for $11 \leq n \leq 20$

For alkylbenzenes group, the following expression was used for estimating the densities (in kg. m^{-3}):

$$\rho = A + BT + CT^2 + DT^3 \quad \text{(D.2.2)}$$

where,

$A = -32.04n + 1422.6$ for $8 \leq n \leq 9$

$A = 0.0477n^2 - 0.4141n + 1082.6$ for $10 \leq n \leq 20$

$B = 0.1831n - 2.824$ for $8 \leq n \leq 9$

$B = 0.0004n^2 - 0.0062n - 0.7017$ for $10 \leq n \leq 20$

$C = -0.0005n + 0.0056$ for $8 \leq n \leq 9$

$C = 0$ for $10 \leq n \leq 20$

$D = 6 \times 10^{-7}n - 7 \times 10^{-6}$ for $8 \leq n \leq 9$

$D = 0$ for $10 \leq n \leq 20$

For naphthalenes group, the following expression was used for estimating the densities (in kg. m^{-3}) with the following coefficients for diaromatics group:

$$\rho = A + BT \quad \text{(E.2.3)}$$

where,

$A = 1.45n^2 - 55.715n + 1671.9$ for $10 \leq n \leq 20$

$B = 0.0087n - 0.8084$ for $10 \leq n \leq 20$

For tricycloalkanes and phenanthrenes groups, equation E.2.3 was used for estimating the densities (in kg. m^{-3}) with the following coefficients for tricycloalkanes and phenanthrenes groups:

tricycloalkanes: $A = 1151.17$, $B = -0.69469$

phenanthrenes: $A = 1374.16$, $B = -0.819355$

For diaromatics group, equation E.2.2 was used for estimating the densities (in kg. m^{-3}) with the following coefficients:

$A = 1224.98$

$B = -0.721739$

$C = -8.65342 \times 10^{-5}$

$D = 1.63332 \times 10^{-9}$

E.3. Liquid viscosity

The liquid viscosity (in Pa. s) was approximated using the following expressions:

$$\mu = 10^{-3}\left[10^{(T)^{b(n)}} - 0.8\right] \quad \text{(E.3.1)}$$

Equation E.3.1 was used for the estimation of viscosity for all hydrocarbon groups of diesel fuel apart from tricycloalkanes, diaromatics and phenanthrenes. The coefficient $b(n)$ was obtained for each hydrocarbon group.

E.3.1. alkanes

$b(n) = -5.745 + 0.616\ln(n) - 40.468n^{-1.5}$

E.3.2. cycloalkanes

$b(n) = -9.001 + 2.35\log_{10}(14n)$

E.3.3. bicycloalkanes

$b(n) = -9.513 + 2.248\log_{10}(14n - 2)$

E.3.4. alkylbenzenes

$b(n) = -9.692 + 2.261\log_{10}(14n - 6)$

E.3.5. indanes and tetralines

$b(n) = -9.411 + 2.217\log_{10}(14n - 8)$

E.3.6. naphthalenes

$b(n) = -9.309 + 2.185\log_{10}(14n - 12)$

For tricycloalkanes. phenanthrenes and diaromatics groups, the liquid viscosity was estimated as follows:

$$\mu = \mathrm{MW}(n) \exp\left\{\frac{\eta_a - 597.82}{T} + \eta_b - 11.202\right\} \quad \text{(E.3.2)}$$

The coefficients for each group are:

tricycloalkanes: $\mathrm{MW} = 262.47$, $\eta_a = 3107.93$, $\eta_b = -9.936$

phenanthrenes: $\mathrm{MW} = 178.23$, $\eta_a = 1613.54$, $\eta_b = -3.372$

diaromatics: $\mathrm{MW} = 168.23$, $\eta_a = 2199.18$, $\eta_b = -5.395$

E.4. Liquid heat capacity

The liquid heat capacity (in $\mathrm{J.kg^{-1}.K^{-1}}$) was approximated using the following expressions:

$$c_l = 10^3 \left[\frac{43.9 + 13.99(n-1) + 0.0543(n-1)T}{\mathrm{MW}(n)}\right] \quad \text{(E.4.1)}$$

where $\mathrm{MW}(n)$ is the molar weight.

Equation E.4.1 was used for the estimation of liquid heat capacity of alkanes group only.

For all other hydrocarbon groups of diesel fuel, the following expression was used:

$$c_l = \frac{R}{\mathrm{MW}(n)}\left[a + b\left(\frac{T}{100}\right) + c\left(\frac{T}{100}\right)^2\right] \quad \text{(E.4.2)}$$

The coefficients a, b and c are shown below for each hydrocarbon group and $R = 8314$ $\mathrm{J.kmol^{-1}.K^{-1}}$ is the universal gas constant.

E.4.1. cycloalkanes

$a = 33.75209 + 2.7345(n - 10)$

$b = -5.21095283 + 0.122732(n - 10)$

$c = 2.78089 - 0.123482(n - 10)$

E.4.2. bicycloalkanes

$a = 19.2782 + 2.7345(n - 11)$

$b = 4.722955 + 0.122732(n - 11)$

$c = 0.08912 + 0.123482(n - 11)$

E.4.3. alkylbenzenes

$a = 15.1109 + 2.7345(n - 7)$

$b = 0.68109 + 0.122732(n - 7)$

$c = 1.96346 - 0.123482(n - 7)$

E.4.4. indanes and tetralines

$a = 14.136 + 2.7345(n - 11)$

$b = 6.43698 + 0.122732(n - 11)$

$c = 14.136 - 0.123482(n - 11)$

E.4.5. naphthalenes

$a = 9.67805 + 2.7345(n - 11)$

$b = 5.982952 + 0.122732(n - 11)$

$c = 0.2688 + 0.123482(n - 11)$

E.4.6. tricycloalkanes, diaromatics and phenanthrenes

tricycloalkanes: $a = 32.9773$, $b = 8.243707$, $c = 0.93225$

diaromatics: $a = 17.9997$, $b = 3.230018$, $c = 0.5203$

phenanthrenes: $a = 2.43092$, $b = 12.11225$, $c = 0.80569$

E.5. Liquid thermal conductivity

For alkanes group, the following expression was used for the estimation of the liquid thermal conductivity (in $\mathrm{W.m^{-1}.K^{-1}}$):

$$k = 10^{\left[A+B\left(1-\frac{T}{T_c}\right)^{\frac{2}{7}}\right]} \quad \text{(E.5.1)}$$

where:

$A = 0.002911n^2 - 0.071339n - 1.319595$

$B = -0.002498n^2 + 0.05872n + 0.710698$

For all other hydrocarbon groups, the following expression was used:

$$k = \frac{0.0264}{\sqrt{MW(n)}} \times \frac{3+20(1-T_r)^{2/3}}{3+20(1-T_{br})^{2/3}} \quad \text{(E.5.2)}$$

where: $T_r = \frac{T}{Tc}$ and $T_{br} = \frac{T_b}{Tc}$

E.6. Enthalpy of evaporation

The enthalpy of evaporation (in $\mathrm{J.kg^{-1}}$) was estimated using the following expression:

$$L = 10^{-6}\frac{A(1-T_r)^B}{\mathrm{MW}(n)} \quad \text{(E.6.1)}$$

Equation E.6.1 was used for the estimation of viscosity for all hydrocarbon groups of diesel fuel apart from bicycloalkanes, tricycloalkanes, diaromatics and phenanthrenes. The coefficients A and B were obtained for each hydrocarbon group.

E.6.1. alkanes

$A = 0.0066n^2 + 4.697n + 20.258$ for $n \leq 20$

$B = -0.1143n^2 + 7.853n - 8.8344$ for $n > 20$

The used values of B were: $B = 0.439$ for $n = 8$, $B = 0.377$ for $n = 9$, $B = 0.451$ for $n = 10$, $B = 0.413$ for $n = 11$, $B = 0.407$ for $n = 12$, $B = 0.416$ for $n = 13$, $B = 0.418$ for $n = 14$, $B = 0.419$ for $n = 15$, $B = 0.422$ for $n = 16$, $B = 0.433$ for $n = 17$, $B = 0.451$ for $n = 18$, $B = 0.448$ for $n = 19$, $B = 0.409$ for $n = 20$, $B = 0.38$ for $n > 8$.

E.6.2. cycloalkanes

$A = -0.0085n^3 + 0.4134n^2 - 2.556n + 56.345$

$B = 0.38$

E.6.3. alkylbenzenes

$A = 0.0007124n^5 - 0.05315n^4 + 1.4963n^3 - 19.83n^2 + 128.65n - 276.8$

$B = -0.007n^2 + 0.1172n - 0.0989$ for $8 \leq n \leq 10$

$B = -0.0062n^2 + 0.1829n - 0.9093$ for $11 \leq n \leq 14$

$B = -0.0013315n^3 + 0.0634n^2 - 0.9842n + 5.3794$ for $15 \leq n \leq 20$

$B = 0.38$ for $n > 20$

E.6.4. indanes and tetralines

$A = -0.0793n^2 + 6.3293n + 5.7796$

$B = 0.303$ for $n \leq 10$

$B = 0.38$ for $n > 10$

E.6.5. naphthalenes

$A = 0.2607n^2 - 2.1791n + 66.218$ for $10 \leq n \leq 16$

$A = -0.1929n^2 + 10.926n - 37.384$ for $n \geq 17$

$B = -0.0003165n^3 + 0.01545n^2 - 0.2495n + 1.722$

For bicycloalkanes group, the following expression was used:

$$L = -\frac{RT_c}{\mathrm{MW}(n)}\Phi(T_r, \omega) \quad \text{(E.6.2)}$$

where,

$\Phi = [(-6.09648 - 15.6875\omega) + (1.28862 + 13.4721\omega)T_r - 6(0.169347 + 0.43577\omega)T_r^7]$ for $\mathrm{T_r} < 0.6$

$\Phi = 7.08(1 - \mathrm{T_r})0.354 + 10.95\omega(1 - T_r)^{0.456}$ for $\mathrm{T_r} \geq 0.6$

$\omega = -0.001n^2 + 0.0679n - 0.3039$

For tricycloalkanes, diaromatics and phenanthrenes groups, the following expression was used:

$$L = -\frac{R}{\mathrm{MW}(n)}\frac{\ln(P^{\mathrm{sat}})}{\ln\left(\frac{1}{T}\right)} \quad \text{(E.6.3)}$$

E.7. Saturated vapour pressure

The saturated vapour pressure (in Pa) was estimated using the following expression:

$$\log_{10}[0.001p^{\mathrm{sat}}(n)] = A(n) - \frac{B(n)}{T + C(n)} \quad \text{(E.7.1)}$$

Equation E.7.1 was used for the estimation of the vapour pressure for n-alkanes, cycloalkanes, alkylbenzenes, tricycloalkanes, diaromatics and phenanthrenes groups. The coefficients $A(n), B(n)$ and $C(n)$ were obtained for each hydrocarbon group.

E.7.1. alkanes

$A(n) = 0.022n + 5.8474$

$B(n) = 52.807n + 981.92$

$C(n) = -5.0431n - 31.205$

E.7.2. cycloalkanes

$A(n) = 0.0201n + 5.8268$

$B(n) = 47.34n + 1115.2$

$C(n) = -5.4145n - 23.03$

E.7.3. alkylbenzenes

$A(n) = 0.0007n^2 - 0.0064n + 6.0715$

$B(n) = 51.811n + 1049.1$

$C(n) = 0.1215n^2 - 9.6892n + 11.161$

E.7.4. tricycloalkanes, diaromatics and phenanthrenes

tricycloalkanes: $A(n) = 15.14702$, $B(n) = 6103.355$, $C(n) = 0$ for $301 \leq T \leq 321$ K

$A(n) = 6.38684$, $B(n) = 2334.129$, $C(n) = -92.028$ for $322 \leq T \leq 464$ K

diaromatics: $A(n) = 9.79557$, $B(n) = 3740.286$, $C(n) = 0$ for $273 \leq T \leq 298$ K

$A(n) = 6.19796$, $B(n) = 1885.888$, $C(n) = -88.292$ for $299 \leq T \leq 647$ K

phenanthrenes: $A(n) = 11.631$, $B(n) = 4873.4$, $C(n) = 0.05$ for $306 \leq T \leq 321$ K

$A(n) = 6.37081$, $B(n) = 2329.54$, $C(n) = -77.87$ for $321 \leq T \leq 650$ K

For bicycloalkanes, indanes and tetralines, and naphthalenes, the vapour pressure was estimated using the following expression:

$$\ln\left(\frac{p^{\text{sat}}}{p_c}\right) = f^0 + \omega f^1 \qquad \text{(E.7.2)}$$

where,

$f^0 = 5.92714 - \frac{6.09648}{T_r} - 1.28862\ln(T_r) + 0.169347T_r^6$

$f^1 = 15.2518 - \frac{15.6875}{T_r} - 13.4721\ln(T_r) + 0.43577T_r^6$

The coefficients the critical pressure (p_c in Pa) and the acentric factor (ω) were obtained for each hydrocarbon group.

E.7.5. bicycloalkanes

$p_c = 10^5(0.0711n^2 - 3.8116n + 60.998)$

$\omega = -0.001n^2 + 0.0679n - 0.3039$

E.7.6. indanes and tetralines

$p_c = 10^5(0.0693n^2 - 3.8821n + 63.771)$

$\omega = 0.617\ln(n) - 1.11$

E.7.7. naphthalenes

$p_c = 10^5(0.2009n^2 - 8.443n + 104.09)$

$\omega = -0.0018n^2 + 0.0997n - 0.5082$

Appendix F. Thermodynamic Properties of Biodiesel

All the thermodynamic properties of biodiesel fuels were inferred from [58] as follows:

F.1. Boiling and critical temperatures

The dependences of boiling and critical temperatures and critical pressures on the carbon number (n) was approximated based on the number of Double Bonds (DB) existed in the methylester structure as:

F.1.1. $DB = 0$

$T_b = 348.7 + 0.8478\text{MW}(n)$

$T_c = 534.3 + 0.784\text{MW}(n)$

F.1.2. $DB = 1$

$T_b = 350 + 0.8463\text{MW}(n)$

$T_c = 538.5 + 0.777\text{MW}(n)$

F.1.3. $DB = 2$

$T_b = 352.1 + 0.8463\text{MW}(n)$

$T_c = 542.6 + 0.772\text{MW}(n)$

F.1.4. $DB = 3$

$T_b = 353.82 + 0.8472\text{MW}(n)$

$T_c = 546.8 + 0.7711\text{MW}(n)$

F.2. Liquid density

The liquid density (in kg. m^{-3}) was approximated using the following expression:

$$\rho = \rho_o - \alpha_T(T - 288.15) \quad \text{(F2)}$$

where,

$\rho_o = 851.471 + \frac{250.718\text{DB}+280.899}{1.214+n}$

$\alpha_T = \frac{7.536}{\ln(n)+3.584} - 0.446$

F.3. Liquid viscosity

The liquid viscosity (in Pa. s) for saturated methyl esters (zero double bond) was approximated using the following expressions:

$$\mu = \rho \left[\exp\left(-2.177 - 0.202n + \frac{403.66}{T} + \frac{109.77n}{T}\right)\right] \times 10^{-6} \quad \text{(F.3.1)}$$

The liquid viscosity (in Pa. s) for unsaturated methyl esters was approximated using the following expressions:

$$\mu = \rho(20)\mathrm{MW}(n) \left[\exp\left(A + \frac{B}{T}\right)\right] \times 10^{-6} \quad \text{(F.3.2)}$$

where, $\rho(20)$ is the density at $T = 20$℃. Coefficients A and B are:

$A = -10.83$ for DB $= 1$

$A = -9.93$ for DB $= 2$

$A = -9.03$ for DB $= 3$

$B = 2009$ for DB $= 1$

$B = 1721$ for DB $= 2$

$B = 1343$ for DB $= 3$

F.4. Liquid heat capacity

The liquid heat capacity (in J. kg^{-1}. K^{-1}) was approximated using the following expressions:

$$c_l = (a + bT + cT^2) \times 10^3 \quad \text{(F.4)}$$

where the coefficients a, b and c are:

$a = 1.816$ for DB $= 0$

$a = 1.915$ for DB $= 1$

$a = 2.018$ for DB $= 2$

$a = 2.115$ for DB $= 3$

$b = -1.462 \times 10^{-3}$ for DB $= 0$

$b = -2.163 \times 10^{-3}$ for DB $= 1$

$b = -2.878 \times 10^{-3}$ for DB $= 2$

$b = -3.580 \times 10^{-3}$ for DB = 3

$c = 7.51 \times 10^{-6}$ for DB = 0

$c = 8.29 \times 10^{-6}$ for DB = 1

$c = 9.09 \times 10^{-6}$ for DB = 2

$c = 9.92 \times 10^{-6}$ for DB = 3

F.5. Liquid thermal conductivity

The following expression was used for the estimation of the liquid thermal conductivity (in $\mathrm{W.m^{-1}.K^{-1}}$):

$$k = \frac{0.0713 T_b^{1.2}(1-T_r)^{0.38}}{\mathrm{MW}(n) T_c^{0.167} T_r^{1/6}} \quad \text{(F.5)}$$

F.6. Enthalpy of evaporation

The enthalpy of evaporation (in $\mathrm{J.kg^{-1}}$) was estimated using the following expression:

$$L = \big(a + b\mathrm{MW}(n)\big)\Phi \quad \text{(F.6)}$$

where,

$$\Phi = \left(\frac{T_c - T}{T_c - T_b}\right)^{0.38}$$

where the coefficients a and b are:

$a = 1.506 \times 10^7$ for DB = 0

$a = 1.389 \times 10^7$ for DB = 1

$a = 1.270 \times 10^7$ for DB = 2

$a = 1.154 \times 10^7$ for DB = 3

$b = 1.814 \times 10^5$ for DB = 0

$b = 1.822 \times 10^5$ for DB = 1

$b = 1.834 \times 10^5$ for DB = 2

$b = 1.843 \times 10^5$ for DB = 3

F.7. Saturated vapour pressure

The saturated vapour pressure (in Pa) was estimated using the following expression:

$$p^{\mathrm{sat}} = 10^3 a_{N0}\left[a(\mathrm{DB}+1) + b + \frac{c}{\mathrm{DB}+1}\right]\exp(a_{N1}n) \tag{F.7}$$

where,

$a_{N0} = 1.908\exp(0.01715T)$

$a_{N1} = -5.656 + 0.02649T - 4.5417\times10^{-5}T^2 + 2.6571\times10^{-8}T^3$

For $\mathrm{DB} = 0$

$a = c = 0, b = 1$

For $\mathrm{DB} > 0$

$a = 5.05 - 0.0306T + 4.62\times10^{-5}T^2$

$b = -9.93 + 0.0339T$

$c = 9.62 + 0.0297T$

Appendix G. Diffusion Coefficients

G.1. Liquid diffusion coefficient

The liquid diffusion coefficient was approximated based on the following expression [60]:

$$D_{jm} = \left(D_{mj}^{0}\right)^{x_j}\left(D_{jm}^{0}\right)^{x_m} \tag{G.1.1}$$

where m refers to the mixture of all other components, D_{mj}^{0} and D_{jm}^{0} are diffusivities of dilute solute j in solvent m, and dilute solute m in solvent j respectively. The difference between D_{mj}^{0} and D_{jm}^{0} was not important. Therefore, it was assumed that $D_{mj}^{0} = D_{jm}^{0}$.

$$D_{mj}^{0} = \frac{7.4\times10^{-15}\sqrt{\mathrm{MW}_v}\,T}{\mu V_v^{0.6}} \tag{G.1.2}$$

where MW_v is the average molar weight obtained as [60]:

$$MW_v = \left[\sum_{m=1}^{m=m_{\text{final}}}\sum_{i=1}^{i=N}\frac{Y_{im}}{MW_{im}}\right]^{-1} \tag{G.1.3}$$

where i is the i^{th}specie in the group m.

$$V_v = \left(\frac{\sigma_v}{1.18}\right)^3 \tag{G.1.4}$$

σ_v is the Lennard–Jones length (in $\dot{A}$). For individual components, this length could be estimated based on the following formula [60]:

$$\sigma_v^3 = 0.17791 + 11.779\left(\frac{T_c}{p_c}\right) - 0.049029\left(\frac{T_c}{p_c}\right)^2 \tag{G.1.5}$$

G.2. Vapour diffusion coefficient

The diffusion coefficient in ($\mathrm{m}^2.\mathrm{s}^{-1}$) were estimated for each fuel. Following a number of publications, including [71], the diffusion coefficient of gasoline and diesel fuels were approximated to that of iso-octane and n-dodecane, respectively. According to [136], the binary diffusion coefficient of iso-octane and dodecane in air is representative of the average diffusion coefficient of gasoline and diesel, respectively, in air with errors under 5% for the temperature range 350 – 700 K.

G.2.1. *ethanol*

$$D_v = 10^{-4} \times (-5.89\ 10^{-2} + 3.6615\ 10^{-4}T + 7.6299\ 10^{-7}T^2)/p \quad \text{(G.2.1)}$$

G.2.2. *gasoline (iso-octane)*

$$D_v = 2 \times 10^{-4}(-0.0578 + 3.0455 \times 10^{-4}T + 3.4265 \times 10^{-7}T^2)/p \quad \text{(G.2.2)}$$

G.2.3. *diesel (n-dodecane)*

$$D_v = 5.27 \times 10^{-6}\left(\frac{T}{300}\right)/p \quad \text{(G.2.3)}$$

G.2.4. *biodiesel*

Following [58], all diffusion coefficients of biodiesel fuels were rather close. Therefore, the following average values of this coefficient for the mixtures of methyl esters was used:

$$D_v = 2 \times 10^{-10}T^{1.75}/p \quad \text{(G.2.4)}$$

Appendix H. Blending Rules

For the work conducted in this thesis, the following blending rules were used to make the properties of the mixture [60]:

H.1. Liquid density

$$\rho = \left[\sum_{i=1}^{i=N} \left(\frac{Y_i}{\rho_i}\right)\right]^{-1} \quad \text{(H1)}$$

H2. Liquid viscosity

$$\ln \mu = \sum_{i=1}^{i=N} X_i \mu_i \quad \text{(H.2)}$$

H.3. Liquid heat capacity

$$C_p = \sum_{i=1}^{i=N} Y_i C_{p_i} \quad \text{(H.3)}$$

H.4. Liquid thermal conductivity

$$k = \left(\sum_{i=1}^{i=N} Y_i K_i^{-2}\right)^{-1/2} \quad \text{(H.4)}$$

H.5. Enthalpy of evaporation

$$L = \sum_{i=1}^{i=N} X_i L_i \quad \text{(H.5)}$$

H.6. Vapour diffusion coefficient

$$D = \sum_{i=1}^{i=3} X_i D_i \quad \text{(H.6)}$$

Note that the vapour diffusion coefficient includes up to three binary diffusion coefficients in air (in the case of blending three fuels such as ethanol/gasoline/diesel or ethanol/biodiesel/diesel).

Appendix I. Components/Quasi-Components

Table I.1. The numbers of components/quasi-components (C/QC) (top line), and the compositions of C/QC, used in the MDQDM for approximating E85-5.

Group	119	90	63	45	20	16
Alkanes (Diesel)	8	8	8	8.91 (C8–C9)	10.33 (C8–C12)	10.33 (C8–C12)
	9	9	9			
	10	10	10	10.38 (C10–C11)		
	11	11	11			
	12	12	12	12.49 (C12–C13)		
	13	13	13			
	14	14	14	14.54 (C14–C15)	15.05 (C13–C17)	15.05 (C13–C17)
	15	15	15			
	16	16	16	16.52 (C16–C17)		
	17	17	17			
	18	18	18	18.52 (C18–C19)		
	19	19	19			
	20	20	20	20.39 (C20–C21)	19.38 (C18–C22)	19.38 (C18–C22)
	21	21	21			
	22	22	22	22.33 (C22–C23)		
	23	23	23			
	24	24	24	24.34 (C24–C25)	23.84 (C23–C27)	23.84 (C23–C27)
	25	25	25			
	26	26.42 (C26-C27)	26.42 (C26-C27)	26.42 (C26-C27)		
	27					
Cycloalkanes (Diesel)	10	10	10.74 (C10-C11)	10.74 (C10-C11)	12.56 (C10–C15)	12.56(C10–C15)
	11	11				
	12	12	12.43 (C12-C13)	12.43 (C12-C13)		
	13	13				
	14	14	14.47 (C14-C15)	14.47 (C14-C15)		
	15	15				
	16	16	16.49 (C16-C17)	16.49 (C16-C17)		
	17	17				
	18	18	18.51 (C18-C19)	18.51 (C18-C19)	18.29 (C16–C21)	18.29 (C16–C21)
	19	19				
	20	20	20.35 (C20-C21)	20.35 (C20-C21)		
	21	21				
	22	22	22.26 (C22-C23)	22.26 (C22-C23)		
	23	23				
	24	24	24.37 (C24-C25)	24.37 (C24-C25)	22.98 (C22–C27)	22.98 (C22–C27)
	25	25				
	26	26.42 (C26-C27)	26.42 (C26-C27)	26.42 (C26-C27)		
	27					
Bicycloalkanes (Diesel)	10	10.60 (C10-C11)	10.60 (C10-C11)	11.1 (C10–C12)	14.74(C10–C25)	14.74(C10–C25)
	11					
	12	12.40 (C12-C13)	12.40 (C12-C13)			
	13					
	14	14.43 (C14-C15)	14.43 (C14-C15)	13.86 (C13–C15)		
	15					
	16	16.57 (C16-C17)	16.57 (C16-C17)	17.09 (C16–C18)		
	17					
	18	18.60 (C18-C19)	18.60 (C18-C19)			

	19 20 21 22 23 24 25	20.32 (C20-C21) 22.41 (C22-C23) 24.42 (C24-C25)	20.32 (C20-C21) 22.41 (C22-C23) 24.42 (C24-C25)	19.31 (C19–C21) 22.92 (C22–C25)		
Alkylbenzenes (Diesel)	8 9 10 11 12 13 14 15 16 17 18 19 20 21 22 23 24	8 9 10 11 12 13 14 15 16 17 18 19 20 21 22 23.49(C23-C24)	8.86 (C8-C9) 10.15 (C10-C11) 12.26 (C12-C13) 14.42 (C14-C15) 16.45 (C16-C17) 18.38 (C18-C19) 20.41 (C20-C21) 22.74 (C22-C24)	8.86 (C8–C9) 10.15 (C10–C11) 12.26 (C12–C13) 14.42 (C14–C15) 16.47 (C16–C17) 18.38 (C18-C19) 20.41 (C20-C21) 22.74 (C22-C24)	10.207 (C8–C13) 16.23 (C14–C19) 21.08 (C20–C24)	10.72(C8–C16) 19.02 (C17–C24)
Indanes & tetralines (Diesel)	10 11 12 13 14 15 16 17 18 19 20 21 22	10 11 12 13 14 15 16 17 18 19 20 21.32 (C21-C22)	10.51 (C10-C11) 12.47 (C12-C13) 14.45 (C14-C15) 16.46 (C16-C17) 18.39 (C18-C19) 20.57 (C20-C22)	11.41 (C10–C13) 15.34 (C14–C17) 19.24 (C18–C22)	12.49 (C10–16) 18.61 (C17–C22)	13.83 (C10–C22)
Naphthalenes (Diesel)	10 11 12 13 14 15 16 17 18 19 20	10 11 12 13 14 15 16 17 18 19.51 (C19-C20)	10.56 (C10-C11) 12.35 (C12-C13) 14.44 (C14-C15) 16.42 (C16-C17) 18.98 (C18-C20)	11.53 (C10–C15) 17.90 (C16–C20)	12.39 (C10–C20)	12.39 (C10–C20)
Diesel T.	19	19	19	19	-	-
Diesel Dia.	13	13	13	13	-	-
Diesel Phe.	14	14	14	14	-	-
N-alkanes	4 5 6	5.24 (C4-C12)	5.24 (C4-C12)	5.24 (C4-C12)	5.24 (C4-C12)	5.24 (C4-C12)

		10 12					
Iso-alkanes (gasoline)		4 5 6 7 8 9 10 11	7.37 (C4-C8) 9.74 (C9-C11)	7.37 (C4-C8) 9.74 (C9-C11)	7.37 (C4-C8) 9.74 (C9-C11)	7.37 (C4-C8) 9.74 (C9-C11)	7.41 (C4-C11)
Alkylbenzenes (gasoline)		8 9 10 11	9.07 (C8-C11)	9.07 (C8-C11)	9.07 (C8-C11)	9.07 (C8-C11)	9.07 (C8-C11)
Gasoline	Ind.	9	-	-	-	-	-
	Cyc.	8	-	-	-	-	-
	Ole.	9	-	-	-	-	-
Ethanol		2	2	2	2	2	2